CARDIFF
UNIVERSITY

PRIFYSGOL
CAERDYDD

BINDING SERVICES
Tel +44 (0)29 2087 4949
Fax +44 (0)29 20371921
e-mail bindery@cardiff.ac.uk

CHARACTERISATION OF SUBSTATION EARTH GRID UNDER HIGH FREQUENCY AND TRANSIENT CONDITIONS

A thesis submitted to the University of Wales, Cardiff

in candidature for degree of

Philosophiae Doctor

By

Buthenah Zedan

School of Engineering,

Cardiff University

June 2005

ACKNOWLEDGEMENT

First of all, I would like to thank my academic supervisors Mr. H. Griffiths and Dr. Haddad for their guidance, encouragement and invaluable advice throughout the duration of this research. And a very special thank for their great support during the writing of this thesis over the last year, I am very grateful.

The Aga Khan Foundation provided the financial support for this research. I would like to thank his Highness Karim Aga Khan for all the support he provides to education throughout the developing countries. I would like to extend my thanks to all the people in the foundation in Syria or Switzerland, and a special thanks to Miss Catherine Hieronymi and Mr Ilias Khalaf for all the help they provided.

The input, support and of the following within the high voltage group has been invaluable: N. Mohamad Nor Miza, Suriya Srisakot, Ahmed Mghairbi, Niamat Ullah, Jackline Crespo-Sandoval, Freddie van der Linde, Davide Lazzari, and Noureddine Harid.

A special thanks to everyone I left behind to follow my dreams, there was not a day that passed without any thoughts of you. My love and gratitude to you all.

SUMMARY

Earthing systems are designed to perform satisfactorily under normal system voltage conditions as well as power frequency faults. The performance of most earth electrode geometries is now fairly well understood under these conditions. However, the response of earthing systems under high frequency and transient conditions is yet to be fully clarified, and there are several aspects of earthing systems that require further investigations.

In this thesis, both modelling and experimental studies were carried out using high frequency and impulse current injection. Generic earth electrodes as well as the full earthing grid of an operating substation were investigated. The studies carried out in this work have confirmed some of the previous findings published in the open literature, and have clarified some aspects of conduction in earthing systems. The literature review on injuries due to lightning currents has highlighted the importance of good earthing systems.

A comprehensive parametric simulation study was conducted on vertical rods, horizontal electrodes as well as earth grids under variable frequency and impulse currents. The effects of geometry and soil characteristics were also studied. It was demonstrated that significant inductive effects appear at high frequency, and the size of the earthing systems was found to reach an "effective dimension" beyond which negligible performance benefit is obtained. For horizontal electrodes the concept of effective length is investigated and for grids the effective area was used instead.

The Simulation techniques developed for these simple electrodes were applied to an operating transmission substation, and similar trends were seen under high frequency and impulse current conditions. The safety voltages were calculated but no conclusion could be drawn as there are no recommended safety guidelines for safety at high frequency and impulse current.

These Generic studies have led to a new proposal for earthing systems so that the short fall of poor performance due to inductive effects and "effective dimensions" are minimized. It was shown that this proposal is a major improvement on the existing enhancement techniques currently used in practice.

Parallel to the simulation programme, an experimental set up was used to study the performance of laboratory earth electrode models under fast impulse current. It was found that highly non-linear conduction phenomena take place in such configurations. These complex conduction processes were explained by thermal effects and soil ionisation.

CHARACTERISATION OF SUBSTATION EARTH GRID UNDER HIGH FREQUENCY AND TRANSIENT CONDITIONS

CHAPTER ONE: INTODUCTION

CHAPTER TWO: LIGHTNING AND ELECTRICAL INJURIES REVIEW OF PREVIOUS WORK

CHAPTER THREE: CHARACTERISATION OF EARTH ELECTRODES UNDER VARIABLE FREQUENCY

CHAPTER FOUR: QUANTIFICATION OF EXISTING AND NEW PROPOSED EARTH GRID ENHANCEMENTS TECHNIQUES.

CHAPTER FIVE: TRANSIENT PERFORMANCE OF EARTHING SYSTEMS

CHAPTER SIX: THE PERFORMANCE OF AN OPERATIONAL SUBSTATION EARTHING SYSTEM UNDER HIGH FREQUENCY AND TRANSIENT CONDITIONS

CHAPTER SEVEN: LABORATORY CHARACTERISATION OF SOIL IONISATION UNDER FAST TRANSIENTS

CHAPTER EIGHT: GENERAL CONCLUSIONS AND FURTHER WORK

CHAPTER ONE

Introduction

1.1 Introduction

Lightning strikes subject the electrical power system to a high magnitude and fast rising transient current and voltage. Using the Optical Transient Detector (OTD), it was possible to estimate that more than 1.2 billion lightning flashes take place all over the world every year [1.1].

Benjamin Franklin was the first to prove that lightning is an electrical phenomenon. The whole idea of earthing systems was his when he invented the lightning rod in the early 1750's [1.1].

" It has pleased God in his Goodness to Mankind, at length to discover to them the Means of securing their Habitation and other Buildings from Mischief by Thunder and Lightning. The method is this: Provide a small Iron Rod (it may be made of the Rod-iron used by the Nailers) but of such Length, that one End being three or four Feet in the moist ground, the other may be six or eight Feet above the highest Part of the Building. To the upper End of the Rod fasten a Foot of brass Wire the Size of a common Knitting-needle, Sharpened to a fine Point; the Rod may be secured to the House by a few small Staples. If the House or Barn be long, there may be a Rod and Point at each End, and a middling Wire along the Ridge from one to the other. A House thus furnished will not be damaged by Lightning, it being attracted to the Points, and passing thro the Metal into the Ground without hurting any Thing. Vessels also, having a sharp pointed rod fix'd on the Tops of their Masts, with a Wire from the Foot of the Rod reaching down, round one of the Shrouds, to the Water, will not be hurt by Lightning"

The use of lightning rods to protect buildings and ships became common in the United States in the 1750s and 1760s. In Europe scientists encouraged installation of the lightning rods on government buildings, ships and churches. However, religious believers refused to install the lightning rod on church steeples thinking that God protects churches. The main reason for the delay in installing the lightning rod in

England was the distrust of scientific theories from the newly independent United States.

Years later and after a few incidents where significant damage and loss of lives resulted from churches hit by lightning, the lightning rod was used in Europe. The first Lightning Rod conference was held in London in 1882. Recommendations from this conference were published that year and again in 1905. Since then, the earthing systems have developed markedly and research work is still in progress aiming to provide the highest standards of protection for humans and equipment.

In this thesis, the performance of earthing systems under high frequency and transient conditions is investigated, the effect of the electrode geometry and soil parameters is quantified and a new proposal for an earthing system is introduced and investigated. In addition, laboratory experiments were devised and used to investigate the conduction phenomena in soil when subjected to fast high-magnitude impulse currents.

1.2 Earthing Systems

Electrical power systems should be designed so that high magnitude and fast transient surges are dissipated to the ground, diminishing personal injuries and damage to equipment while also reducing disturbances to power system operations. Although high voltage distribution and transmission systems are protected from lightning, the effectiveness of the lightning protection depends mainly on its connection to earth.

1.2.1 Earthing System Components and the Soil Medium

Although earthing systems are mainly designed to be safe under power frequency earth fault conditions, they are also required to perform satisfactorily under fast-front surges so that the power system can be protected against excessive voltages. The characteristics of an earthing system under these conditions are very different from those under power frequency and, therefore, the design of earthing systems to perform satisfactorily is more difficult.

Certain equipment within substations such as surge arresters will provide the transient currents with a path to earth. The dissipation of a transient current to earth involves above-ground conductors which are connected to a buried earth electrode system. For power frequency earth faults, the self-impedance of the electrode and the connected conductors is very small. Consequently, the effect of above-ground downleads can be neglected. For transient conditions, the self-impedance of the above-ground downlead is of significant value and must, therefore, be considered.

The earth electrodes are generally solid copper conductors, which are buried below the equipment being protected. The earthing system usually consists of a vertical earth rod, short horizontal electrode or a combination of both, for small, pole-mounted or ground-mounted equipment. In larger substations, the electrodes are arranged in the form of a buried grid occupying the entire area under where the equipment is installed.

In the case of transient currents, the standards recommend the installation of a "high frequency earth electrode", usually a vertical earth rod [1.2]. The phrase "high frequency earth electrode" suggests that the main function of the earth rod is to dissipate to earth all the high frequency components of the transient. In reality, every single part of the earthing system may play a role in the dissipation of both power frequency faults and the transient conditions.

The most difficult parameter to quantify in earthing system performance estimation is the electrical characteristics of the earth itself [1.3]. The soil can change structurally in both horizontal and vertical directions, but it can be approximated to a model consisting of one or more uniform horizontal layers each with a particular resistivity.

1.2.2 Standards Applicable to Earthing System

A number of national and international standards provide guidelines to earthing system design. These standards are concerned with power frequency design and give only limited guidance under transient conditions. These standards are:

- Engineering Association Technical Specification 41-24 (EA TS 41-24), "Guidelines for the Design, Testing and Maintenance of Main Earthing Systems in Substations" (UK) [1.2]. This standards states that '*unless a low-impedance earth connection is provided...the effectiveness of the surge arrester could be impaired*'. The same standard also recommends that the connection from the equipment to earth should be '*as short, and as free from changes in direction, as is practicable*' and that '*the effectiveness of the arrester can be improved .. by connecting ..(it) to a high-frequency earth electrode in the immediate vicinity, for example an earth rod*'.
- ANSI/IEEE Std.80, "IEEE Guide for Safety in AC Substation Grounding", (USA) [1.4], this standard is widely used throughout the world. In this standard,

it is considered that designing according to power frequency principles will '*provide a high degree of protection against steep wave front surges...*'. It also considers issues related to the '*safety in grounding*', and defines step and touch voltages and provides equations to calculate their values.

- CENLEC HD 637 S1, "Power Installation Exceeding 1kV ac or 1.5kV dc" [1.5]. It suggests measures to reduce the amount of interference created when surges are dissipated to earth. These include minimising the inductance of the current paths by the 'significant meshing' of earth electrodes and earthing conductors.
- BS 6651, 'Code of Practice for Protection of Structures Against Lightning' (UK) [1.6]. It provides the only transient earthing design limit; the earthing systems designed for lightning protection should have an earth resistance of less than 10Ω. This 10Ω value is adopted in most of the electricity companies in the UK.
- IEC 479 "Guide to effects of current on human beings and livestock" [1.7]. This standard consists of four parts. Parts one, two and three provide data regarding human body tolerable current for DC and low frequency currents. Part 4, which it is still in draft form, discusses the effect of lightning strokes on human beings and livestock, but still does not provide quantitative limits.

The IEEE standard also provides safe step and touch voltage thresholds applicable to people working within and around the substations. The thresholds are determined from tolerable current magnitude and duration, and using assumed values of the human body impedance.

The behaviour of earthing systems subject to surges has been examined for many years. Extensive experimental studies and threshold analysis have been carried out. However, despite this research, there are many aspects which remain unaddressed. Furthermore, quantitative guidelines have not been established for the design of large earthing systems under high frequency and transient conditions.

1.3 Lightning Parameter Data

To investigate the behaviour of earthing systems under surge conditions, it is important to have accurate data about the lightning current magnitudes and rise-time. Therefore, the definition of the impulse shape is described below as noted by previous investigations

Figure 1.1 illustrates the cumulative frequency distribution of lightning current amplitudes. The data was collected from lightning discharges (101 negative and 26 positive lightning strokes) to a tower on Mount San Salvatore, in Switzerland. For negative lightning strokes, the maximum recorded magnitude was about 90kA while the average value was 30kA. Current magnitudes higher than 90kA were observed and they were related to the positive strokes [1.8].

The lightning impulse is characterised by three parameters, the peak current magnitude, the time to peak current and time to half peak current which is the time required for the current impulse to decay to half of its peak value.

The standard lightning impulse shape is generally described by the peak current (or voltage) and by T_1 and T_2 written as T_1/T_2. Figure 1.2 presents a typical lightning impulse curve. The current rises from zero to its peak value I_p in a time of T_1 known as the rise-time, after that it decays to half its peak value $I_{p/2}$ at a time of T_2. For current impulses, the 8/20 shape is used in power systems applications.

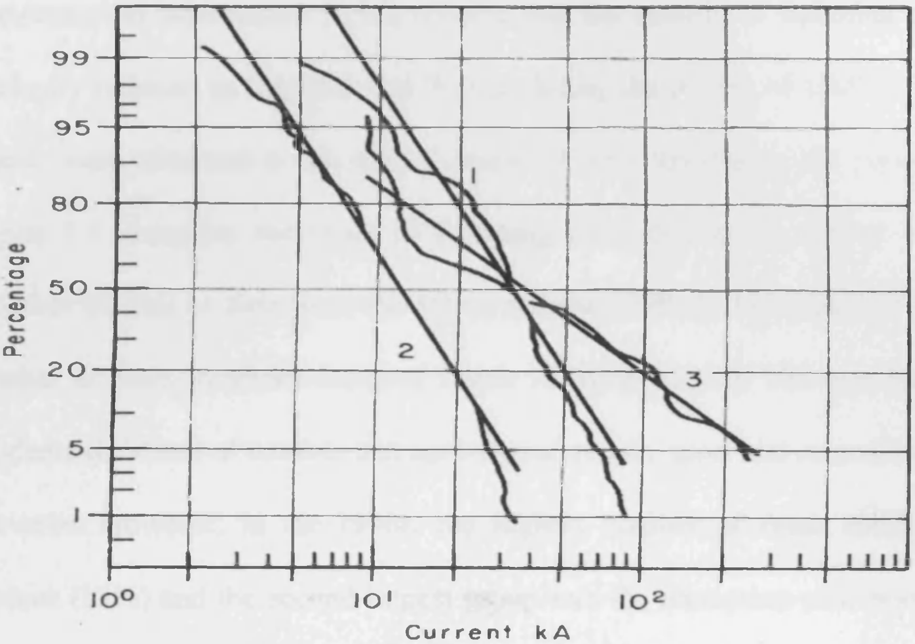

Figure 1.1 Cumulative frequency distributions of lightning current amplitudes

1: Negative first strokes, 2: Negative subsequent strokes, 3: Positive strokes.[1.8]

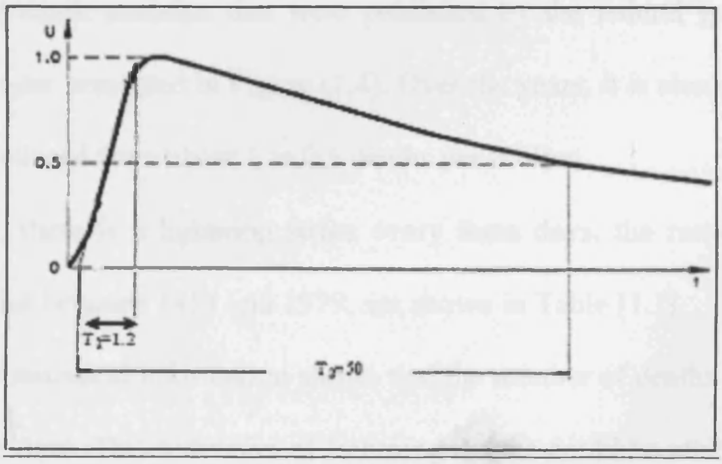

Figure 1.2 Standard Lightning Impulses [1.9]

1.4 Consequences of Insufficient Earthing under Lightning Conditions

1.4.1 Lightning Casualty

The statistical information [1.10] showed that the number of lightning casualties was markedly reduced in England and Wales, during the period of 1920 to 1976. Similar results were obtained in the United states of America during the period 1950-1974. Figure 1.3 compares the types of lightning casualties in the United States for two different periods of time from the 1890s and the 1990s [1.1]. In the 1890s, the highest number of death incidents occurred inside buildings (23%). The next largest group of incidents consisted of outdoor and agricultural events, sport and recreation incidents did not exist. However, in the 1990s, the highest number of death incidents happened outdoor (15%) and the second largest group was the recreation and sport events while the indoor and agriculture incidents were reduced to only 2% and 0.1 % respectively. These fatalities are caused by cardiac arrest, respiratory arrest and massive burns.

The changes of the number of deaths resulting from lightning were investigated over a period from 1900 to 1991 in the United States of America [1.11]. The data were taken from the annual death statistics that were published by the federal government since 1900. All results are presented in Figure (1.4). Over the years, it is clear that the number of deaths have reduced from about 6 to 0.5 deaths per million.

In Japan [1.12], there is a lightning strike every three days, the resulting number of deaths and injuries between 1954 and 1979, are shown in Table [1.1].

All the previous statistical information shows that the number of deaths due to lightning is reducing with time. This reduction of lightning deaths could be attributed to several reasons such as; immigration to urban areas, progressive development of rural areas. It could also be due to improved medical treatment, education, meteorological warnings, improved fire resistance and electrical systems of houses and very importantly the increasing use of earthing systems.

1.4.2. Equipment Damage and Financial Loss

Serious damage to power system equipment can result from an inadequate earthing system. The transformer is the most expensive item of equipment within electrical substations. The cost of transformers can range from a few hundred pounds for a small pole mounted transformer to millions of pounds for a large transmission transformer. A British electricity company reported 850 failed 11kV pole-mounted transformers in 1985, 53% of that failure was due to lightning[1.13]. Assuming the same failure rate throughout the country, this would result in over 2500 damaged transformers due to lightning in one year. Beside the transformers, surge arresters and insulators can also be damaged by flashover to earth. The total cost of lightning damage to the electricity distribution system in the UK was estimated to be approximately four million pounds per annum in 1997[1.14].

In the United States of America, the problem is much worse. Recent reports estimated the cost of lightning damage to be $100 million per annum[1.15]. In one case, a lightning strike to a communication tower caused the failure of a 66kV/12kV transformer and communication equipment. As a result, the communication services had to be routed through third party equipment at a cost of $100,000 per hour [1.16]. The costs mentioned above are just examples of the seriousness of the damage caused by lightning. However, more efficient lightning protection systems including the earthing system could provide significant and more cost effective benefits.

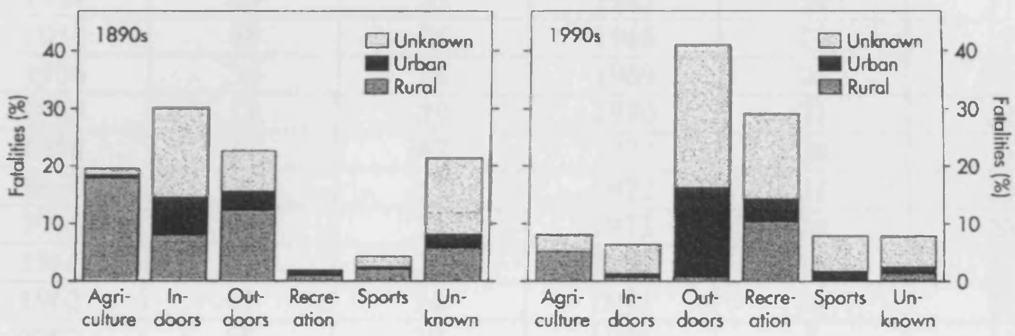

Figure 1.3 Types of U.S. Lightning Casualty Incidents (%) from 1891 to 1894 compared with 1991 to 1994. [1.1]

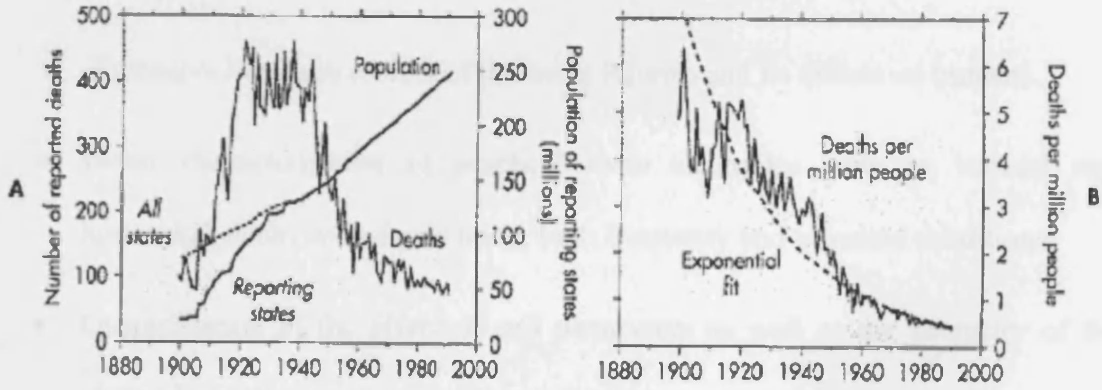

Figure 1.4 The yearly number of lightning deaths [1.1,1.13]

Table 1.1 Annual number of Lightning Accidents In Japan (reference 1.14)

Year	Death	Injury	Year	Death	Injury
1954	29	21	1967	50	57
1955	48	26	1968	22	19
1956	34	34	1969	24	25
1957	18	30	1970	21	22
1958	31	47	1971	20	35
1959	34	57	1972	21	23
1960	41	21	1973	24	20
1961	41	26	1974	16	28
1962	41	34	1975	30	43
1963	58	30	1976	6	11
1964	21	47	1977	6	8
1965	26	57	1978	16	22
1966	21	40	1979	17	19

1.5 Contribution of the thesis

The investigations carried out in this work have led to the following:

- Extensive literature review of lightning injuries and its effects on humans.
- Better characterisation of practical earth electrodes such as vertical rod, horizontal electrode and grid under high frequency and transient conditions.
- Quantification of the effect of soil parameters as well as the geometry of the electrode on the impedance of the earthing system.

- Clarification of the concept of effective length and effective area of earth electrode.
- Comprehensive analysis of the earthing system of substation under variable frequency and transient conditions.
- A new proposal for enhancing the performance of earthing systems.
- Characterisation of laboratory earth electrode systems under fast transient and clarification of the associated non-linear conduction phenomena including soil ionisation.

1.6 Content of Thesis

Chapter Two: Literature Review: An extensive review of the published studies: related to electrical and lightning injuries, is presented in this chapter. The factors that affect the severity of these injuries are determined. These studies were based on laboratory experiments and data collected from hospital reports and medical research that concentrated on the long term behaviour of the victims of electrical or lightning injuries.

Chapter three*: Characterisation of Earth Electrodes under Variable Frequency:* a comprehensive parametric analysis of earthing systems (vertical rod, horizontal electrode and earth grid) response to high frequency is conducted. The important parameters affecting the performance of earth grids are examined, such as soil resistivity and relative permittivity. The geometry of the earth electrode is also investigated.

Chapter four: Quantification of Existing and New Proposed Earth Grid Enhancement Techniques: to improve the performance of the earthing systems under high-frequency and transient conditions, existing recommendations and a new proposal for earthing systems arrangements are examined. These are based on existing guidelines provided by the relevant standards, and they include: increasing the overall or local mesh density of an earth grid, and adding vertical rods to the perimeter of the earth grid or locally close to the injection point. The new proposal suggests the use of above ground enhancement to reduce inductive effects and helps distribute injected current to remote parts of the grid.

Chapter Five: Transient Performance of Earthing Systems: the earthing systems (vertical rod, horizontal electrode and earth grid) performance under transient conditions is quantified. The effect of the earthing system dimensions and the various soil conditions on this transient performance is addressed. The transient performance under different impulses is compared in this chapter.

Chapter Six: The Performance of an Operational Substation Earthing System under High Frequency and Transient Conditions: the characterisation procedures investigated above are applied to the earthing system of an operational-substation. At the chosen substation, safety issues are investigated and transient step and touch voltages are calculated.

Chapter Seven: Laboratory Characterisation of Soil Ionisation under Fast Transients: laboratory experiments are designed to investigate the soil conduction processes including the soil ionisation phenomenon. The non-linear behaviour of soil is investigated under different soil conditions and electrode arrangements.

CHAPTER TWO

Lightning and Electrical Injuries: Review of Previous Work

2.1 Introduction

Lightning has always been looked at with awe and anxiety and, even in ancient times, people saw lightning as a powerful force that could not only destroy and kill people but also provide a source of fire before they had learned how to start a fire. It has always been a mysterious phenomenon, being depicted in ancient cultures and religions dating from the Akkadian time (2200 BC) up to the eighteenth century when this mystery was finally solved by Benjamin Franklin, the first person to prove that lightning was an electrical phenomenon. Subsequent investigations have concentrated on the mechanism of lightning and lightning protection.

Several reviews have been conducted by the Cardiff High Voltage Group on the performance of earthing systems under high frequency and transient conditions [2.1]. To add new dimensions and contributions to the group's knowledge, the effect of current on the human being is reviewed. This chapter presents a review of work investigating the effect of lightning parameters, the mechanism of the lightning strike and various other different factors concerning lightning injuries. The damage resulting from a lightning strike on a human being is described in detail. The injuries resulting from electrical current are also mentioned to show the different effects of lightning and electrical current on the organism.

2.2 Electrical Injuries

2.2.1 Mechanism of Electrical Injuries

The IEEE 80 standard [2.1] and IEC 479 [2.3], describe the mechanism of electrical accidents in substations and the different accidental scenarios that may apply to the victim. Figure (2.1) shows how the different voltages may affect a person working in a substation or even walking somewhere near a substation. These voltages are defined as follows[2.2, 2.3]:

"Ground potential rise (GPR): the maximum electrical potential that a substation grounding grid may attain relative to a distant grounding point assumed to be at the potential of remote earth.

Mesh voltage: the maximum touch voltage within a mesh of ground grid.

Metal-to-metal touch voltage: the difference in potential between metallic objects or structures within the substation site that may be bridged by direct hand-to-hand or hand-to-feet contact.

Step voltage: the difference in surface potential experienced by a person bridging distance of 1m with the feet without contacting any other grounding object.

Touch voltage: the potential difference between a ground potential rise and the surface potential at the point where a person is standing while at the same time having a hand in contact with a ground structure.

Transferred voltage: is a special case of touch voltage where a voltage is transferred into or out of the substation from or to a remote point external to the substation site."

2.2.2 Pathophysiology of Electrical Injuries

Dalziel, in 1941 [2.4], conducted an experiment where electrical shocks of different frequencies and different magnitudes were applied on 120 men over different periods

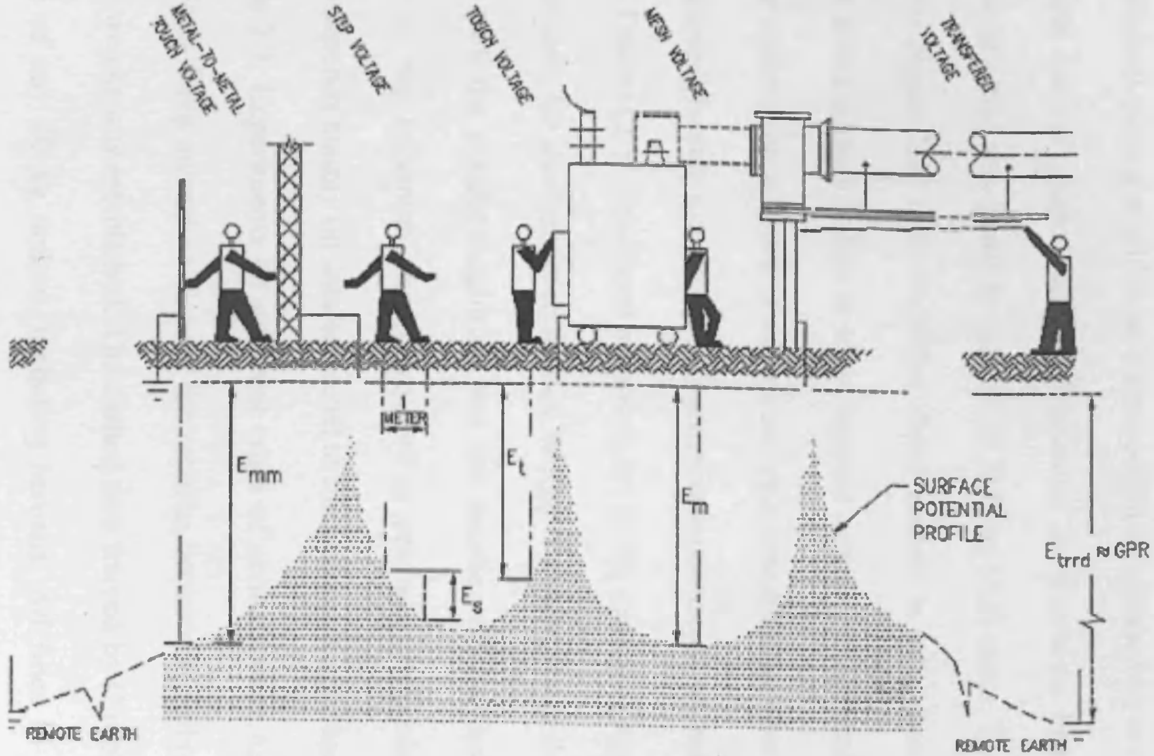

Figure 2.1 Basic electrical shock situation in a work place reported by IEEE [2.2]

of time. Most of the men were between 21 and 25 years old and about 15 of them aged between 26 and 46 years. He identified the let-go threshold as;

"...the highest current at which an electrode can be released by muscular control..."

The let-go current plotted against frequency is shown in Figure 2.2. The body resistance at 60Hz was found to vary from 1570 to 4430 ohms. Direct current data are plotted on Figure 2.2. It is clear that direct current is safer than alternating current although direct current results in some internal heating of the hands and the arms, the muscular contraction is much smaller than that generated by alternating current. It is very interesting to note that the let-go current is minimum at around 60Hz.

In 1953, Dalziel [2.5] introduced a new aspect to the electrical injuries research when concluded that, for short-duration shocks, energy is a main factor that affects the injury together with the current magnitude and the duration of the shock. He proposed a criterion for the minimum energy required to produce ventricular fibrillation. This criterion depends mainly on data collected at the Colombia University and reproduced in Figure 2.3. Experiments on different types of animals were used to produce this figure. For a 70kg animal or human, the relation between the fibrillation current and the body weight was established. The dashed area framed by C represents the possible response of any 70 kg animal, including humans. All lines in Figure 2.3 can be represented by the following equation: $I^2 \times t = k^2$ (2.1)

Where t is the shock duration in seconds
I is the current in r.m.s milliamperes
k is the energy constant

The threshold of danger for a 70 kg man is based on half of 1% of a large group of people who would suffer from ventricular fibrillation if subjected to an electrical shock. Using the values of I and t represented in curve C, the energy constant was found to be 0.027, giving a probable energy safety criterion of:

$$I^2 \times t = 0.027 \qquad (2.2)$$

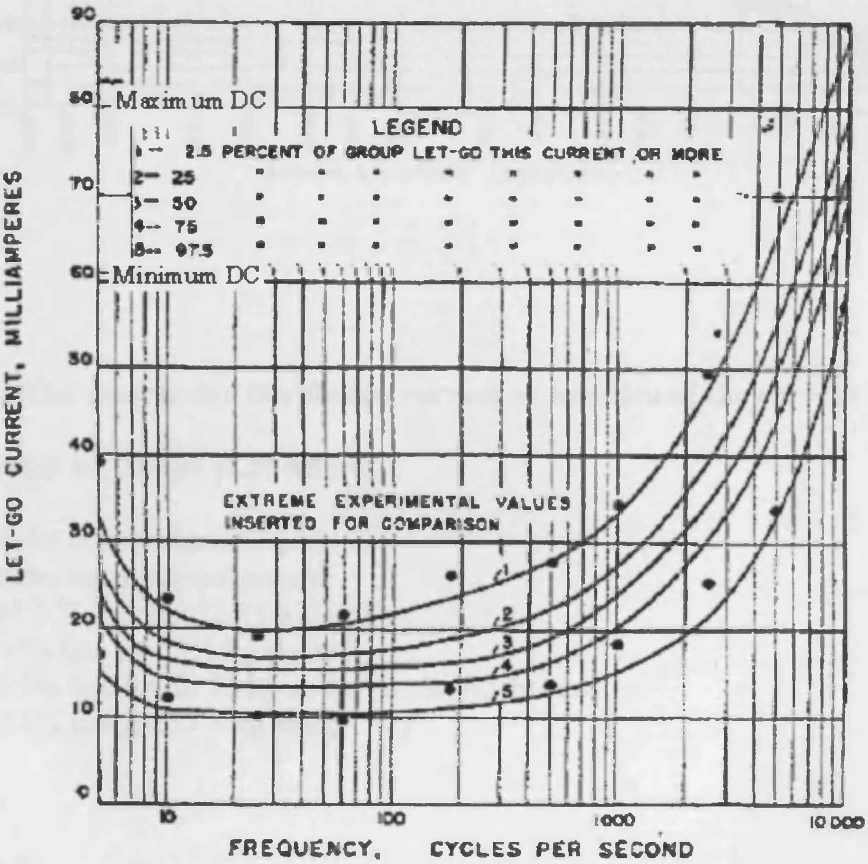

Figure 2.2 Let-go current against frequency [2.4]

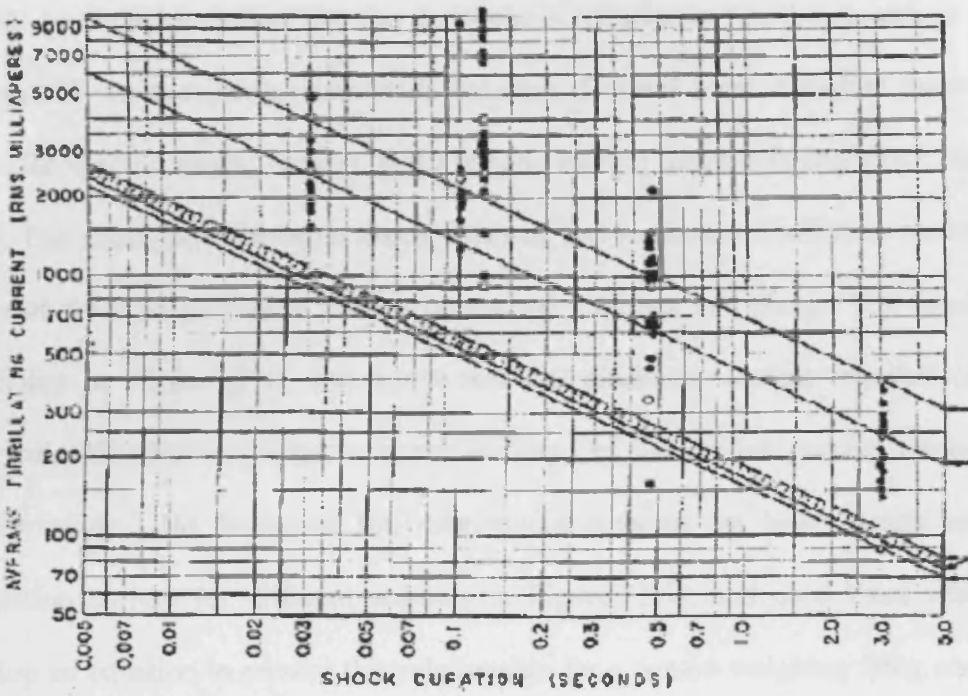

Figure 2.3 The ventricular fibrillation current as function of the current duration as suggested by Dalziel [2.5] where;

•	Refer to experimental points.
o	Refer to calculated points.
A	99.5 % line for 57.4 kg sheep
B	50% line for 57.4 kg sheep
C	0.5% line for all 70 kg animal including human
D	0.5% line for 57.4 kg sheep

Dalziel continued to investigate the threshold of ventricular fibrillation and, in 1968, he was able to establish a relationship between the three most important factors that affect the electric shock; namely, body weight, current magnitude and shock duration [2.6]. The relationship between shock duration and minimum fibrillation current was obtained from experimental studies conducted on dogs and sheep. The results are illustrated in Figure (2.4), and show that the minimum current required causing ventricular fibrillation decreases as the duration of the current passing through the body increases. He illustrated the relationship between the body weight and the fibrillation current for different animals in Figure (2.5), and used these results to develop an equation to present this relationship for a person weighing 50kg and for a current duration more than 8.3ms and less than five seconds.

$$I = \frac{116}{\sqrt{t}} \quad \text{to} \quad I = \frac{185}{\sqrt{t}} \quad \text{(mA.)} \qquad (2.3)$$

For longer shock durations, 5 to 30 seconds, the minimum fibrillation current drops only slightly. For longer durations, the asphyxial changes may increasingly apply their influence and reduce the threshold level even more. In a subsequent study [2.7], the time limits were extended to 60 seconds and it was found that the threshold current does not change greatly after 5 seconds.

Kitagwa et al [2.8, 2.9] determined that the minimum energy required to cause death is about 40 J/kg. Golde and Lee [2.10] also believed that the injury which may result from electrical shock depends on two important factors; the current magnitude and duration. They also reported that direct current shock is less dangerous compared with

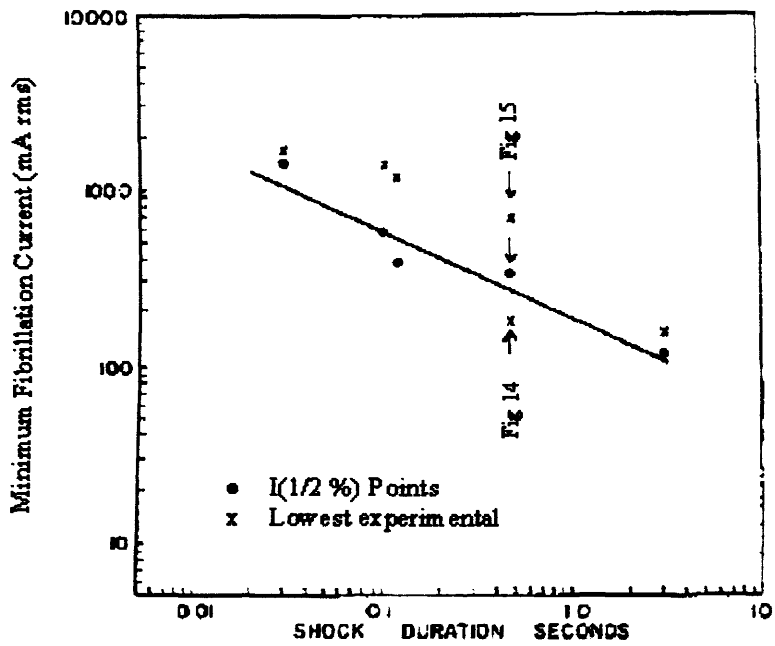

(a) Sheep

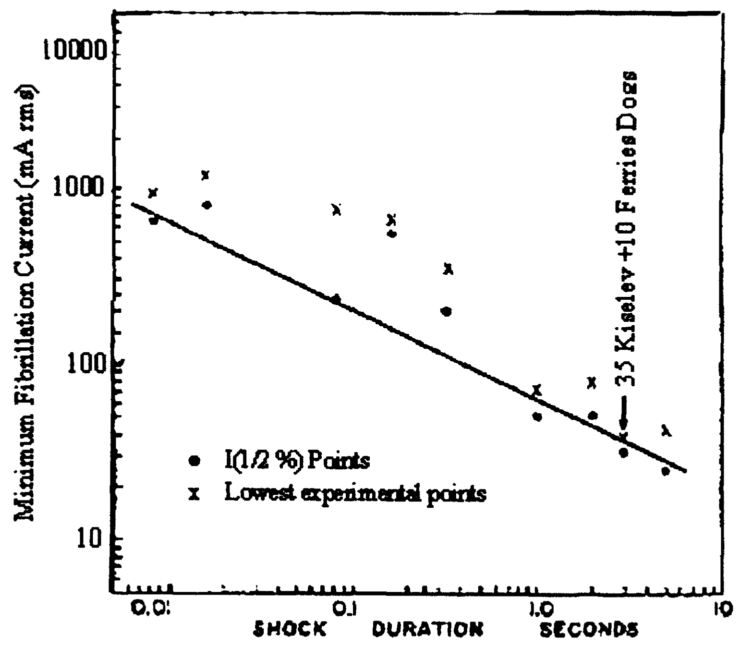

(b) Dogs

(c) Figure 2.4 The fibrillation current as a function of duration time for dogs and sheep [2.6]

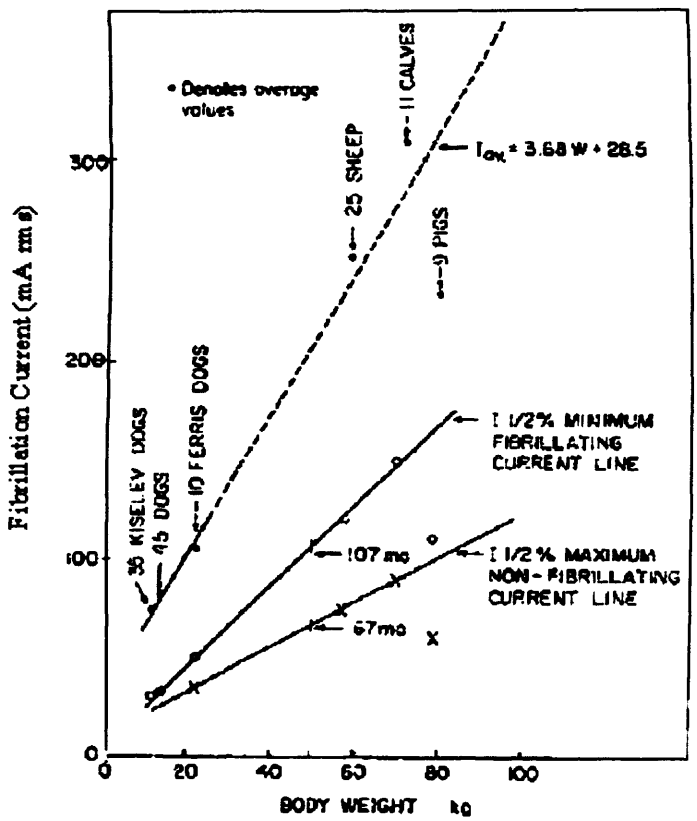

Figure 2.5 The fibrillation current as function of body weight for different animals [2.6]

the alternating one for the same voltage. To have the same effect, the DC level has to be greater than the AC level by a ratio of 5:1. Golde and Lee [2.10] also questioned the work of previous authors (Osypka [2.11]) who adopted a different approach to understanding hazard of electric shock. Osypka [2.11] suggested that the hazard resulting from an electric shock is determined by the total charge (I x t). Golde and

Lee thought that Osypka's conclusion must be treated with caution for different reasons: Firstly, he concentrated his work on increasing the total charge and omitted the effect of current duration, secondly, his case study was only based on a small number of victims (6) where ventricular fibrillation occurred.

It is possible for respiratory arrest to occur as a result of an electric shock. This effect may occur only if the current passes through the respiratory centre. Golde and Lee also reported the work of Andreuzzi who simulated the electric shock on a rabbit by passing a 50Hz current from the head to the back of the neck; the results are shown in Table 2.1

Cooper et al [2.12, 2.13] investigated high voltage injuries and concluded that there are various factors that affect the severity of these injuries;

i. Circuit type: the direct current causes a single muscle spasm and is most likely to throw the victim away from the source resulting in a traumatic, blunt injury. While an alternating current is about three times more dangerous than a direct current of the same magnitude and it produces an incessant muscle contraction or tetany occurs after the muscles are fibred for 40 to 110 times per second. Hands are most likely to be the entrance point of the current as they are the grasp tool. The person should be able to release the current source as long as the current is less than the let-go threshold (6 to 9mA).

ii. Resistance: The nerves, muscles, mucous membranes and blood are good conductors of electrical current because of their water content. The tendon, fat and bone have a very high resistance. All other parts of the body have an intermediate resistance. The skin is a main resistor to the current flowing through the body. However, the sweat could reduce the skin's resistance to a value of between 2500 and 3000Ω while immersion in water can result in a further reduction of 1200 to 1500Ω, which would allow more energy to flow through the body and cause an electrocution with cardiac arrest and surface burns.

iii. Duration: Generally, the longer the duration of contact with sources, the larger the damage will be. The body response to different current magnitude passing through the body is shown in the Table 2.2.

iv. Voltage: Electrical injuries could be divided into low and high voltage. The common division between both levels is considered to be 500V or 1000V as both low and high voltage can result in a significant morbidity and mortality. However, high voltage is most likely to cause tissue damage resulting in severe injuries leading to major amputations.

v. Pathway: the path that a current takes is very important to determine the tissues at risk and the type of injury caused. For example, current passing through the heart will cause cardiac arrhythmias and direct myocardial damage, while current passing through the brain will result in respiratory arrest, seizures, paralysis and brain damage. As the current density increases, the current starts flowing through the tissues randomly, treating the body as a conductor volume.

Table 2.1 The effect of current magnitude and duration on the respiratory centre [2.10]

Current (mA)	Duration	Respiratory arrest (%)
200-300	6 cases for 5 s 9 cases for 10s	100 (15 out of 15)
350-450	5 cases for 5 s 5 cases for 10 s 5 cases for 15 s	53 (8 out of 15)
500-600	4 cases for 5 s 4 cases for 10s 4cases for 20s 4cases for 25s 9cases for 30s	32 (8 out of 25)

Table 2.2 The body response for different current magnitude[2.13]

The body response	mA
Tingling sensation from household current	1-2
Let-go current Man Woman Child	 7-9 6-8 3-5
Tetany (freezing to circuit)	10-20
Respiratory arrest from thoracic muscle tetany	20-50
Ventricular fibrillation	50-100

2.2.3. Injuries resulting from Electrical Shock

In 1984, M. Daniel et al [2.14] investigated the neuropsychological and emotional problem, resulting from an electrical shock on eleven patients (ten male and one female), aged between 23 to 51 years, none of the patient had a history of psychiatric treatment, and there was no information available regarding the current applied to the patients but the voltage ranged from 220 to 8000 volts.

Present complaints: 91% of the patients had memory dysfunction, and 91 % had emotional difficulties such as anxiety, increased irritability and depression. 64% had pain as a lasting problem while 55% of patients had general weakness and lack of coordination. Dizziness, concentration problems and confusion were reported in 36% of the patients while 27% of these eleven patients suffered from insomnia, para- and dysesthesias, fatigue and dysphasia.

Neuropsychological problem: the patients were subjected to an individual neuropsychological test. It was found that the neuropsychological behaviour of these patients could be determined by different factors such as age, time elapsed since the injury, length of unconsciousness after the shock, the shock parameters, the current path through the body, additional injuries resulting from falling or being thrown away and cardiac and respiratory complications.

A statistical analysis of the relationship between all these factors and the patients' behaviour could not be achieved due to the small number of patients used in this investigation.

In 1989, Hooshmand, Radfar and Beckner [2.15] conducted their research into Neuro-physiological aspects of electrical injuries. This research was based on observations of sixteen patients of electrical current injuries and the patients were observed for between five and nine years after the accident. The group consisted of thirteen males and three females, ranging in age from 21 to 47 years. Eleven of them were married. These patients had been exposed to an electrical current in the work environment or even at home, however, the voltage they were exposed to varied from 120 volts up to 500,000 volts. The authors classified the clinical complications into early and late forms. Early complications of all the patients were dangerous enough to keep the patients a few days in hospital, they included loss of consciousness and pain in the extremities. The late complications, generally, are neurological and psychological. Within 3 months to a year, all patients developed a disturbance in their life concerning recent memory, concentration, judgments and verbal and non-verbal achievements. Around 88% of patients suffered a demanding depression which disabled them from having a normal personal or professional life. After 5 years, eleven out of thirteen employed patients lost their jobs and nine of the eleven married patients were divorced. 75% of the patients had one or more attacks of seizure, however, only two of them (17%) continued to have the attacks after 9 years of observation. Dizziness was present in ten patients, six of them continued to suffer with it even after five years.

They noticed that patients with current passing from one hand to another developed post-traumatic depression, atonic seizures, and spinal cord injury. While amongst the patients with a hand to feet current path the neurologic problems were not that extreme. All patients suffered from extreme anxiety and depression, they also had poor recent memory, poor judgments and concentration problems.

In 1993 Grossman et al [2.16] observed that it is always hard to decide if the long-term symptoms of electrical shock resulted from post traumatic stress disorder (PTSD) or a neurobehavioral disorder (PNBD). The authors studied a group of patients who had an electric shock strong enough to cause a symptom but not so severe as to result in obvious brain damage. The study was conducted over six years and included 101 patients who were divided into two groups. The first group consisted of forty eight patients who had an electric-current injury where the current had actually flown through the body, while the second group included the remaining fifty three patients who had received a flash, contact or arc burns without actual current entry. All patients were checked for auditory and neurologic damage. Consequently, 34 patients received psychiatric treatment, (16 from the first group and 18 from the second group) over a period varying from a few months up to two years. Unfortunately, the remaining 67 suffered gross damage to the head and central nervous system making them poor candidates for applying the techniques used in the study.

The results showed that twelve of the 16 patients of the first group met the criteria of PNBD. This included short-term memory problems, difficulties in carrying out tasks and everything seemed to take longer to achieve, difficulty in socialising with people due to obvious patient issues, but an inability on the part of the observer to ascertain the exact nature of the complaint. One patient did meet the criteria of the PTSD. For example, flashback, disturbing imagery and nightmares. Out of 18 patients in group two, only 4 met the criteria of the PTSD after one year and none of them met the criteria of PNBD. Eight patients in group one and none in group two demonstrated auditory changes, hearing loss was always neurosensory. There was no evidence of conduction loss or ruptured tympanic membrane. Peripheral nerve damage was reported in nine patients where current had passed through and in four of them the damage was permanent. There were two other patients who sustained permanent peripheral nerve damage without the current passing through their bodies.

In September 1995, Cooper [2.12] summarised a set of electrical physical and psychological injuries. She found that electrical injuries could occur in different ways such as direct contact, arc contact, side flash, thermal and blunt trauma. The worst indirect injury occurs when a person is in series with an electrical arc. The high temperature of the arc (about 2500 degrees Celsius) could cause cloth to ignite and result in secondary thermal burns. The burns are, generally, on the surface and will rarely be deep burns. A blunt injury may occur when a person is thrown away from the electric source, it may also result from falling from a height.

High voltage electrical injuries are disturbing, with massive burns, muscle damage (necrosis), amputations and vascular and neural tissue damage. Cervical spine injury or even spine and long bones fractures are possible and have been reported. Approximately 6% of high-voltage electrical victims develop cataracts and all these injuries lead to long and complicated hospitalizations. A brain injury is possible as the skull is a very common contact point. However, death from electric shock is possible and may result from asystole, ventricular fibrillation, or a respiratory paralysis, depending on the voltage and the current path. Most high-voltage electrical injury victims suffer from loss of consciousness, a long coma with recovery in some cases, confusion, and short term memory difficulties. They may suffer a concentration problem. Seizure may develop after the electrical shock. The author summarized the main complication of electrical injuries in the same order of occurrence as; cardiopulmonary arrest, overwhelming injuries, cardiac arrhythmias, hypoxia and intracranial injury, myoglobinuric renal failure, abdominal injuries, sepsis, tetanus, and finally suicide.

2.3 Lightning Injuries

2.3.1 Mechanism of lightning injuries

Golde and Lee 1976 [2.10] investigated the mechanism of lightning and they concluded that lightning has four different strike patterns and ways to injure somebody, these are;

i. Direct stroke: in this case the person has to be outdoors and has failed to find a safe location.

ii. Side flash: this takes place when lightning hits an object and splashes onto a person who is close to that object, a splash could happen indoors as well as outdoors.

iii. Contact voltage: this happens to a person who is touching an object such as a tree which is either hit directly, or splashed by a lightning strike.

iv. Step voltage: occurs when lightning hits the ground and a person is walking nearby, where one foot is close to the strike and the other is further away. The voltage difference between both feet produces a current flow through the person's body. This case is least likely to result in fatality. It was stated [2.17] that step voltage could be calculated using equations found in his earlier work;

$$u = i \times \frac{\rho}{2\pi} \times \frac{s}{d(s+d)}$$

Where d is the distance between the place hit by the strike and the front foot (m)
s is the distance between both feet (m)
ρ soil resistivity (Ωm)
I is the lightning current amplitude (A)

Mary Ann Cooper, 1995, [2.12] classified two additional mechanisms of lightning injuries, the first one is orifice entry which occurs when lightning strikes a victim near the head and the current may enter through the eyes, nose or ear to flow internally.

The second one is blunt injury which may take place when the victim is thrown away by the impulsive force resulting from the immediately heated and rapidly cooled lightning current pathway.

Later in 1997, Copper and Andrews [2.18] specified that lightning injuries may happen as a result of direct strike, splash, contact, step voltage or blunt trauma. In a subsequent work 2001, Cooper et al [2.13] divided lightning injuries into direct and indirect categories. Direct lightning injuries could be the result of three different factors; electrical effect, heat production and excessive force, it may happen in different ways; direct, splash, touch and step voltage. Lightning may also cause some indirect injuries resulting from forest or house fire and objects falling on an occupied building.

Gatewood and Zane [2.19] and Gourbiere 2004 [2.20] appear to agree with Cooper's [2.18] view of lightning injury mechanisms.

Cooray et al [2.21] has not only confirmed the main four mechanism of lightning injuries, (direct strike, side flash, contact voltage and step voltage), he also added three more important mechanisms of the lightning injuries,

i. Subsequent strokes: Generally, lightning consists of more than one stroke. If one stroke hit an object close to a person and then a subsequent stroke hits the person directly, this person will be subjected to a step voltage from the first strike and a direct strike from the second hit.

ii. Connecting leader: This mechanism has been identified recently. During a lightning strike, as the stepped leader reaches a few hundred metres from the ground, several uprising streamers may start from a high object on the ground, trying to make the connection with the down-coming leader. Only one of these uprising streamers will make the connection. If this streamer started from the head of a person, the discharge current could be as high as few hundred Amperes, and it may last for up to several tens of microseconds. This is a very dangerous condition.

iii. Stroke wave: The temperature of the lightning channel increases rapidly to reach 25,000 K in a few microseconds. This results in a pressure increase in the channel causing a rapid expansion of the air, creating a shock wave. This shock wave may cause injury to a person present in the vicinity of the lightning channel.

2.3.2 The Body Model

In Japan in 1982, Ishikawa [2.22] conducted an artificial lightning experiment; a maximum negative voltage impulse of 1300kV was applied, on dummies with a height of 170 cm and a resistance of between 300–500Ω. The discharge current was first observed in the form of a flashover surrounding the body. As a result, the charging voltage decreased to approximately 50kV and the current passing through the dummy was about 167A. The potential gradient which triggered the flash-over was 2.7 kV/cm. The lightning current ran mostly outside the body and the current passing through the body was about 10% of the total current. It was confirmed that metal pieces attached to the body had an effect on attracting a lightning strike although this did not occur in all cases.

Another discharge experiment on a rabbit showed that in the case of discharge to the head, the fatal threshold is determined by the energy dissipated throughout the body not the flash-over current.

Later in 1986, Ishikawa et al. [2.23] observed that when external flashover takes place along the victim's body, the possibility of survival is relatively high (56%). However, the possibility of survival is only 15% when no external flash-over occurs. Experiments on rats proved that the external flashover reduces the current within the body, hence, the energy dissipation through the body.

A mathematical model for the human body was developed by Andrews [2.24-2.27] and is shown in Figure 2.6. The impedance of the human body was divided into two parts: firstly, the internal part including the arms, torso and the legs and this is purely resistive. Secondly, the skin impedance consisting of a high value resistance in parallel with a capacitance. The skin is assumed to break down at 5kV across its impedance, while the body surface is assumed to break down at a gradient of about 2.7kV/cm.

Using this mathematical model, a direct strike on a human being was studied considering two different cases - first a direct strike without external flashover. An impulse of 5kA, 8/20 was applied directly to the top of the head. Figures 2.7 shows the electrical test circuit and Figures 2.8 shows the analytical results. It is clear that internal current and voltage increase exponentially. At 1.1 and 1.7μs, the skin elements break down, which has a minor effect on the internal current, this increases to reach its maximum value of 5kA. The subsequent current will mainly decrease. Secondly, a direct strike with an external flashover occurs, Figure 2.7 also presents the equivalent circuit in this case as well and the analytical results are displayed in Figure 2.9. The voltage between the victim's head and the ground (G4 in Figure 2.7) rises exponentially and it reaches a maximum value of 500kV, where an external flashover takes place at 340ns. At this point, the body current has increased to approximately 800A. When the flashover takes place, both current and voltage drop dramatically to zero. Most of the current has been transmitted externally. In this case, the skin voltage will not increase to 5kV and skin breakdown will not take place.

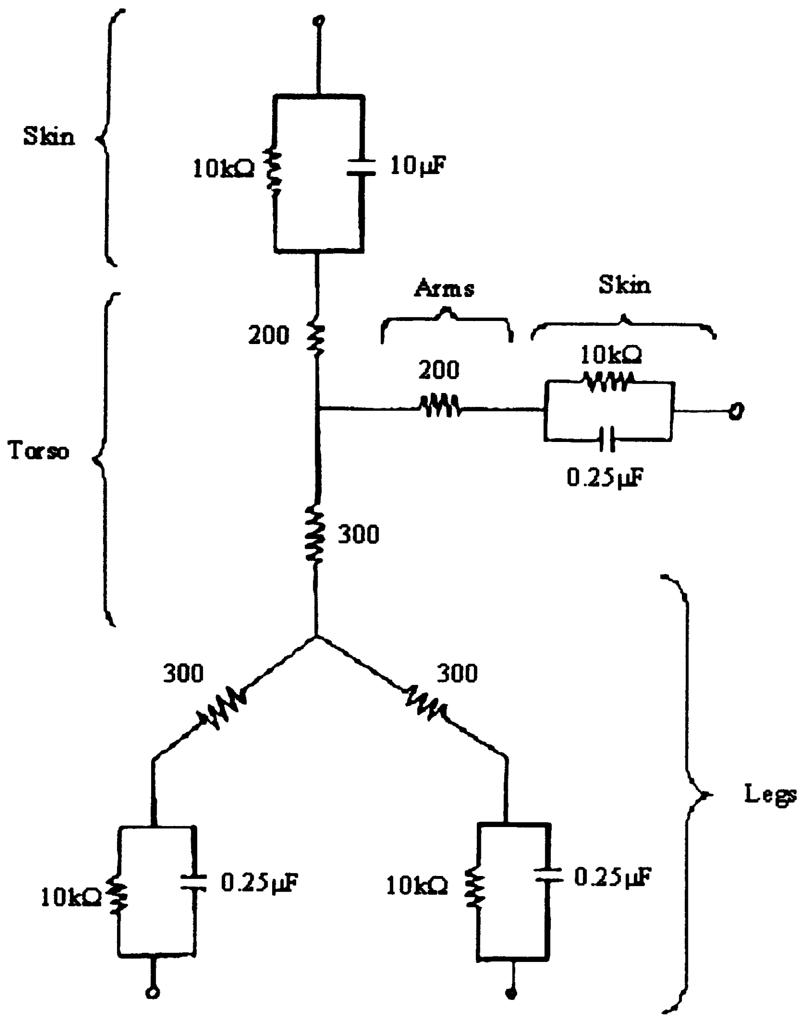

Figure 2.6 The body model [2.24-2.27]

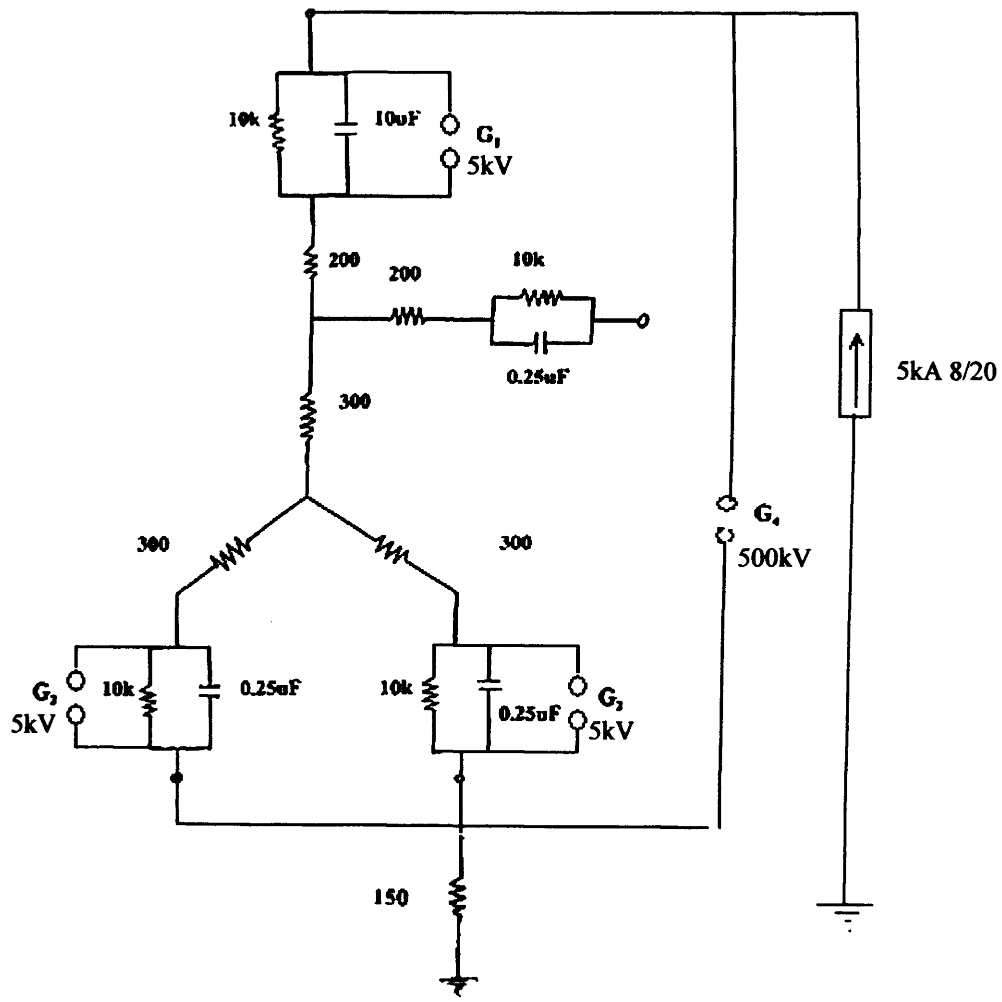

Figure 2.7 The equivalent circuit of direct strike [2.24-2.27]

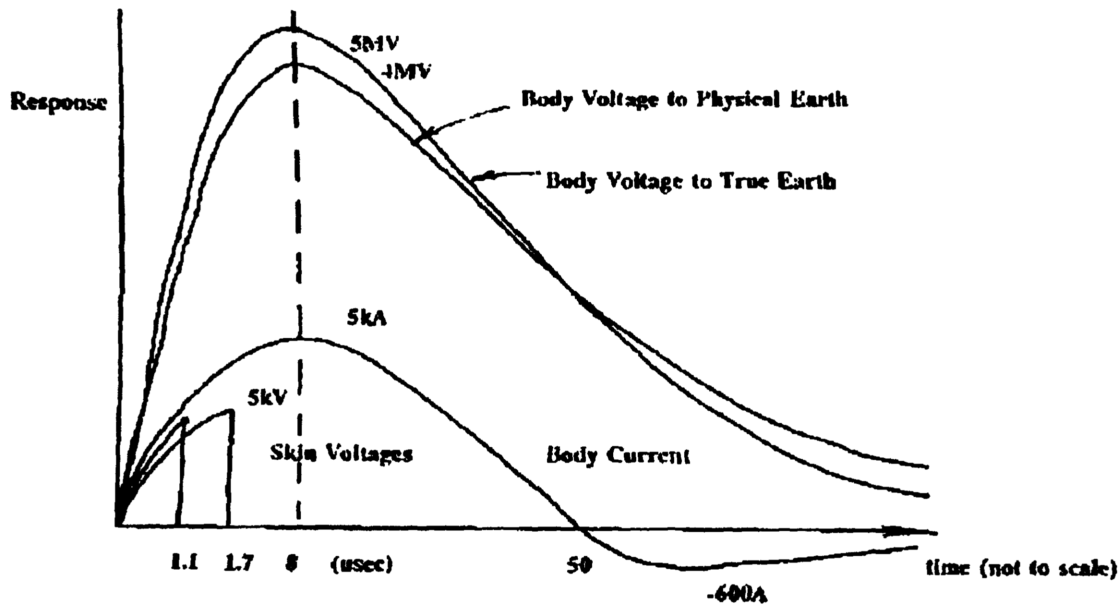

Figure 2.8 Voltage and current through the body without external flshover

[2.24-2.27]

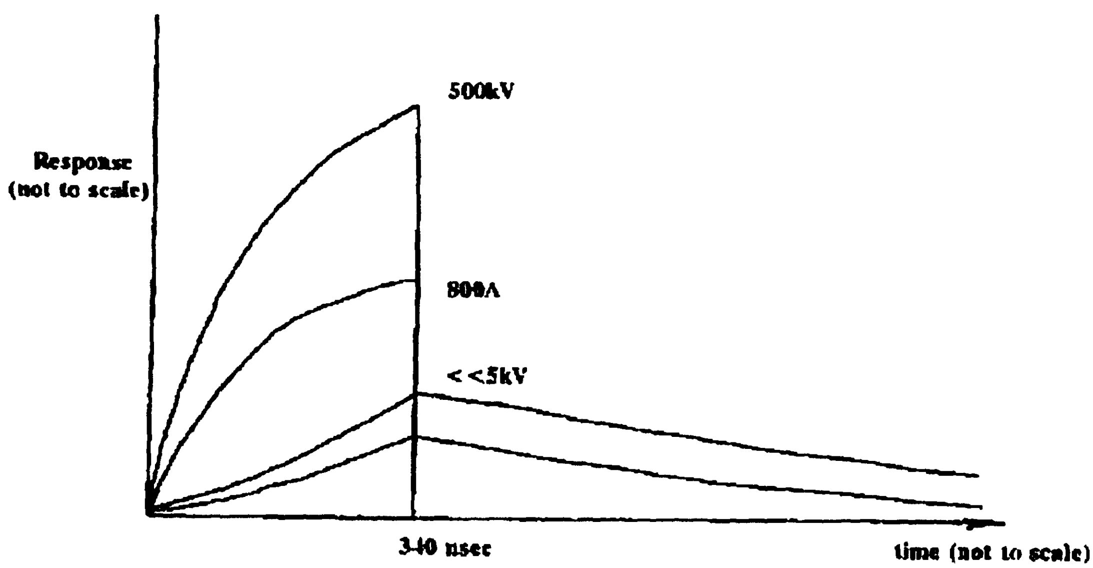

Figure 2.9 Voltage and current through the body with external flashover

[2.24-2.27]

2.3.3 *Pathophysiology of lightning injuries*

There are four factors that determine the type and severity of lightning injuries, these factors are

- Frequency and type of circuit: lightning is neither a direct, nor an alternating current. It is a massive current impulse that has a very short duration and that is why the lightning effect on the human body is not fully understood [2.13, 2.18, 2.19]
- Energy absorbed during lightning: as the voltage difference between the cloud and the ground disappears at the moment of lightning connection, it is not easy to apply Ohm low or even to calculate the power (P). Therefore it is necessary to find an alternative formulation of these equations. This is the energy dissipated in the body which is determined in the following equation:

$$\text{Energy(heat)} = \text{Current}^2 \times \text{Resistance} \times \text{Time}$$

  When low electrical energy is encountered by a human body, most of this energy will be dissipated by the skin, causing superficial burns which are typically not accompanied by internal injuries [2.13, 2.18, 2.19].
- Pathway, duration of current and flashover effect: in 1982, experiments conducted on dummies by Ishikawa [2.22] resulted in an estimation that about 10% of the total current passes through the body. Later in 1997, a mathematical model was introduced by Andrews [2.13, 2.18], yet, an accurate quantitative study of how much current passes through or over the body was not available. Cooper et al [2.13] added, the degree of harm is variable, and it depends on the

pathway of the breakdown and the current density in this path. The worst-case scenario is when the current is led directly to the heart through the vessels and probably conducted through the veins. In this case, the cross-sectional area is about $7cm^2$ and the current density is extremely high.

- Effect of current flow in tissues: any electric current which passes through the tissues will result in a heating of the tissues under Joule's law. The cell wall safety, enzyme reaction, protein shape and structure, the cell membrane gate and pumps operate by changes in the order of microvolt. Therefore, the current passing through the tissues may cause significant thermal damage and permanent changes in the cell functions, leading to the cell death or dysfunction [2.13, 2.18].

Cooper et al. [2.13] also investigated one more factor that affects the severity of lightning injuries which is the magnetic field effect. They proved that the danger resulting from the magnetic field effect is very small in normal circumstances, but it may exist in certain, special conditions such as when a pacemaker is used.

2.4 Comparing Electrical and Lightning Injuries

Margaret et al. [2.28], compared the frequencies of the most common after shock effects reported by lightning and electrical injury survivors, the results are summarised in the following table:

Table 2.3 Comparison of lightning and electrical injuries [2.28]

Symptom	Electrical injury sample (%)	Lightning Injury Sample (%)
Neurobehavioral		
Sleep disturbance	74	44
Memory deficit	71	52
Attention deficit	68	41
Headaches	65	30
Irritability	60	34
Inability to cope	60	29
Reduced libido	55	26
Unable to work	54	29
Chronic fatigue	48	32
Dizziness	48	38
Easily fatigued	48	38
Communication problem	46	25
Incoordination	40	28
Confusion	38	25
Chronic pain	29	21
Weakness	25	29
Symptom	Electrical injury sample (%)	Lightning Injury Sample (%)
Neurologic		
History of coma / loss of consciousness	9	15
History of convulsions	11	7
Seizure disorder	12	12
Aphasia	8	6
Paralysis	8	11
Inability to walk	11	11
Ataxia	3	5
Deafness	12	13
Dry eyes	23	9
Cardiovascular		
Heart problem	14	12
History of heart attack	6	10
Irregular electrocardiogram	3	3
Elevated heart rate	6	6
Drop in heart rate	3	4
Hypertension	5	6

Table 2.3 Comparison of Lightning and electrical injuries [2.28] (Continued)

Sensory		
Numbness	63	36
Paresthesias	60	40
Tinnitus	48	33
Photophobia	46	34
Hearing loss	31	25
Visual acuity reduced	25	20
Emotional		
Depression	63	32
Flashbacks	51	20
Agoraphobia	46	29
Emotional problems	38	24
Personality changes	29	19
Storm phobia	7	29
Nightmares	26	12
Others		
Muscle spasm	63	34
External burns	54	32
Decreased grip strength	51	34
Stiff joints	48	35
Back problems	46	25
Inability to sit long	45	32
Arthritis	38	19
Hyperhidrosis	31	25
Internal burn	28	21
Bowel Problems	25	23
Others		
Amputation	6	2
Pinched nerves	18	17
Bladder problems	18	17
Kidney problems	11	10
Skin problems	18	12
Random fears	17	11
Suicidal thoughts	11	6
Out of body experience	18	5
No known after effects	0	4

2.3 Conclusions

A literature review of electrical and lightning injuries has been conducted. It was found that most investigators have attempted to determine the factors that affect the severity of an electrical injury or a lightning injury. The investigations involved applying low or high voltage electrical shock to laboratory animals, or even trying to represent a lightning strike using fast transient currents applied to dummies. Most of the data were collected from hospital reports and medical research, this concentrated on the long term behaviour of the victims of electrical or lightning injuries.

The electrical injury depends on the energy dissipated inside the body, the body weight of the individual, the current magnitude and the shock duration. The type of current is a very important factor, as it was found that direct current is safer than alternating current.

The severity of lightning injury depends on frequency, voltage, current magnitude and duration, pathway, and the behaviour of the tissue. A body model was introduced to represent the body in the case of a lightning strike. Two different cases were assumed; firstly, when an external flashover occurs; in this case the current passing through the body is 10 % of the total current, and secondly, no external flashover was observed; in this case most of the current passes through the body and is extremely dangerous. It was found that the possibility of survival is 56% if external flashover takes place, this reduces to 15% if no external flashover occurs.

Victims may survive a lightning strike, though they could suffer from injuries that may be immediate or long term injuries. In both cases, the injuries could be neurological, physical or psychological.

CHAPTER THREE

Characterisation of Earth Electrodes under Variable Frequency

3.1 Introduction

Earthing systems are required to provide a complete protection from high-magnitude fault currents, switching operations and fast-front surge currents caused by lightning strikes. The earthing systems response to these conditions is very different from that for the power frequency and, therefore, the earthing system design and dimensions are far more complicated.

The earthing system behaviour at power frequencies is fairly well understood [3.1], but its performance under a high-magnitude, fast impulse current is more complex, and most of the previous work [3.2-3.10] on this subject has concentrated on simple grounding arrangements such as vertical rods or horizontal electrodes. Few researchers [3.11-3.18] have studied the performance of earth grids under high frequency and transient conditions, investigating the factors that affect the performance of earth grids in an attempt to improve that performance. Detailed guidelines are provided in the earthing standards [3.19, 3.20], for the design of substation earthing grids under power frequency conditions. However, for surge conditions, only brief and qualitative recommendations are given.

In this chapter, a comprehensive parametric study of the earthing systems response to high frequency is conducted. The effects of soil resistivity and soil permittivity on the performance of earthing systems (simple electrode, earthing grid) are investigated, the effect of electrode length, grid size and different injection points are also investigated.

A range of soil conditions is examined by varying both the soil resistivity and permittivity over a frequency range from DC to 10 MHz.

3.2 Earthing Systems Arrangements and Models

To study the different types of earthing systems 'found in practice' three simple earth electrode arrangements are adopted for this study. Figure 3.1 shows the electrode arrangements adopted, and these are:

(a) *5m vertical earth rod*

The rod is assumed to be made of copper with a radius of 1cm. The rod is buried at 1 m below the earth surface.

(b) *100m horizontal earth electrode*

The copper horizontal electrode is buried at 1m below the soil surface and assumed to have a 1cm radius.

(c) *100m x 100m earth grid*

The horizontal copper grid has overall dimensions of 100m x 100m and the number of meshes is varied between 4 and 100. The grid is buried at a depth of 1m below the surface of the soil. The conductors forming the grid are assumed to have a radius of 1cm.

Each of the above earth electrodes are simulated for different earth conditions with a soil resistivity of (10 to 10,000Ωm) and a relative soil permittivity of (1 to 50).

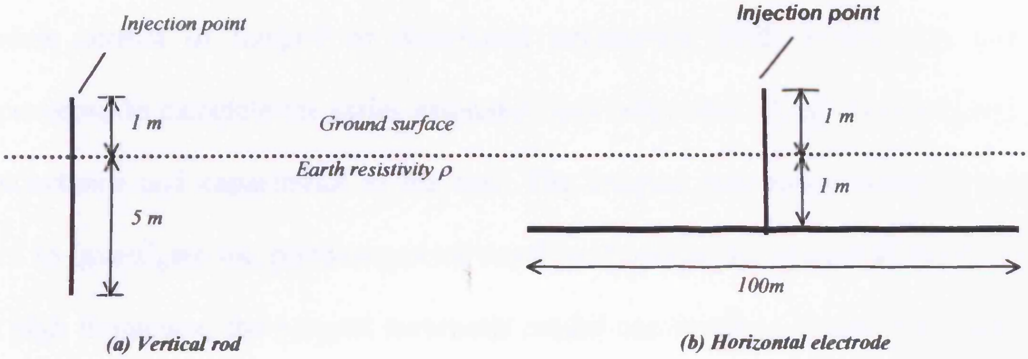

(a) Simple vertical rods and horizontal electrodes used in the simulations

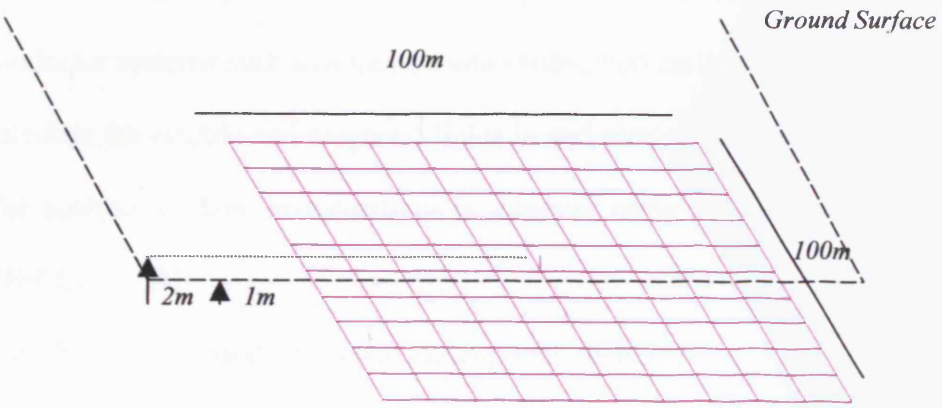

b) The earth grid used in the simulations of soil resistivity and permittivity effects.

Figure 3.1 The earthing system arrangements

The impedance for the earth electrode system is calculated for each arrangement using an injected current of 1A. The impedance of an earth electrode can be calculated using an equivalent circuit model or field-based numerical techniques. The equivalent circuit models consist of lumped or distributed parameters. Both models use analytical expressions to calculate the series resistance and inductance of the electrode, and shunt conductance and capacitance in the soil. The lumped parameters model is generally used to investigate the performance of small earth electrode systems at low frequency. At high frequency, the lumped parameter model can result in significant errors when estimating the earth electrode impedance [3.2]. The distributed parameter model can offer more accuracy for calculating the earth impedance of simple configurations such as vertical rod and horizontal electrode, at high frequency.

The field-based numerical techniques have several advantages over the equivalent circuit model; they can be used to analyse complex and arbitrarily oriented buried conductor systems such as a transmission substation earthing systems, and they can also calculate the electric and magnetic fields in and around the substation [3.11, 3.21-3.23]. The analysis in these investigations is achieved using a field based computer software HIFREQ [3.24].

The HIFREQ is based on several assumptions such as:

- In case of a uniform soil medium, the medium is assumed to be a half-space of air and soil, separated by a horizontal plane. The soil and air are assumed to be homogenous media.

- The earth electrodes are assumed to be cylindrical, metallic conductors. (Non cylindrical conductors must be converted to equivalent cylindrical conductors, keeping the same equivalent surface area).
- The conductors are modelled as cylindrical segments, the degree of segmentation affect the result accuracy particularly at high frequencies. The number of segments must be chosen so that the length of the segments satisfy two conditions: i) the thin wire condition where the segment length must be at least 5 times longer than its radius. ii) the segment length must allow the leakage current distribution over the segment to be approximated by a constant value. This means that shorter segment should be used wherever the current is expected to vary rapidly in space, (close to the points of injection). It is shown[3.2, 3.24] that at higher frequencies, where the current tends to vary sinusoidally along the conductors, with a wavelength (λ) can be expressed as follows:

  In air $$\lambda = \frac{3\times 10^{8}}{f} \quad \text{(m)} \qquad (3.1)$$

  In soil $$\lambda = 3160 \times \sqrt{\frac{\rho}{f}} \quad \text{(m)} \qquad (3.2)$$

  For reliable results, the maximum length of a segment should be about 1/6 of the wavelength.

In all of the simulations conducted in this thesis, the minimum segment length to radius ratio was 5. A sensitivity analysis was carried out to determine the appropriate level of segmentation for the main simulations. A 100mx100m grid was simulated under high frequencies (100 kHz and 1MHz), and the segment's length decreased for each set of the simulation. The corresponding earth grid impedance is shown in Tables 3.1 and 3.2. According to the wavelength calculated using Equation (3.2) the segment's length should be about 5.27m and 16.655m for 1MHz and 100kHz respectively. Tables 3.1 and 3.2 show that lower earth grid impedance corresponds to segments length equal or less than these values.

Table 3.1 The effect of conductors segmentations on the earth grid impedance at 1 MHz

Segment Length	4 meshes		16 meshes		100 meshes	
	Z	ϕ	Z	ϕ	Z	ϕ
20m	18.309	69.113	18.423	69.087	25.279	60.135
10m	18.533	69.056	18.533	69.063	18.958	68.369
6.7m	17.873	66.626	17.966	64.915	18.272	64.482
5m	17.755	64.414	17.758	65.419	18.039	65.027
4m	17.71	64.979	17.820	64.984	18.105	64.639
3.3	17.763	64.917	17.766	64.922	18.045	64.857
2.9	17.765	64.888	17.768	64.892	18.051	64.571

Table 3.2 The effect of conductors segmentations on the earth grid impedance at 100 kHz

Segment Length	4 meshes		16 meshes		100 meshes	
	Z	ϕ	Z	ϕ	Z	ϕ
20m	4.373	49.596	4.55	50.974	5.395	65.173
10m	4.298	49.182	4.507	50.852	3.968	61.755
6.7m	4.312	48.965	4.523	50.689	4.012	60.721
5m	4.312	48.860	4.522	50.564	3.986	61.332
4m	4.309	48.861	4.518	50.593	3.977	61.350
3.3	4.312	48.834	4.521	50.573	3.981	61.313
2.9	4.308	48.835	4.517	50.583	3.973	61.322

3.3 Effect of Soil Resistivity

3.3.1 Vertical Rod

The frequency response of a 5 m vertical rod is illustrated in Fig 3.2. The impedance magnitudes and angles are calculated for different soil resistivities and a relative permittivity of 1.

The impedance magnitude shown in Figure 3.2(a) indicates that each curve has; i) a lower frequency range over which the impedance magnitude is almost constant. Therefore, the earth electrode is predominantly resistive, and ii) A higher frequency range where an inductive and capacitive effect become evident. In a medium of low soil resistivity, the impedance magnitude increases suddenly above a particular frequency, this frequency is related to the soil resistivity i.e 100 kHz for 10Ωm and 1MHz for 100Ωm soil resistivity. The impedance angle has a similar trend to that of impedance magnitude; the angle is positive and increases to a value of 80 degrees. This shows that the inductive effect may be highly significant under these conditions, and this may explain the increase in the impedance magnitude. These results are similar to those obtained by Davies et al. [3.2 , 3.3].

In a high soil resistivity medium, the impedance of the vertical earth rod decreases above a particular frequency also related to the soil resistivity. At 100kHz and above, the impedance angle starts decreasing to negative values to reach - 80° just below 10 MHz. This may indicate that capacitive effects could be very important in high soil resistivity media and over a high frequency range. This may explain the reduction in impedance magnitude.

3.3.2 Horizontal Electrode

Figure 3.3 shows the impedance magnitude and angle for a 100m horizontal electrode, in different soil resistivity media and over a range of frequency DC to 10MHz.

As expected, the trend is similar to that of the vertical rod, where the electrode impedance is mainly resistive up to a particular frequency, related to the resistivity, and above that frequency, the inductive effect becomes dominant and the impedance magnitude increases markedly as the frequency increases. The inductive effects are apparent at much lower frequencies than for the case of 5m vertical rod.

For a medium of high soil resistivity (10 kΩm) and for frequencies above 1 MHz, a resonant-like effect appears in the impedance magnitude. By examining the phase angle curves, capacitive effects are indicated by a reduction in the phase angle. Above 1 MHz, a resonant effect appears in the impedance angles.

Figure 3.4 presents the comparison of a vertical rod and a horizontal electrode of the same length (20m) for different soil resistivities, and unity soil permittivity. As can be seen, the earth impedance of the horizontal electrode is slightly higher than that of the vertical rod in the low frequency range before inductive effects become significant. Similar results were published earlier, [3.4, 3.5]. In the high frequency range, the difference becomes much smaller and the impedances of the vertical rod and the horizontal electrode tend to converge to the same magnitude.

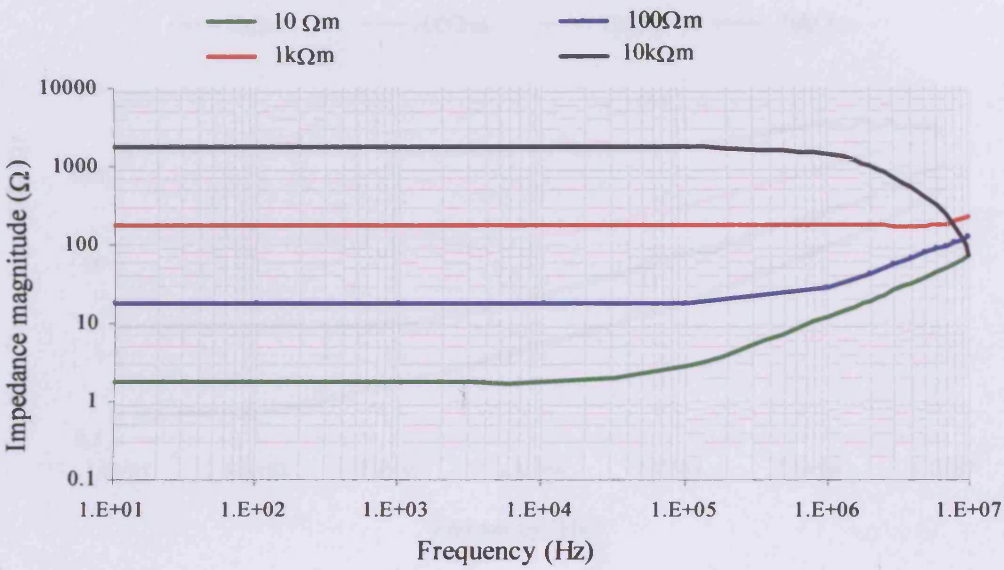

(a) Earth impedance magnitude

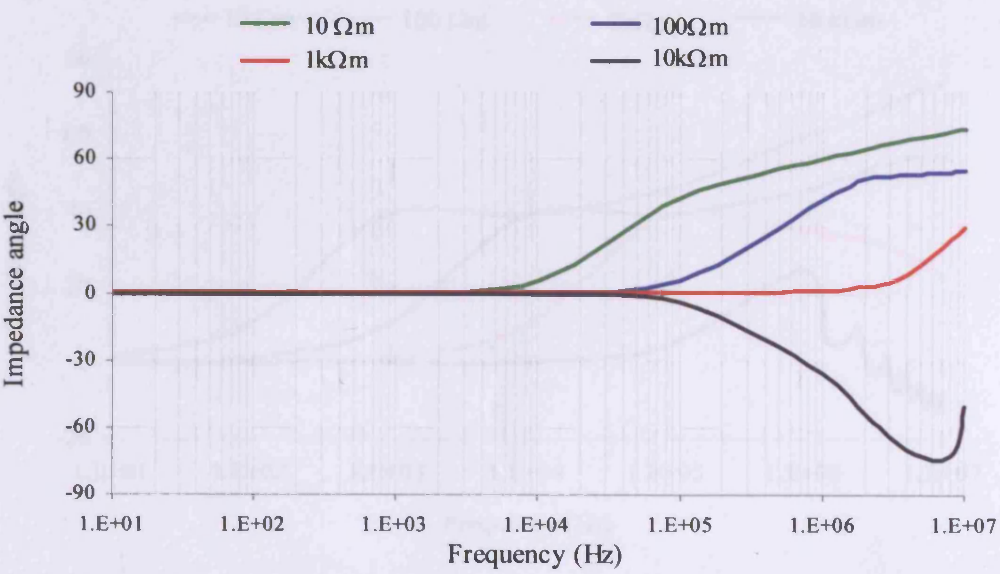

(b) Earth impedance angle (ϕ)

Figure 3.2 Frequency response of a 5 m vertical rod for different soil resistivities (ε_r=1)

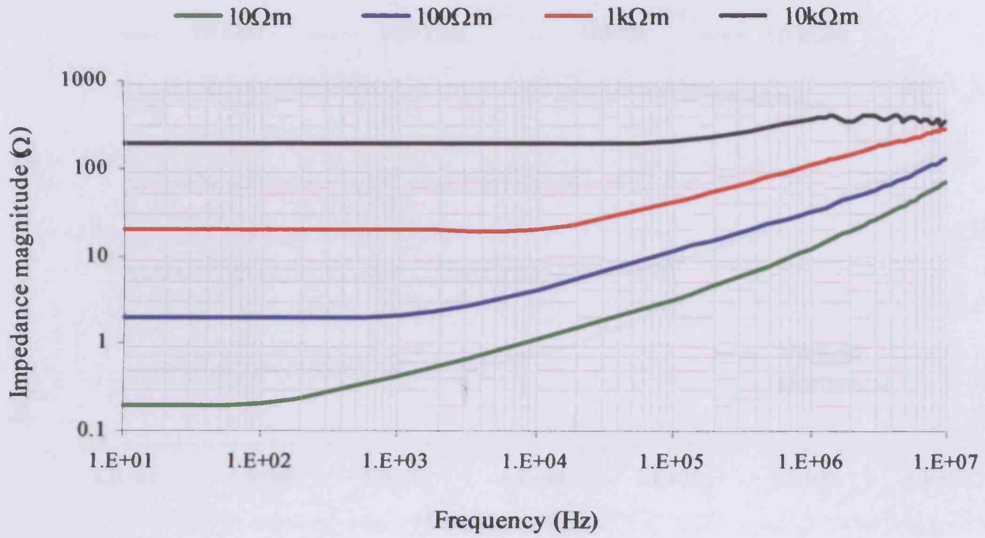

(a) Impedance magnitude

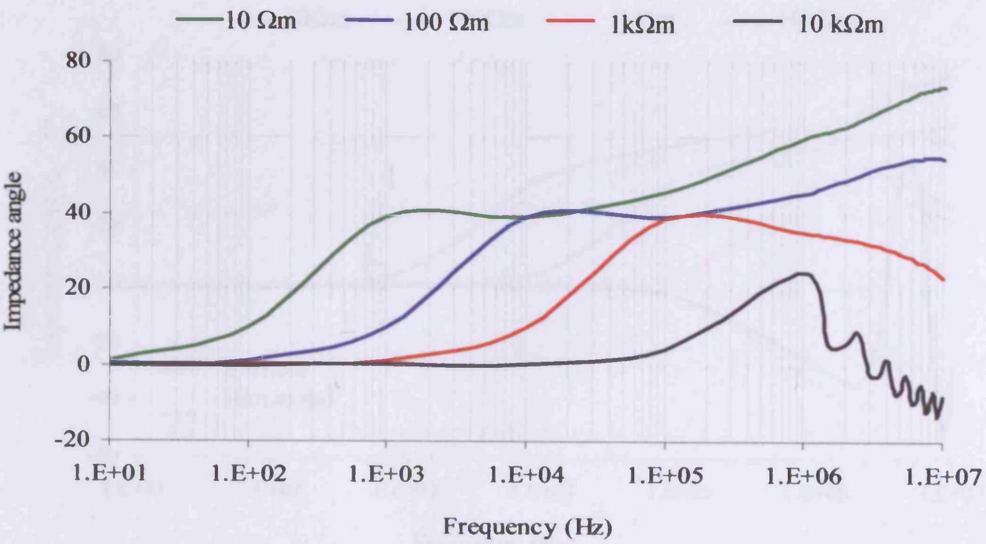

(b) Impedance angle (ϕ)

Figure 3.3 Frequency response of a 100 m horizontal electrode for different soil resistivities (ε_r=1)

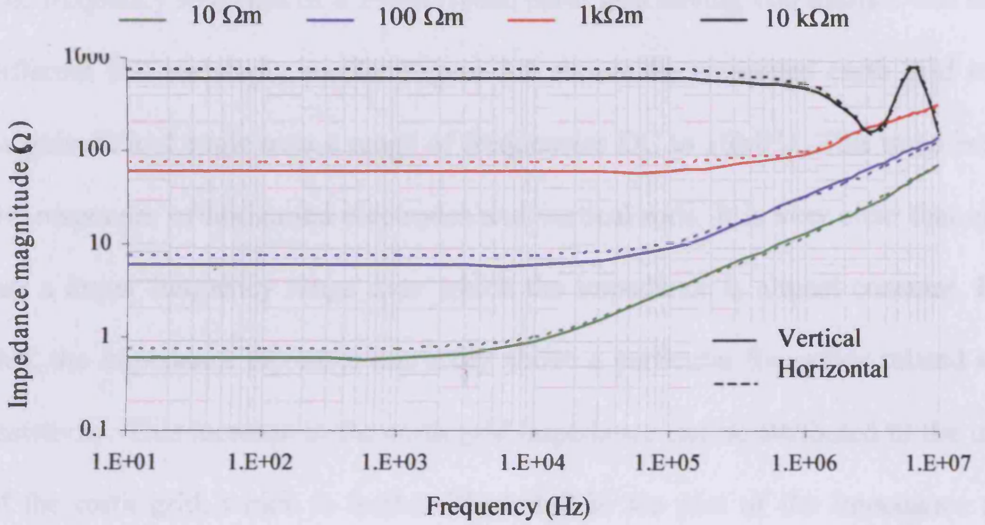

(a) Impedance magnitude

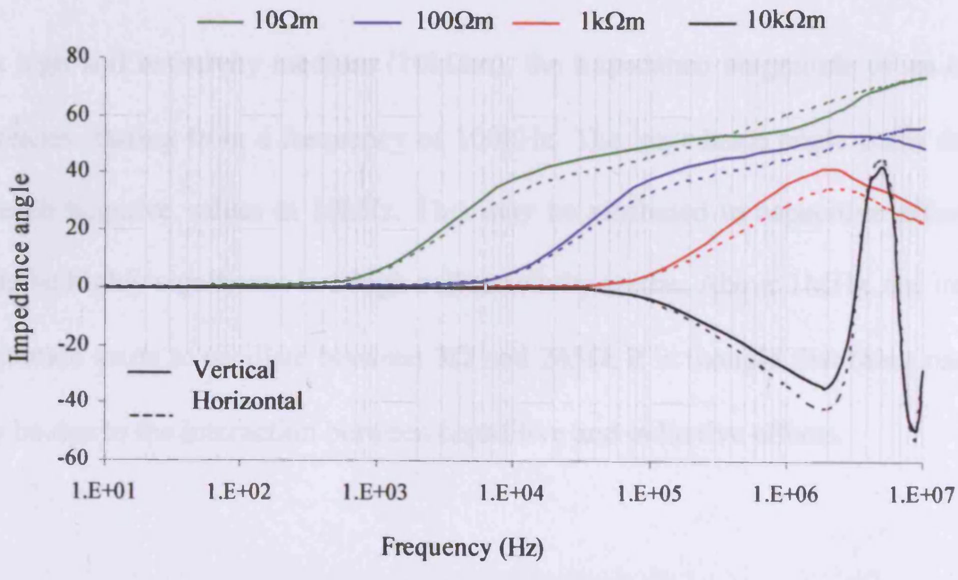

(b) Impedance angle (ϕ)

Figure 3.4 Response of a horizontal electrode and a vertical rod of 20m length

3.3.3 Earth Grid

The frequency response of a 100mx100m earth grid having 100 meshes was studied for different soil resistivity media. Figure 3.5 shows the computed earth grid impedance magnitude and angle over a range of frequencies DC to 10MHz. This trend is similar to the responses of horizontal electrodes and vertical rods. It is very clear that each curve has a lower frequency range over which the impedance is almost constant. Following this, the impedance increases markedly above a particular frequency related to the soil resistivity. This increase in the earth grid impedance can be attributed to the inductance of the earth grid, which is further illustrated in the plot of the impedance angle. As expected, the inductive effects are more significant at low frequencies for low resistivity soil conditions [3.12]. These findings agree with those reported by Heimbach and Grcev [3.11, 3.13-3.15]

In a high soil resistivity medium (10kΩm), the impedance magnitude of an earth grid decreases starting from a frequency of 100kHz. The impedance angle starts decreasing to reach negative values at 10kHz. This may be attributed to capacitive effects which could be highly significant in a high soil resistivity media. Above 1MHz, the impedance magnitude starts to oscillate between 3Ω and 245Ω. It is thought that these oscillations may be due to the interaction between capacitive and inductive effects.

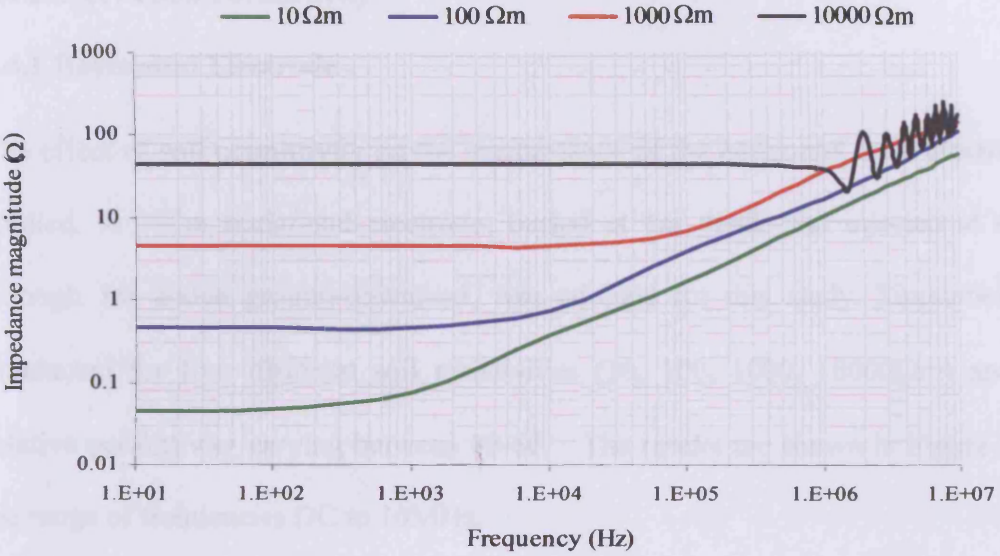

(a) Impedance magnitude

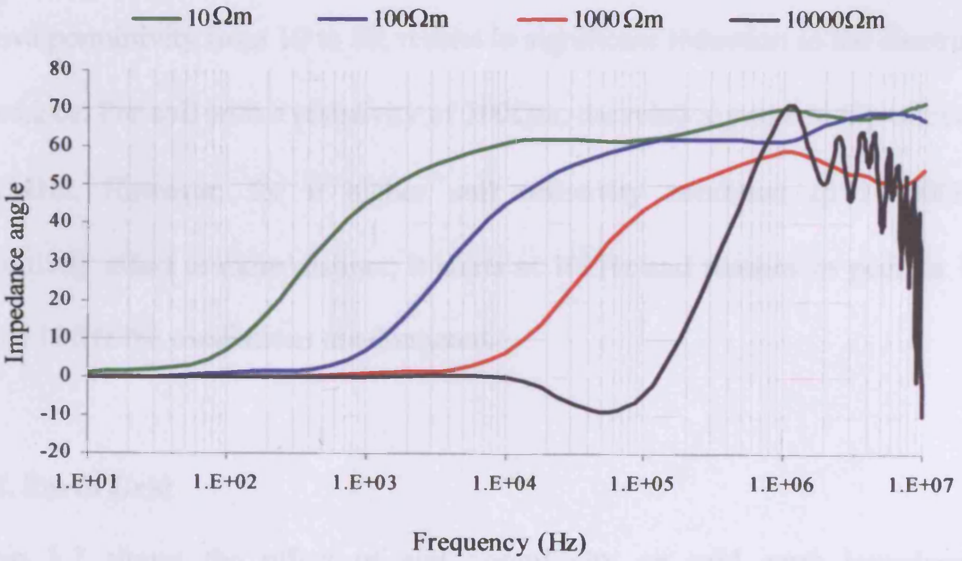

(b) Impedance angle

Figure 3.5 Frequency response of 100mx100m earth grid for different soil resistivities (ε_r=1)

3.4 Effect of Soil Permittivity

3.4.1 Horizontal Electrode

The effect of soil permittivity on the performance of the horizontal earth electrode was studied. A 100m horizontal electrode, buried at 1m depth and injected at one end through 1m above ground-downlead, was adopted for this study. Simulations were conducted for four different soil resistivities (10, 100, 1000, 10000Ωm) and a soil relative permittivity varying between 10-80. The results are shown in Figure 3.6 over the range of frequencies DC to 10MHz.

It is clear that soil permittivity has no major effect on the impedance of the earth electrode under low soil resistivity conditions (ρ=10Ωm). However, the effect of soil permittivity becomes more evident as the soil resistivity increases. Increasing the relative permittivity from 10 to 80, results in significant reduction in the electrode earth impedance. For soil with a resistivity of 100Ωm, the relative permittivity effect appears at 1MHz. However, for a higher soil resistivity condition (ρ=10000Ωm), the permittivity effect is more distinct; it starts at 10kHz and reaches its peak at 100kHz. Above 1MHz the oscillations are dominant.

3.4.2. Earth Grid

Figure 3.7 shows the effect of soil permittivity on grid earth impedance of a 100mx100m grid having 100 meshes. The frequency response is investigated for low and high soil resistivities over the same range (DC to 10 MHz). For low soil resistivity with a value of (ρ=100Ωm), the soil permittivity has no clear effect on the earth grid impedance. For the high resistivity condition (ρ=10000Ωm), there is no marked permittivity effect up to 10kHz, where the impedance magnitude for the various soil permittivity values has a constant value around 45Ω. Above that frequency, increasing the relative permittivity from 10 to 50 results in a significant reduction in the earth impedance, the effect of soil permittivity reaches its maximum value at 100kHz. At the higher frequency of 1MHz, the impedance magnitudes for all values of permittivity are higher than that for 100kHz. Above 1MHz, the impedance magnitude oscillates between 22Ω and 205Ω.

The impedance angle illustrated in Figure 3.7(b) shows that, for low soil resistivity, the inductive effect of the earth grid dominates in the range of frequencies 1kHz to 100 kHz. Above that frequency, the angle starts to decrease indicating a capacitive effect. For high soil resistivity (10kΩm), the capacitive effect is dominant over a range of frequencies (1kHz to 100kHz); the decrease of the impedance angle becomes sharper as the relative permittivity increases. Above this frequency, the earth grid behaves inductively up to 1MHz where the impedance angle starts to oscillate as seen for the impedance magnitude. The capacitive effect starts to play an important role at lower frequencies, in soil with higher relative permittivity. These trends agree with the findings of previously published work [3.11, 3.16-3.18].

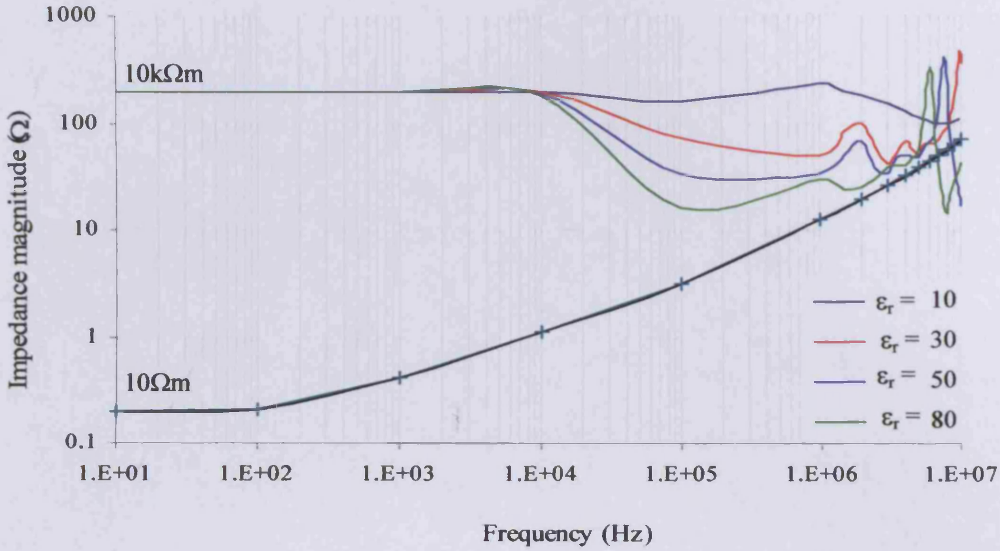

(a) Impedance magnitude (ρ= 10, 10000 Ωm)

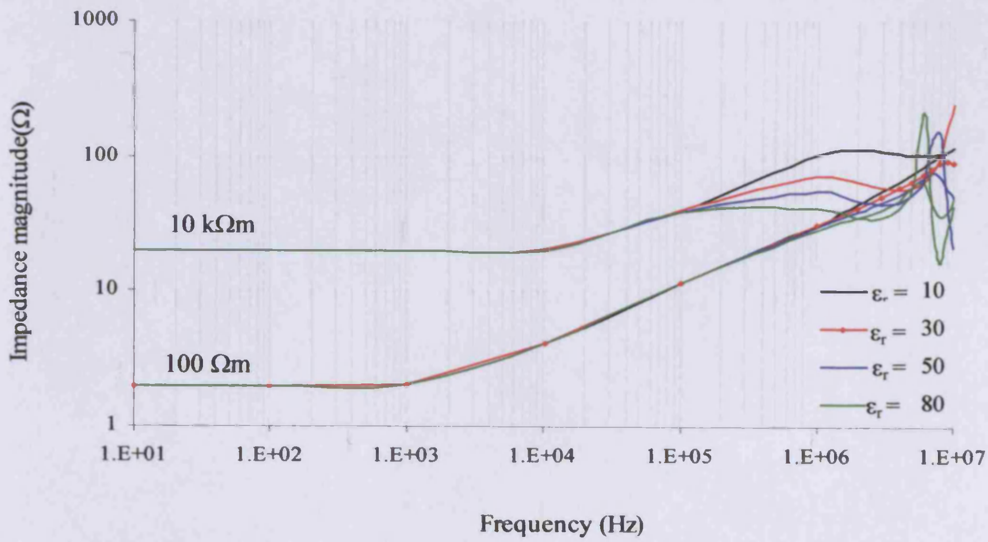

(c) Impedance magnitude (ρ= 100, 1000 Ωm)

Figure 3.6 Impedance magnitudes against frequency for a 100 m horizontal electrode for different soil permittivities

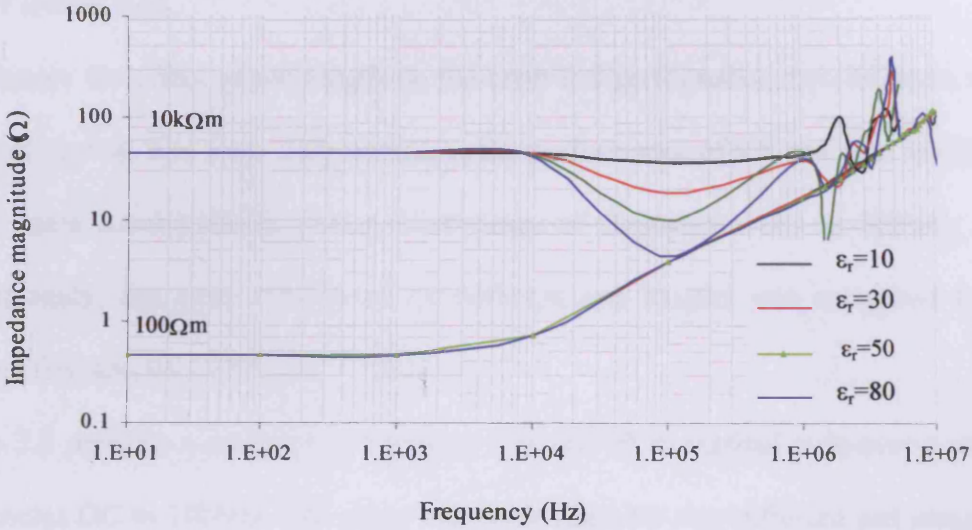

(a) Impedance magnitude

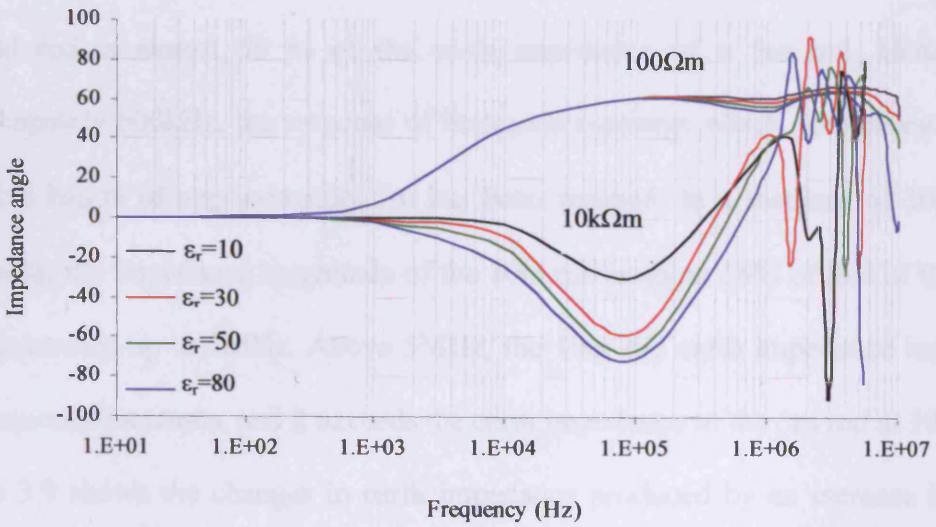

(b) Impedance angle (ϕ)

Figure 3.7 Frequency response of a 100mx100m earth grid-effect of soil permittivity

3.5 The Effect of Earth Electrode Length

3.5.1 Vertical Rod

To evaluate the effect of rod length on the earth rod performance, two different studies were conducted. The first study compares the performance of a 5 and 10m vertical rod of the same specifications, over a wide range of frequencies DC to 10MHz. In the second study, the earth impedance of different rod lengths was compared for two selected frequencies 100Hz and 100kHz.

Figure 3.8 presents a comparison between 5 m and 10 m vertical rods over a range of frequencies DC to 10MHz. The study was conducted for two different soil resistivities 100Ωm and 10 kΩm. It is clear that the impedance magnitude for a 10m vertical rod is smaller than that for a 5m one, up to a particular frequency, which depends on the soil resistivity. For a medium of 100Ωm soil resistivity, the earth impedance of the 10m vertical rod is almost 50 % of the earth impedance of a 5m rod. Hence, above approximately 600kHz, the response of both rods converge which demonstrates that an effective length of approximately 5m has been reached. In a medium of 10kΩm soil resistivity, the impedance magnitude of the 10m rod is about 55% of that of the 5m rod for frequencies up to 5MHz. Above 5MHz, the 10m rod earth impedance increases as the frequency increases, and it exceeds the earth impedance of the 5m rod at 10MHz.

Figure 3.9 shows the changes in earth impedance produced by an increase in the rod length for different soil resistivities and selected frequencies. At both frequencies 100Hz and 100kHZ, the earth impedance magnitude decreases as the length of the earth rod is increased (Figure 3.9).

3.5.2. Horizontal Electrode

To estimate the effect of length on the performance of the horizontal earth electrode, the impedance magnitude of a horizontal electrode varying with its length varying between 3 to 300 m was studied. The results are presented in Figure 3.10 for different soil resistivity media and for two selected frequencies 10Hz and 100kHz.

At a low frequency (Figure 3.10(a)) extending the electrode length results in a marked reduction on the earth electrode impedance for all soil resistivities. At the high frequency, extending the electrode length to a considerable length causes a reduction of the earth electrode impedance, Figure (3.10(b). As can be seen in this figure, the earth impedance of the electrode becomes constant at a particular length, indicating that the electrode has reached its effective length, and an increase in length will no longer reduce the earth impedance. It is clear that the effective length is greater for higher soil resistivities, for example, the electrode impedance becomes constant at 100kHz in 10Ωm soil at a length of 5m, while in 10kΩm soil, it becomes constant at a length of 200m. Previous investigations on horizontal earth electrode [3.8] revealed similar results to these obtained in this work.

The effective length was quantified previously and it was suggested [3.2, 3.6] that the effective electrode length could be estimated by the following expression;

$$\frac{\lambda}{4} \leq \text{effective electrode length} \leq \frac{\lambda}{6} \qquad (3.3)$$

Using Equations (3.1) and (3.2), the wavelength was calculated for different soil resistivities and selected frequencies, the results are shown in Table 3.3. Comparing these results to those shown in Figure 3.10 (a and b), it is clear that the results obtained in this work agree with the effective length calculated using the previous equations. For example, in Figure 3.10 (a), the effective length of the horizontal electrode in soil with 10Ωm resistivity and at 100Hz is between 150 to 200m which is similar to the range shown in Table 3.3.

Table 3.3 The calculated minimum and maximum effective length for different soil resistivities and selected frequencies.

Soil Resistivity	100Hz		100kHz	
	λ/4	λ/6	λ/4	λ/6
10	249	166	7	5
100	790	526	25	16.7
1000	2498	1665	79	52
10000	7900	5266	249	166

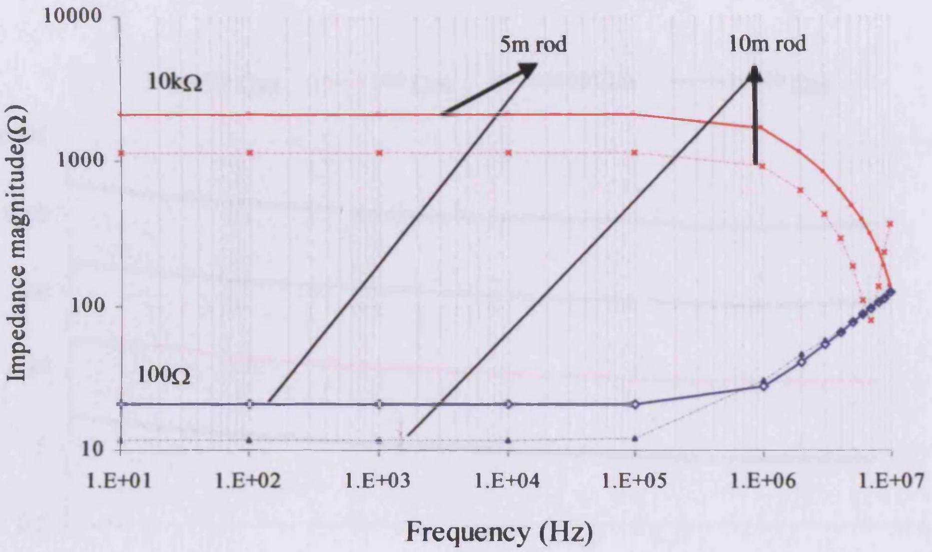

(a) Impedance magnitude (Ω)

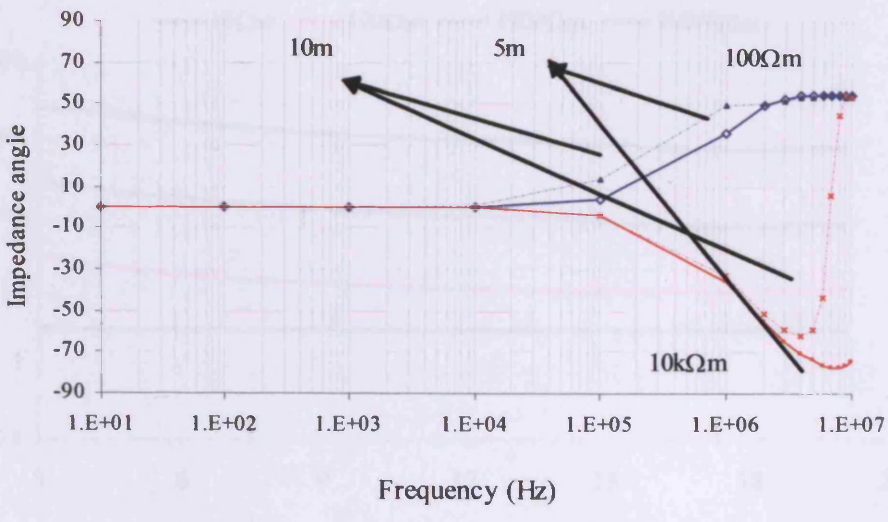

(b) Impedance angle (ϕ)

Figure 3.8 Comparison of 5m and 10m vertical rod frequency response

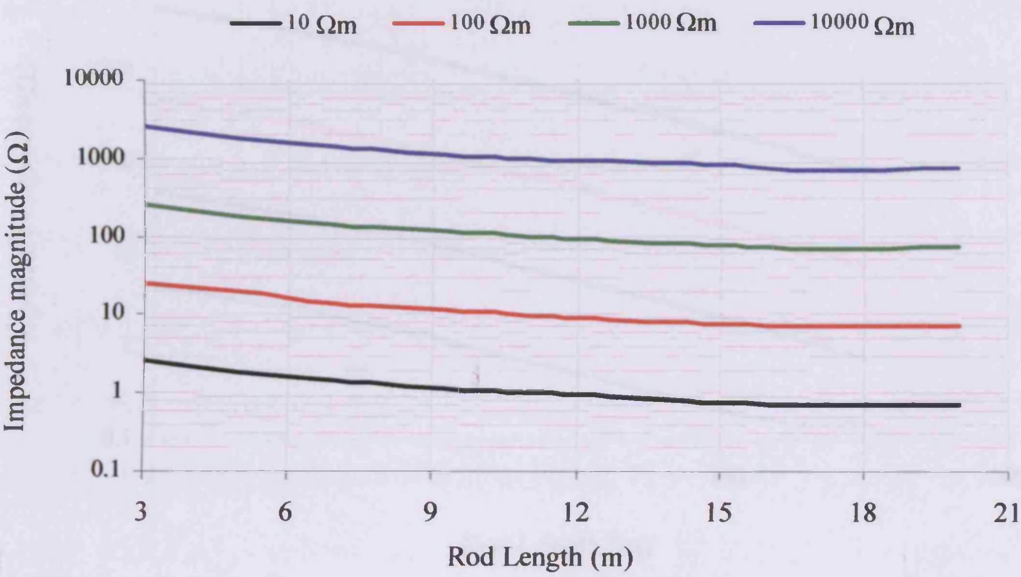

(a) At 100Hz

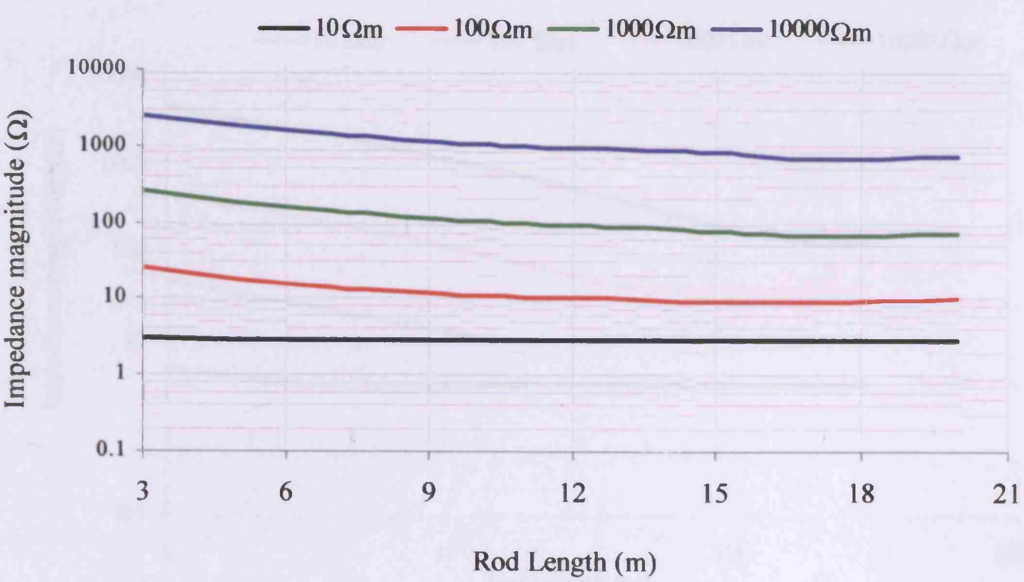

b) At 100kHz

Figure 3.9 Effect of the vertical rod length on earth impedance for different soil resistivities at selected frequencies

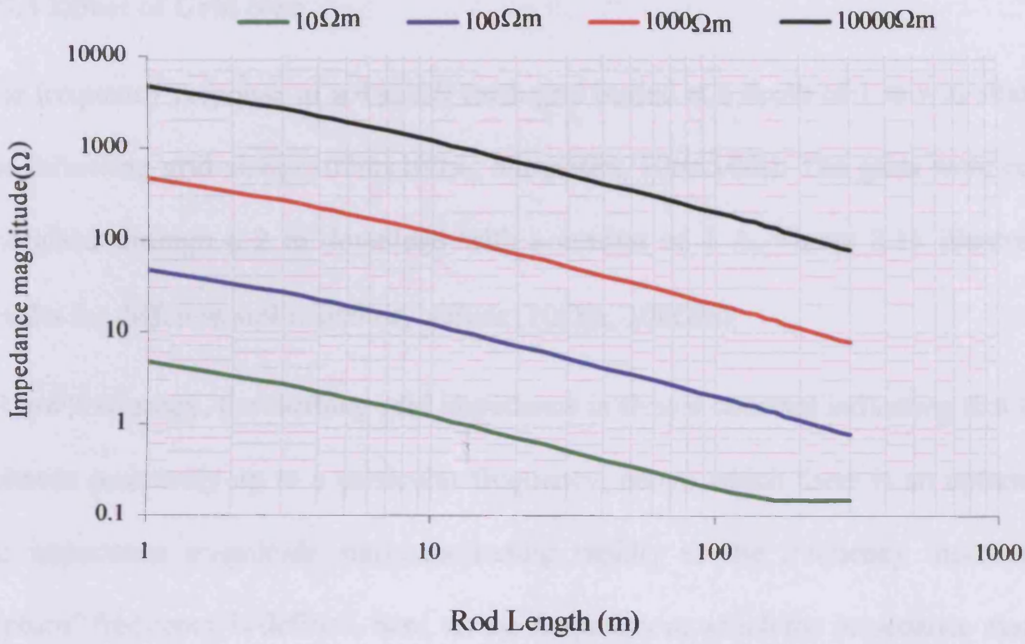

(a) Frequency 100 Hz

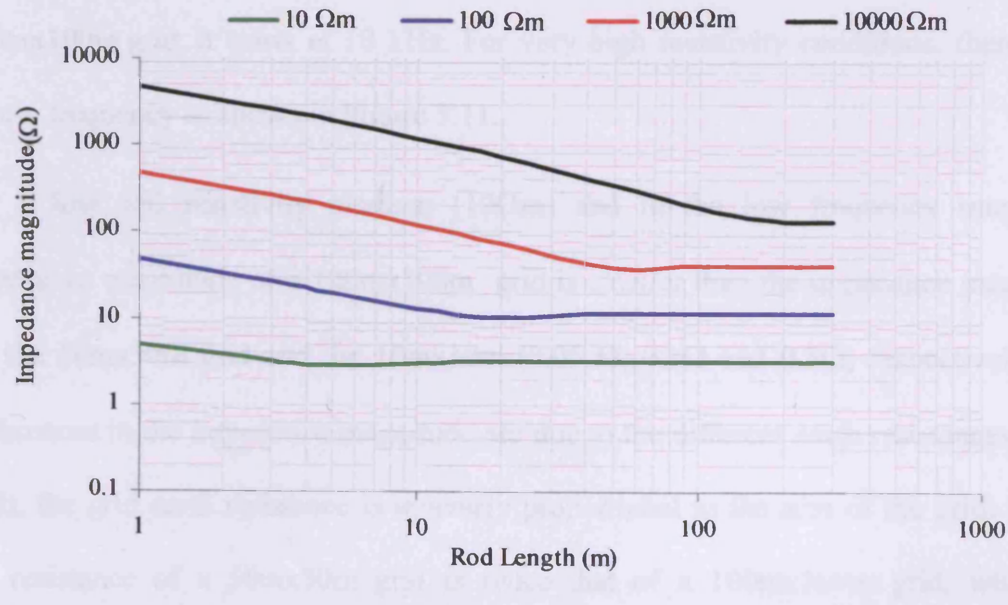

(b) Frequency 100 kHz

Figure 3.10 Effect of the horizontal electrode length on earth impedance for different soil resistivities at selected frequencies

3.5.3 Effect of Grid Size

The frequency response of a 4-mesh earth grid buried at a depth of 1 m was studied for the following grid sizes (100mx100m, 50mx50m, 10mx10m). The grids were centrally energised through a 2 m downlead with a current of 1 A. Figure 3.11 illustrates the results for different soil resistivity values (10Ωm, 10kΩm).

At low frequency, the earthing grid impedance is almost constant indicating that the grid behaves resistively up to a particular frequency, above which there is an upturn where the impedance magnitude starts increasing rapidly as the frequency increases. The "upturn" frequency is defined, here, as the frequency at which the impedance magnitude starts to increase rapidly, depending on the grid size and soil resistivity. For low soil resistivity (10Ωm), the inductive effect starts at 100Hz for a 10mx10m grid, while for 100mx100m grid, it starts at 10 kHz. For very high resistivity conditions, there is no upturn frequency as shown in Figure 3.11.

For a low soil resistivity medium (10Ωm) and in the low frequency range, the impedance magnitude of a 100mx100m grid is smaller than the impedance magnitude for the 50mx50m grid and the 10mx10m (0.05 Ω, 0.1Ω and 0.5Ω) respectively. The differences in the impedance magnitude are due to the different earth resistances of the grids, the grid earth resistance is inversely proportional to the area of the grid. Hence, the resistance of a 50mx50m grid is twice that of a 100mx100m grid, while the 10mx10m is ten times higher. Above the "upturn" frequency, the earth grid impedance of all grid sizes converges at approximately 100kHz.

For high soil resistivity conditions (10kΩm), the resistive behaviour region extends to a much higher frequency (100kHz). However, unlike the low soil resistivity conditions the impedance of the different sized grid do not converge at high frequency. Rather these are changing in impedance with frequency.

These results can partly be explained by using the effective area concept [3.9, 3.10, 3.14-3.17,], where the effective area is defined as a certain grid area beyond which increasing the grid size will result in no appreciable changes in the earth grid impedance.

3.6 Effect of Injection Point Location

The effect of injection point location has been examined by several authors [3.2, 3.10, 3.11, 3.15-3.17]. Here, this effect is examined at three different frequencies (100Hz, 1MHz, 10MHz) A 4-mesh 100mx100m earth grid is simulated in 100Ωm soil resistivity. The grid was injected with a current of magnitude 1A at the corner and the central points via a 2 m downlead.

Figures 3.12 to 3.14 show the potential distribution at the surface of the soil for both the corner and central injection points, for the selected frequencies. Figure 3.12 shows the potential profile for a frequency of 100Hz. The imprint of the earth grid can be seen clearly for both central (a) and corner (b) injection points. The potential is higher above the conductors because of the high current density in this region. The potential magnitude is the same in both central and corner injection points as the point of injection has no effect on the potential profile at low frequency, as shown in figure 3.15. For a frequency of 1MHz (Figure 3.13), it is evident that the potential profile on the soil surface is significantly different from the 100Hz profile, the grid imprint is not recognisable anymore, and the potential is high in a small area around the injection point. However, the potential magnitude has increased markedly compared to 100Hz. At 10MHz, the imprint of the grid can barely be seen (Figure 3.14) but the potential magnitude at the injection point is still increasing. This increase in the ground potential rise can be attributed to the inductive effect of the grid itself. This explains why the highest voltage gradient can be found near the current injection point.

Although the potential characterisations on the surface of soil for both the corner and central injection points have the same trend, there is a marked difference in the potential magnitude itself; for the corner injected grid the magnitude is higher than that for the centrally injected grid. For a frequency of 1MHz, the peak magnitude of the surface potential is 4000V for a central injection point and 4400V for the corner-injected point, and. At 10MHz, the peak magnitude is about 6600V for the centrally-injected grid and 7400V for the corner-injected grid.

Figure 3.15 shows a comparison of the frequency response of centrally-injected and corner-injected earth grids. Figure 3.15 shows that the earth grid response to different injection positions could be divided into two frequency ranges. First, the low frequency range where the impedance magnitude is constant and the earth grid is predominantly resistive. Over this range, the location of the point of injection has no effect and the impedance magnitude is identical for both injection positions. Secondly, a higher frequency range when the inductive effect becomes dominant and the impedance magnitude increases markedly. Over this range, the centrally-injected grid has a smaller impedance magnitude than the corner injected grid. At a very high frequencies of 10MHz, the difference is so small indicating that both curves may tend to converge just above 10MHz.

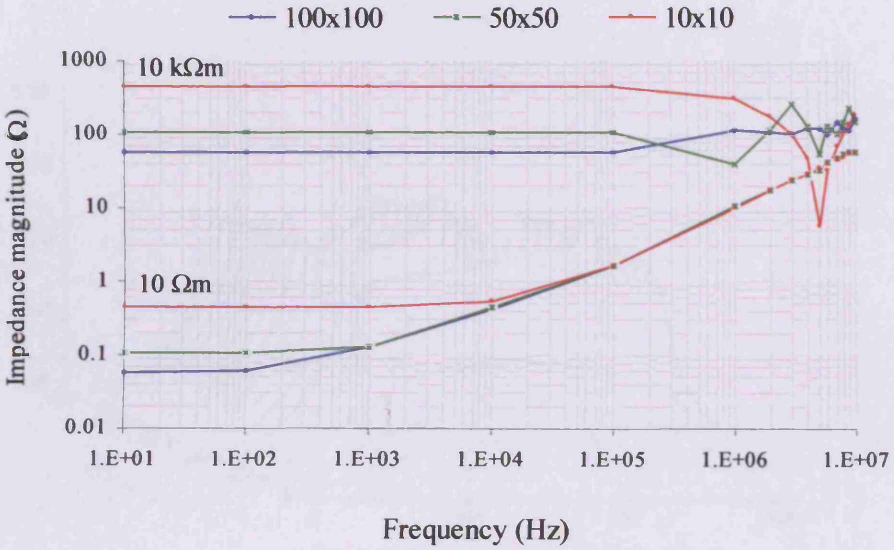

(a) Impedance magnitude (Ω)

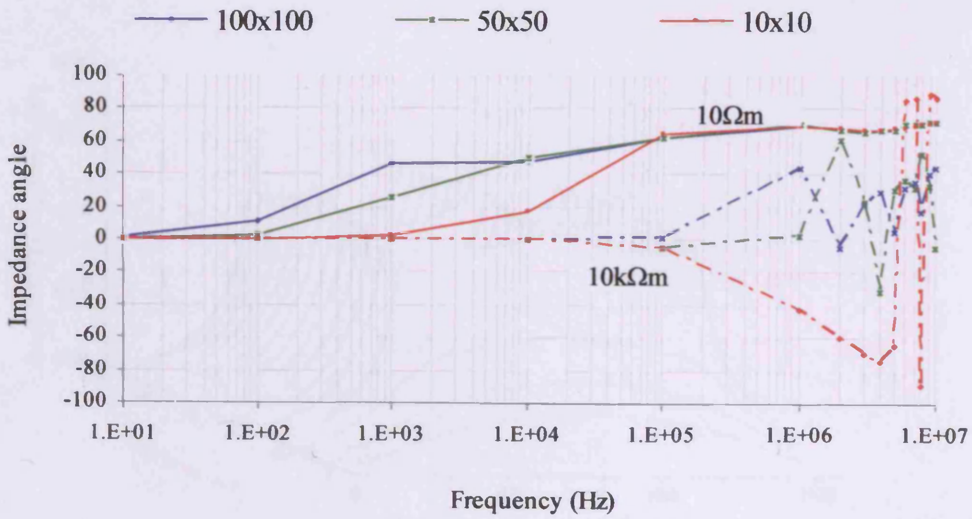

(b) Impedance angle (ϕ)

Figure 3.11 Effect of grid size on earth grid impedance

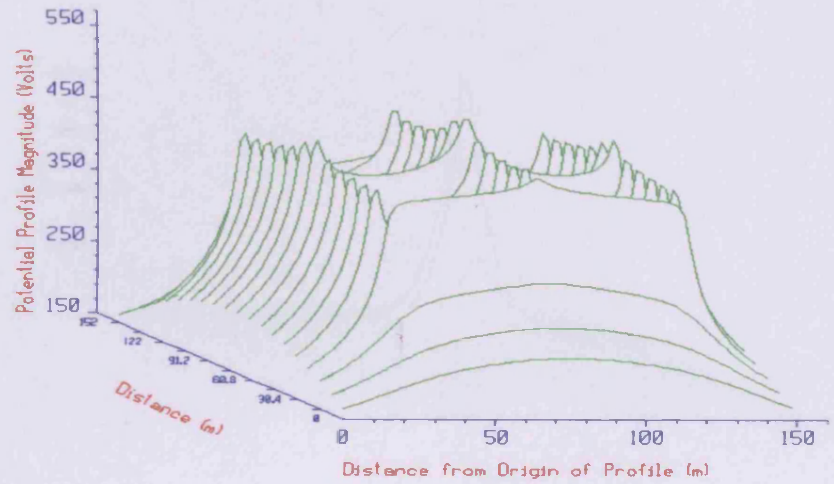

Central injection

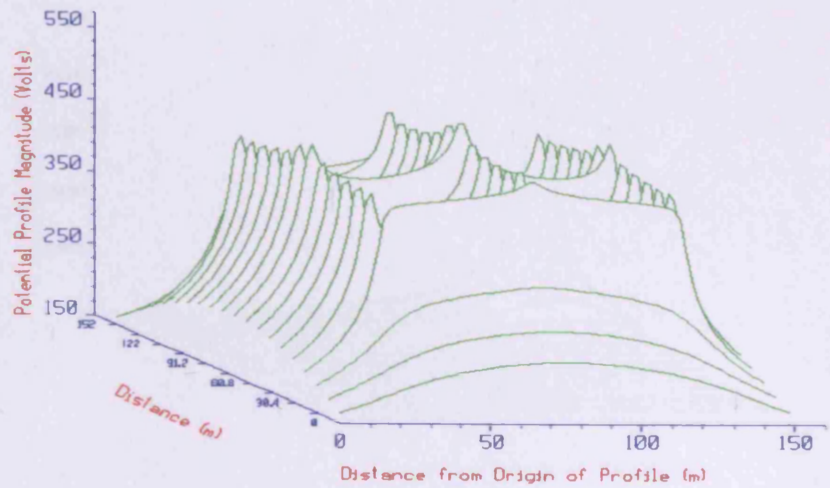

b) Corner injection

Figure 3.12 Surface potential of soil above 100mx100m earth grid (100Hz)

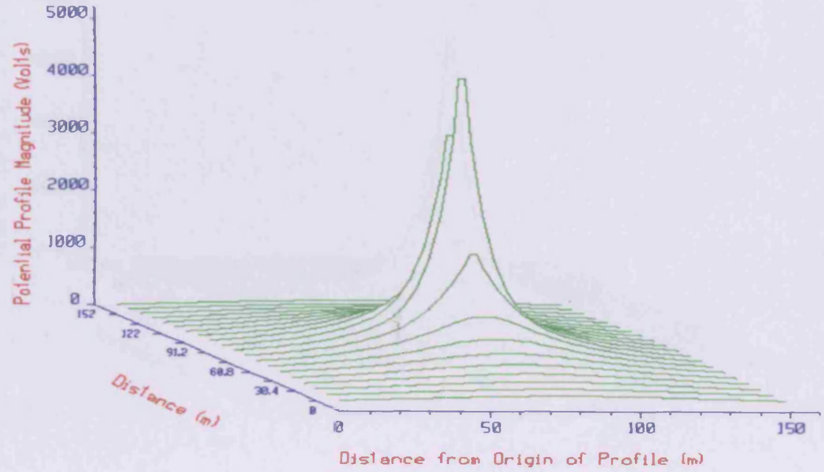

a) Central injection

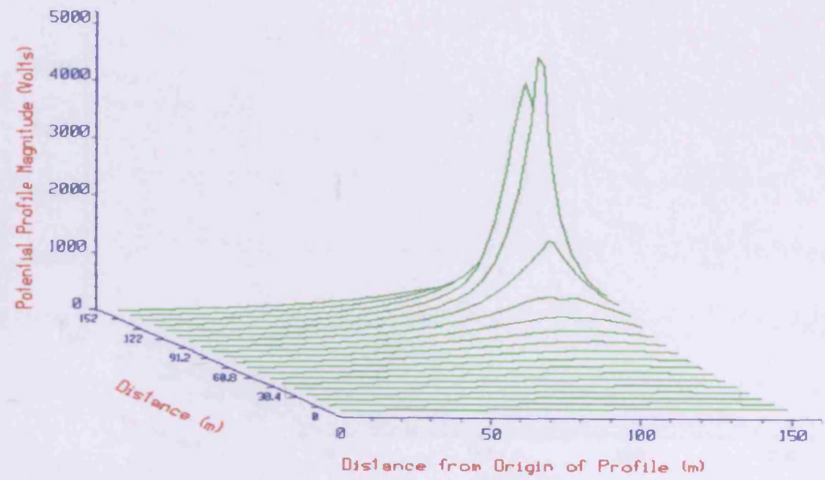

b) Corner injection

Figure 3.13 Surface potential of soil above 100mx100m earth grid (1MHz)

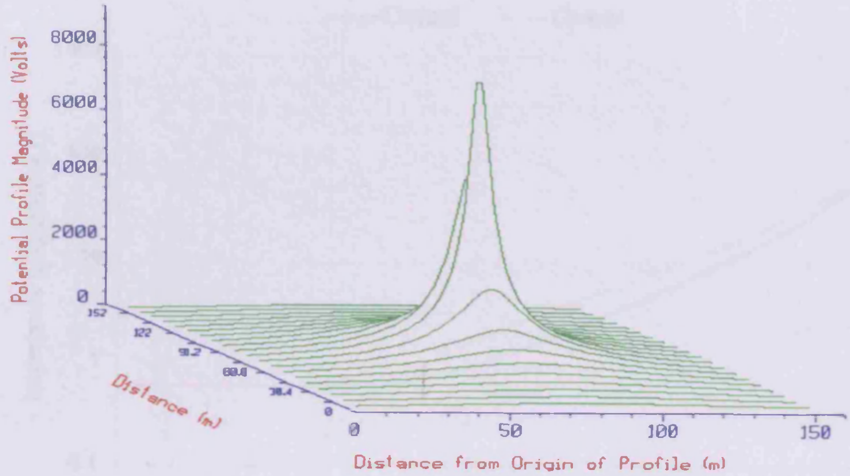

a) Central injection

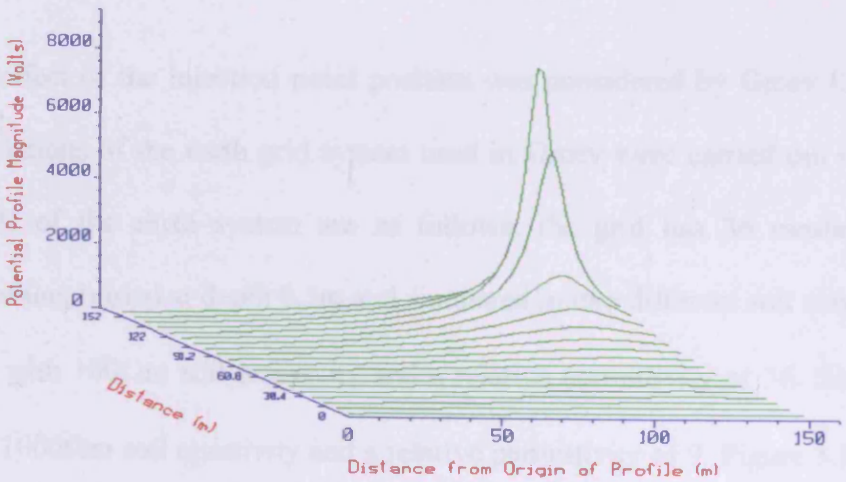

b) Corner injection

Figure 3.14 Surface potential of soil above 100mx100m earth grid

(10MHz, corner injection)

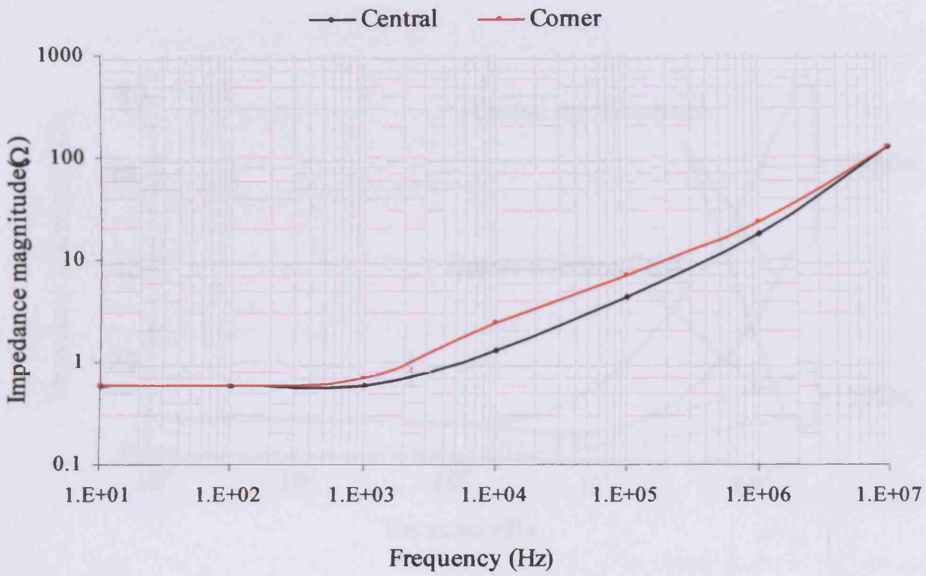

Figure 3.15 Effect of different injection points for 100mx100m 4 mesh-Grid (Soil resistivity of 100Ωm)

The effect of the injection point position was considered by Grcev [3.11, 3.13- 3.15]. Simulations of the earth grid system used in Grcev were carried out in CDEEGS. The details of the earth system are as follows; the grid has 36 meshes, of dimension 60mx60m, buried at depth 0.5m and simulated in two different soil conditions: first, wet sand with 100Ωm soil resistivity and a relative permittivity of 36. Secondly, dry sand with 1000Ωm soil resistivity and a relative permittivity of 9. Figure 3.16 and 3.17 show the results obtained from Grcev and the results obtained from the present investigation, respectively. The figures show that both results are in a good agreement. One small difference was noticed, that was the impedance magnitude for dry sand, obtained by Grcev is found to be slightly higher than that obtained in this investigation. This could be due to the injection downlead. Grcev did not specify the parameters of injection downlead, whereas, in this work, it was assumed to be 3m above ground.

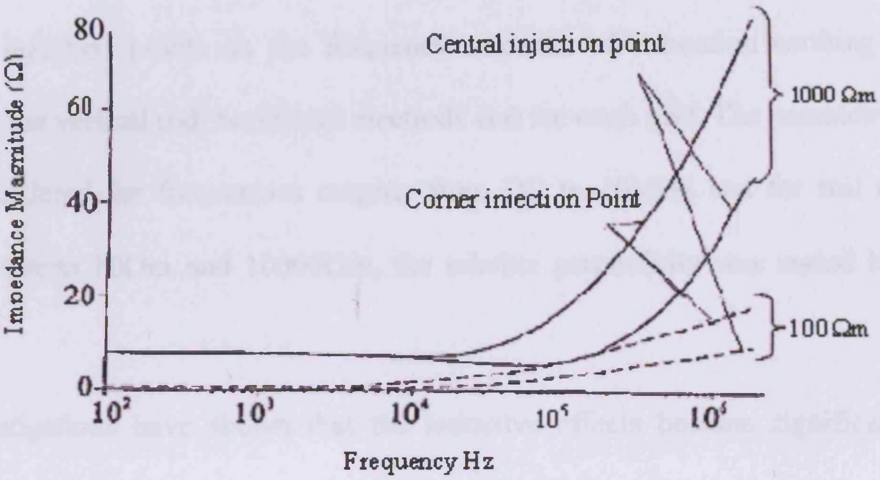

Figure 16 The effect of soil resistivity and the injection point position on the frequency response of earth grid (obtained by Grcev)

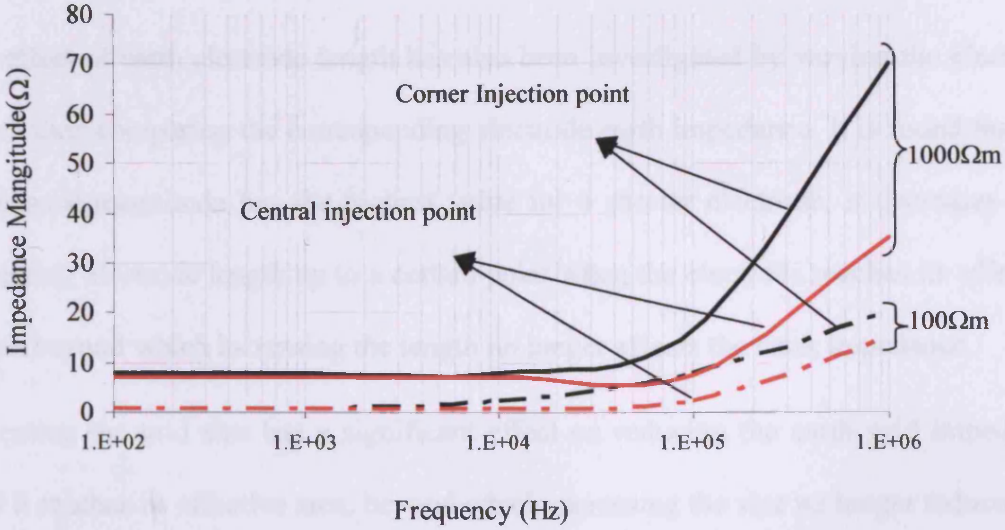

Figure 17 The effect of soil resistivity and the injection point position on the frequency response of earth grid. (Simulated using CDEGS)

3.7 Conclusions

This chapter demonstrates the influence of soil resistivity, soil permittivity, grid size and different injection points on the frequency response of substation earthing systems, including the vertical rod, horizontal electrode and the earth grid. The parametric studies were considered for frequencies ranging from DC to 10MHz and for soil resistivity values between 10Ωm and 10000Ωm, the relative permittivity was varied between 1 and 80.

The investigations have shown that the inductive effects become significant for all electrode systems above a threshold frequency for a given soil resistivity, resulting in an increase in the earth grid impedance magnitude. At higher frequencies and for a soil resistivity of 10kΩm, the impedance magnitude of a simple earth electrode tends to drop with increasing frequency which could be attributed to capacitive effects. The impedance also starts oscillating under the same conditions.

The effect of earth electrode length has also been investigated by varying the electrode length then comparing the corresponding electrode earth impedance. It is found that the impedance magnitude has the highest value for a shorter electrode, it decreases with increasing electrode length up to a certain point when the electrode reaches its effective length beyond which increasing the length no longer affects the earth impedance.

Increasing the grid size has a significant effect on reducing the earth grid impedance until it reaches its effective area, beyond which increasing the size no longer reduces the earth grid impedance.

For the 100x100m grid in 100Ωm soil resistivity, the injection point has no effect on the earth grid impedance in the low frequency range. Over an intermediate range of frequency, a centrally-fed ground grid has lower impedance than the corner injected grid. This may be attributed to the difference in inductance between the central and corner injection current paths. This effect becomes smaller at higher frequencies indicating that it may vanish above 10MHz where the impedance is no longer sensitive to the point of injection.

CHAPTER FOUR

Quantification of Existing and New Proposed Earth Grid Enhancement Techniques

4.1 Introduction

In Chapter 3, a comprehensive parametric study of the earthing system response to high frequency was examined. The effects of soil resistivity and soil permittivity on the earth grid impedance were studied together with the effective length of the earth electrode, the grid size and the different injection positions. The effective length and effective areas of electrode were quantified. These studies lead to consideration of how the earthing grid can be enhanced to improve performance under high frequency and transient conditions.

IEEE 80 [4.1] EA 41-24 [4.2] and CENELEC HD 637 S1 [4.3] recommend a number of qualitative measures to improve the performance of the earthing system under high-frequency and transient conditions. These recommendations concentrate on local earthing system enhancements such as:

i. 'High- frequency' earth rods connected to the main earth grid (EA 41-24)
ii. Multiple downleads (CENELEC HD)
iii. Increasing the grid mesh density (CENELEC HD).

In this chapter, careful investigations are conducted in order to quantify the benefits of these recommendations. This study investigates the high frequency response of an earth grid considering the effect of:

i. Number of local and perimeter-located rods

ii. Proposed new above ground arrangements and bonding between surge arrester bases

iii. Local and overall mesh density.

4.2 Effect of Mesh Density

To evaluate the effect of mesh density on the earth grid performance, two different studies were conducted. First, the overall mesh density was varied from 4 to 400 meshes. Second, the local mesh density was varied by increasing the number of meshes within a 20mx20m area around the injection point. A 100mx100 m earth grid was studied for low and high soil resistivity media and for a soil relative permittivity 1. The grid was centrally injected with 1A current through a 2m downlead. Figures 4.1 and 4.2 show the models adopted for this study.

4.2.1 Overall Mesh Density

Figures 4.3 present the influence of grid mesh density on the earth grid impedance over a range of frequencies DC to 10MHz, and over three different soil resistivities. At low frequency, increasing the mesh density has a very small effect on reducing the earth grid impedance, for all soil conditions. This could be attributed to the resistive behaviour of the earth grid as discussed previously. At higher frequencies, the earth impedance, for all mesh densities, converges to the same value; the frequency at which convergence takes place is a function of the soil resistivity. It is obvious from Figure 4.3 that there is a particular range of frequencies, over which the mesh density has an important effect on the earth grid impedance. This frequency range depends on soil conditions; for a low soil resistivity medium (10Ωm), the effect of increasing mesh density becomes more pronounced between 100Hz and 10kHz, it reaches its maximum at 1kHz where the impedance magnitude varies between 0.13Ω for a grid with 4 meshes and 0.064Ω for a grid with 400 meshes, which means about 50% reduction. For a medium of high soil resistivity (1000Ωm), the reduction of the earth grid impedance with mesh density reaches its maximum at 100kHz where the impedance magnitude varies between 12.9Ω for a grid with 4 meshes to 6.3Ω for a grid of 400 meshes resulting in a reduction of approximately 51%. This behaviour could be attributed to the different effective areas of the earthing system for different soil resistivities as argued in Chapter 3

4.2.2 Local Mesh Density

As expected, the earth grid responds in a similar way to the local enhancement of mesh density. Figure 4.4 illustrates the impedance magnitude and angle for a 100mx100m grid of 4 meshes with local mesh density enhancements. This study was conducted for two different soil conditions; low soil resistivity (10Ωm) and high soil resistivity (1kΩm). At low frequencies and for both soil resistivities, the impedance magnitude of the grid is less affected by the local meshing than by the overall mesh density. The reduction in the earth grid impedance is very small and is hardly observable in Figure 4.4. At higher frequencies, increasing local mesh density results in a reduction in the earth grid impedance over a particular range of frequencies depending on the soil resistivity. In a medium of low soil resistivity (10Ωm), the impedance magnitude decreases with local mesh density enhancements for frequencies between 1kHz and 100kHz. The largest reduction is seen at 10kHz where adding 4 and 36 extra local meshes produces a reduction of 12% and 30% respectively.

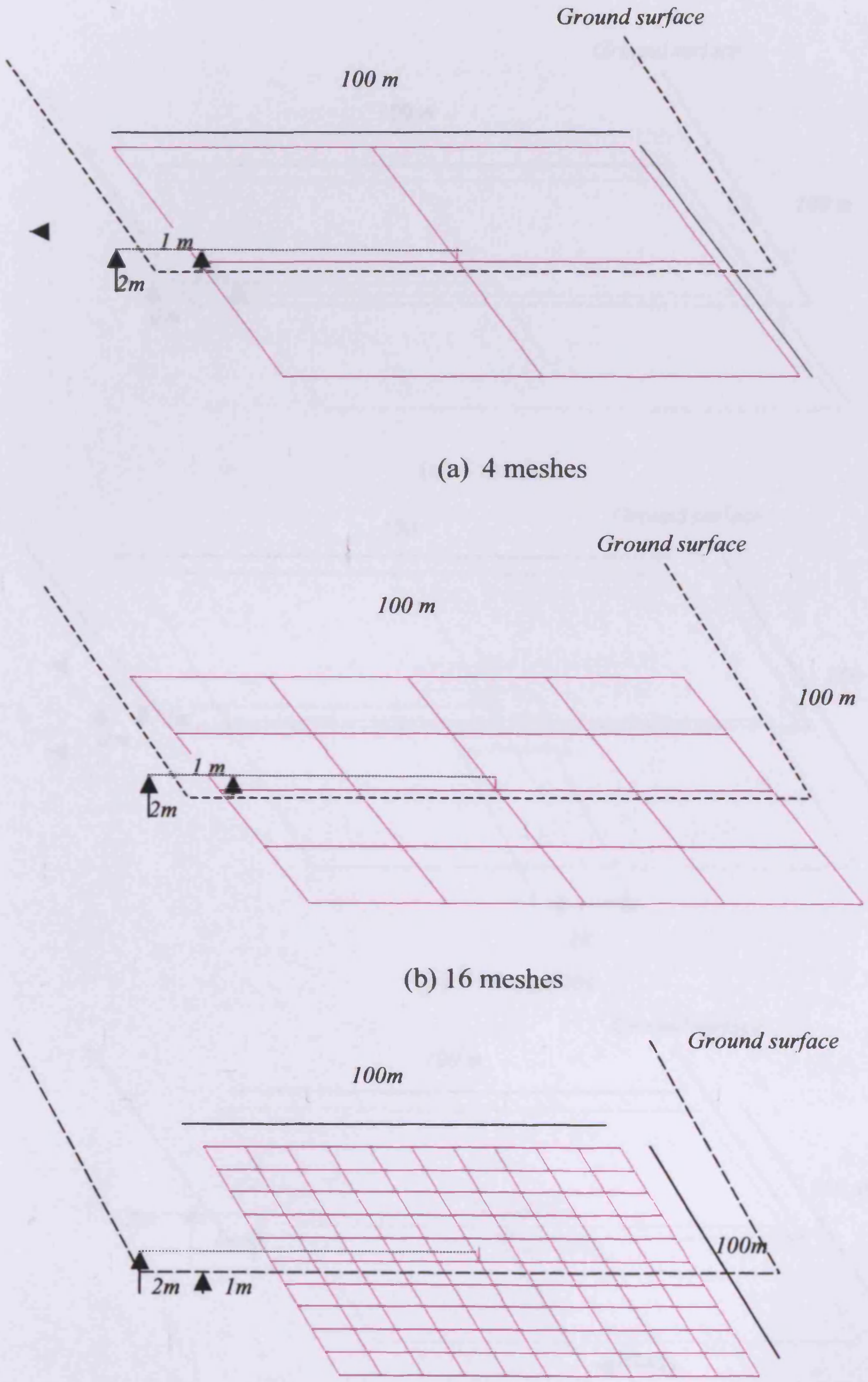

(a) 4 meshes

(b) 16 meshes

(C) 100 meshes

Figure 4.1 100mx100m grid, adopted for investigating the effect of overall mesh density

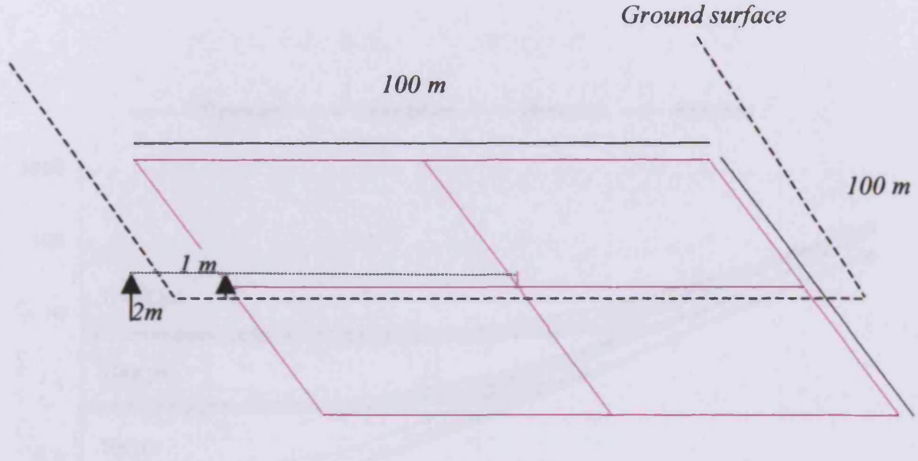

(a) 4 meshes

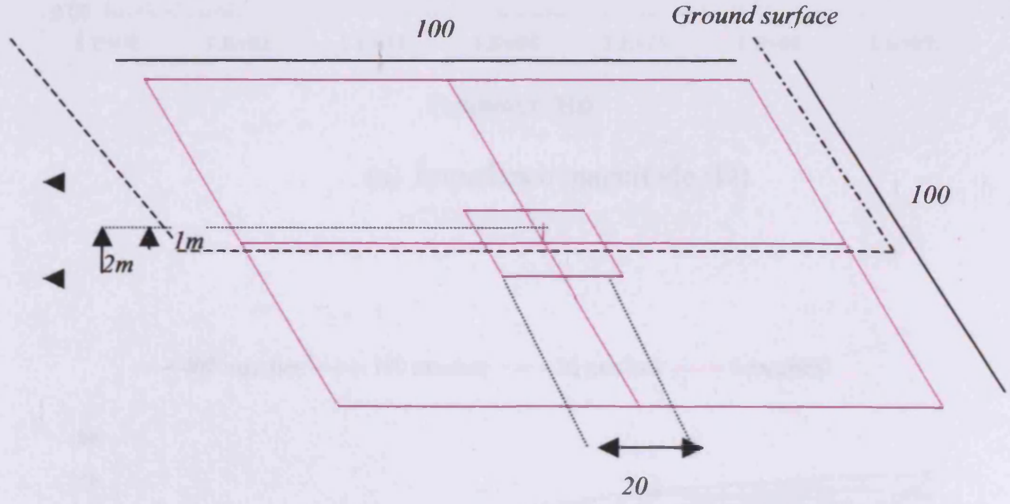

(b) 4+4 meshes

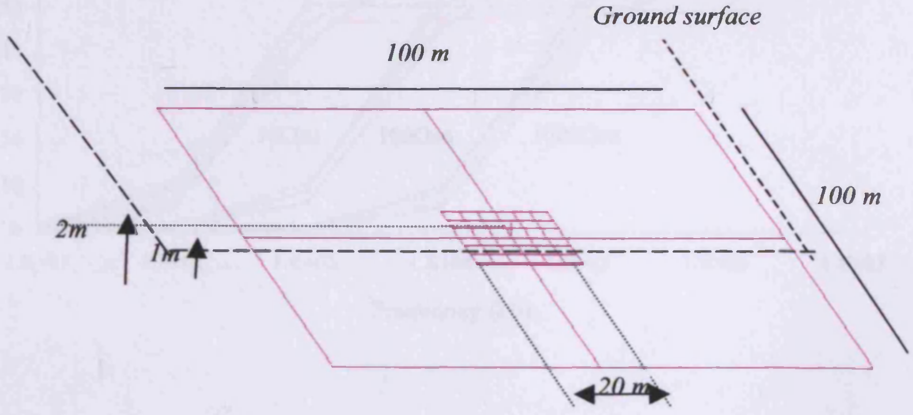

(c) 4+36 meshes

Figure 4.2 100mx100m grid, adopted for investigating the effect of local mesh density

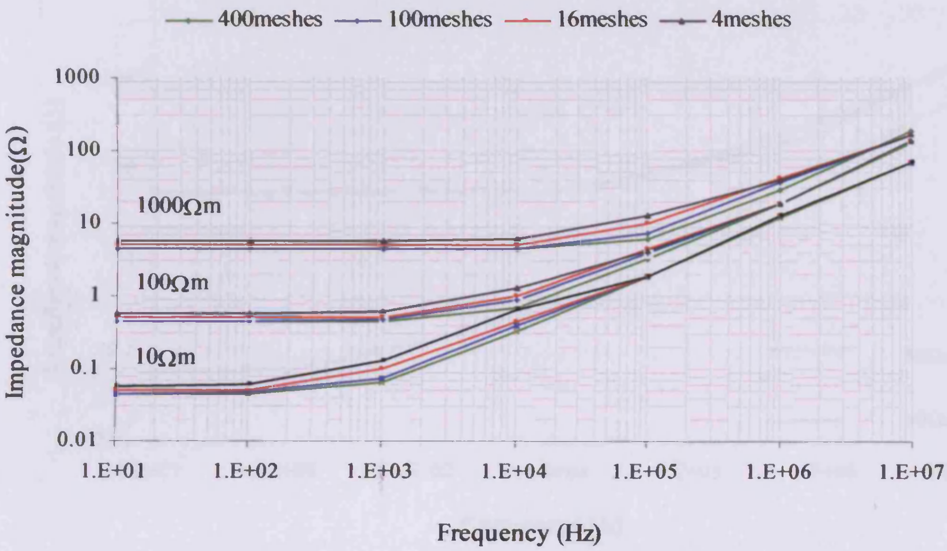

(a) Impedance magnitude (Ω)

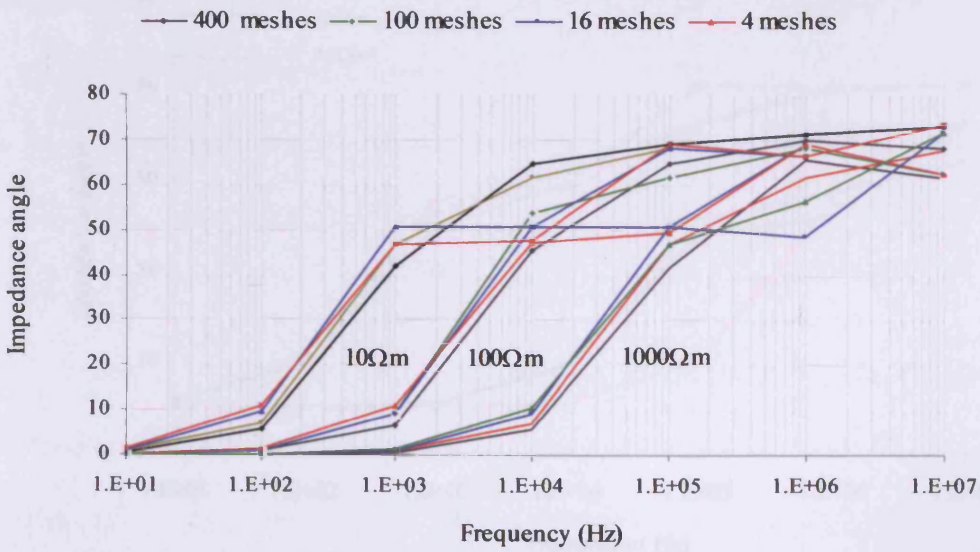

(b) Impedance angle (ϕ)

Figure 4.3 Effect of overall mesh density with soils of 100 and 1000 Ωm

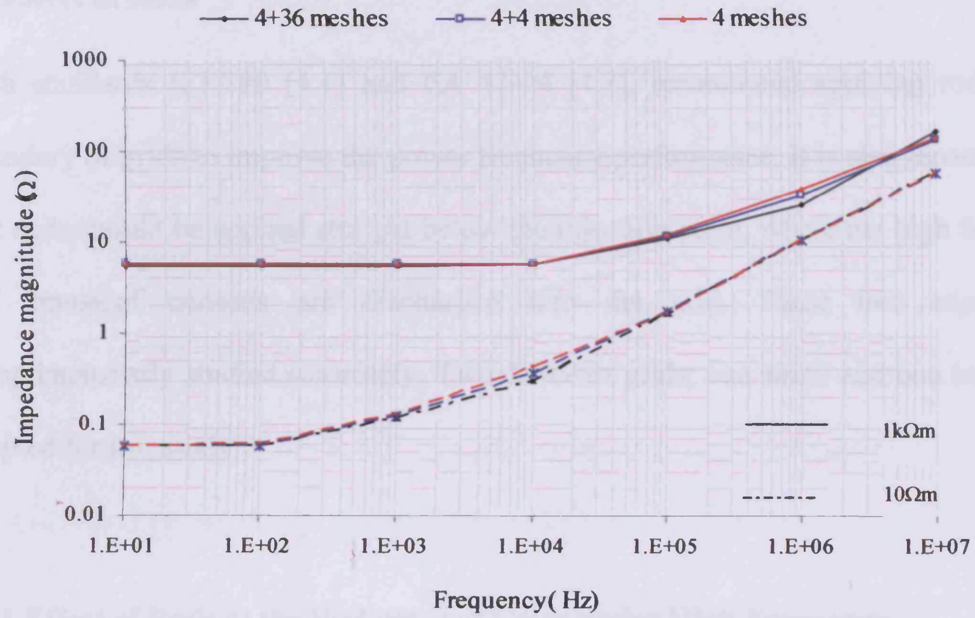

(a) Impedance magnitude(Ω)

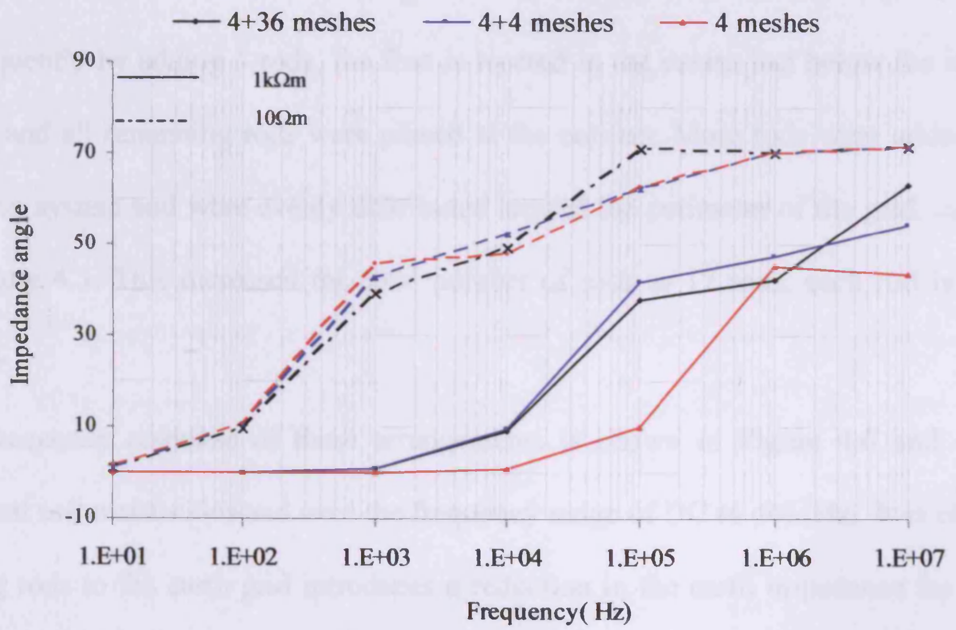

(b) Impedance angle (ϕ)

Figure 4.4 Effect of enhancing mesh density locally around the injection point for soil resistivity of 10 and 1000 Ωm.

4.3 Effect of Rods

Both standards IEEE80 [4.1] and EA 41-24 [4.2], recommend applying rods at the boundary of grids to improve the power frequency performance. It is also recommended that rods should be applied straight below the injection point, where the high frequency and transient currents are discharged into the grid. These two cases were comprehensively studied separately. Two different grids; one small and one large were adopted for this study.

4.3.1 Effect of Rods at the Perimeter of Grids under High Frequency

A 12mx12m 16-mesh grid buried at a depth of 1m and is centrally injected with a 1A current through a 3.3 m above ground downlead. This model was developed subsequently by adding 5 rods, the first is located in the centre just below the injection point, and all remaining rods were placed at the corners. More rods were added to the earthing system and were evenly distributed around the perimeter of the grid, as shown in Figure 4.5. This increased the total number of rods to 17 rods, each rod is 5 m in length.

The frequency response of these arrangements is shown in Figure 4.6 and 4.7, for different soil resistivities and over the frequency range of DC to 10MHz. It is clear that adding rods to the earth grid introduces a reduction in the earth impedance for all soil resistivities. This occurs for frequencies below the upturn frequency where the inductive effect becomes dominant. Above that frequency, the impedance magnitude for a grid with and without rods converges. In high soil resistivity (10kΩm), the addition of rods results in a reduction on the earth grid impedance up to a higher frequency (4MHz). Above that frequency, the impedance magnitude for all grids will converge in a similar way to its behaviour in lower soil resistivities.

It is evident that increasing the number of rods added to the grid results in a bigger reduction on the earth grid impedance. In this study, adding 5 rods to the grid introduces an approximate 14% reduction in the earth grid impedance for all soil resistivities, while increasing the number of rods to 17 causes a reduction of 26% of the original value of the earth grid impedance when no rods are added.

Figure 4.8 presents the frequency response of the same grid with two different sets of 17 rods distributed evenly around the perimeter of the grid. The first one is 5m in length while the others are 10m rods. This study was conducted for low and high soil resistivities (10Ωm and 10kΩm), and over the same range of frequency DC to 10MHz. As can be seen in Figure 4.8, increasing the rod length from 5m to 10m results in a significant reduction in the earth grid impedance over the entire frequency range where the rods are effective. As described previously, the addition of 17 rods of 5m in length to the earth grid introduces a reduction of about 26% to the earth grid impedance. An increase of the rod length to 10m is accompanied by a reduction of 44% of the original value of the earth grid impedance where no rods were added.

4.3.2 Effect of Rods Close to the Point of Injection

A 100mx100m 4-mesh grid was chosen for this study, the grid is buried at 1 m depth and injected with current through 2m downlead. The grid was modified by adding one rod 5m in length, the rod is located at the point of injection as recommended in the EA 41-24 as a "high frequency" electrode.

Figure 4.9 illustrates the frequency response of an earth grid with and without the "high frequency" electrode, for a low and high soil resistivity media (10Ωm, 10kΩm). For low soil resistivity, the addition of the rod has a very small effect on the frequency response of an earth grid and results in a reduction of less than 1%. For the high soil resistivity medium, the addition of the rod just below the injection point results in a slight reduction on the earth grid impedance for frequencies up to approximately 4MHz. Above 4MHz, the rod effect becomes more significant and produces a reduction of around 17% of the earth grid impedance at 8MHz.

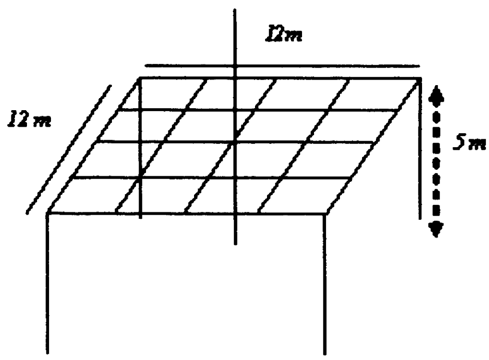

(a) 5 Rods

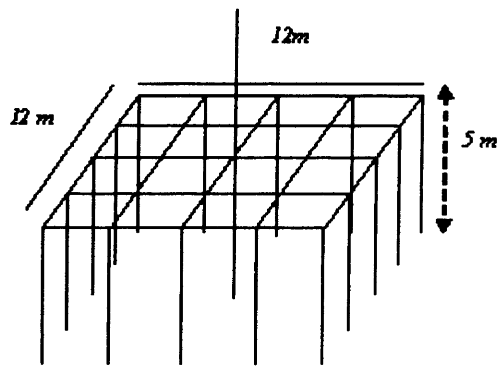

(b) 17 Rods

Figure 4.5 Earth grid configurations adopted for the rods study

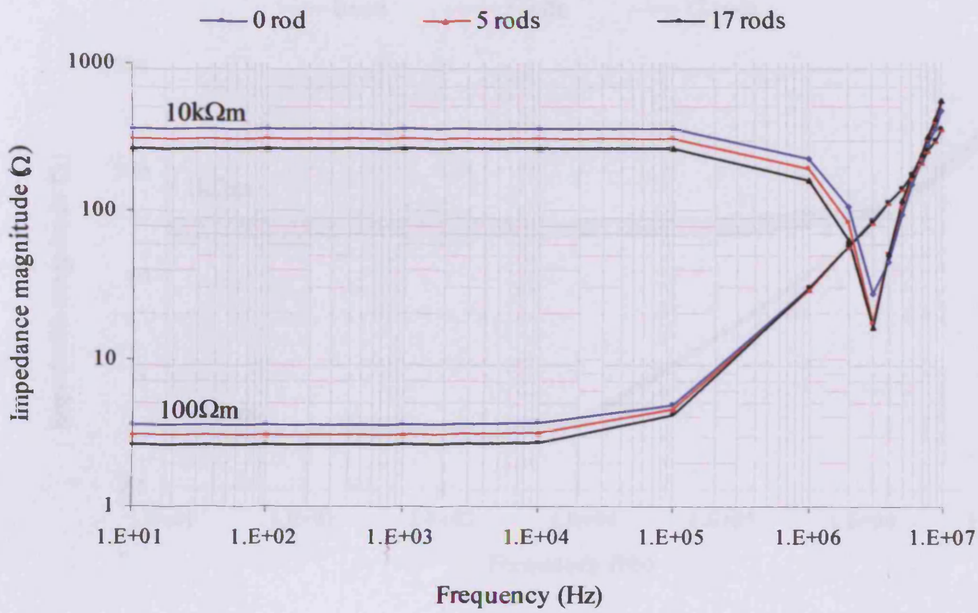

(a) Impedance magnitude (Ω)

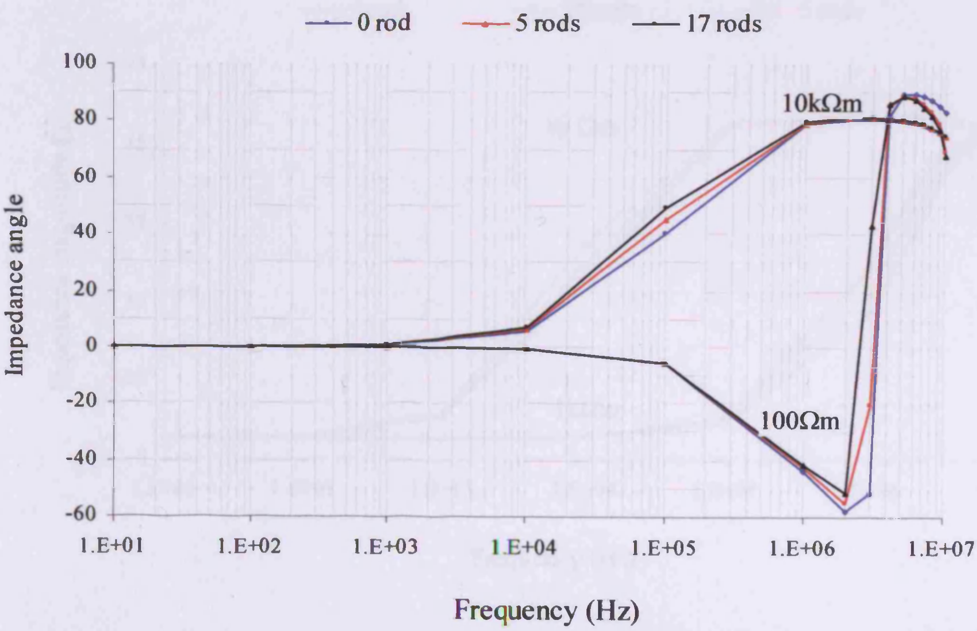

(b) Impedance angle (ϕ)

Figure 4.6 Effect of additional rods for 12mx12m 16-mesh grid (100Ωm and 10kΩm soil resistivity)

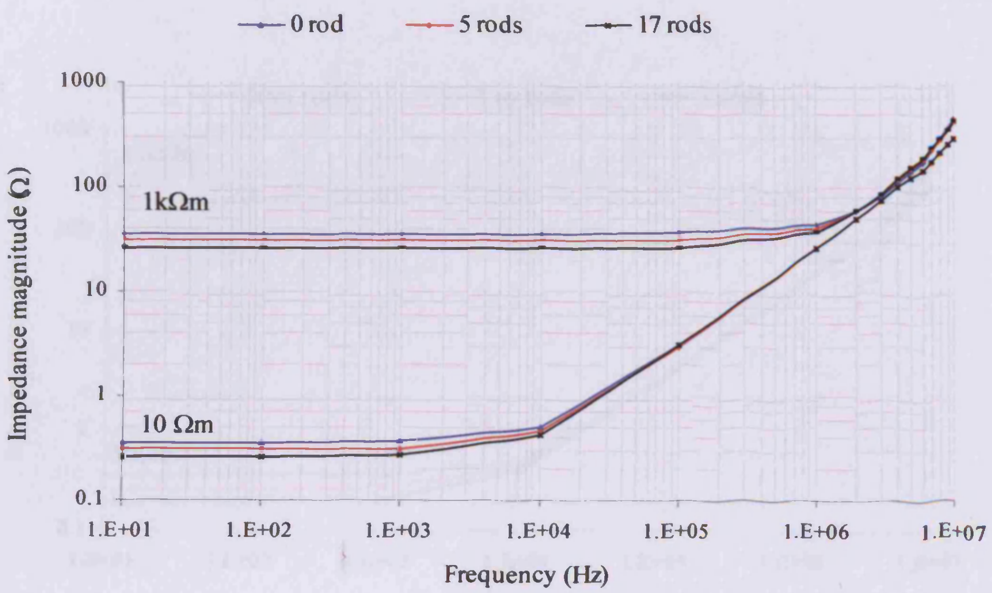

(a) Impedance magnitude (Ω)

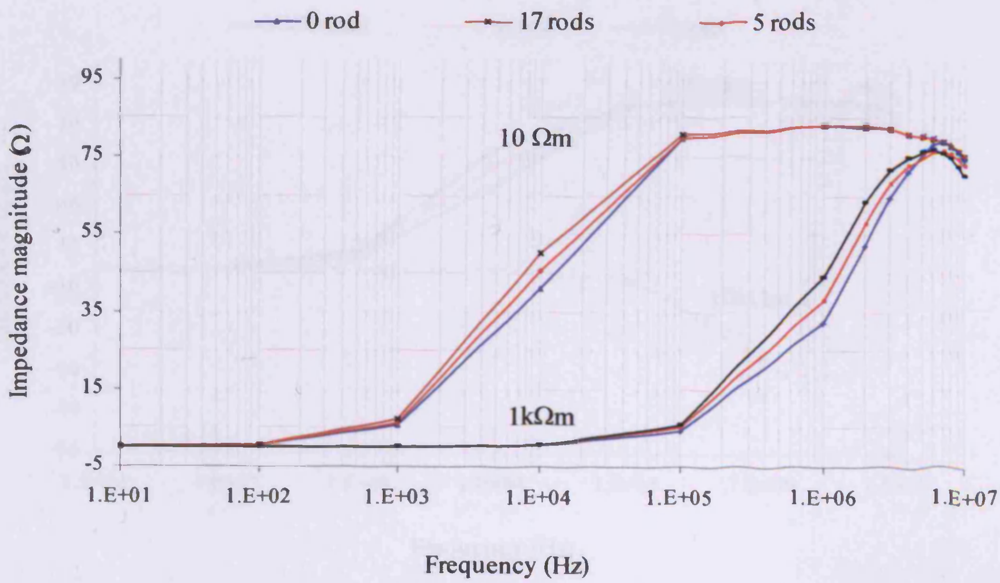

(b) Impedance angle (ϕ)

Figure 4.7 Effect of additional rods for 12mx12m 16-meshes grid

(10Ωm and 1 kΩm soil resistivity)

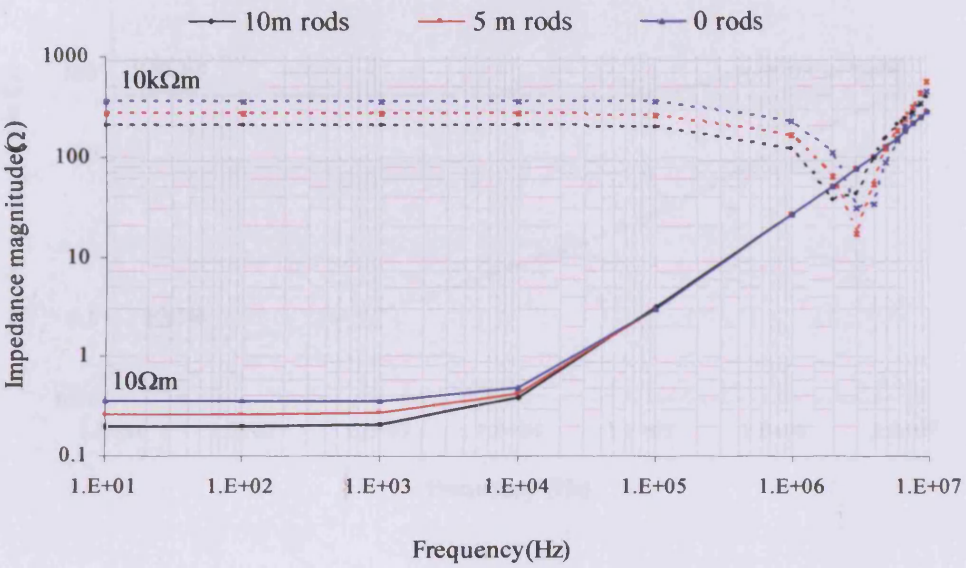

(a) Impedance magnitude (Ω)

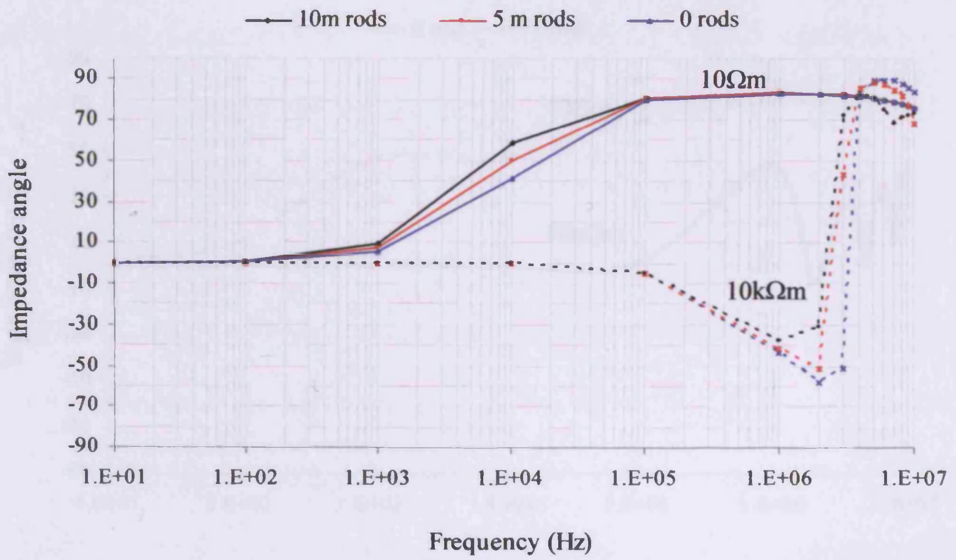

(b) Impedance angle (ϕ)

Figure 4.8 Effect of additional rods for 12mx12m 16-mesh grid with 5m and 10 m rods, (10Ωm and 10kΩm soil resistivity)

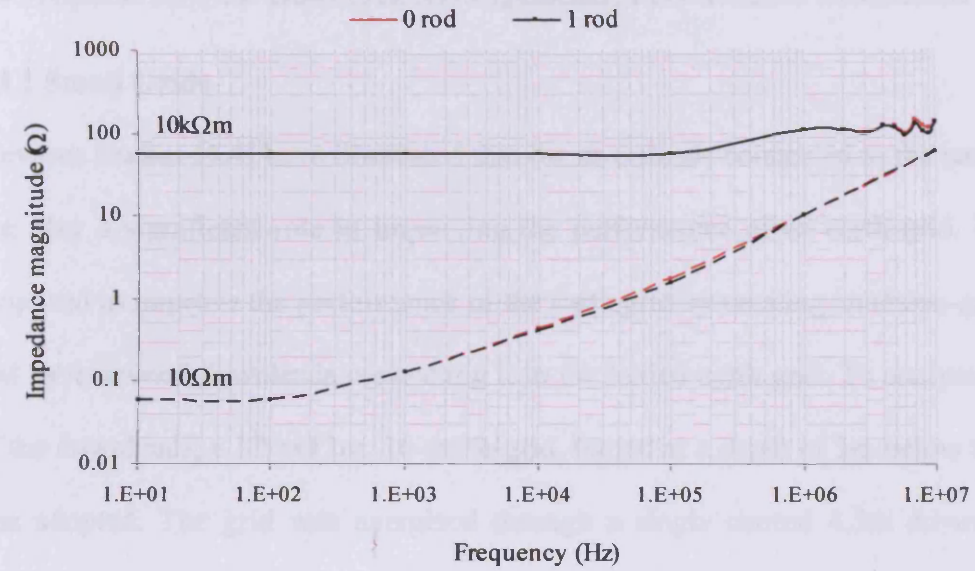

(a) Impedance magnitude (Ω)

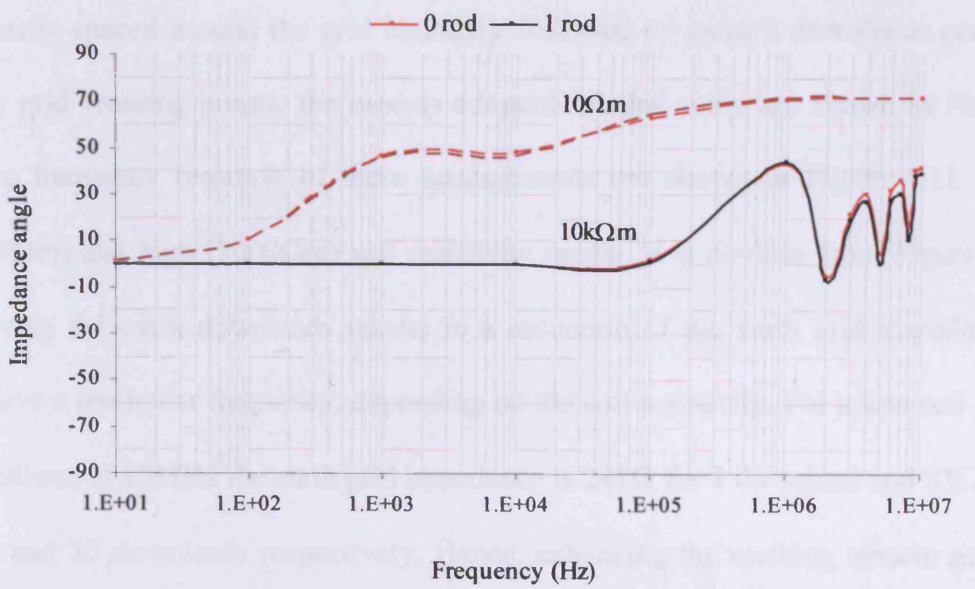

(b) Impedance angle (ϕ)

Figure 4.9 Performance of grids with and without "high frequency" Electrode [10Ωm and 10kΩm] ,(100m x 100m 4-mesh grid)

4.4 Proposal for New Downlead Arrangements: Performance Assessment

4.4.1 Small Grids

Previous studies [4.4] have illustrated that the downleads connected to the earthing grid can play a significant role in improving the performance of an earth grid. Here. It is proposed to improve the performance of the earth grid by creating an above-ground grid and have several downleads connecting it to the buried earth grid. To analyse the effect of the downleads, a 12mx12m, 16-mesh-grid, buried at a depth of 1m below the ground was adopted. The grid was energised through a single central 4.3m downlead. This arrangement was subsequently improved by adding a grid identical to the buried grid, 3m above ground, to increase the number of current paths to earth. These two grids were connected through two different sets of downleads. Firstly, 17 downleads were equally-spaced around the grid boundary followed by extra 8 downleads connected to the grid crossing points, the models adopted for this study are shown in Figure 4.10. The frequency response of these arrangements are shown in Figure 4.11 for a low (10Ωm) and high (1000Ωm) soil resistivity media. It is obvious from Figure 4.11 that having the extra downleads results in a reduction of the earth grid impedance value above a particular frequency, depending on the soil resistivity. For a low soil resistivity medium, at 10MHz the earth grid impedance is 241Ω for 1 downlead and 85Ω, 53Ω for 17 and 25 downleads respectively. Hence, enhancing the earthing system generated a reduction of approximately 65% in the case of the 17 downleads and 78% in the case of the 25 downleads. For a high soil resistivity medium, at 10MHz, enhancing the earthing system results in a reduction of about 87% in the case of the 17 downleads and 89 % in the case of the 25 downleads. These very large reductions can be explained by the reduction in the inductance between the point of injection and the grid as a results of increasing the number of downleads, therefore, increasing the current paths.

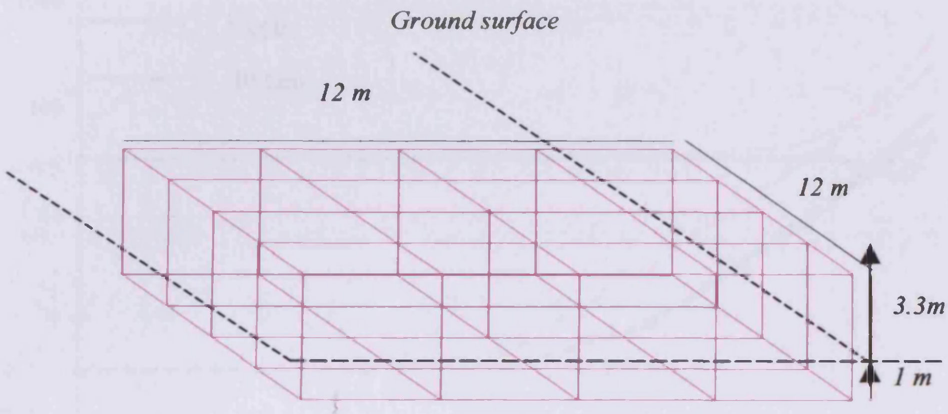

(a) 17 downleads

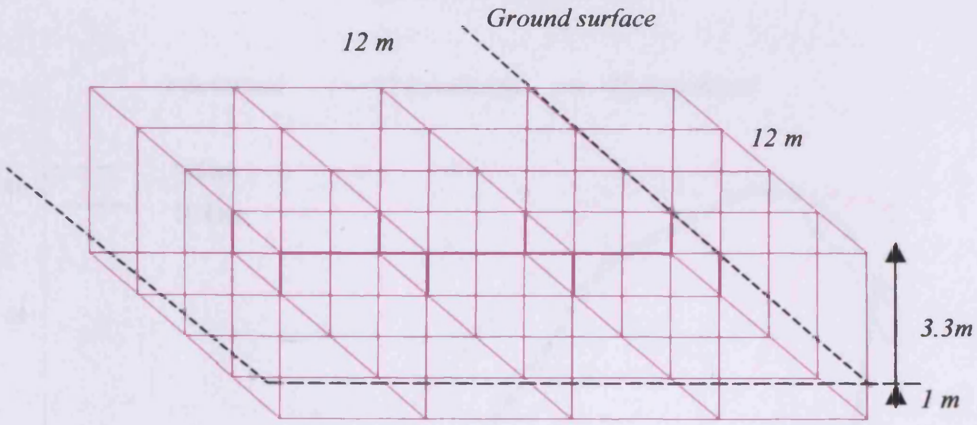

(b) 25 downleads

Figure 4.10 12mx12m grid, 16 meshes downleads arrangements

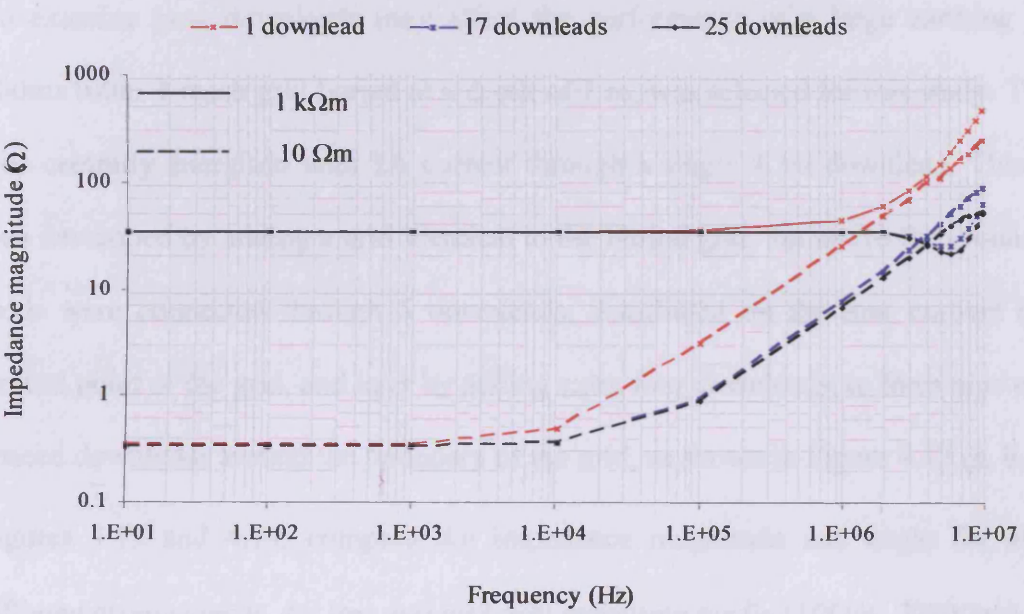

(a) **Impedance magnitude**

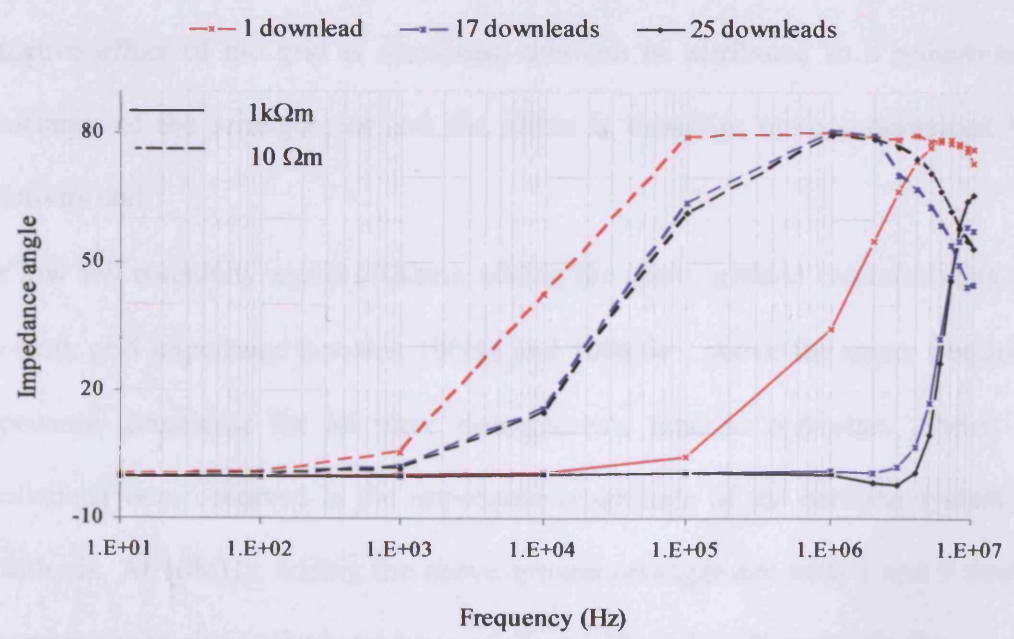

(b) Impedance angle (ϕ)

Figure 4.11 Effect of above-ground enhancements (12mx12m 16-meshes grid)

4.4.2 Large Grids

To examine how downleads may affect the performance of a large earthing grid, a 100mx100m 4-mesh grid buried at a depth of 1 m, was selected for this study. The grid was centrally energised with 1A current through a single 4.3m downlead. This model was developed by adding a grid identical to the buried grid, 3m above the ground. Both grids were connected through 5 downleads, distributed on the four corners and the central point of the grid, and later by adding extra four downleads, to form nine equally-spaced downleads around the boundary of the grid, as shown in Figure 4.12 (a, b, and c)

Figures 4.13 and 4.14, compare the impedance magnitude and angle for all three different arrangements, for low and high soil resistivity media (10Ωm, 1000Ωm).

It is evident that the addition of the above ground arrangements has an important effect in reducing the earth impedance for frequencies above the upturn frequency. Where the inductive effect of the grid is dominant, this can be attributed to a reduction in the inductance of the arrangement and the effect is therefore more pronounced for low resistivity soil.

For low soil resistivity media (10Ωm), adding the above ground enhancements reduces the earth grid impedance between 100Hz and 100kHz , above the upper frequency the impedance magnitude for all three arrangements tend to converge. Above 3MHz, oscillations were observed in the impedance magnitude of the earthing system with 9 downleads. At 10MHz, adding the above ground arrangement with 5 and 9 downleads generates a reduction in the impedance of about 21% and 25 % respectively.

In a high resistivity medium, a similar trend is observed, the above-ground arrangements results in a reduction in the earth impedance above 10kHz. At 10MHz, the above-ground arrangements with 5 and 9 downleads introduce reductions in the impedance of approximately 45% and 72 % respectively.

It is clear from Figure 3.13 and 3.14 that the earth grid impedance for the above-ground arrangements is higher than the impedance magnitude for grid with 1 downlead, in particular frequency range 600kHz to 2 MHz. Further investigations need to be conducted to explain the negative effect of the downleads arrangement on the earth grid impedance, over some particular frequency ranges.

4.4.3. Further Practical Improvement to the Proposed Above-Ground Arrangement with Downleads

The results shown in the previous section have clearly demonstrated that the above ground enhancements play a beneficial role in reducing the earth grid impedance, thus improving the performance of an earthing system. However, the previously- studied models are impractical, as it would be impossible to implement an overhead earthing system in a substation due to plant arrangements. To overcome this problem, alternative arrangements were adopted for this study. Instead of above ground mesh at 3m height, an identical installed grid just above the natural ground surface (6cm) is added (Figure 4.12.d). This makes it possible to bury the entire earthing system below the surface of the chippings. The grids are connected through short downleads distributed over all cross points and on the boundary of the grid.

Figure 4.15 presents the impedance magnitude and angle for different soil conditions, over a range of frequencies DC to 10MHz. As expected, the above ground arrangements result in a reduction of earth grid impedance. Above the upturn frequency, where the inductive effect becomes dominant, the effect of the above ground enhancement is greater in a low soil resistivity medium. For soil resistivity of 10Ωm, the effect of the above ground enhancements starts at 100Hz and continues for all higher frequencies. For example, at 1000Hz the above ground arrangements result in a reduction of 17 %, of the earth impedance. This reduction increases as the frequency increases, it reaches 27% at 10MHz. For high soil resistivity (10kΩm), the effect of the above ground starts at just over 100kHz and reaches its maximum at 1MHz, where adding the above ground enhancements produces a reduction of about 47%. This effect becomes smaller as the frequency increases, and the two curves will converge at higher frequencies.

4.5. Case Study: Effect of Interconnecting Earth Leads at Surge Arresters Bases

The effect of above-ground arrangement on the transferred potential is investigated using a small grid (6mx12m) with 8 meshes. Three downleads of 4m length are placed on the grid as shown in Figure 4.12 (e). This study is conducted with two stages; firstly, a 1A current is injected at the top of the central then the outer downlead without providing an interconnection between the three downleads. Secondly, the same study is repeated after connecting the three downleads. This study is conducted for a medium having 100Ωm soil resistivity and unity soil relative permittivity.

Figures 4.16 and 4.17 compare the frequency response of the potential observed from the injection point and the transferred potential per-unit-current at the other downleads for both central and outer injection points. Connecting the downleads in a substation, results in a significant reduction of the potential magnitude at the injection point. This occurs only above a particular frequency where the inductive effect becomes dominant.

At the same time, it increases the potential at the other downleads.

Figure 4.16 presents the case when the current is injected through one of the outer arresters. There is a considerable difference in the potential at the injection point and the potential at different downleads; for 10MHz, the potential at points 2 and 3 is about 18% and 11% (respectively) of the potential at the injection point. Connecting the downleads introduces a reduction in the potential at the injection point by approximately 27%, and an increase of around 235% and 340% for the potential at the other downleads in respect to the distance from the injection point. Therefore, the difference in potential at the injection point and the potential at a different downleads is less for 10MHz. The potential at downleads 2 and 3 is respectively 77% and 61% of the potential at the injection point.

Figure 4.12 shows the second case: when the injection point is central. It is obvious that the potential at the two outer downleads is symmetrical. As expected, the difference in the potential at the injection point and the potential at both outer downleads is still observed; for 10MHz, the potential is approximately 18% of the potential at the point of injection. Connecting the downleads introduces a 233% increase of the potential at both outer downleads, and an average reduction of 34% of the potential at the injection point over a range of frequencies higher than 100kHz. At 10MHz, connecting the downleads introduces a slight reduction in the potential at the point of injection, less than 1 %.

Although connecting downleads has a benefit in reducing the potential, and therefore, the earth impedance at the injection point, this comes with the disadvantage of transferring a higher potential over a larger area of the substation.

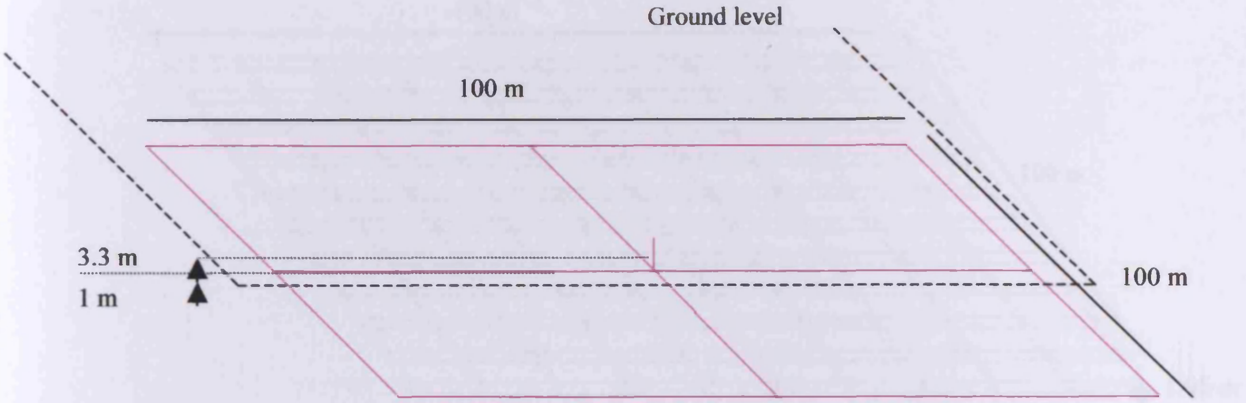

a) 100x100 me 4 meshes,

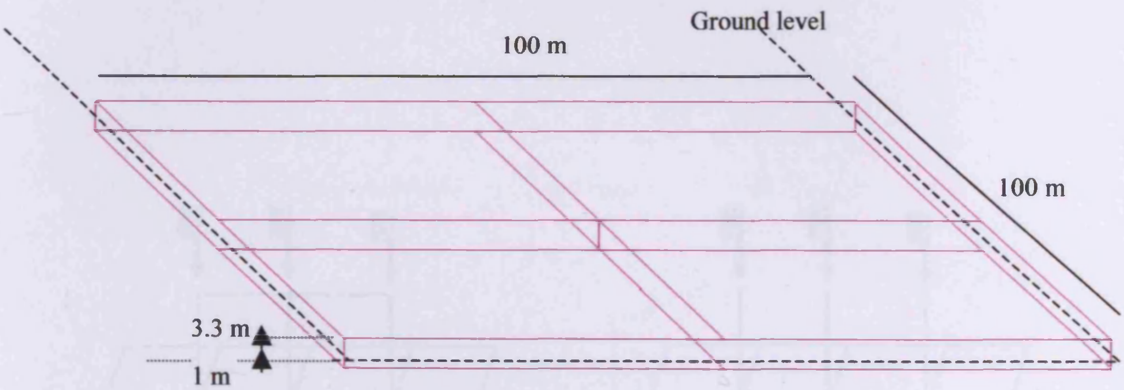

b)100x100 m -4 meshes grid with 5 downleads

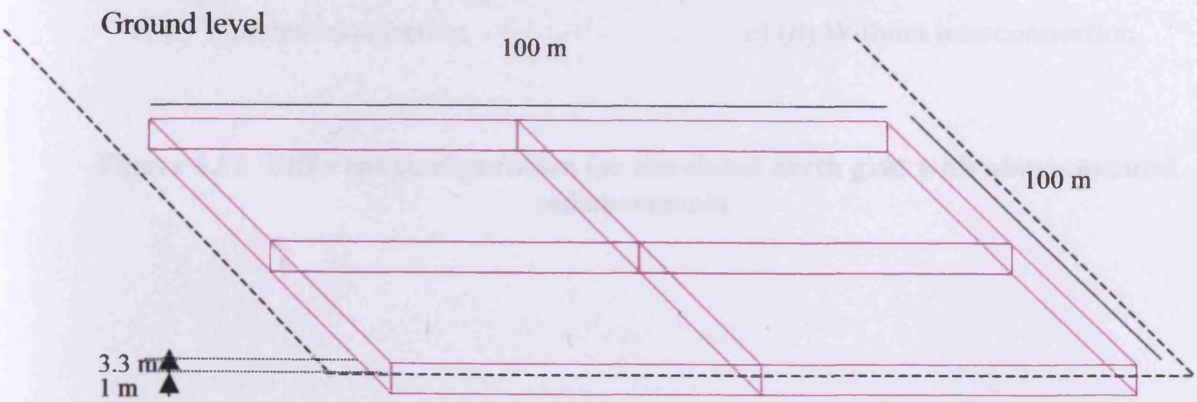

c) 100x100 m -4 meshes grid with 9 downleads

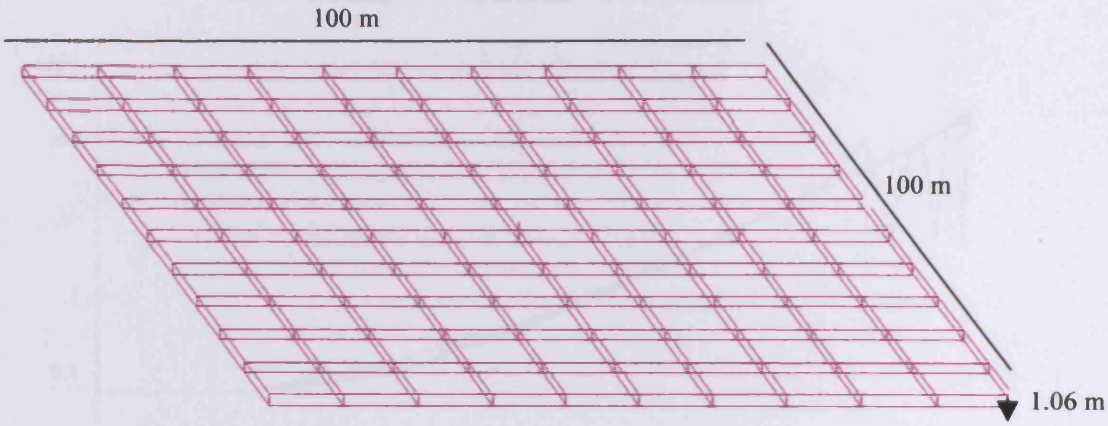

d) 100x100 m -100 mesh grid with downleads 6 cm in length

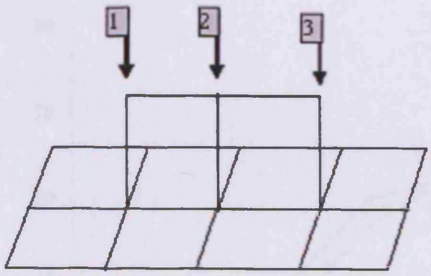

e) (*i*) With interconnection

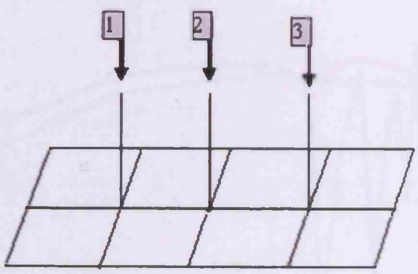

e) (*ii*) Without interconnection

Figure 4.12 Different configuration for simulated earth grid with above-ground enhancements

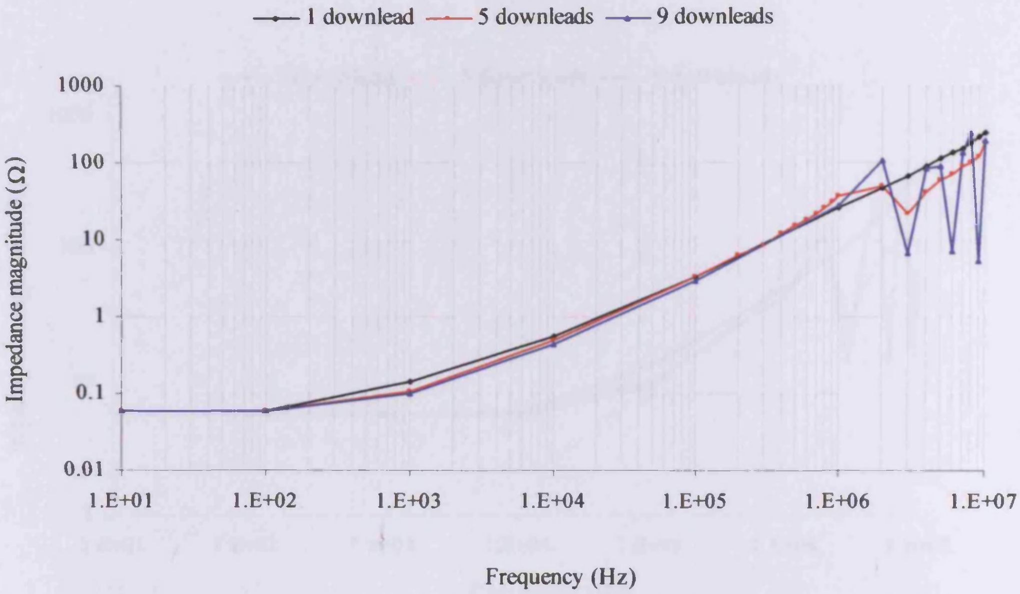

(a) Impedance magnitude

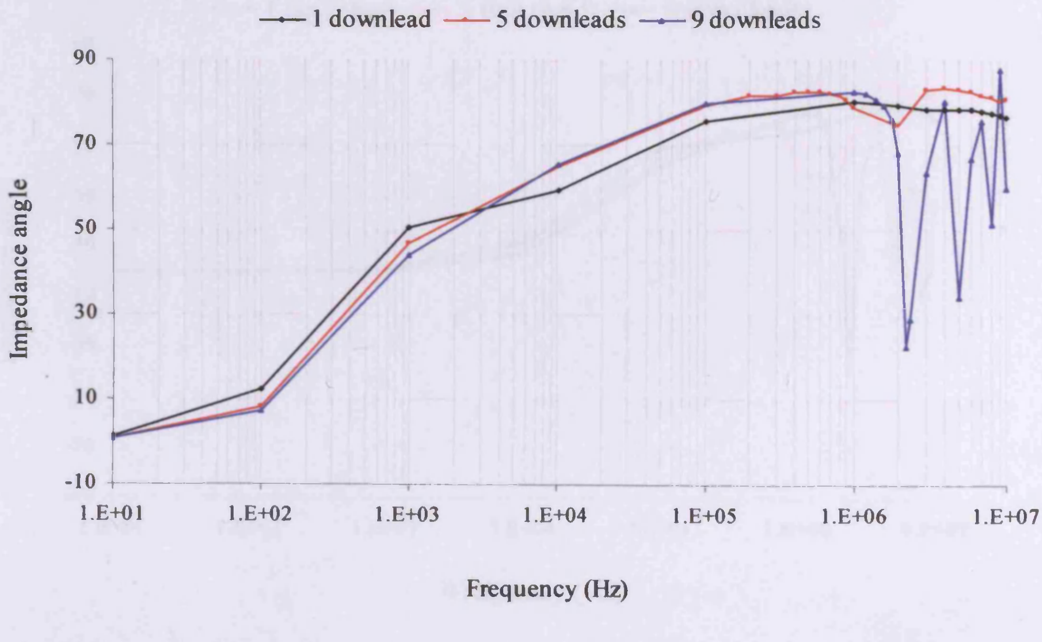

b) Impedance angle (ϕ)

Figure 4.13 Effect of above ground enhancements (100mx100m 4 Mesh Grid 10Ωm)

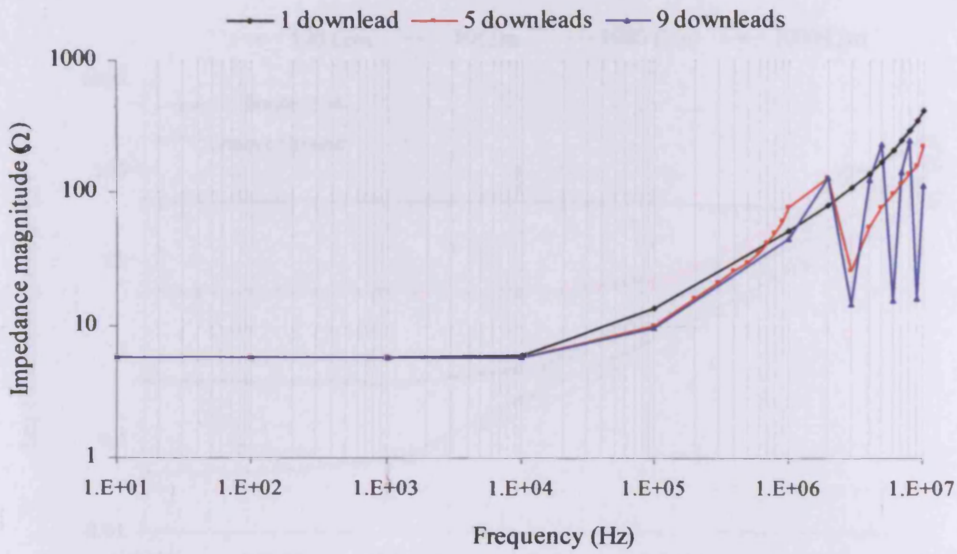

(a) **Impedance magnitude**

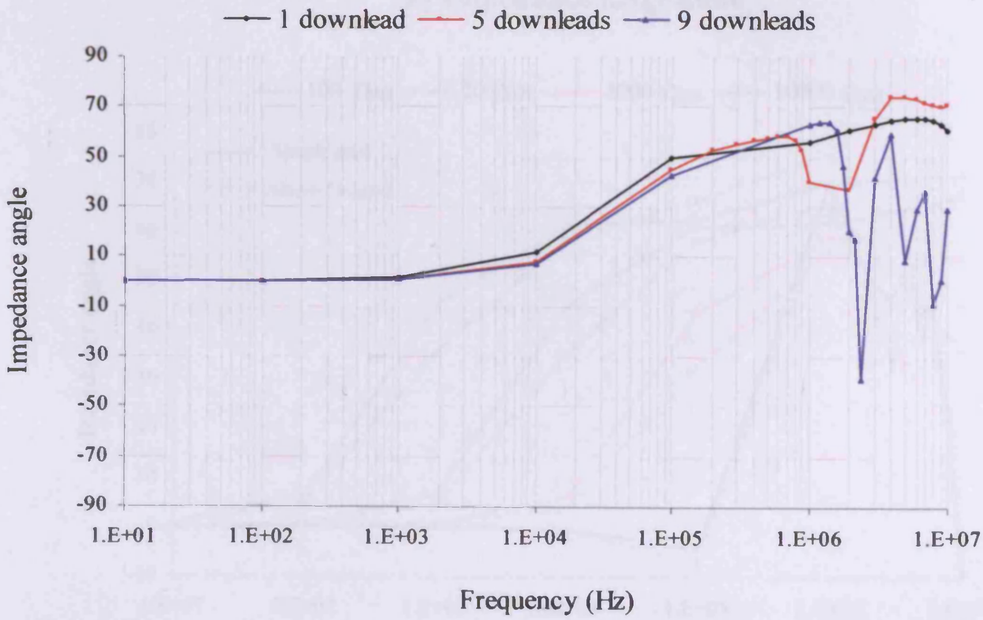

(a) Impedance angle (ϕ)

Figure 4.14 Effect of above ground enhancements (100mx100m 4 mesh grid 1 kΩm)

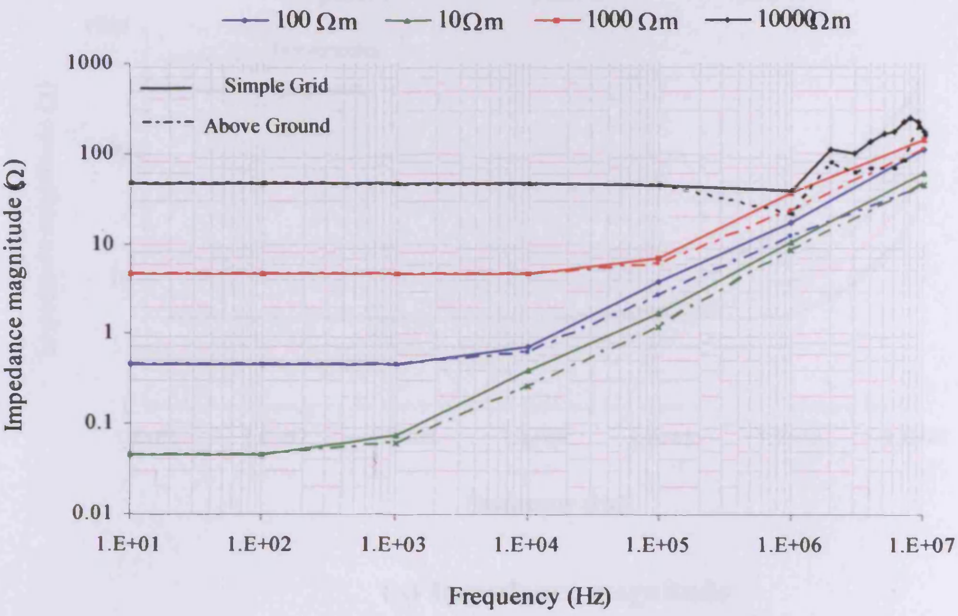

(a) Impedance magnitude

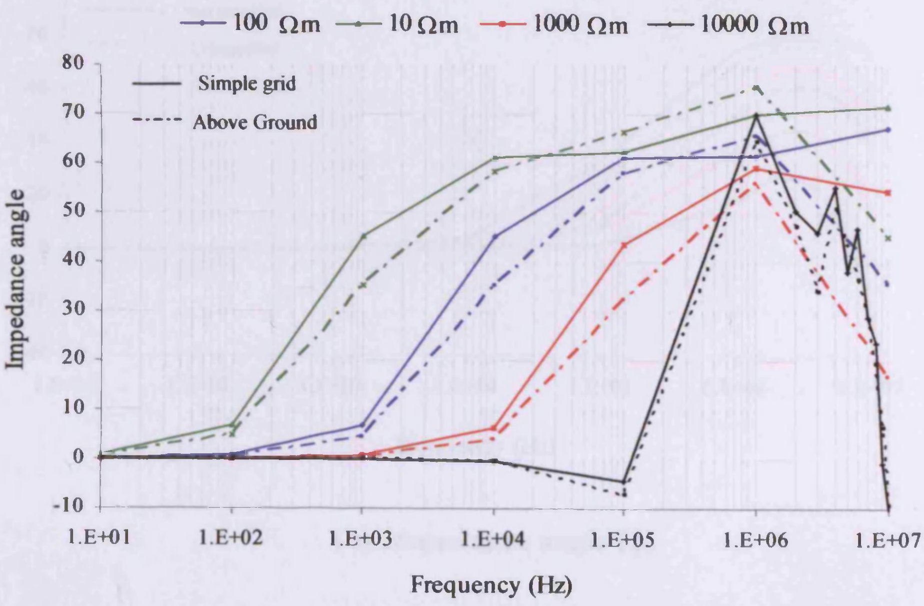

(b) Impedance angle (ϕ)

Figure 4.15 Effect of above ground enhancements for a 100mx100m 100 mesh grid with identical 6cm-above ground grid (different soil resistivity)

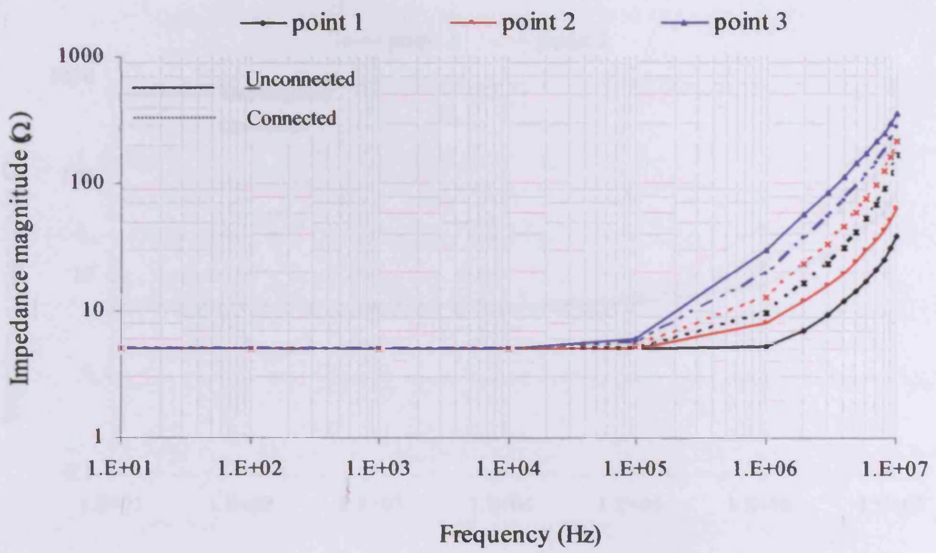

(a) Impedance magnitude

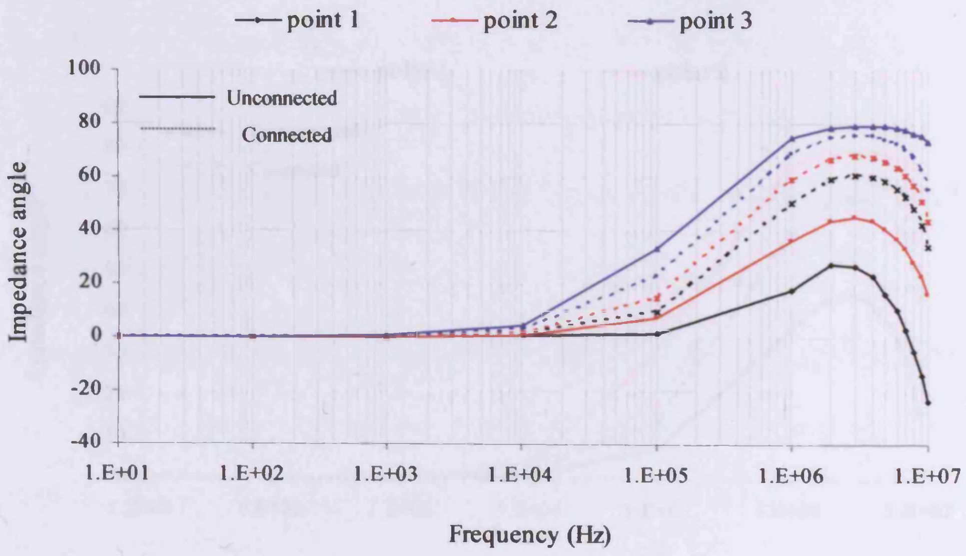

(b) Impedance angle (ϕ)

Figure 4.16 Effect of bonding surge arresters, current injected at location (3) for 100Ωm soil resistivity

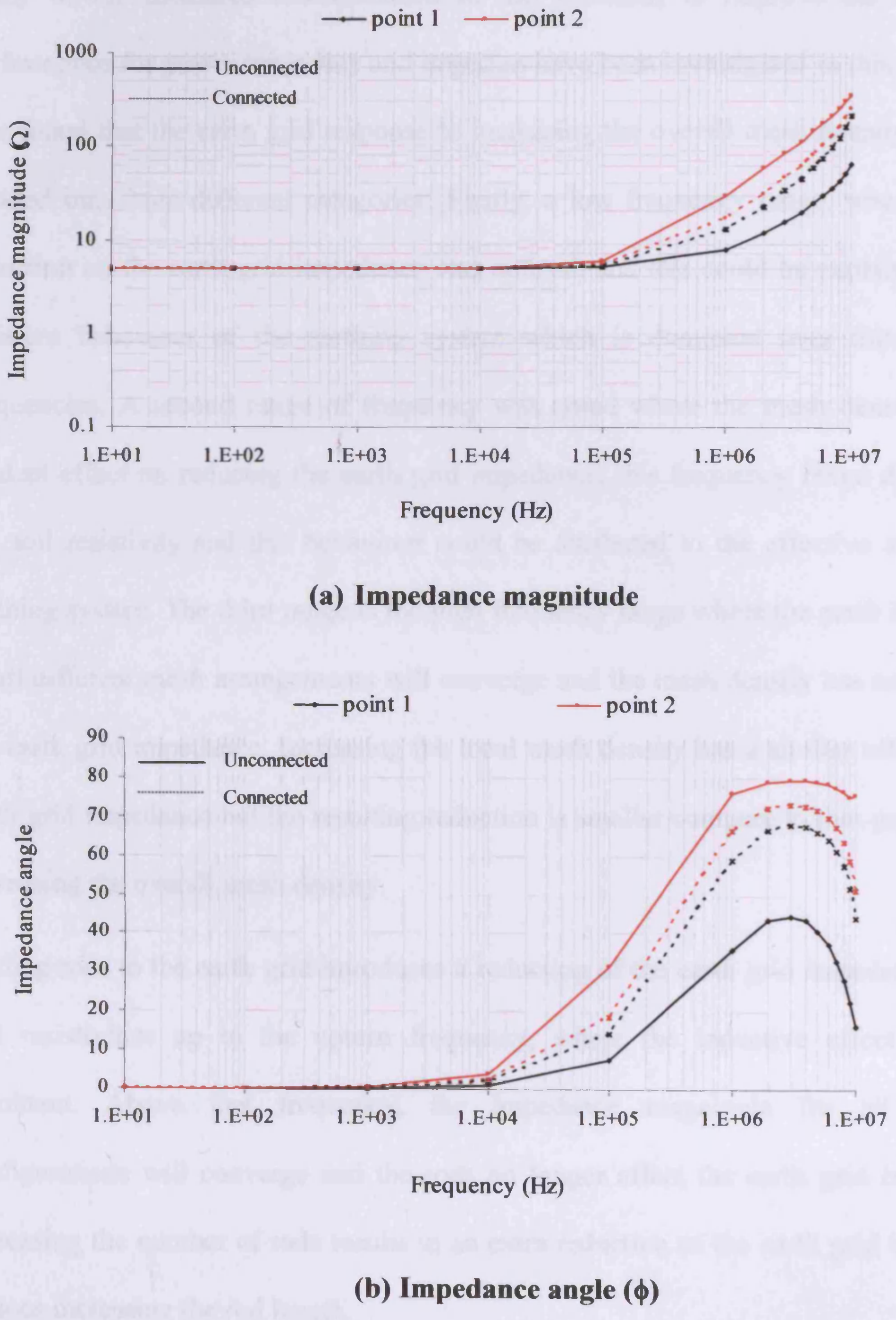

(a) Impedance magnitude

(b) Impedance angle (ϕ)

Figure 4.17 Effect of bonding surge arresters, current injected at location (2) for 100Ωm soil resistivity

4.6 Conclusions

Many of the measures recommended in the standards to improve the earth grid performance for power frequency and impulses have been investigated in this chapter. It was found that the earth grid response to increasing the overall mesh density could be divided into three different categories: Firstly, a low frequency range, where a small reduction on the earth grid impedance was noticed, and this could be explained by the resistive behaviour of the earthing system which is dominant over this range of frequencies. A second range of frequency was noted where the mesh density has an evident effect on reducing the earth grid impedance, this frequency range depends on the soil resistivity and this behaviour could be attributed to the effective area of the earthing system. The third range is the high frequency range where the earth impedance of all different mesh arrangements will converge and the mesh density has no effect on the earth grid impedance. Increasing the local mesh density has a similar effect on the earth grid impedance but the resulting reduction is smaller compare to that gained from increasing the overall mesh density.

Adding rods to the earth grid introduces a reduction of the earth grid impedance for all soil resistivities up to the upturn frequency, where the inductive effect becomes dominant. Above that frequency, the impedance magnitude for all different configurations will converge and the rods no longer affect the earth grid impedance. Increasing the number of rods results in an extra reduction of the earth grid impedance as does increasing the rod length.

A new proposal for enhancing earth grid systems is shown to play an important role in reducing the earth grid impedance for a small earthing grid above a particular frequency, depending on the soil resistivity. This may be explained by the impedance of the downlead itself which becomes dominant in the high frequency range. For a large earthing grid, the reduction in the earthing grid impedance occurs over a range of frequencies where the inductive effect is dominant. This is because, at these frequencies, the inductance of the earthing grid system is smaller. Therefore, the effect of downleads is more pronounced in low soil resistivity media. At high frequencies, the earth grid impedance of all arrangements tend to converge until oscillations start taking place at much higher frequencies above MHz.

A significant reduction of the potential, hence, the earth grid impedance, at the injection point is obtained by connecting the downleads above ground. However, this results in an increase in the transferred potential to a wider area around the injection point.

CHAPTER FIVE

Transient Performance of Earthing Systems

5.1 Introduction

A comprehensive parametric study of the frequency response of a number of earth electrode systems is investigated in Chapter Three. In Chapter Four techniques to improve the performance of earthing system under high frequency were investigated. In order to consider these measures for quantitative earth design guidelines, an extensive investigation has been carried out to study the earth grid performance under transient conditions caused by lightning and switching.

These lightning and switching impulse currents have short durations and the standard impulse shape can be described [5.1] by double-exponential time functions of the form

$$i(t) = I(e^{-\alpha t} - e^{-\beta t}) \qquad (5.1)$$

where I, α and β are positive constants that define the waveform. Impulse currents could also be described [5.2] by the front-time T_1 as defined in section 1.3, which is "the virtual parameter defined as 1.67 times the interval T between the instants when the impulse is 30% and 90% of the peak value", and the time, T_2, it takes for the wave tail to decay to 50% of the peak value.

The dispersal of impulse currents through the earthing system affects the power system in different ways. The high magnitude and fast rate of change of the currents mean that high voltages can occur in nearby metallic objects and structure. In addition, differences in soil surface potential may cause a safety risk, although these are very difficult to quantify accurately.

Many theoretical [5.3-5.26] and experimental studies [5.27-5.32] of the response of the earth electrode system to impulse currents have been published. These studies analyse vertical rods, horizontal electrodes substation grids and combinations of them. In these studies, a variety of impulse currents were considered and particular quantities determined such as the rise in potential of the earth electrode system, the electromagnetic field in the vicinity of the earth electrode and current distribution and dispersion. Electromagnetic, transmission-line and simple circuit models have been adopted in these investigations. In this chapter, the behaviour of earth electrode systems under standard lightning impulse current 8/20 was investigated, using a software developed for calculating electromagnetic fields (CDEGS)[5.33]. In order to analyse the impulse behaviour, it was necessary to use two components of the software FFTSES and HIFREQ. This analysis requires a minimum of three operations:

- Taking the Fast Fourier Transform of the current impulse wave form using FFT.
- Calculating the response of the earth electrode at each frequency recommended by the FFT using the HIFREQ.
- Calculating the Inverse Fourier Transform using IFT .

The transient ground potential rise (TGPR) was calculated for each electrode configuration at the mid-point of the energized segment. The energized lead was assumed to be 1 m above ground. The number of segments in the energized lead was kept constant (2 segments) so the transient ground potential rise was always calculated at 0.75 m above ground level on the energized lead. Because of inductive effects, it is expected that the TGPR will be higher for long above ground leads.

5.2 Effect of Soil Resistivity

5.2.1 Vertical and Horizontal Electrode

The time-domain behaviour of a 20m vertical rod buried at a depth of 1m was studied for different soil resistivities and a relative permittivity of 1. The vertical rod was subjected to a standard lightning impulse current of 8/20 shape having 1A peak value. Figure 5.1 illustrates the injected lightning impulse current 8/20 and the transient ground potential rise (TGPR) for a vertical rod for 100Ωm soil resistivity and relative permittivity of 1. The TGPR reaches its peak value at 6μs, about 2μs before the injected current impulse, the TGPR impulse is faster than the injected current which indicates that the inductive effect of the electrode is present.

Figure 5.2 presents the transient ground potential rise peak magnitude and front-time for four different values of soil resistivity 10Ωm to 10kΩm. As expected, the TGPR peak magnitude increases as the soil resistivity increases. A similar trend in the TGPR peak value was observed by Nixon [5.21] when a 1.8m driven rod, injected with 0.4/23 and 3.4/58 current impulse was investigated, for soils with 100 and 1000Ωm and constant relative permittivity. The transient ground potential rise front-time increases as the soil resistivity increases.

Figure 5.3 illustrates the TGPR peak magnitude and the front-time plotted as a function of soil resistivity for a 20m horizontal electrode buried at a depth of 1m. Both the peak magnitude and front-time have a similar trend to that found in the vertical rod, the TGPR peak magnitude increases as the soil resistivity increases and so does the front-time. Figure 5.4 (a and b) shows a comparison of the time domain behaviour of a 20m horizontal electrode and a 20m vertical electrode for two different soil resistivities (100Ωm and 10kΩm) . For both soil resistivities, it is clear that the TGPR for the horizontal electrode is much higher than that for the vertical rod. As shown in Figure 5.4(b) The TGPR peak magnitude, for 10kΩm, is about 720V for the horizontal electrode, while it is about 110V for the vertical rod. The front-time and TGPR peak magnitude are illustrated in Figures 5.5 and 5.6 for different soil resistivities. It is evident that, at low soil resistivity, the TGPR peak magnitude for the horizontal electrode is slightly higher than that for the vertical electrode. This difference increases as the soil resistivity increases. At 10kΩm, the TGPR peak for vertical rods is about 15% of the TGPR for the horizontal electrode.

It is clear from Figure 5.6 that the front-time for both vertical rod and horizontal electrode is less than the impulse current front-time (8μs), this indicates that the inductive effect is dominant for both electrode cases.

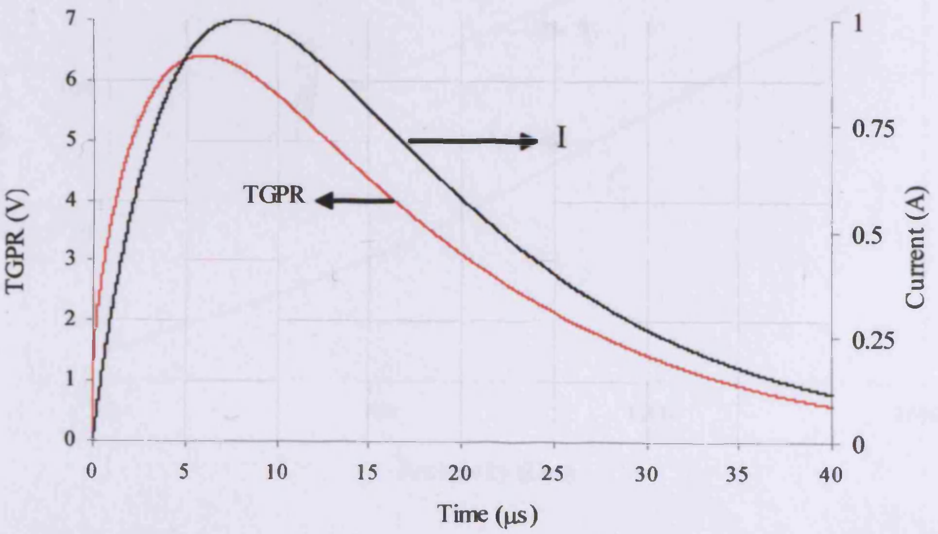

Figure 5.1 Transient ground potential rise (TGPR) of a 20m vertical rod injected with a 1A 8/20 current impulse (ρ=100Ωm and ε_r=1).

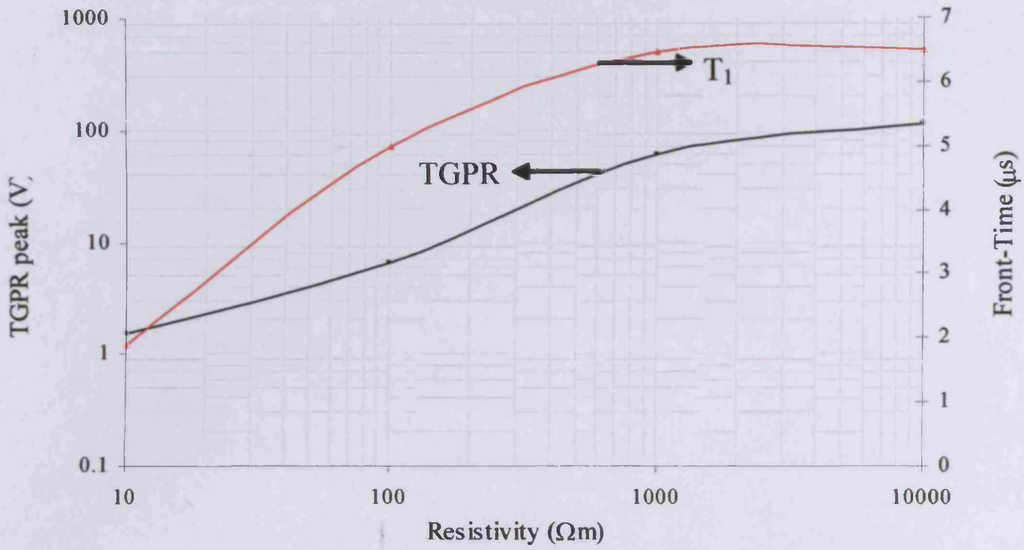

Figure 5.2 Effect of soil resistivity on the (TGPR) peak magnitude and front-time of a 20m vertical rod injected with a 1A 8/20 current impulse. (ε_r=1).

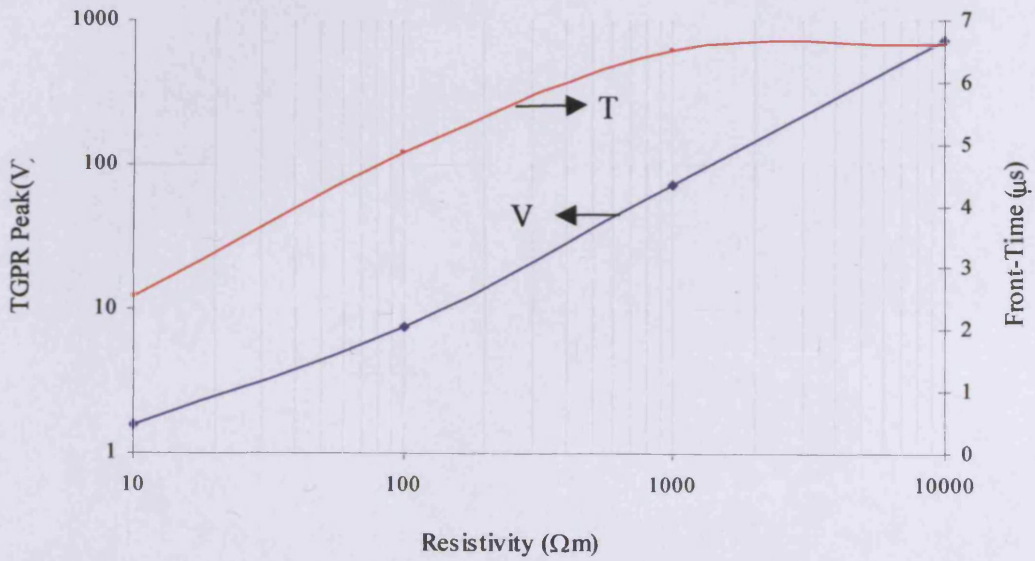

Figure 5.3 Effect of soil resistivity on the (TGPR) peak magnitude and front-time of a 20m horizontal electrode injected with a 1A 8/20 current impulse. (ε_r=1).

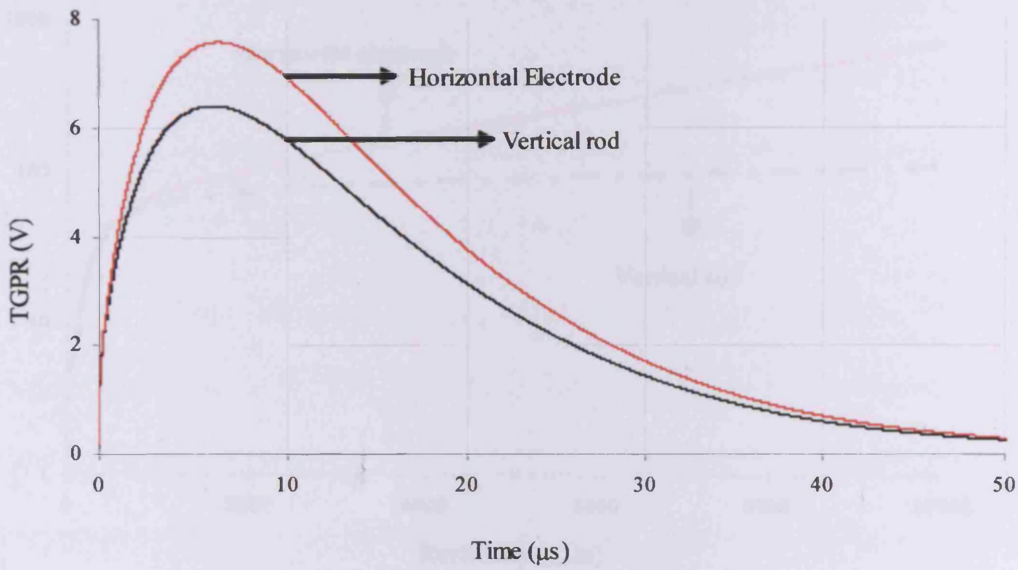

a) 100 Ωm, ε_r=1

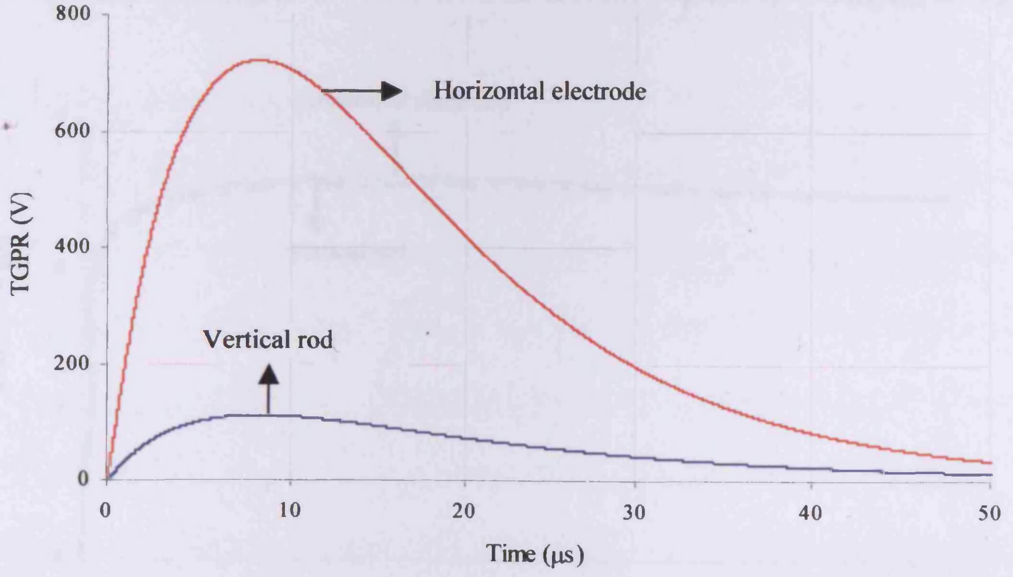

b) 10kΩm, ε_r=1

Figure 5.4 Response of a 20m horizontal electrode and 20 m vertical rod, both injected with a 1A 8/20 current impulse with different soil resistivities.

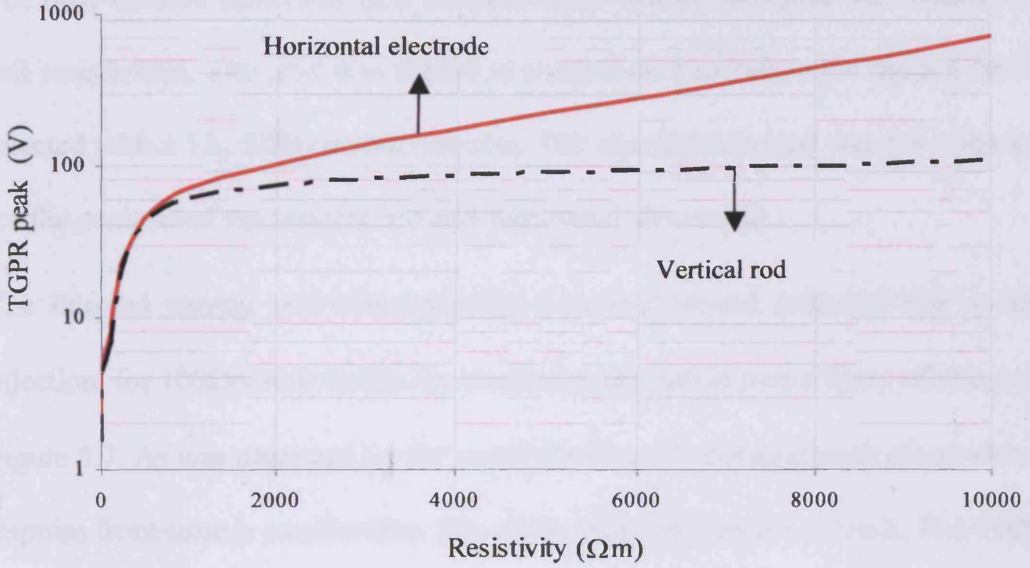

Figure 5.5 TGPR peak magnitudes of a 20m horizontal electrode and a 20 m vertical rod, both injected with a 1A 8/20 current impulse (ρ= 10kΩm, ε_r=1).

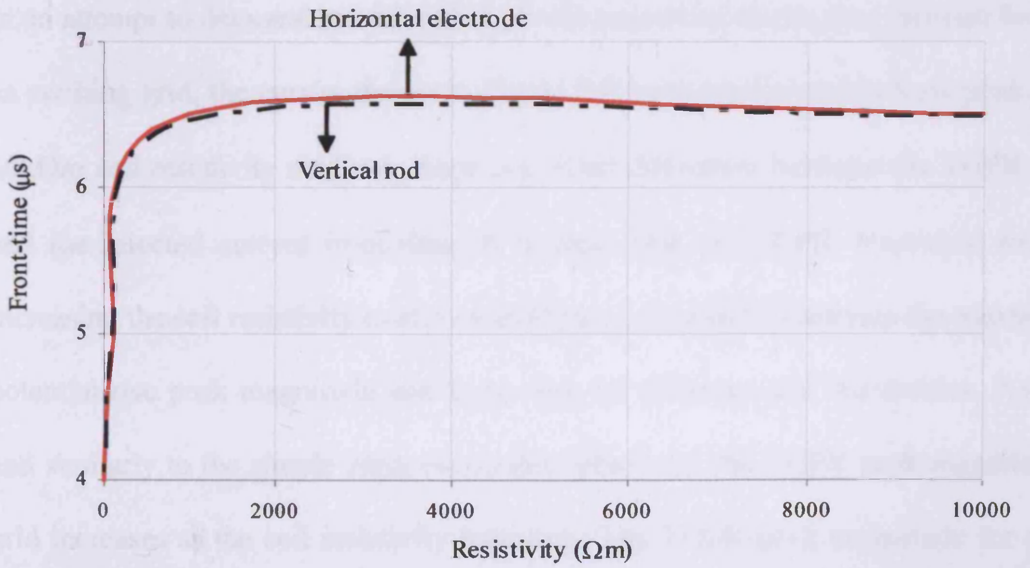

Figure 5.6 TGPR front-time of a 20m horizontal electrode and a 20 m vertical rod, both injected with a 1A 8/20μs current impulse (ρ= 10 kΩm, ε_r=1).

5.2.2 Earth Grid

The time-domain behaviour of a 100mx100m, 4-mesh earth grid was studied for different soil resistivities. The grid was buried at a depth of 1 m below the ground surface, it was injected with a 1A, 8/20 current impulse. The energisation lead was the same as that used for the analysis of the vertical rod and horizontal electrodes.

The injected current and corresponding transient ground potential rise at the point of injection, for 100Ωm soil resistivity medium and relative permittivity of one, are shown in Figure 5.7. As was observed for the vertical rod and horizontal earth electrodes, the TGPR impulse front-time is smaller than that of the injected impulse current. The TGPR impulse decreases rapidly compared with the injected impulse current. This behaviour indicates that the dominance of the electrode characteristics by an inductive effect. This fast decay of the grid TGPR has also been obtained by other authors [5.8-5.12, 5.16].

In an attempt to demonstrate the effect of soil resistivity on the time domain behaviour of an earthing grid, the curves shown in Figure 5.8 were normalised to their peak value. For 10kΩm soil resistivity medium, there is a small difference between the TGPR front-time and the injected current front-time. It is clear that the TGPR front-time increases by increasing the soil resistivity as shown in Figure 5.9, which illustrates the transient ground potential rise peak magnitude and front-time for different soil resistivities. As expected, and similarly to the simple earth electrodes behaviour, the TGPR peak magnitude for the grid increases as the soil resistivity increases. The TGPR peak magnitude for a grid in a medium of 10Ωm soil resistivity is about 0.9V. This magnitude increases gradually, and it is about 57.4V for a soil medium having a resistivity of 10kΩm.

5.3 Effect of Soil Permittivity

To investigate the effect of soil permittivity on the time-domain behaviour of a complex earthing system, a 100mx100m, 4-mesh earth grid was adopted. The grid was simulated for a wide range of soil resistivities (10-10000Ωm) and relative permittivities (1-50). The grid was buried at a depth of 1m below the ground surface, it was injected with a 1A, 8/20 current impulse, the energisation lead was the same as that used for the analysis of simple earth electrode.

Figure 5.10 presents the injected current and the resulting transient ground potential rise at the point of injection, for 10kΩm soil resistivity medium and different values of relative permittivity. It is clear that the transient ground potential rise magnitude decreases as the soil permittivity increases.

To analyse this effect in more detail, the TGPR peak magnitude and front-time for different soil conditions are plotted in Figures 5.11 and 5.12 respectively. It is obvious from Figure 5.11 that the soil permittivity has no effect on the TGPR peak magnitude in a medium of low soil resistivity above 1kΩm; increasing the soil relative permittivity has a significant effect on reducing the TGPR peak magnitude.

As seen in Figure 5.12, the TGPR front-time increases with the increase of relative permittivity. It is clear that for low soil resistivity and low relative permittivity, the TGPR front-time is smaller than that for an injected current indicating that the inductive effect of the earth grid is dominant at these soil conditions. For a 10kΩm soil resistivity and permittivity of 30 and above, the TGPR front-time is longer than that of the injected current, suggesting that a capacitive effect is dominant under these soil conditions, and that the changes in relative permittivity have a significant effect on the TGPR front-time. These results were published earlier during the course of this work [5.34].

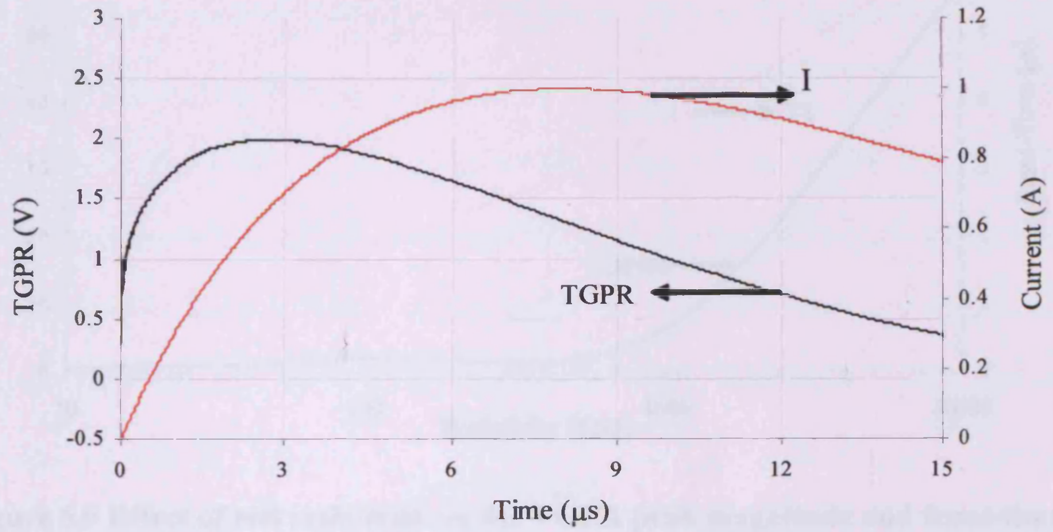

Figure 5.7 Transient ground potential rise of a 100mx100m, 4 mesh-grid injected with a 1A, 8/20 current impulse

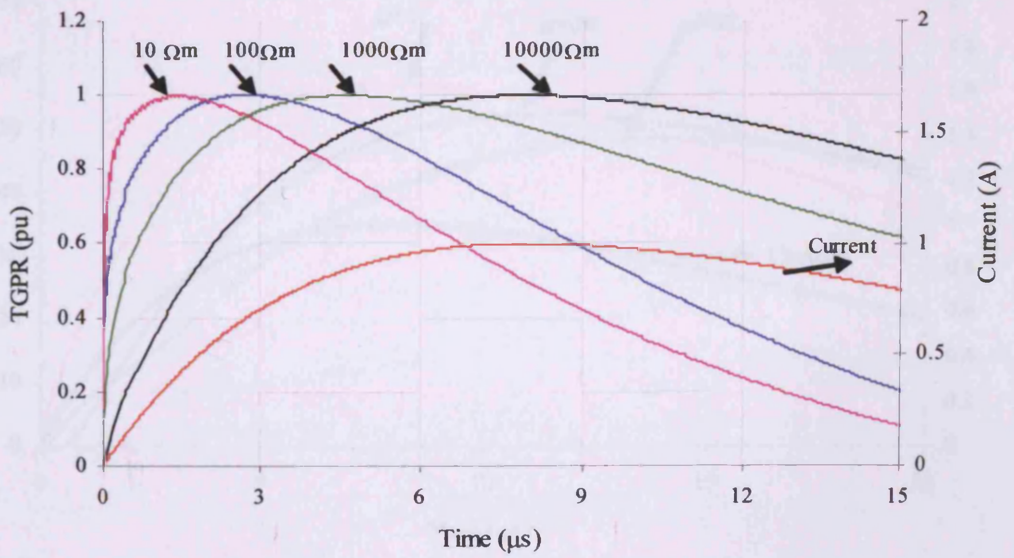

Figure 5.8 Effect of soil resistivity on the TGPR of a 100mx100m, 4 mesh-grid injected with a 1A, 8/20 current impulse, ε_r=1.

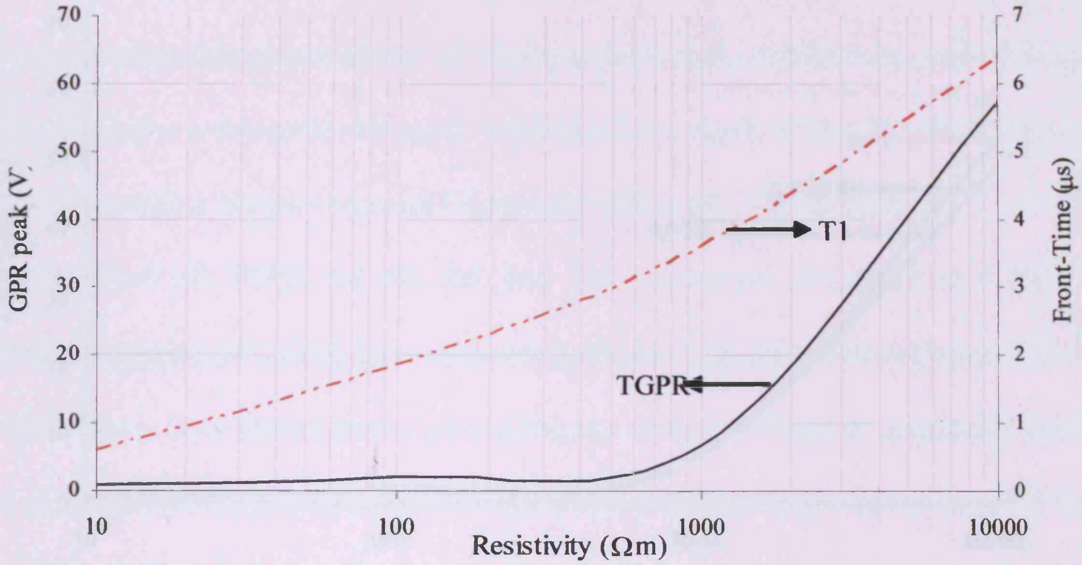

Figure 5.9 Effect of soil resistivity on the TGPR peak magnitude and front-time of 100mx100m, 4-mesh grid injected with a 1A, 8/20 current impulse, ε_r=1.

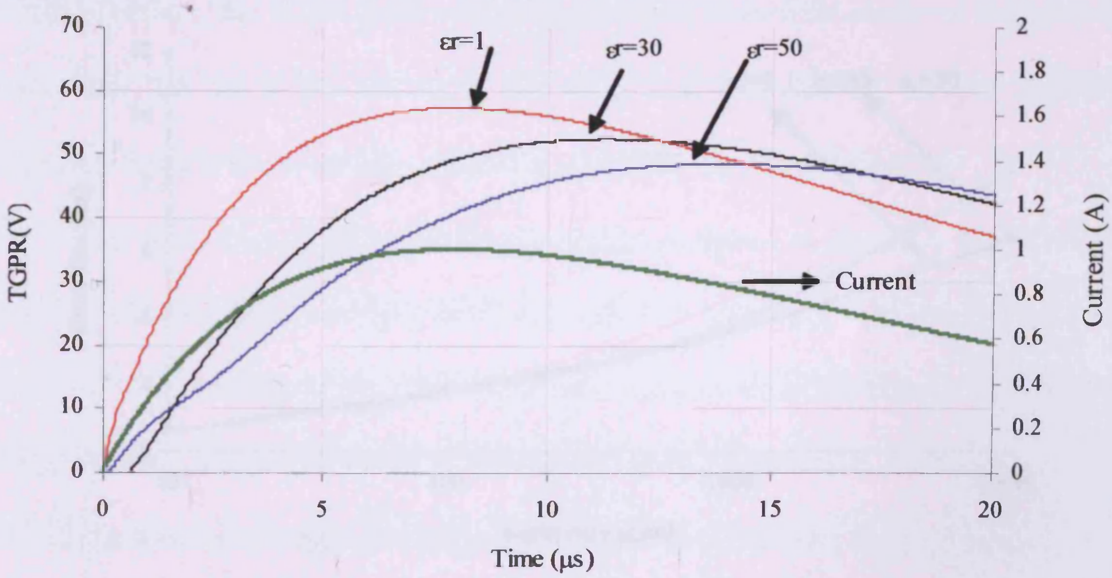

Figure 5.10 Effect of soil permittivity on the TGPR of 100mx100m, 4-mesh grid injected with a 1A, 8/20 current impulse, ρ=10kΩm

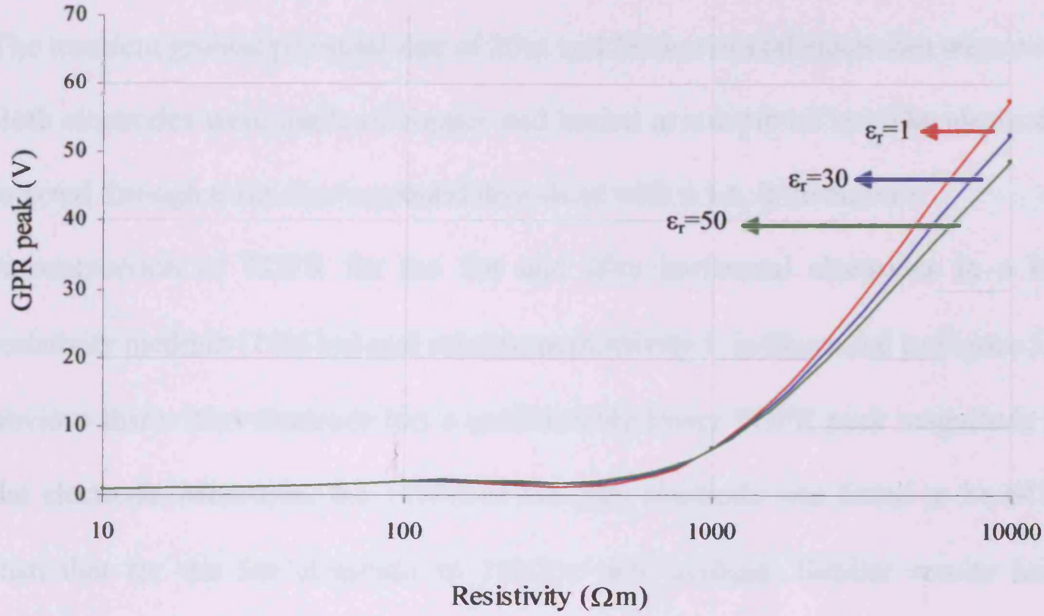

Figure 5.11 Effect of soil permittivity on the TGPR peak magnitude of 100mx100 m, 4-mesh grid injected with a 1A 8/20 current impulse.

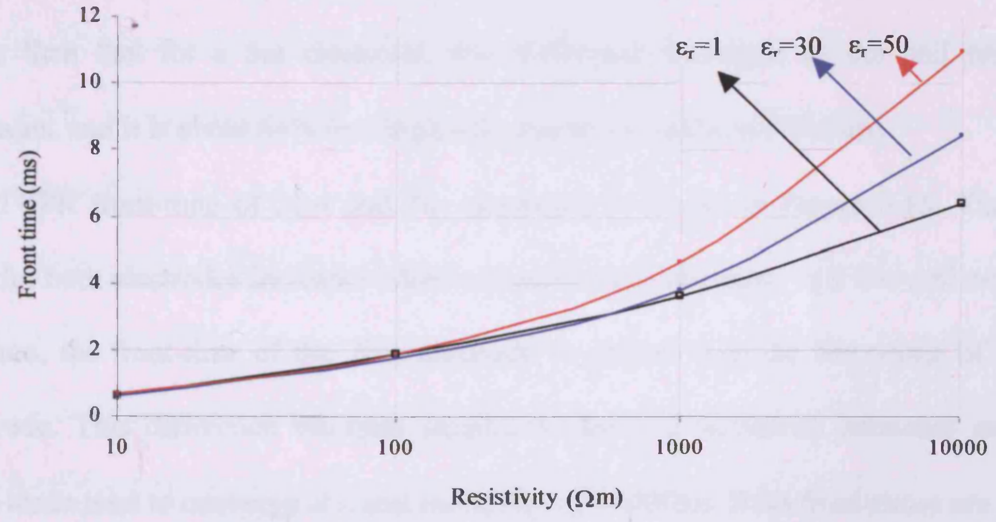

Figure 5.12 Effect of soil permittivity on the TGPR front-time of 100mx100m, 4-mesh grid injected with a 1A, 8/20 current impulse.

5.4 Effect of Extending Earthing System Dimensions

5.4.1 Horizontal Earth Electrode

The transient ground potential rise of 20m and 5m horizontal electrodes were compared. Both electrodes were made of copper and buried at a depth of 1m, The electrodes were injected through a 1m above-ground downlead with a 1A, 8/20 current.

A comparison of TGPR for the 5m and 20m horizontal electrodes in a high soil resistivity medium (10kΩm) and relative permittivity 1, is illustrated in Figure 5.13. It is obvious that a 20m electrode has a considerably lower TGPR peak magnitude than the 5m electrode. Moreover, the TGPR of the 20m electrode was found to be 64% lower than that for the 5m electrode in 10kΩm soil medium. Similar results have been observed earlier [5.4, 5.12, 5.34].

Figure 5.14 compares the transient ground potential rise peak magnitude of 20m and 5m horizontal electrodes for four different values of soil resistivity. In a low soil resistivity medium (10Ωm), the TGPR peak magnitude of a 20m horizontal electrode is about 40% lower than that for a 5m electrode, this difference increases as the soil resistivity increases, and it is about 64% in a high soil resistivity medium (10kΩm).

The TGPR front-time of 20m and 5m electrodes is shown in Figure 5.15. The front-time for both electrodes increases when soil resistivity increases. In a low soil resistivity medium, the front-time of the 20m electrode is shorter than the front-time of the 5m electrode. This difference becomes smaller as the soil resistivity increases and both front-times tend to converge at a soil resistivity of 1000Ωm. Both front-times are shorter than the injected current front-time.

5.4.2 Earth Grid

To investigate the effect of grid size on the time domain behaviour of an earthing system, a 4-mesh square grid of three different dimensions (10mx10m, 50mx50m, and 100mx100m) was adopted. The grids were buried at a depth of 1m and were centrally injected through 1m above-ground downlead with a current impulse of 8/20 shape and a peak value of 1A.

Figure 5.16 presents the TGPR peak magnitude as a function of the grid area for low and high soil resistivity (10Ωm, 10kΩm). In a low soil resistivity medium, increasing the grid area produces a very small reduction in peak TGPR. The peak TGPR of a 10mx10m grid is about 9% higher than that of a 100mx100m grid. In contrast, in a high soil resistivity medium, the grid size plays an important role. It is clear that increasing the grid size results in a significant reduction on the TGPR peak magnitude. A high reduction was achieved by increasing the grid size to 50mx50m, beyond this further increases in the grid size generate less reduction on the TGPR peak magnitude. For example, increasing the grid size from 10mx10m to 50mx50m produces a reduction of 76%, while increasing the grid size from 50x50m to 100x100m results in a further reduction of 47%.

These results indicate that there may be an effective area beyond which increasing the grid size has no effect or a very small effect on the performance of an earthing grid. This effective area may be in the order of $100m^2$ in low soil resistivity, while in high soil resistivity medium, the effective area could be higher than $2500m^2$. It is important to note that the transient effective area is different from that at single frequency, as discussed in Chapter Three. Similar results have been noted by other authors together with the effective area concept. [5.12, 5.13, 5.15, 5.35].

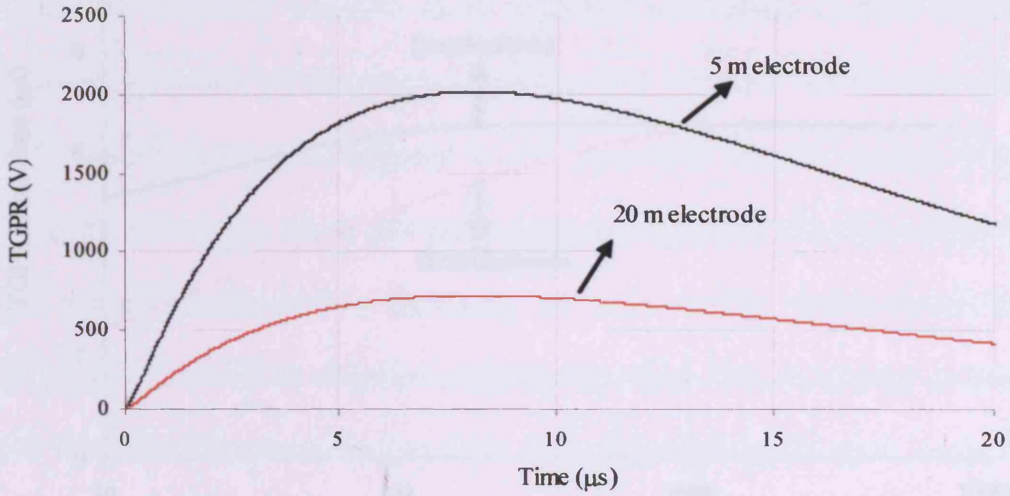

Figure 5.13 TGPR of a 20 m and a 5m horizontal electrodes, injected with 1A 8/20 current impulse, (ρ=10000Ωm, ε_r=1)

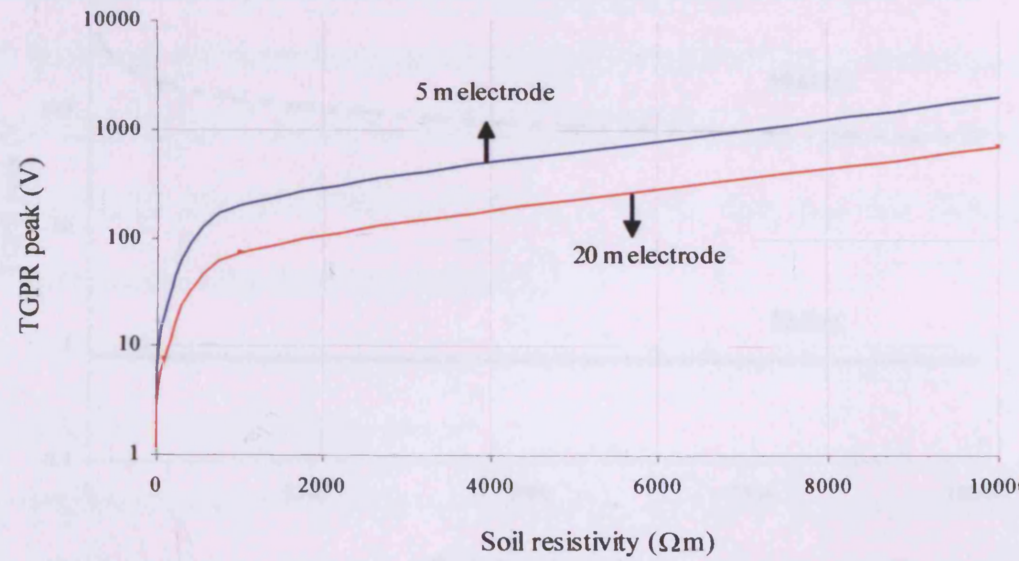

Figure 5.14 TGPR peak magnitude of a 20 m and a 5m horizontal electrodes, injected with 1A 8/20 current impulse, for different soil resistivities.(ε_r=1).

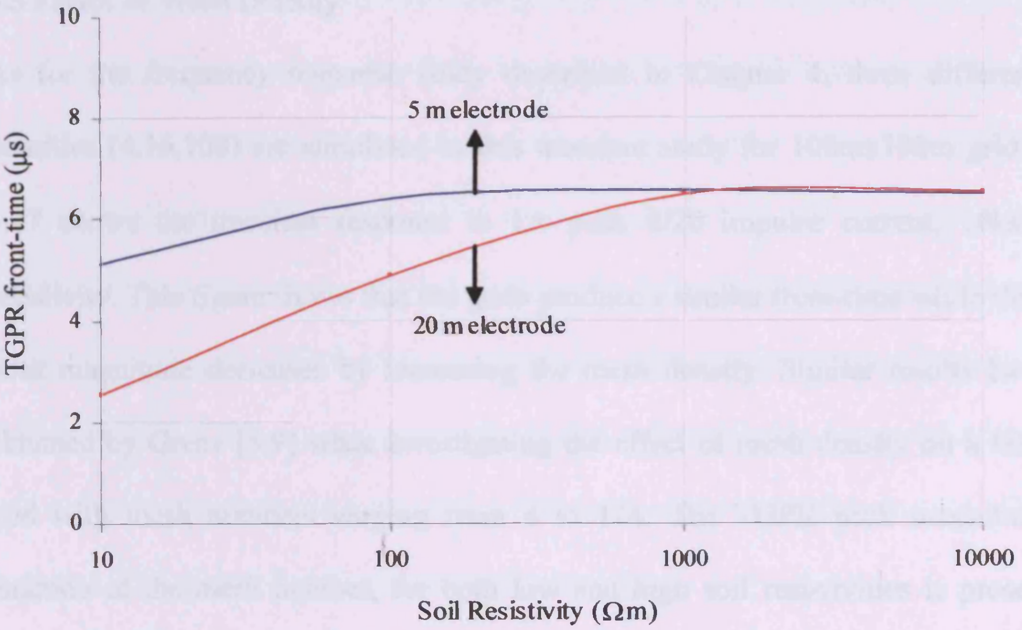

Figure 5.15 TGPR front-time of a 20m and a 5m horizontal electrodes, injected with a 1A 8/20 current impulse, for different soil resistivities (ε_r=1).

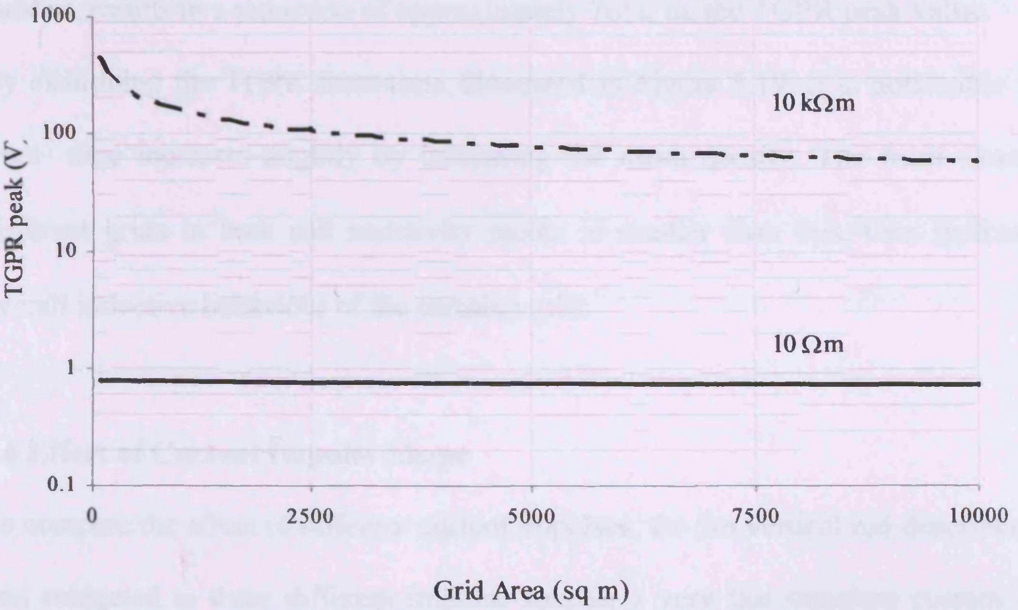

Figure 5.16 Effect of grid size on the TGPR peak magnitude of 4-mesh grid, injected with a 1A 8/20 current impulse, (ε_r=1).

5.5 Effect of Mesh Density

As for the frequency response study described in Chapter 4, three different mesh densities (4,16,100) are simulated in this transient study for 100mx100m grid. Figure 5.17 shows the transient response to 1A peak 8/20 impulse current, 10kΩm soil resistivity. This figure shows that the grids produce a similar front-time while the TGPR peak magnitude decreases by increasing the mesh density. Similar results have been obtained by Grecv [5.9] when investigating the effect of mesh density on a 60mx60m grid with mesh numbers varying from 4 to 124. The TGPR peak magnitude as a function of the mesh number, for both low and high soil resistivities is presented in Figure 5.18. In low soil resistivity, increasing the number of meshes results in a very small improvement on the TGPR peak magnitude, only a very small reduction could be seen. In a high soil resistivity medium, increasing the mesh density from 4 to 100 meshes, results in a reduction of approximately 76%, on the TGPR peak value.

By examining the TGPR front-time illustrated in Figure 5.19, it is noticeable that the front- time increases slightly by increasing the mesh density. The front–time for all different grids in both soil resistivity media is smaller than 8μs, thus indicating the overall inductive behaviour of the earthing grid.

5.6 Effect of Current Impulse Shape

To compare the effect of different current impulses, the 5m vertical rod described earlier was subjected to three different impulse shapes; a very fast transient current impulse 1/5, standard lightning current impulse 8/20 and a switching current impulse (30/80). Simulations were conducted for soil resistivity varying between 10Ωm and 10kΩm and a relative permittivity of 30.

Figure 5.20 shows the relationship between the TGPR peak magnitude and the impulse shape for the selected soil resistivities. As expected, the 30/80 current impulses produce a TGPR peak magnitude similar to the 8/20 current impulse studied in section 5.2. It was observed that the increase in TGPR peak magnitude with soil resistivity is less for a fast transient impulse current (1/5) than those for both relatively slow current impulses (8/20 and 30/80). The TGPR peak magnitude for a fast transient current impulse (1/5) is higher than for a slower current impulse in low soil resistivity, but it is lower in high soil resistivity medium, thus suggesting that both capacitive and inductive effects are more pronounced in a fast transient impulse current.

Figure 5.21 compares the TGPR front-time for the different current impulses. Front-times were normalised to the front-time of the injected current impulse shape. The increase of front-time with soil resistivity is less for slower current impulses. For 8/20 and 30/80 impulses, the front-time increases with soil resistivity but it does not exceed the front-time of the injected current impulse indicating that the inductive effect is dominant. For a fast current impulse 1/5, the voltage front-time increases with resistivity. For soil resistivity below 1kΩm, the inductive effect is dominant and the front-time is less than that of the injected current. However, for higher soil resistivity, the front-time exceeds that of the current impulse, and capacitive effects are dominant.

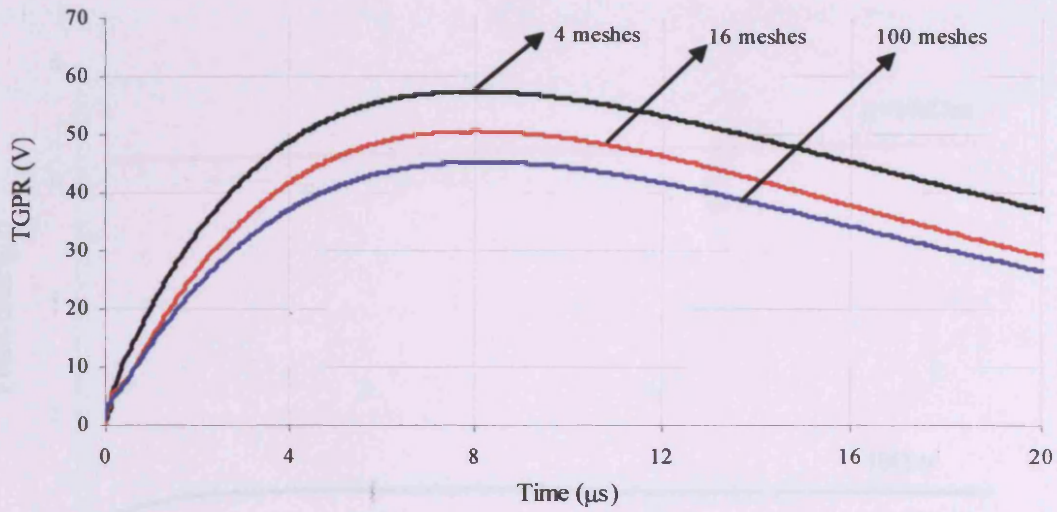

Figure 5.17 Effect of mesh density on the TGPR peak magnitude of 100x100m grid, injected with a 1A 8/20 current impulse, (ρ=10kΩm , ε_r=1).

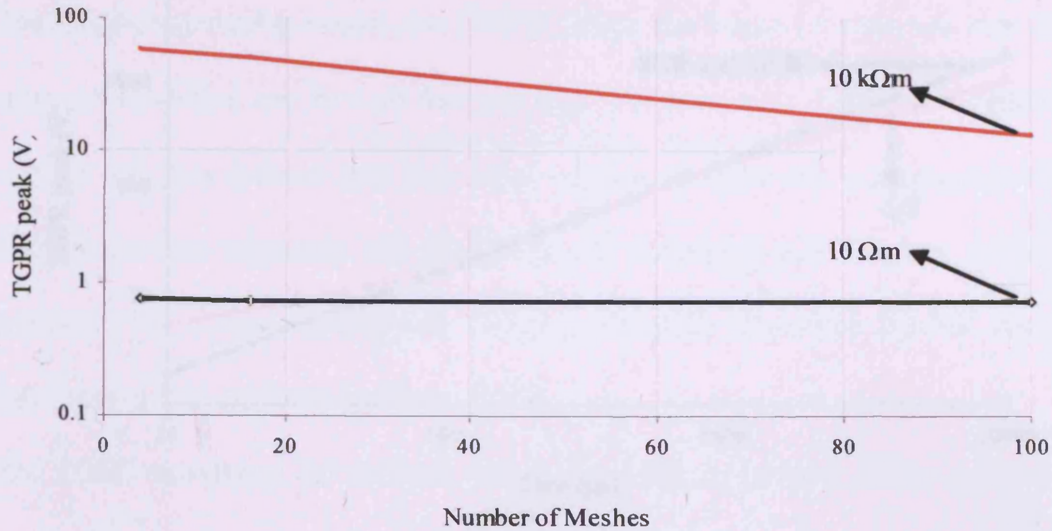

Figure 5.18 TGPR peak magnitude of 100mx100m grid, injected with a 1A 8/20 current impulse (ε_r=1).

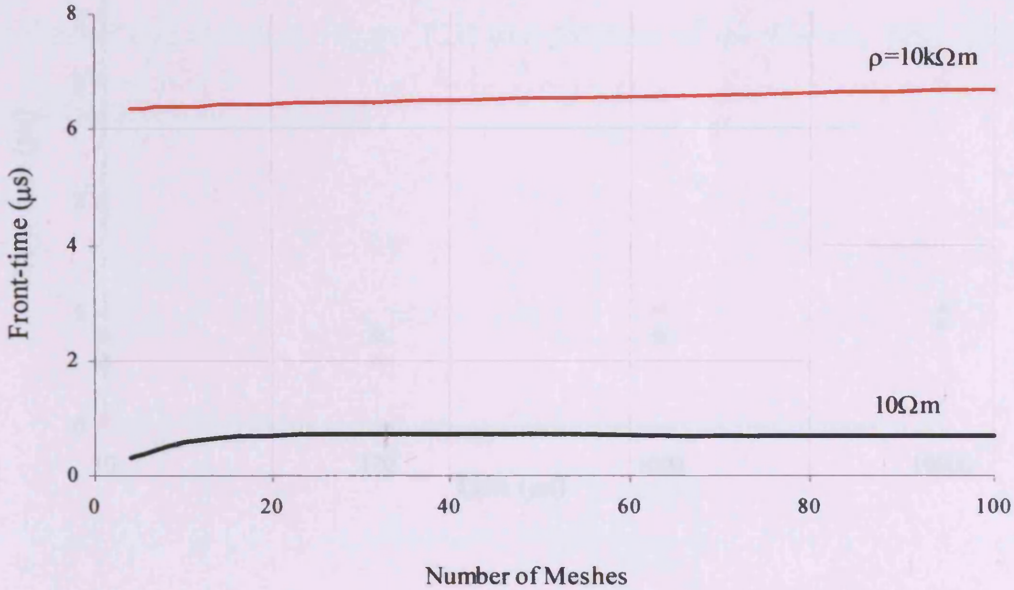

Figure 5.19 TGPR front-time of 100mx100m grid, injected with 1A 8/20 current impulse (ε_r=30)

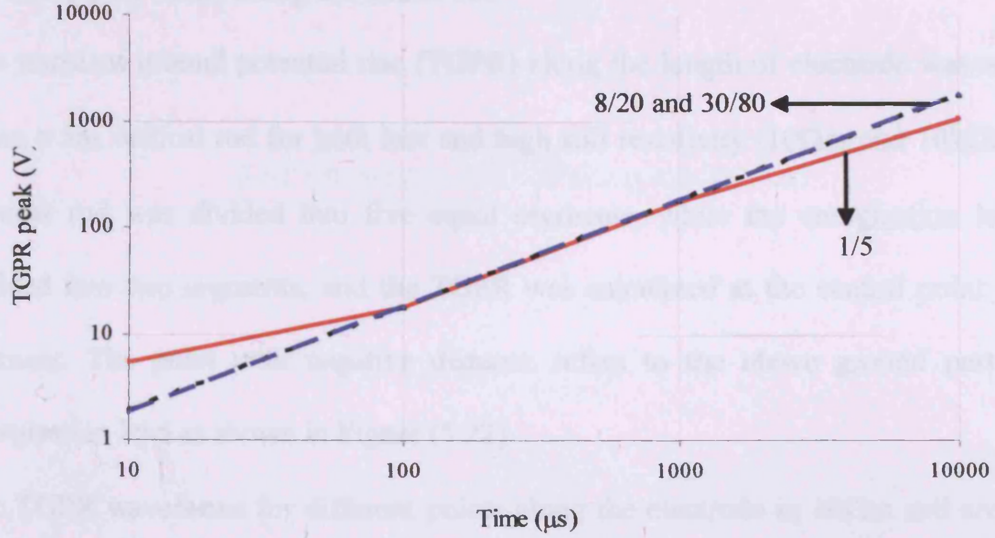

Figure 5.20 TGPR peak magnitude of the 5m vertical rod, injected with three different current impulses: 8/20, 30/80 and 1/5. (ε_r=30)

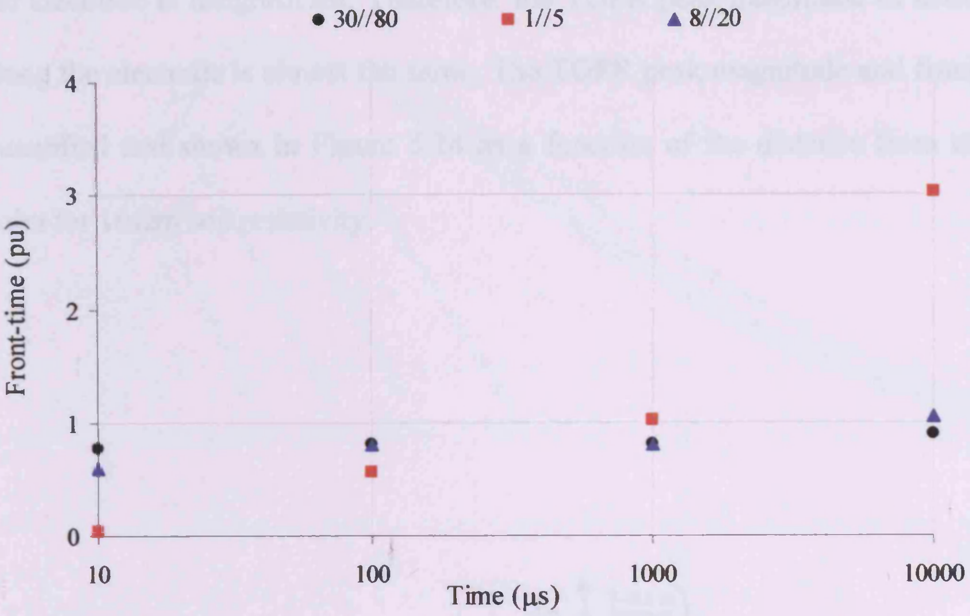

Figure 5.21 TGPR front-time of the 5m vertical rod, injected with three different current impulses 8/20, 30/80 and 1/5. (ε_r= 30)

5.7 Potential Profile along the Electrode

The transient ground potential rise (TGPR) along the length of electrode was analysed using a 5m vertical rod for both low and high soil resistivity (10Ωm and 10kΩm). The vertical rod was divided into five equal segments, while the energisation lead was divided into two segments, and the TGPR was calculated at the central point of each segment. The point with negative distance refers to the above ground part of the energisation lead as shown in Figure (5.22).

The TGPR waveforms for different points along the electrode in 10Ωm soil are shown in Figure 5.23. It is clear that the TGPR peak magnitude decreases, while the front-time increases with distance from the injection point. This behaviour could be attributed to the current leakage from electrode. For high soil resistivity (10kΩm), the leakage from the electrode is insignificant. Therefore, the TGPR peak magnitude of different points along the electrode is almost the same. The TGPR peak magnitude and front-time were quantified and shown in Figure 5.24 as a function of the distance from the injection point for 10Ωm soil resistivity.

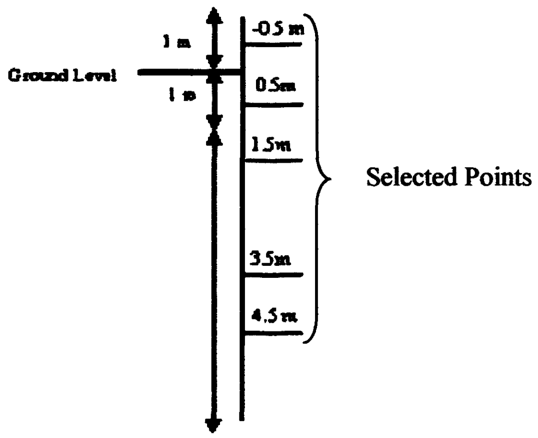

5.22 The points selected along vertical rod

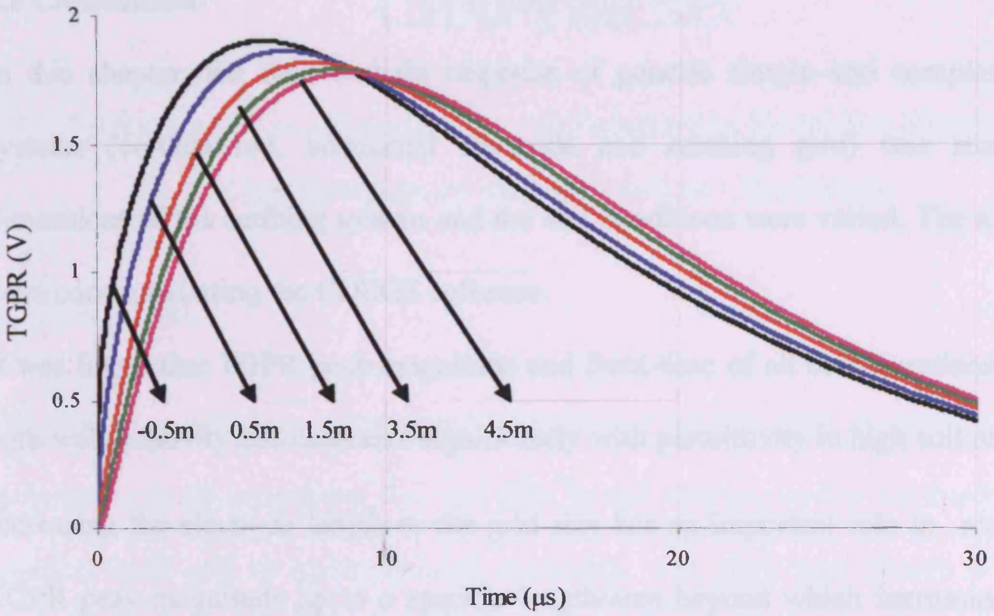

Figure 5.23 TGPR impulse shapes for different points along the 5m vertical rod, injected with a 1A 8/20 current impulse. (ρ=10Ωm ε_r= 1).

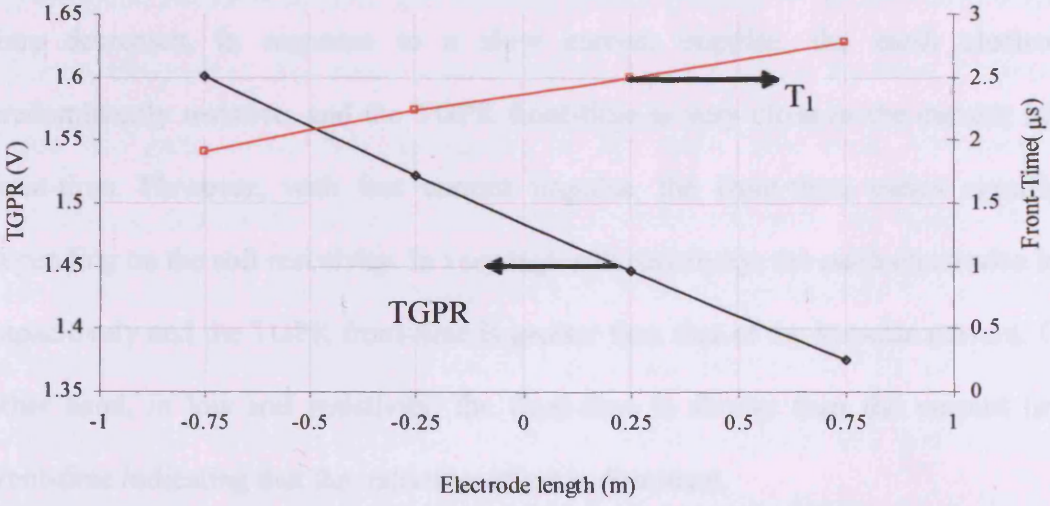

Figure 5.24 TGPR peak magnitude and front-time for different points along the 5m vertical rod, injected with a 1A 8/20 current impulse,(ρ=10Ωm and ε_r=1)

5.8 Conclusions

In this chapter, the time domain response of generic simple and complex earthing systems (vertical rod, horizontal electrode and earthing grid) was studied. The dimensions of the earthing system and the soil conditions were varied. The simulations were conducted using the CDEGS software.

It was found that TGPR peak magnitude and front-time of all configurations increases with soil resistivity and decreases significantly with permittivity in high soil resistivity.

Increasing the electrode length or the grid size has an important role in reducing the TGPR peak magnitude up to a specific length/area beyond which increasing the size will no longer affect the TGPR peak magnitude .

In low soil resistivity, TGPR peak magnitude increases as the front-time of the current impulse decreases, while in high soil resistivity it decreases as the impulse current front-time decreases. In response to a slow current impulse, the earth electrode is predominantly resistive, and the TGPR front-time is very close to the current impulse front-time. However, with fast current impulse, the front-time varies significantly depending on the soil resistivity. In very high soil resistivity, the earth electrodes behave capacitively and the TGPR front-time is greater than that of the impulse current. On the other hand, in low soil resistivity, the front-time is shorter than the current impulse front-time indicating that the inductive effect is dominant.

A potential profile along the electrode was investigated. It was found that, in low soil resistivity, the TGPR peak magnitude decreases and the front-time increases with distance from the injection point. However, in medium to high soil resistivity, the TGPR peak magnitude was found to be constant along the length of the electrode.

CHAPTER SIX

The Performance of an Operational Substation Earthing System under High Frequency and Transient Conditions

6.1 Introduction

The frequency response and transient behaviour of generic earth electrodes have been investigated in chapters three, four and five. In this chapter, studies are conducted on a practical earth grid of an operational substation. The earth grid chosen is shown in Figure 6.1. It consists of a meshed earth grid with 5m rods on the left-hand side of the figure, which is connected to an extended earth electrode system in the form of a ring, shown on the right-hand side of the figure. In addition, 10m earth rods are connected to the extended electrode system. The earthing system consists of copper earth-strips with different dimensions. The strips surrounding the building are a 50x4mm in dimension, while the parts connecting equipment to the main grid have 60x6mm strips. Furthermore, horizontal strips of dimensions 25x4mm are used. All internal strips are 6cm above ground, while the external strips are buried at a depth of 0.6cm. All strips passing through door openings are routed around the door frame. The earthing system includes several vertical rods, 5m in length around the building and 10m further away from the building. All rods are made of copper with a radius of 1cm.

In this chapter, both frequency response and transient behaviour are investigated. The simulations were conducted using the HFREQ and FFT routines from the commercial software package "CDEGS". All conductors are modelled as cylindrical conductors. Therefore, the earthing strips were represented as conductors with cylindrical shapes having the equivalent cross sectional area.

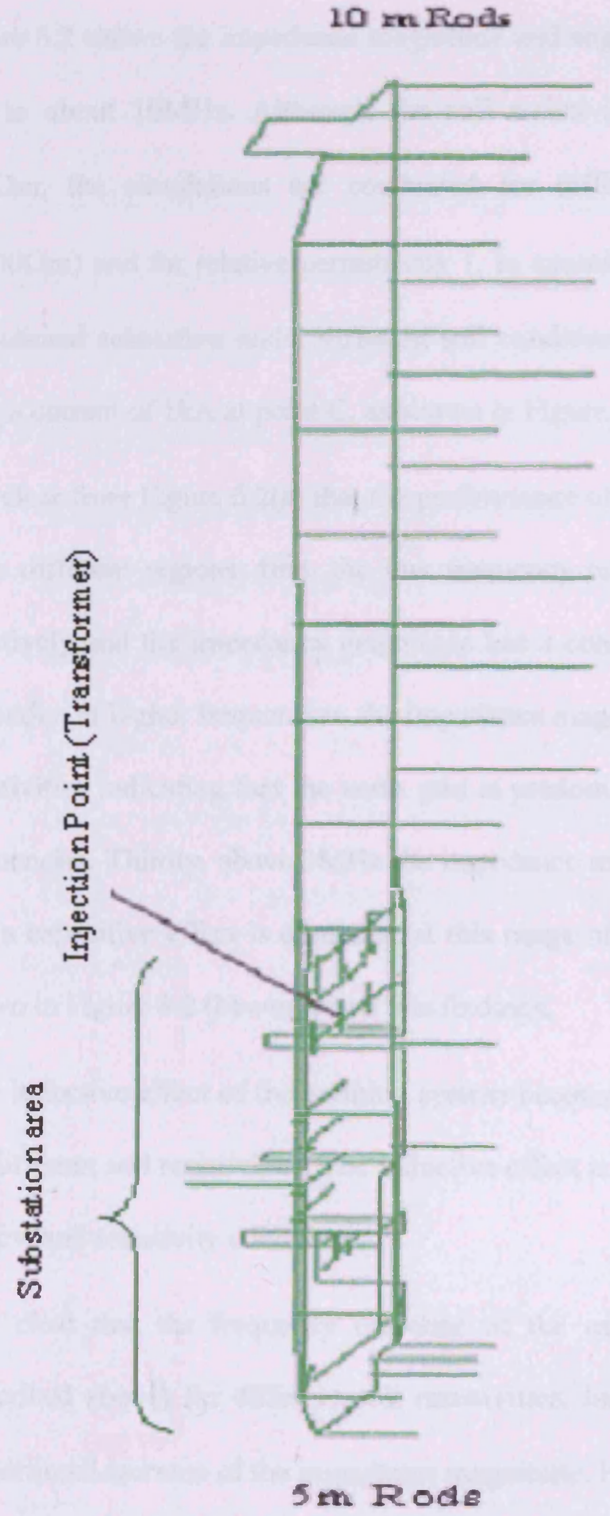

Figure 6.1 The operational substation earthing system

6.2 Frequency Response of the Substation Grid

Figure 6.2 shows the impedance magnitude and angle over a wide range of frequencies DC to about 10MHz. Although the soil resistivity in the substation area is about 100Ωm, the simulations are conducted for different soil resistivities (100, 1000, 10000Ωm) and for relative permittivity 1, to examine of the frequency response of the operational substation under different soil conditions. The earthing system is injected with a current of 1kA at point C, as shown in Figure 6.1.

It is clear from Figure 6.2(a) that the performance of the earth grid could be divided into three different regions: first, the low frequency region where the earth grid behaves resistively and the impedance magnitude has a constant value for each soil resistivity. Secondly, at higher frequencies, the impedance magnitude increases for all different soil resistivities indicating that the earth grid is predominantly inductive over this range of frequencies. Thirdly, above 3MHz the impedance magnitude start decreasing indicating that a capacitive effect is dominant at this range of frequencies. The impedance angle shown in Figure 6.2 (b) confirmed this findings.

The inductive effect of the earthing system becomes dominant at different frequencies for different soil resistivities. The inductive effect is more significant at low frequencies for low soil resistivity conditions.

It is clear that the frequency response of the earthing system has the same trend (described above) for different soil resistivities. Increasing soil resistivity results in a proportional increase of the impedance magnitude. For example, at a 100Ωm soil resistivity and over a low frequency range, the impedance magnitude is about 1Ω. When the soil resistivity increases to 1000Ωm (ten times higher), the impedance magnitude increases and it is in the order of 10Ω (ten times higher).

Comparing the behaviour of this earthing system to that of the simple earth grid, previously investigated in Section 3.3.3, it is clear that both earthing systems behave in a similar way up to 1MHz. Above that frequency two major differences were observed:

- In Figure 3.5, the response of the earth grid to soil resistivity of 10kΩm and frequency above 1MHz shows very clear oscillations, they were thought to be due to interaction between capacitive and inductive effects. These oscillations were not exhibited in the frequency response of this earthing system.
- In Figures 3.2, 3.3 and 3.5 the capacitive effect becomes dominant above 1MHz, only for high soil resistivity (10kΩm). In this study and as shown in Figure 6.2, The capacitive effect is dominant above 3MHz for all different soil resistivities.

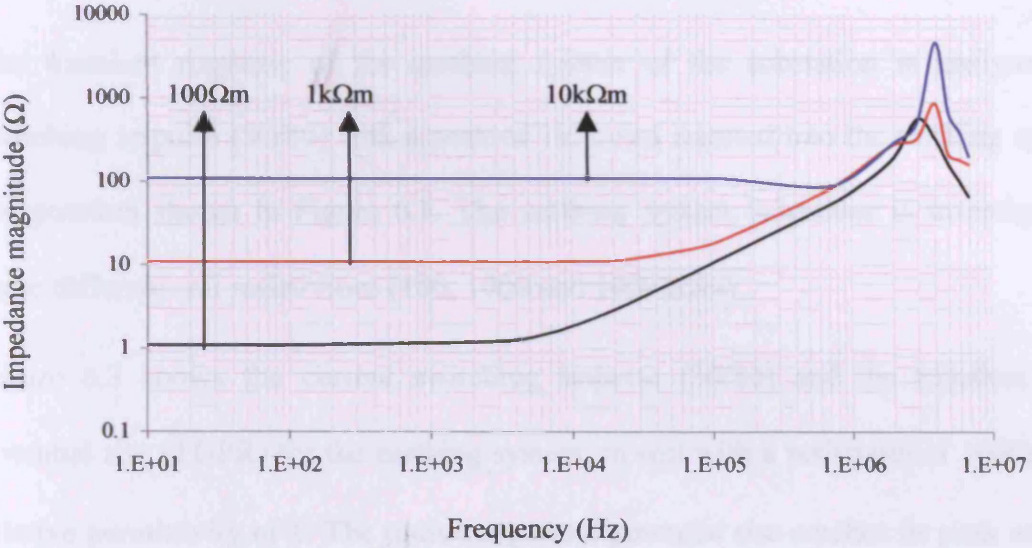

(a) **Impedance magnitude**

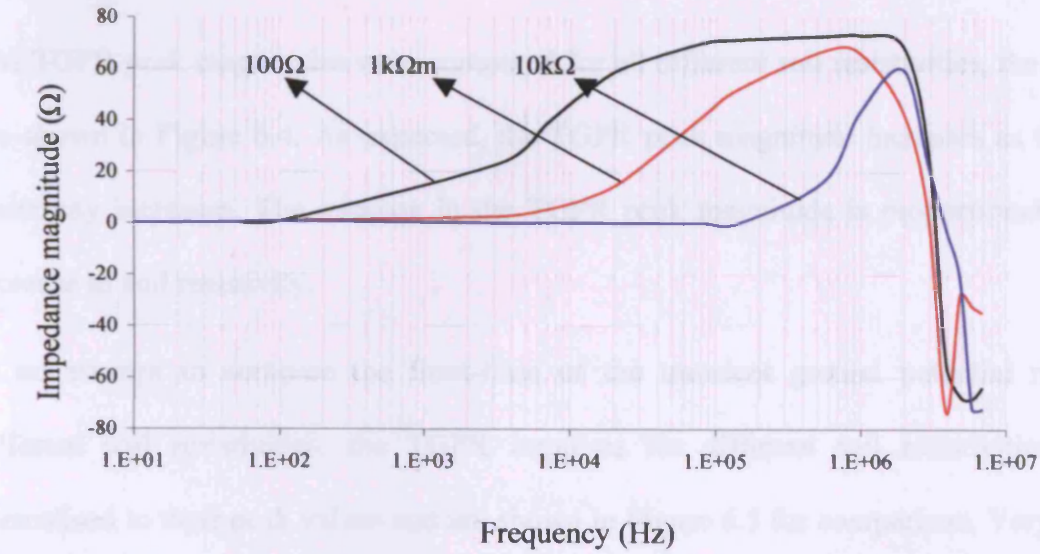

(b) Impedance angle

Figure 6.2 Frequency response of an operational substation- earthing system for different soil resistivities (ε_r=1)

6.3 Transient Behaviour of the Substation Earthing Grid

The transient response of the earthing system of the substation is analysed for a switching impulse (30/80) with a peak of 1kA, and injected into the earthing system at the position shown in Figure 6.1. The earthing system behaviour is investigated for three different soil resistivities (100, 1000 and 10000Ωm).

Figure 6.3 shows the current switching impulse (30/80) and the transient ground potential rise (TGPR) for the earthing system, in soil with a resistivity of 100Ωm and a relative permittivity of 1. The transient ground potential rise reaches its peak at 28.9μs, which is 1.1 μs before the injected current impulse rises to its peak value indicating that the earthing system characteristics are controlled mainly by resistive and inductive effects.

The TGPR peak magnitudes were compared for all different soil resistivities, the results are shown in Figure 6.4. As expected, the TGPR peak magnitude increases as the soil resistivity increases. The increase in the TGPR peak magnitude is proportional to the increase in soil resistivity.

In an attempt to compare the front-time of the transient ground potential rise for different soil resistivities, the TGPR impulses for different soil resistivities were normalised to their peak values and are shown in Figure 6.5 for comparison. Very small differences between the TGPR front-times were observed. To quantify these differences, the TGPR impulse front-times are plotted against soil resistivity, the results are shown in Figure 6.6. The transient ground potential rise front-time increases as the soil resistivity increases.

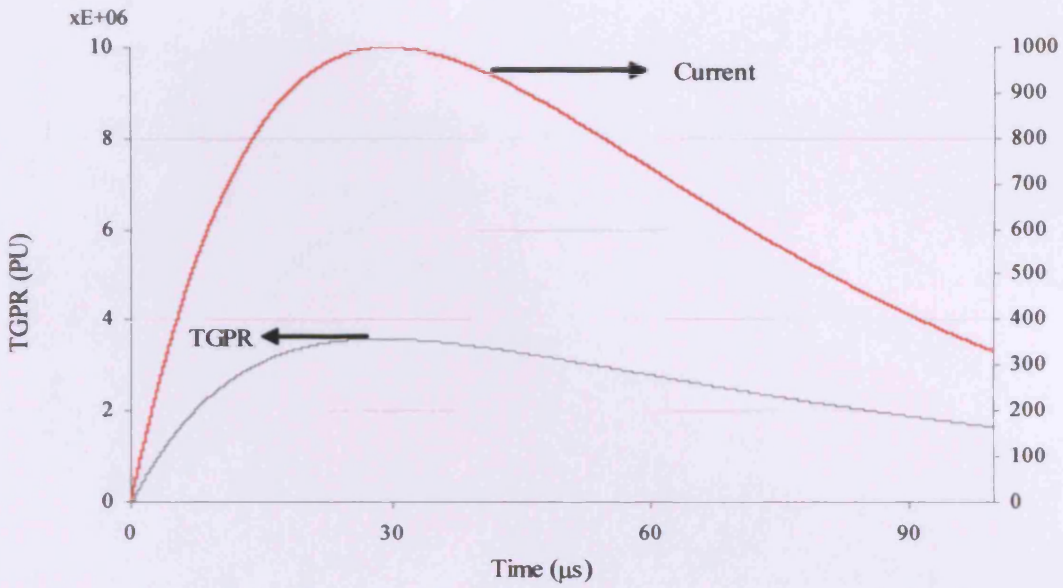

Figure 6.3 The injected current (30/80) and the corresponding TGPR for 100Ωm soil resistivity and relative permittivity 1

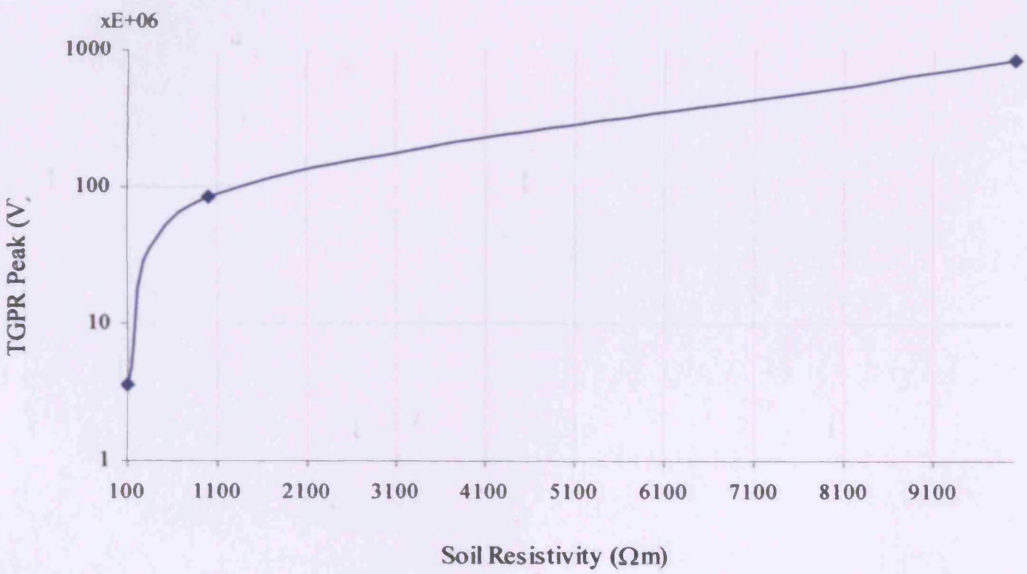

Figure 6.4 TGPR peak magnitude for different soil resistivities

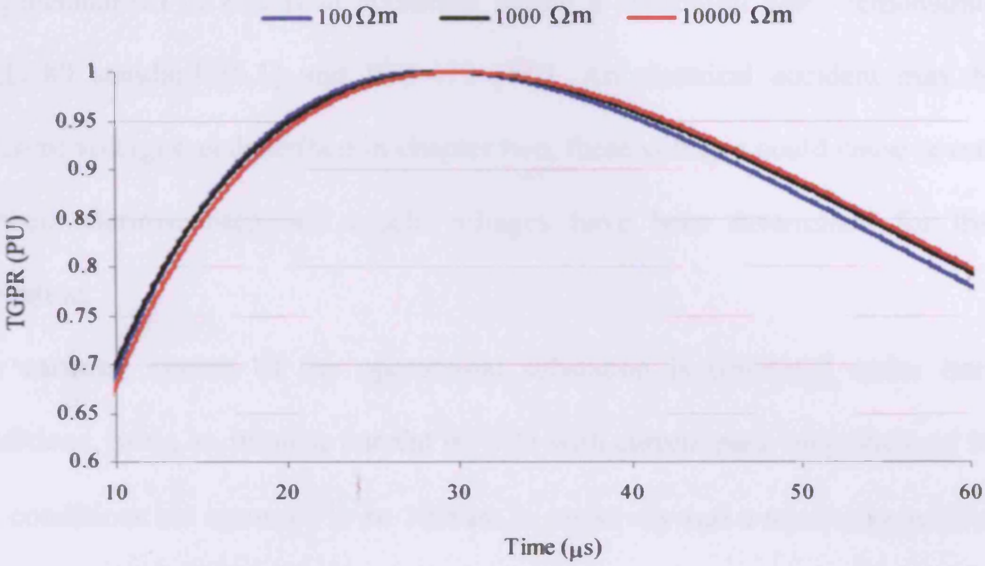

Figure 6.5 Effect of soil resistivity on the TGPR front-time

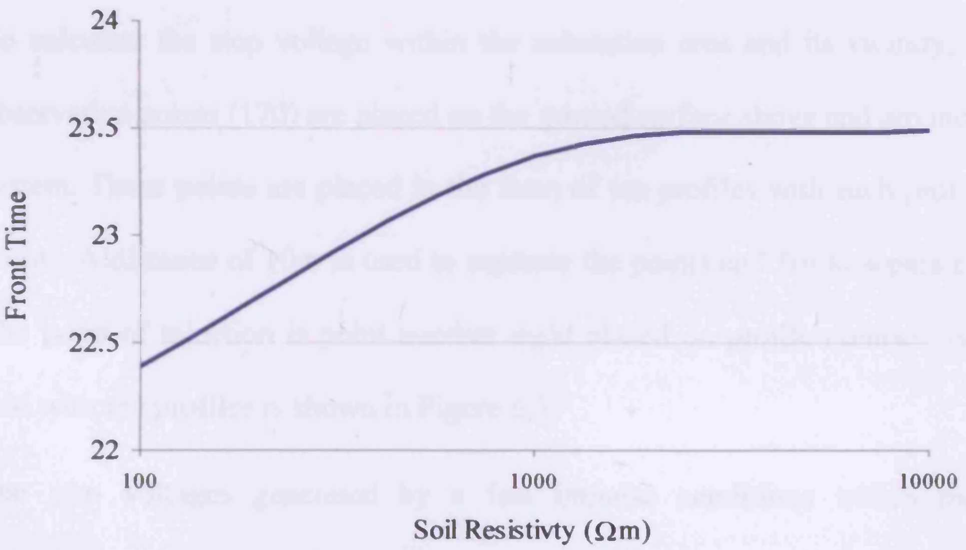

Figure 6.6 TGPR front-time for different soil resistivities

6.4 Safety Issues in Operational Substations

The mechanism of electrical accidents within a substation were demonstrated in the IEEE 80 standard [6.1] and IEC-479 [6.2]. An electrical accident may be due to different voltages as described in chapter two, these voltages could cause severe injuries to their victims. Step and touch voltages have been determined for the studied substation.

The earthing system of the operational substation is simulated under fast impulse conditions, using an impulse current of 1/20 with current peak magnitude of 10kA. The soil conditions are assumed to be 100Ωm in resistivity and a relative permittivity of 36, representing wet soil conditions [6.3].

6.4.1 Step Voltage

To calculate the step voltage within the substation area and its vicinity, a number of observation points (170) are placed on the ground surface above and around the earthing system. These points are placed in the form of ten profiles with each profile having 17 points. A distance of 10m is used to separate the points and 5m to separate the profiles. The point of injection is point number eight placed on profile number five. The earth grid with the profiles is shown in Figure 6.7.

The step voltages generated by a fast impulse conditions within the concerned substation is calculated. Figures 6.8 (a) and 6.8 (b) show the step voltages along each of the ten profiles described earlier. The step voltage along each profile is found to have its highest value at points seven or eight, which are around the injection point. The highest step voltage is observed to be at point nine from profile five, just 10m away from the point of injection. It is clearly seen that the step voltage decreases as the distance from the point of injection increases; profiles one and ten have the lowest step voltages.

The step voltage impulse shapes at selected points along the profiles numbered 1,5 and 10 are shown in Figures 6.9 to 6.11.

6.4.1 Touch Voltage

The touch voltages generated by a fast impulse conditions within the concerned substation are calculated for different observation points and are assumed to be 1m away from metal structure within the substation. Figures 6.12 shows the earthing system within the substation area and the selected points are marked with numbers 1 to 7.

The touch voltages at these selected points are shown in Figure 6.13. The touch voltage is found to reach its highest value next to the point of injection (1m away), and decreases markedly as the distance from the injection point increases. It is clear that the touch voltage at points five and six is lower than the touch voltage at point seven, and this could be due to the presence of the vertical rods closer to these two points.

The safety of a person working in the substation or even walking in the vicinity of the substation during a lightning strike depends on the amount of shock energy that is being absorbed.

Although the IEEE standards determine the critical values of step and touch voltages, under fault conditions, they do not have any recommendations concerning transient and fast impulse events.

The draft IEC479-4 discusses the effect of lightning strokes on human beings and livestock. It briefly explains the cause of lightning death and the most typical consequences. But yet, no quantitative value or limits are provided.

It is very important to clarify that, both step and touch voltages have been calculated in the worst case scenario as the fast impulse current hits the substation directly and the step voltage considered is the peak value.

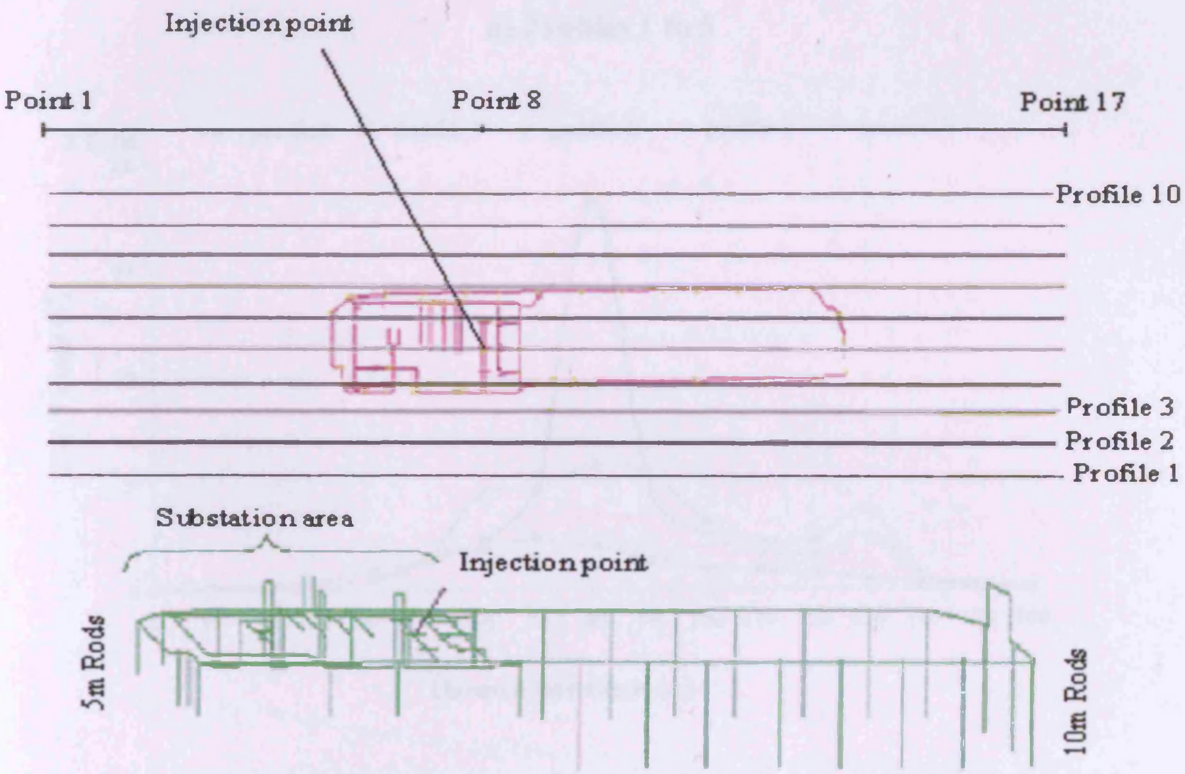

Figure 6.7 The operational substation earthing grid with the profiles

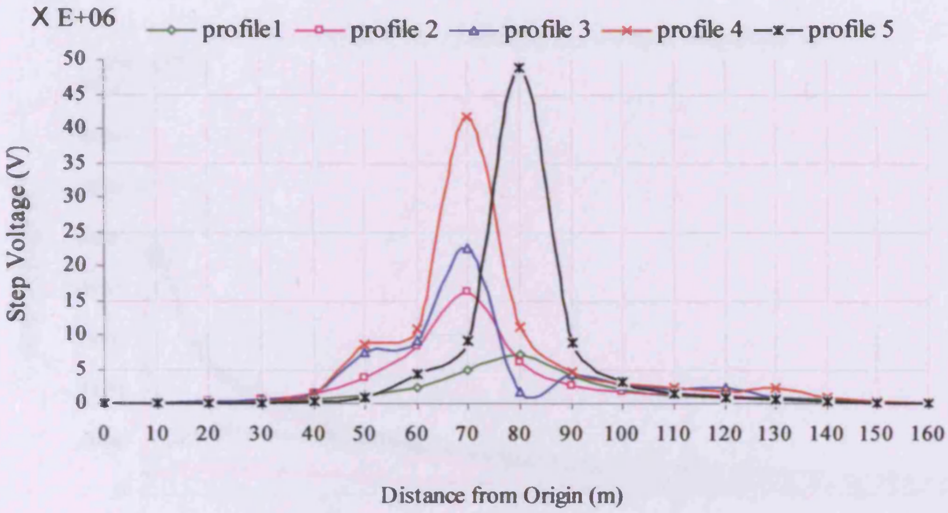

a) Profiles 1 to 5

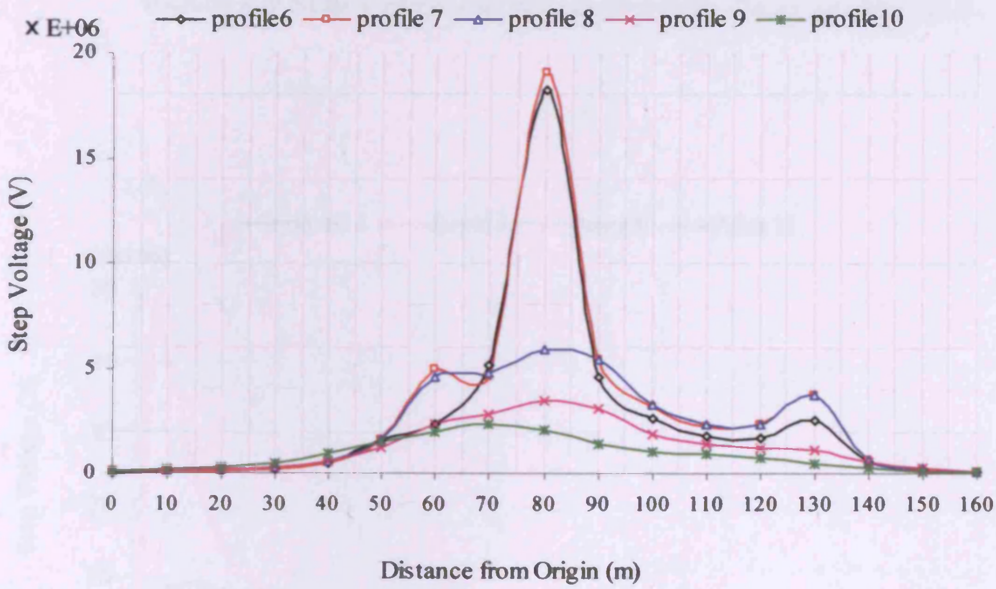

b) Profiles 6 to 10

Figure 6.8 Step voltage along the profiles

(I: 1/20, 10kA, ρ=100Ωm, ε_r=1)

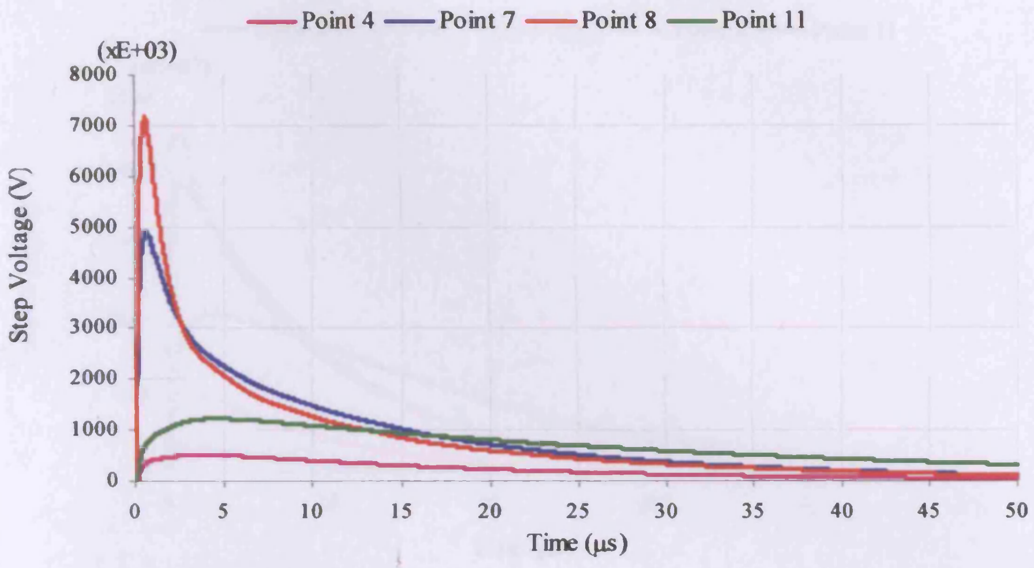

Figure 6.9 Step voltages at different points along profile No.1.

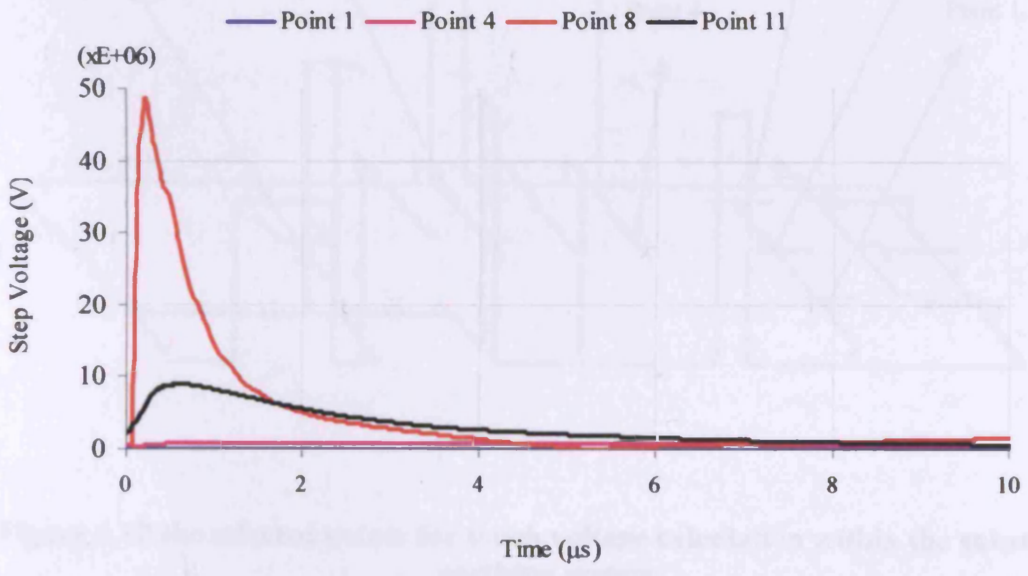

Figure 6.10 Step voltages at different points along profile No.5.

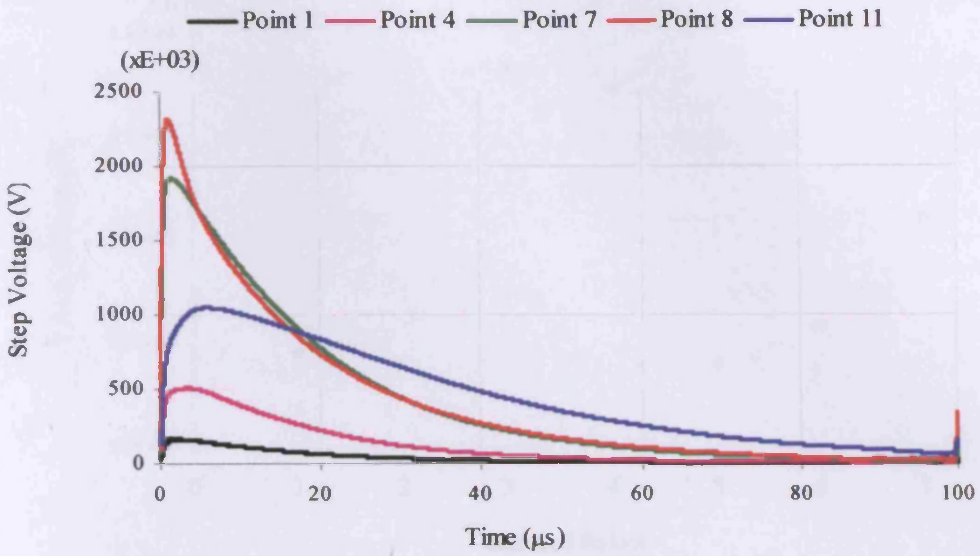

Figure 6.11 Step voltages at different points along profile No.10.

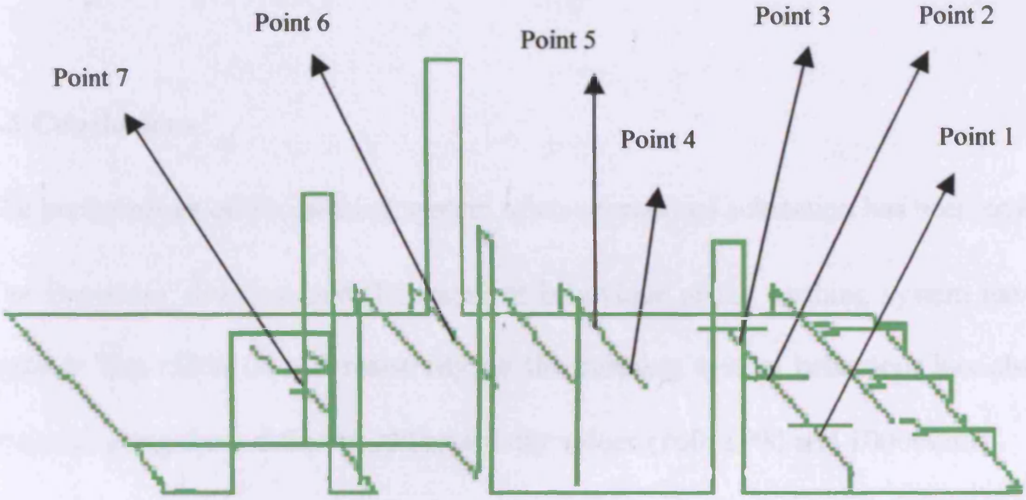

Figure 6.12 the selected points for touch voltage calculation within the substation earthing system

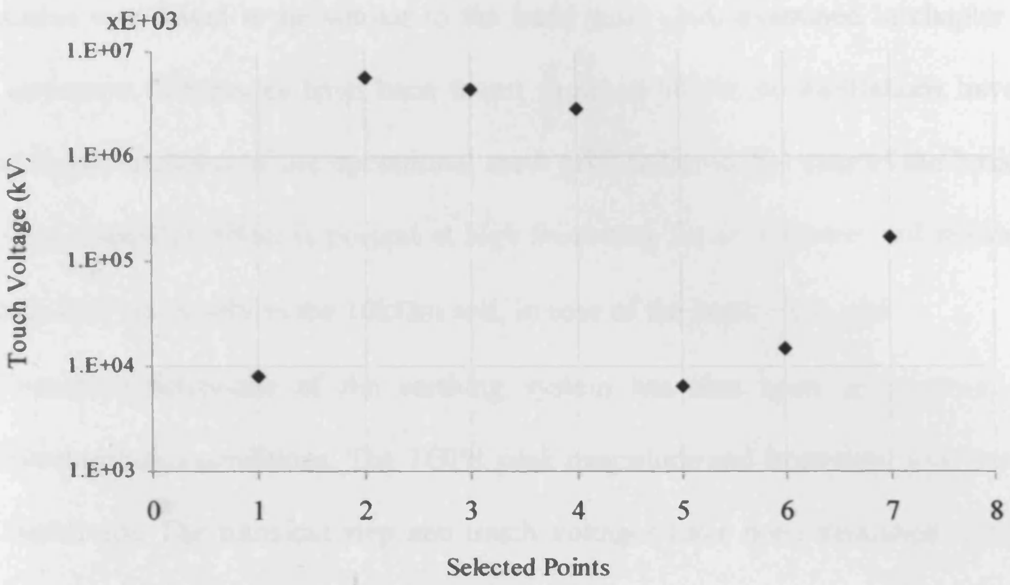

Figure 6.13 Peak touch voltage at selected points within the substation.

6.5 Conclusions

The performance of the earthing system of an operational substation has been analysed.

The frequency response and the transient behaviour of the earthing system have been studied. The effect of soil resistivity on the earthing system behaviour has also been analysed using three different soil resistivity values (100, 1000 and 10000Ωm).

The investigations have shown that the inductive effects become significant above a threshold frequency for a given soil resistivity, resulting in an increase in the earth grid impedance magnitude. At higher frequencies, the impedance magnitude of a simple earth electrode tends to drop with increasing frequency which could be attributed to capacitive effects. Increasing soil resistivity results in a proportional increase of the impedance magnitude. The inductive effect becomes significant at lower frequencies, for lower soil resistivities. Although the frequency response of the operational substation was found to be similar to the basic earth grid, examined in chapter three, two important differences have been found 1) above 1MHz no oscillations have been found in the response of the operational earth grid, unlike in the case of the basic grid, and 2) a capacitive effect is present at high frequency for all different soil resistivities, while it was found only in the 10kΩm soil, in case of the basic earth grid.

The transient behaviour of the earthing system has also been investigated, under switching impulse conditions. The TGPR peak magnitude and front-time, increases with soil resistivity. The transient step and touch voltages have been simulated within and around the substation area, under fast impulse conditions. The simulations show that both step and touch voltages have high magnitudes. As there are no safety criteria recommended by the standards, for fast impulse conditions the results could not be assessed in term of their safety hazard. However, it is important to note that both step and touch voltages have been simulated in their worst-case scenario, when the fast impulse hits the substation and the impulse reaches its peak value.

CHAPTER SEVEN

Laboratory Characterisation of Soil Ionisation under Fast Transients

7.1 Introduction

It is now well-known that earthing systems are designed to have low-magnitude earth impedances so that the high fault current can be diverted effectively and safely to earth. To achieve the low earth impedance magnitude, two different parameters should be considered in designing the earthing system: the electrode geometry and the soil property.

In Chapters Three, Four and Five, the frequency and transient performance of earthing systems were studied and new developments were suggested to improve the performance of the earthing system. In this chapter, the soil characteristics under high transient currents are investigated. Many standards dealing with earthing systems have been published such as: BS 7430-2998 [7.1], ANSI/IEEE Std 81-1983[7-2], IEEE Std 142-1991 [7,3], and IEEE Std. 80-2000 [7,4]. These standards are mainly based on investigations at power frequency voltages and low-level conduction currents in soil. These standards give some recommendations and guidelines on 'the transient earth practice' but they do not quantify it, because only a small amount of research work has been conducted in this area compared with work involving power frequency.

Non-linear soil behaviour under high impulse currents has been observed by Towne as early as 1928 [7.5]. Following this, a number of studies [7.5-7.12] of soil characteristics under high impulse currents were conducted to introduce a better understanding of soil conduction under high impulse current. This non-linear soil behaviour under high current was found to depend on a number of factors: soil properties, the electrode dimensions, current front-time and the impulse polarity, for example.

Two main conduction processes have been suggested to cause non-linear soil behaviour under a high current: thermal and ionisation processes. In the thermal process, two types of conduction processes can take place depending on the energy absorbed by the earthing system. Low energy absorption is where ionic conduction results in an increase of conductivity. While in the case of high energy absorption, vaporisation of the water contained in the soil medium will occur, thus, causing a remarkable reduction in the conduction level of the medium. The ionisation process is due to electric field enhancement in the gaps and interfacial surfaces within the soil medium which introduce local arcing.

In this chapter, the electrode characteristics will be investigated using voltage and current measurements in sand wetted with various percentages of water content. Sand was chosen because it is easy to wet and dry without losing its physical and electrical characteristics. An impulse test was carried out for bounded and unbounded electrode systems, and two different containers were used during the test procedures.

7.2 Laboratory Arrangement

7.2.1 Impulse Current Generator

Two different types of impulse generator were used to achieve this study;

I. A Haefely impulse generator type SGS 400/2KA was used for part of the tests. The generator has four stages. Each stage consists of reservoir capacitor, a front resistor connected in series, a tail resistor connected in parallel, a charging resistor and an adjustable spark gap.

II. A fast-impulse current generator of double exponential circuit type was also used. This current generator includes:

- A DC charging unit with an output voltage of up to 55kV DC and a current of 2 mA. Two resistors of 26kΩ each were used in series as a charging resistor.
- The capacitor bank consists of three low inductance capacitors of 0.15μF, 0.004μH rated at 65kV were connected in parallel and to the SF_6 spark gap.
- A high pressure SF_6 spark gap consisting of two plane electrodes with a spacing of few millimetres. The insulating SF_6 gas was provided from a gas bottle with a suitable pressure into the sealed spark gap. The spark gap was provided with an external triggering source via the remote system for fast switching of the impulse generator. To achieve an effective triggering of the spark gap, a low voltage pulse circuit was used to generate a 300V impulse. This was then applied to a step up pulse transformer generating a narrow pulse of 30kV. When the pressure of the spark gap reaches the appropriate level, triggering can be achieved over a broad range of the charging voltage.

7.2.2 Impulse Current Transducers

For the high impulse test, it is essential to use current transducers that are capable of measuring tens of kiloamper, with a rise-time in the microsecond range. There has been much published research work [7.13-7.18] related to current measurements. Three types of measurement methods were used in high current applications: resistive, inductive and optical current measurements. The optical current measurement offers better performance compared with the resistive and inductive methods. However, there are limiting factors with these methods; limited bandwidth and the low range of current rating and the elevated cost of high performance devices.

The inductive method was adopted for this study. A current transformer (CT) was used for current measurement. The current transformer has the advantage of being completely isolated from the high voltage circuit and the effect of spurious ground current.

A commercial current transformer with a sensitivity of $0.1VA^{-1}$, a response time of 20ns, and a maximum measurable current of 5kA was used. From previous work [7.19, 7.20], this current transformer was shown to produce reliable and accurate measurements, and was subsequently used as a calibrating transducer in the laboratory.

7.2.3 Impulse Voltage Measurements

Voltage measurements may suffer from inductive effects in the measurement loop. As a result, voltage measurements, peak, rise and decay times could be influenced by the characteristics of the test and the physical size of the loops due to the self and mutual inductances between the test current and the measuring loops. One more factor should be considered in voltage measurement, the initial overshoot on the measured trace.

This overshoot could be generated by:

i. The inductive effect of the test circuit combined with the capacitive effect of the test load under study.

ii. The inherent inductive and capacitive effect related to both high and low voltage sides of the voltage divider.

iii. The arrangement of test load should be some distance away from the voltage divider.

In this experimental programme, the adopted voltage transducer was a mixed resistive-capacitive divider (Haefely RC-150) with a ratio of 3750:1 and a response time of 30ns. This transducer was calibrated according to IEC 60 [7.21].

7.3 Laboratory Tests on Single Earth Electrode

7.3.1 Circuit and Procedures

Two different test circuits were used for this study. Figure 7.1 shows the test circuits adopted for this study. The use of the first circuit made it possible to generate high voltages up to 50kV and high current impulse up to 5kA. The impulse was generated by connecting the three, low inductance 0.15μF, 65kV, capacitors in parallel. A 21kΩ tail resistor was used to obtain the required tail wave shapes. The second circuit was adopted for a part of this study using the Haefely impulse generator connected directly to the test load. The circuit was connected and earthed as recommended in [7.22].

A Lecroy 9354A, 500MHz digital storage oscilloscope (DSO), was used for capturing the voltage and current signals. It is important that the measuring system components (current transformer, voltage divider, measuring cables and the digital storage oscilloscope) have adequate bandwidth and response time, as the accuracy of the end shape of the measured signal depends on the slower response-time device. High voltage and high current impulse measurements are normally accompanied by electromagnetic field interference. Therefore, it is necessary to shield the equipment against this interference. In these tests, all the transducer signals were transmitted through shielded triaxial cables to the recording equipment placed in a shielded room, away from the source of interference.

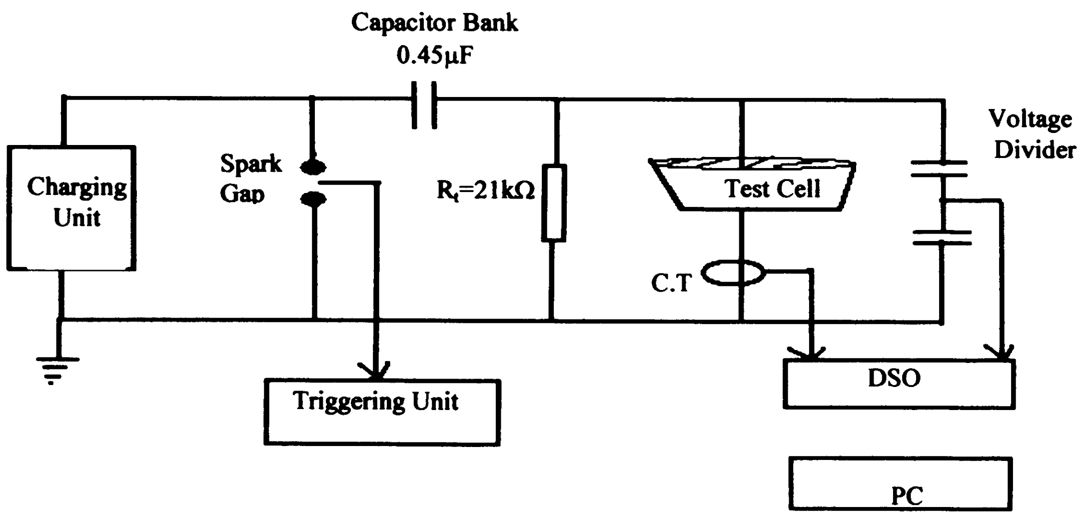

(a) Impulse current test circuit

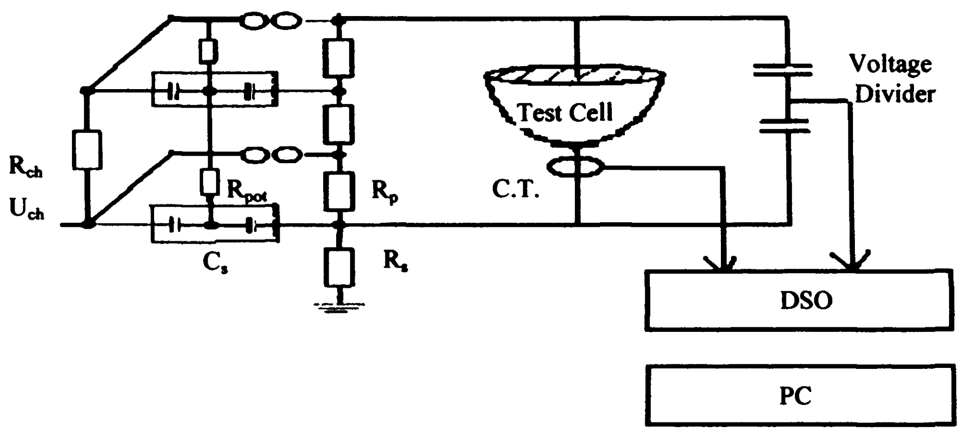

(b) Test Circuit using the Haefely impulse generator

Figure 7.1 Test Circuits

I. Characteristics of the Test Cell

Two different test cells were used in this research, a small hemispherical cell and a large rectangular container. The hemispherical container has radius of 23.8cm. Four connection points were fixed evenly around the perimeter of the container to ensure a uniform current distribution in the test soil. A hemispherical electrode of 3.13cm radius was used for current injection and placed in the centre of the container. The electrode was half buried in the sand to avoid high electric field magnitudes at the interface between the sand and the air. Figure 7.2(a) illustrates the test cell design with the live electrode. The second container was made of plastic and covered inside with a conducting sheet of aluminium to ensure uniform current return. Four connecting points were set on the boundary of the container. The container dimensions and shapes are shown in Figure 7.2 (b). Figure 7.3 shows photographs of the test cell with the live electrode (a) and the laboratory set up (b).

II. Soil Medium Preparation

Sand was chosen for this study because it is easily wetted and dried without any loss of its physical properties. The sand was mixed with a different percentage of water content to control its resistivity. The water content of the sand was calculated as a percentage of the ratio of water mass to the dry soil mass, as specified in BS 1377 [7.23]. A sand mixer was used so that a uniform wetting of the sand was guaranteed. After mixing, the sand was poured into the test container and compacted manually. The active electrode was half buried into the centre of the container. The sand was then compressed manually with hands to avoid sharp edges and prevent air discharges. Following each test, the sand was dried either by using an oven available in the laboratory or by spreading it over the floor, depending on the sand quantity. It is important to note that the sand was always completely dry before any subsequent experiments.

During the test, it was very difficult to keep control of the homogeneity of the sand, as the water was settling by gravity to the bottom of the container very rapidly. To overcome this problem, a periodical mixing of the sand was carried out manually.

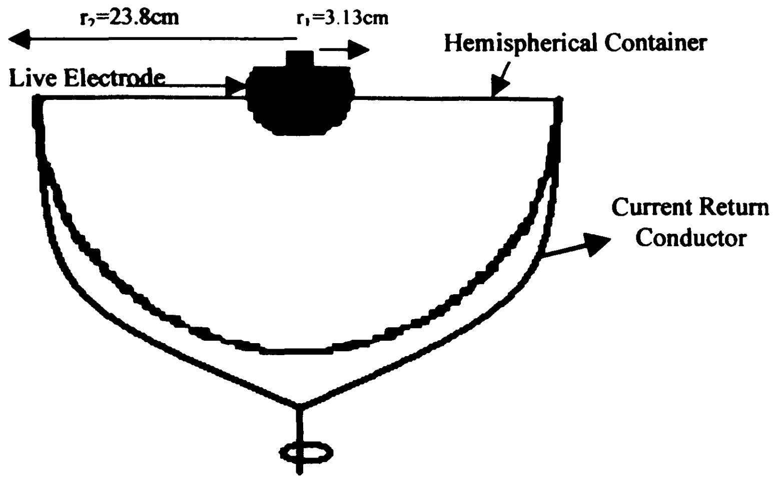

(a) Small hemispherical test cell

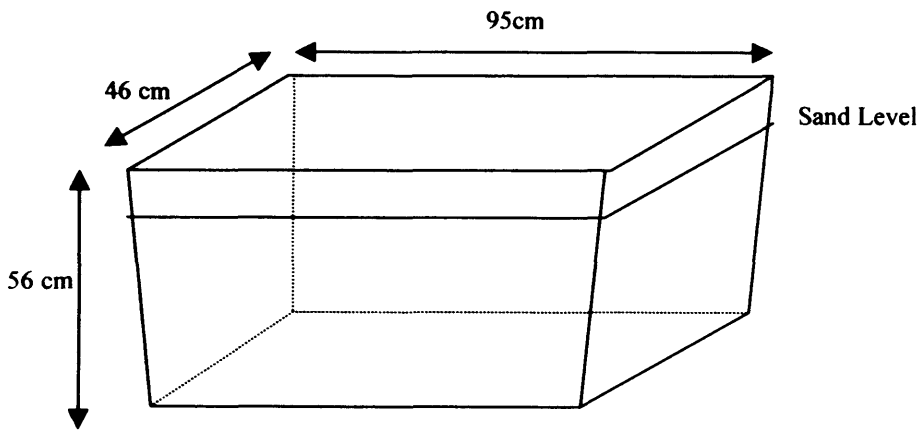

(b) Large plastic test cell

Figure 7.2: Test cells used for testing soil under a high impulse current

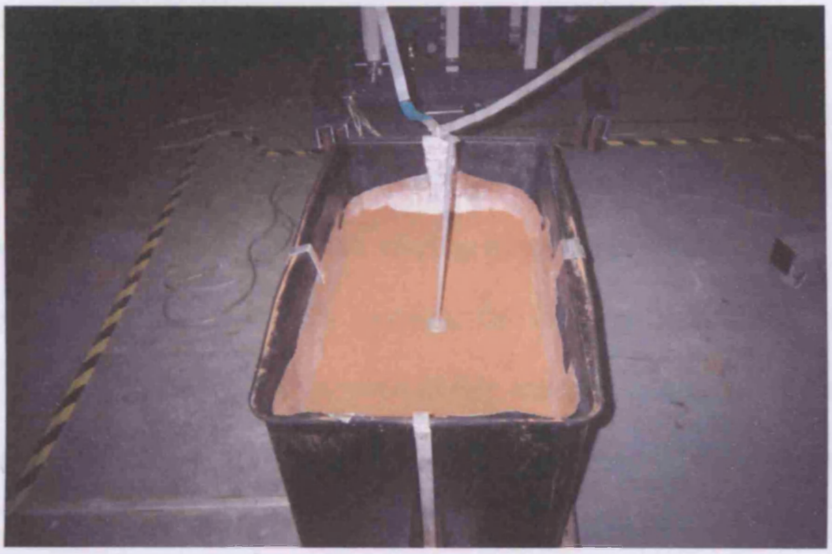

a) The large plastic container with the live electrode

(b) Test circuit

Figure 7.3 The laboratory set up

7.3.2 Impulse Test on a Liquid Medium

An impulse test was conducted on a liquid resistive medium with a conductivity of 1.4mS/cm. The test set up, as previously described was adopted for this study and the hemispherical container was filled with a solution having volume of $0.024m^3$, after that the active electrode was submerged in this medium. The impulse test was then carried out for increasing current magnitudes. The purpose of this test was to associate the response of a resistive medium, which was assumed to have a 'linear behaviour' with the response of wet sand, which is well-known to display non-linear behaviour under high impulse currents.

Figure 7.4 shows typical current and voltage traces for a resistive solution inside the hemispherical container for a 15kV charging voltage. It is very clear that the rise time for impulse voltage is shorter than the rise time of the current impulse and hence, the voltage peak occurs before that of the current. This could be attributed to the inductive effects of the test circuit components.

Figure 7.5 shows the resistance (V at I peak)/(I peak) as function of current magnitude. As expected, the resistance is nearly constant at 34Ω for different current magnitudes. These results concur with previous investigations [7.5,7.9,7.20]. The conductivity of the resistive solution can be calculated using the measured constant resistance of 34Ω using the following:

$$R = \frac{\rho}{2\pi}\left(\frac{1}{r_1} - \frac{1}{r_2}\right) \qquad (7.1)$$

Where ρ is the soil resistivity, r_1 is the radius of the active electrode, r_2 is the radius of the hemispherical container. From Equation (7.2) the calculated conductivity was found to be 1.3mS/cm, which is within 10% of the value measured using the conductivity meter (1.4mS/cm).

The accuracy achieved in this test on a resistive load provides a high degree of confidence in the test set up adopted for these studies.

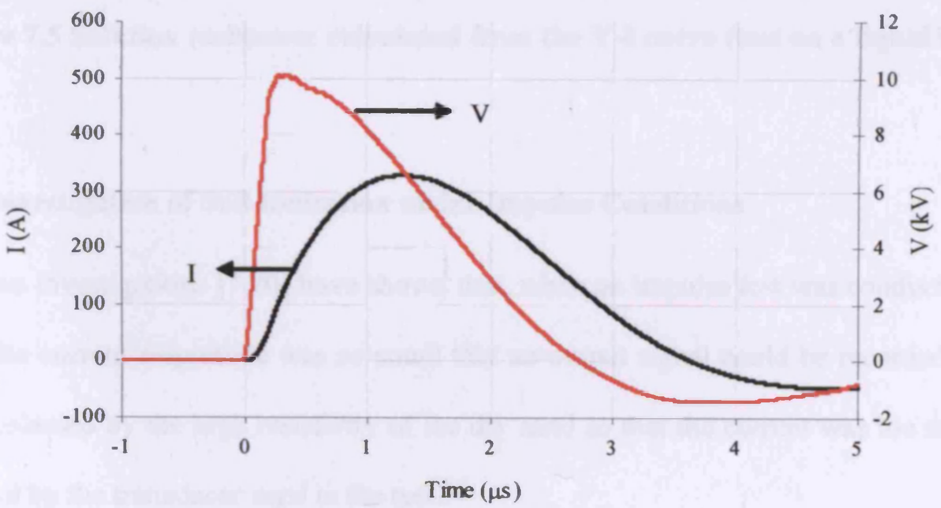

Figure 7.4 Typical current and voltage traces for a resistive solution obtained for a 15 kV charging voltage

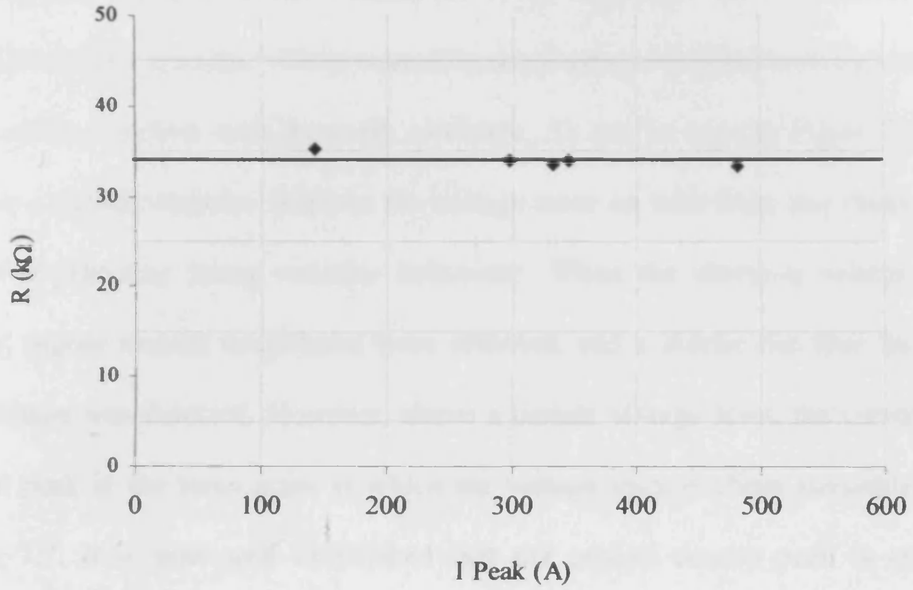

Figure 7.5 Solution resistance calculated from the V-I curve (test on a liquid medium)

7.3.3 Investigation of Soil Ionisation under Impulse Conditions

Previous investigations [7.20] have shown that, when an impulse test was conducted on dry sand, the current magnitude was so small that no output signal could be recorded, and this was explained by the high resistivity of the dry sand so that the current was too small to be detected by the transducer used in the test.

In this work, the effect of soil ionisation under impulse of high magnitude was investigated. Impulse tests were carried out on wet sand with different current magnitudes. Figures 7.6 and 7.7 illustrate the voltage and current traces obtained during these new tests on sand with 5% water subjected to two different applied voltages of 27kV and 33kV respectively. For both applied voltages, initial oscillations were observed. These oscillations could be attributed to the capacitive effects caused by small air spaces between the grains of sand and at the contact surface with the earth electrode. As can be seen in Figure 7.6, the current exhibits a similar impulse shape to the voltage trace on both front and decay times which denote a primarily linear resistive behaviour. When the charging voltage is increased further, higher current magnitudes were obtained, and a shorter rise time for both current and voltage was detected. However, above a certain voltage level, the current exhibited a second peak at the same point at which the voltage trace declines smoothly as shown in Figure 7.7. It is now well established that the second current peak is caused by soil ionisation, as stated in previous work [7.20, 7.24]. It was also stated that the second current peak was not observed in the test applied on sand mixed with a high percentage of water content (15% and more).

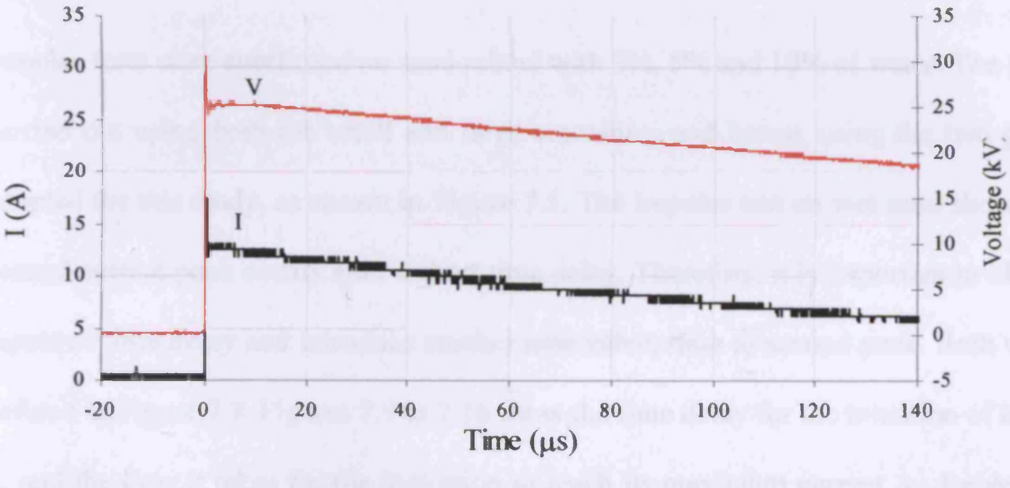

Figure 7.6 Typical voltage and current impulse shapes for sand mixed with 5% water. Large container at a charging voltage of 27kV)

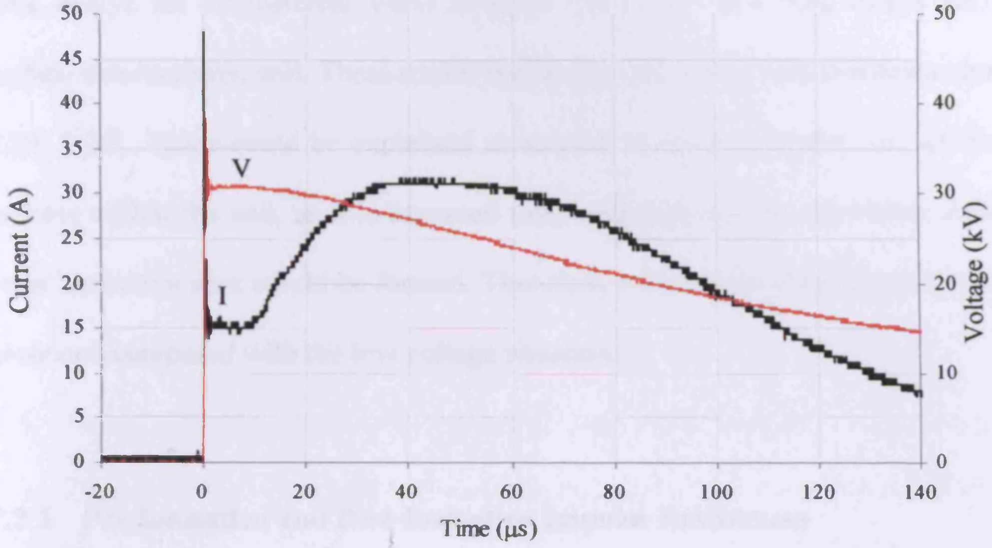

Figure 7.7 Typical voltage and current impulse shape during non-linear conduction for sand mixed with 5% water (large container, charging voltage 33kV)

7.3.4 Measurements of Soil Ionisation Parameters

Impulse tests were conducted on sand mixed with 3%, 5% and 10% of water. The tests were carried out using both the small and large containers and hence, using the two generators adopted for this study, as shown in Figure 7.1. The impulse test on wet sand shows that the second current peak occurs after a short time delay. Therefore, it is important to identify the aspect of time delay and introduce another new value, time to second peak. Both values are defined in Figure 7.8. Figures 7.9 to 7.16 show the time delay for the initiation of ionisation, t_d, and the time it takes for the ionisation to reach its maximum current, t_2, for sand mixed with different water contents and for both test cells. The results are similar for both test cells. It is clear that increasing voltage and current magnitudes results in a reduction in both time delays for all different water contents. However, both time delays are shorter for higher- conductivity, soil. These results are in agreement with previous research work [7.20, 7.24, 7.25]. These could be explained as a result of the propagation rate of the ionisation process within the soil, as it is expected that, with high voltage and higher conductivity, a large ionisation area would be formed. Therefore, a faster rate of conduction expansion was produced compared with the low voltage situation.

7.3.5 Pre-Ionisation and Post-Ionisation Impulse Resistances

Having two different current peaks allows the definition of two different resistances;

i) Pre-ionisation resistance corresponds to the soil properties before the soil ionisation and its influence takes place. It represent the non-linear conduction behaviour controlled by thermal effects.

ii) Post-ionisation resistance, corresponds to the last condition of conduction after the ionisation area has reached its maximum volume within the test cell.

These two resistance values were measured using the following equations:

$$R1 = \frac{V \text{ at } I_{peak1}}{I_{peak1}} \qquad (7.2)$$

$$R\,2 = \frac{V \text{ at } I_{peak2}}{I_{peak2}} \qquad (7.3)$$

Figures 7.17 to 7.20 illustrate the changes that occur with both resistances as the impulse voltage is increased up to the breakdown level of the test cell. The graphs show the resistances as a function of corresponding current peak and for all different water contents, as adopted in this study.

As shown in Figures 7.17 to 7.20, the pre-ionisation resistance R1 is decreasing as the current magnitude is increased, which could be explained by a non-linear conduction process in the test medium resulting from a thermal effect. As a result of the heating effect (I^2R) when the current magnitude is increased, the conductivity of the medium is increased. Therefore, the resistivity of the soil could be reduced. However, there are different factors that affect the trend of R1 and these could be related to: a) the number of shots applied to the same test cell which affects the mechanism controlling the heating process in the sand. and b) the water movements in the sand and the settling process which is presently uncontrolled. In some tests, it was found that R1 increases with current magnitude instead of decreasing, which could be attributed to extreme heating occurring in the soil. This heating will result in a water vaporisation which leads to a reduction in the conductivity, hence, increasing the resistivity. To overcome this problem, it was suggested to minimize the number of impulse shots applied to the same test medium or to leave a time-gap long enough to allow the test medium to cool and, consequently, reduce the heating effect.

The post-ionisation resistance R_2 is always lower than the pre-ionisation resistance R_1. Both R_1 and R_2 decrease as the current magnitude increases, as is clear from Figures 7.19 and 7.20. This reduction is larger in sand mixed with 3% water than for sand mixed with 10% water. Close examination of the fall ratio of the post ionisation resistance

R1/R2 , revealed that sand mixed with 3% water content has the highest fall ratio of 0.82.

However, this ratio decreases as the water content increases and it is 0.01 for 10% water content. This indicates that sand with 3% water has a higher ionisation effect than sand with higher water content. This behaviour may be attributed to the vaporisation process which produces dry areas that allow field enhancements to take place in the dry area and a higher field in the air gaps within the dry sand. This process is expected to promote ionisation by expanding the effective radius of the active electrode, therefore, reducing the resistance.

The investigation of soil ionisation was extended to consider the soil breakdown phenomena. Above a certain voltage, a breakdown occurs between the live electrode and the test cell container through the test soil. This breakdown could be observed on both voltage and current impulse shape. After the current first peak and just before the second peak, a sudden large increase in current occurs, coinciding with a drop in voltage and indicating the soil breakdown. There was no evidence of glassification but a few tubular holes were observed in the test soil, following the breakdown, when the active electrode was carefully removed. Therefore, it was important to remove the electrode after every breakdown, mix and compress the sand to avoid any capacitive effect which may result from these air gaps. Figure 7.21 shows a typical current-voltage trace obtained during the soil breakdown.

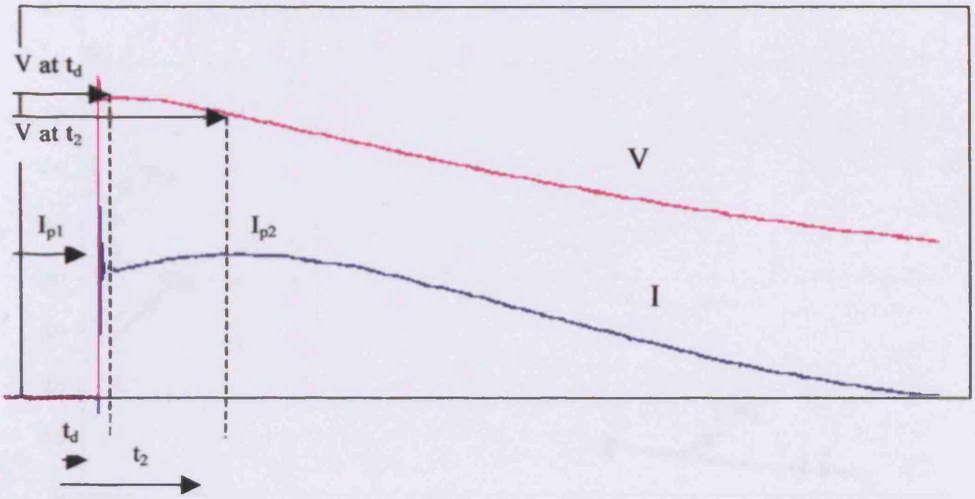

Figure 7.8 Definition of time initiation of the second current peak, td, and time of the second current peak, t2.

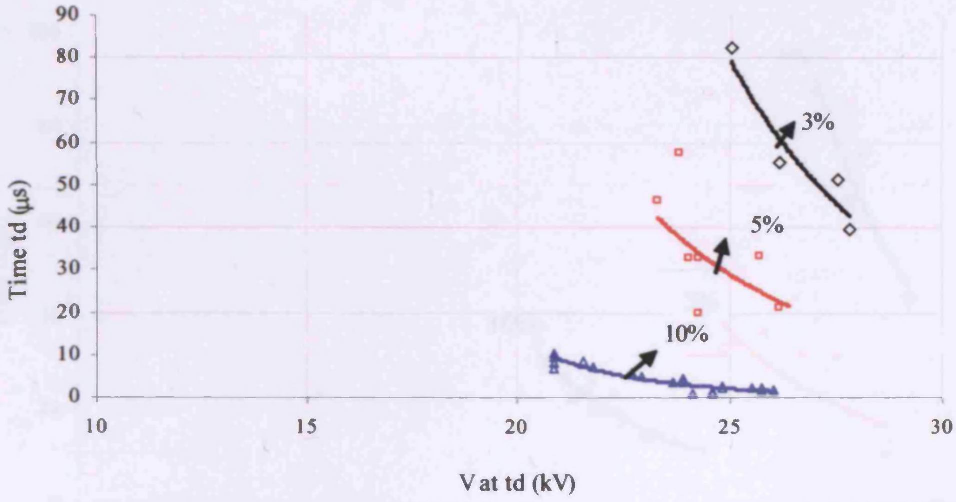

Figure 7.9 Ionisation time delay (t_d) as a function of its corresponding voltage for sand mixed with different water contents in the hemispherical container.

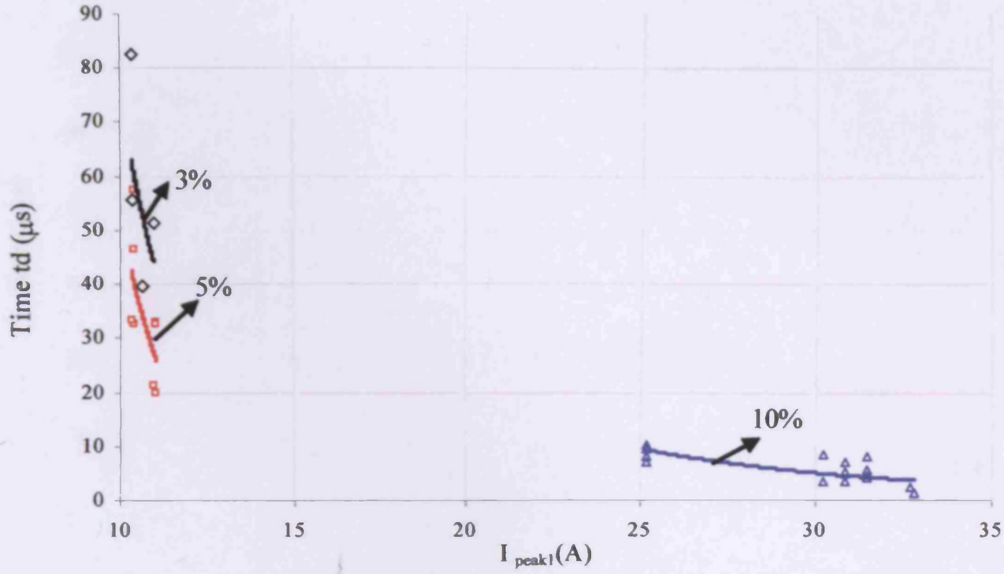

Figure 7.10 Ionisation delay time (Td) as a function of I $_{peak1}$ for sand mixed with different water contents in the hemispherical container.

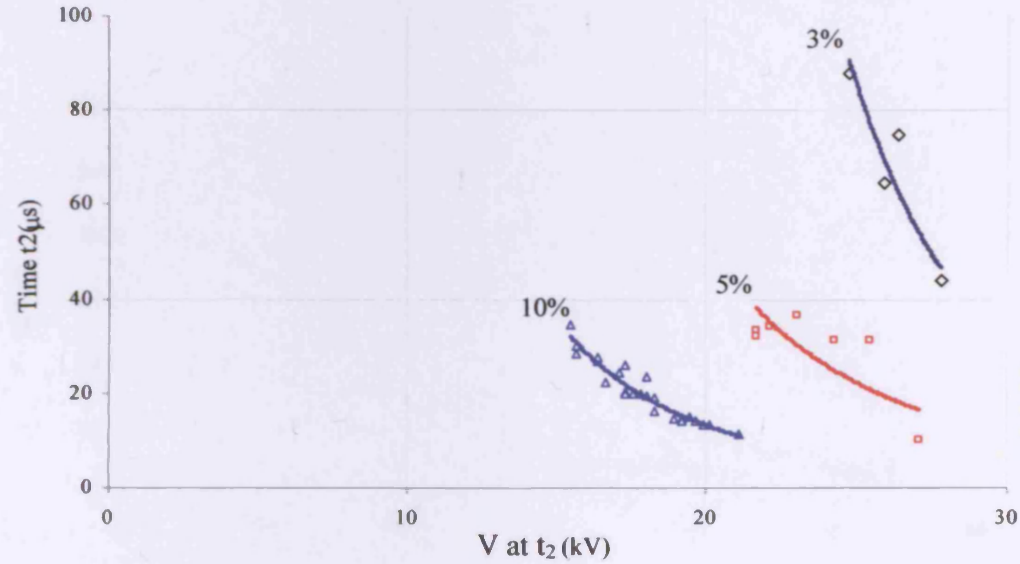

Figure 7.11 Time to peak ionisation (t_2) as a function of its corresponding voltage for sand mixed with different water contents in the hemispherical container.

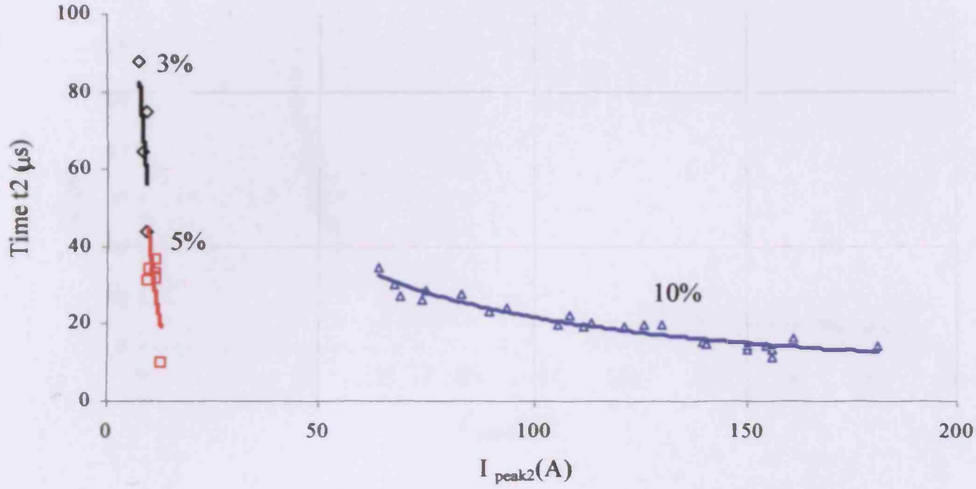

Figure 7.12 Time to peak ionisation (t_2) as function of I_{peak2} for sand mixed with different water contents in the hemispherical container.

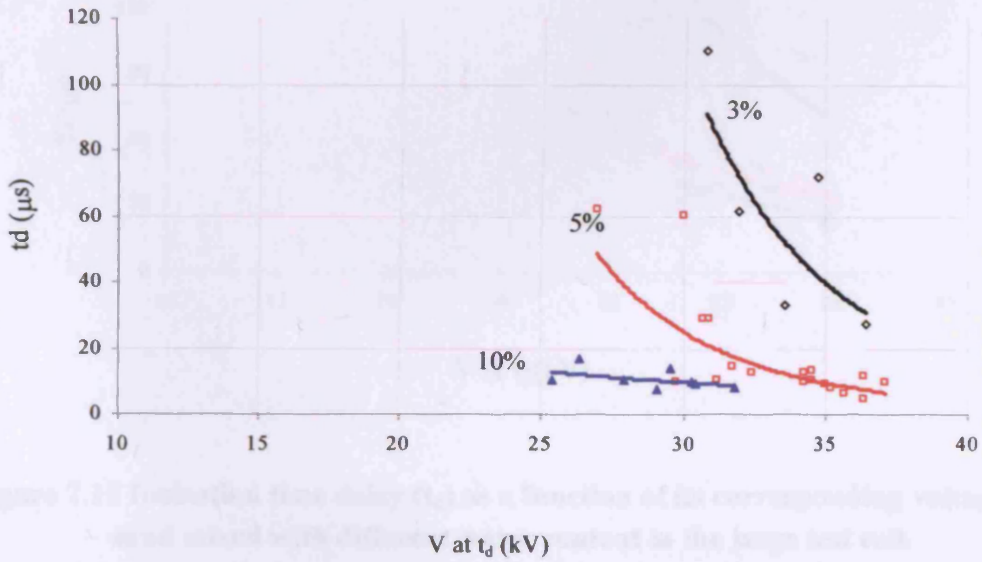

Figure 7.13 Ionisation time delay (t_d) as function of its corresponding voltage for sand mixed with different water contents in the large test cell.

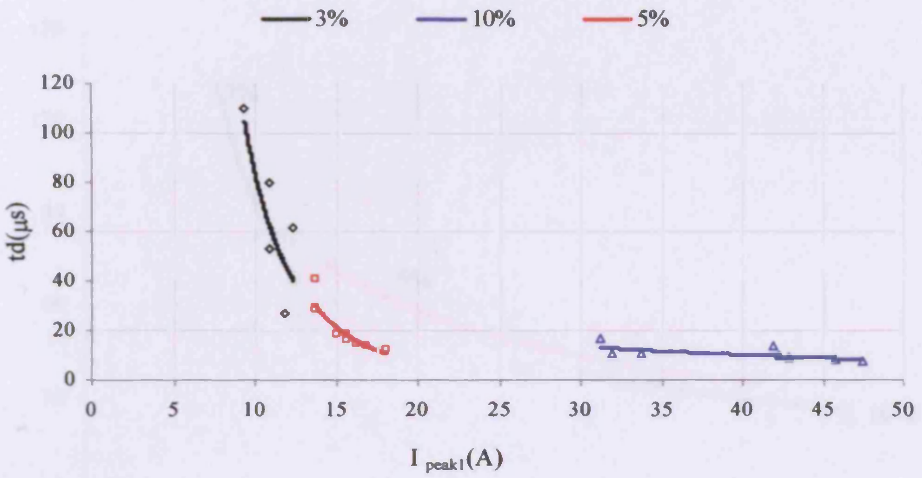

Figure 7.14 Ionisation time delay (t_d) as a function of I_{peak1} for sand mixed with different water contents in the large test cell.

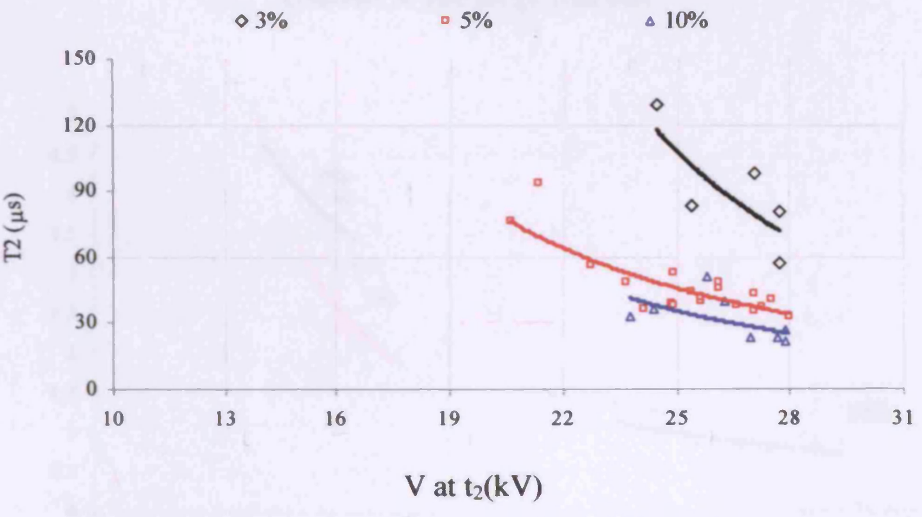

Figure 7.15 Ionisation time delay (t_d) as a function of its corresponding voltage for sand mixed with different water content in the large test cell.

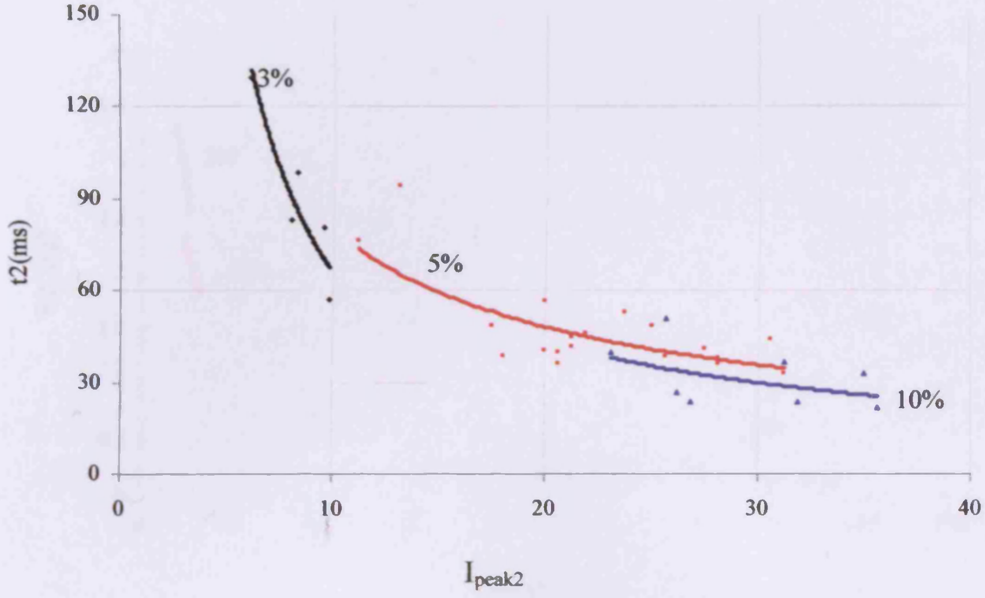

Figure 7.16 Ionisation time delay (t_d) as function of I $_{peak1}$ for sand with varying water content in the large test cell

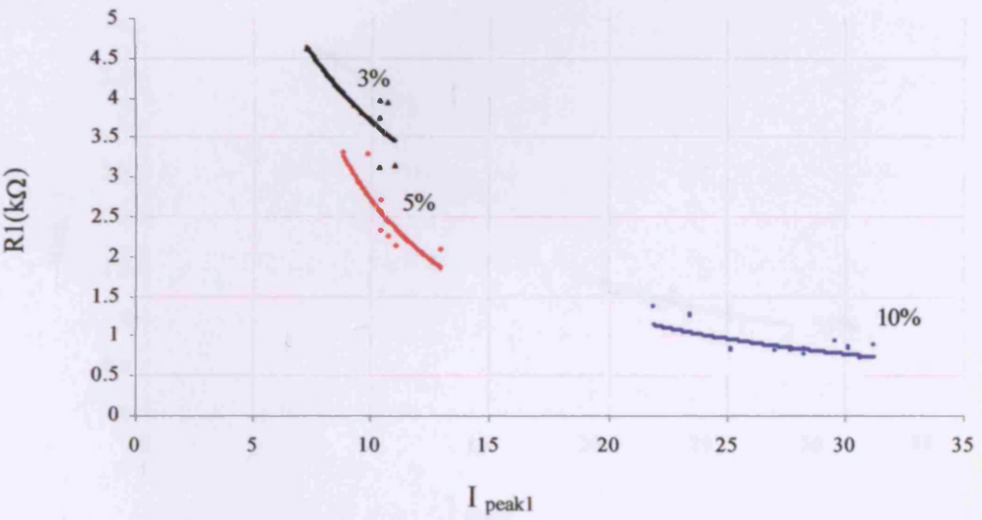

Figure 7.17 Pre-ionisation resistance R_1 (kΩ) for sand with different water content in the hemispherical container.

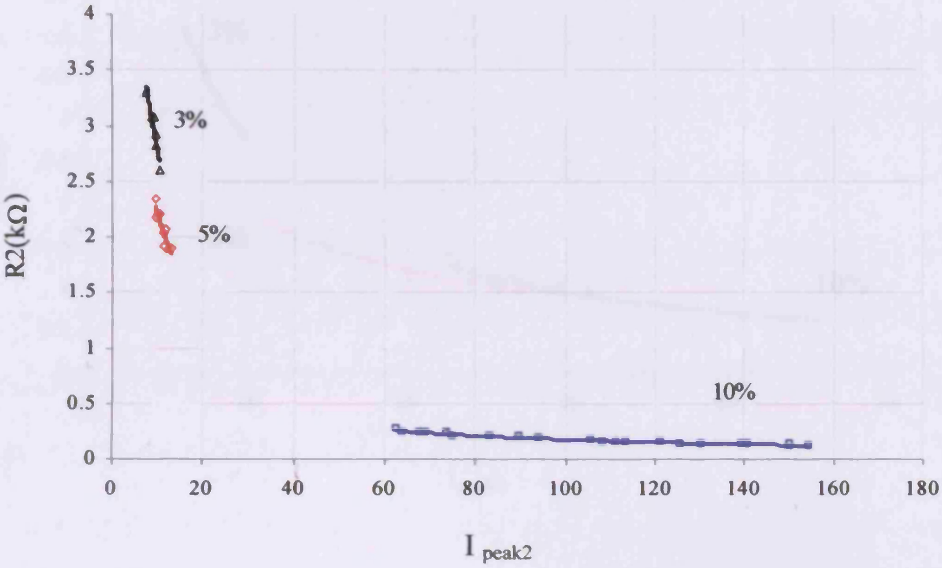

Figure 7.18 Post-ionisation resistance R_2 (kΩ) for sand mixed with different water contents in the hemispherical container.

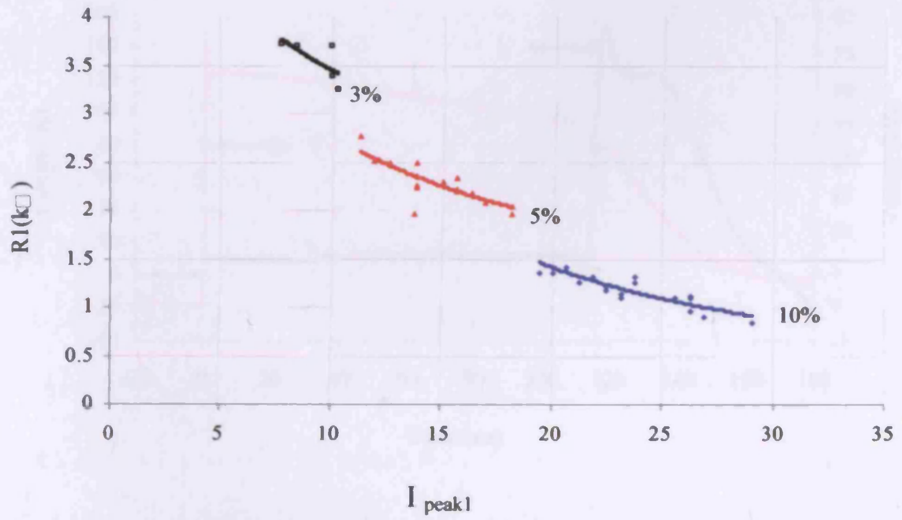

Figure 7.19 Pre-ionisation resistance R_1 (kΩ) for sand mixed with different water contents in the large test cell.

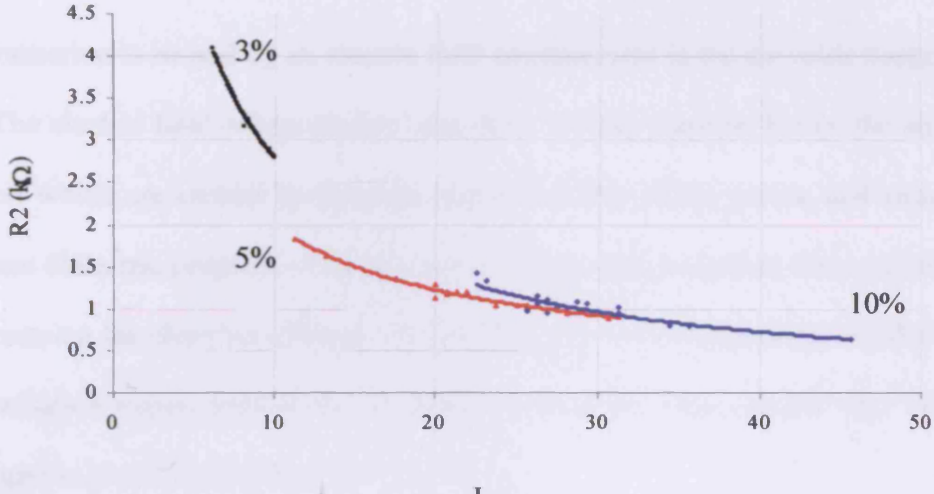

Figure 7.20 Post-ionisation resistance R_2 (kΩ) for sand mixed with different water contents in the large test cell.

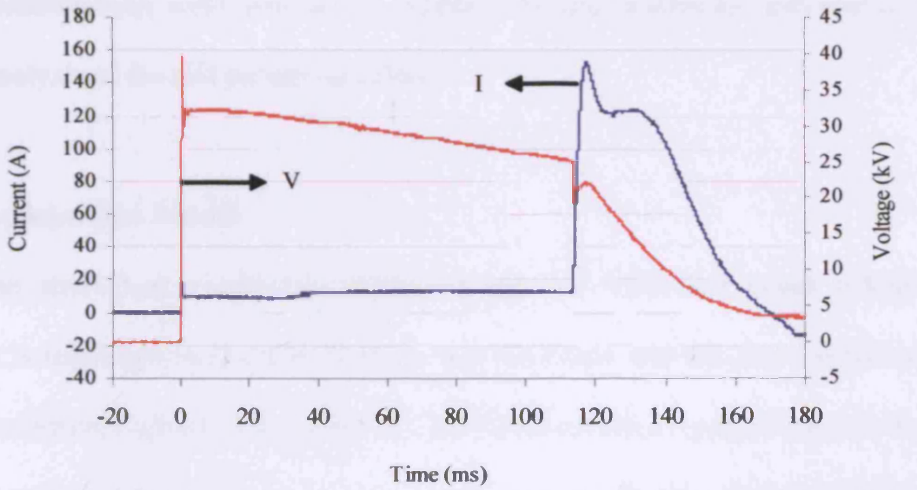

Figure 7.21 Typical voltage-current traces when breakdown occurs in sand mixed with a 3% water content (charging voltage 34kV).

7.4 Equivalent Circuit Model

Soil ionisation is caused by an electric field enhancement in the air voids trapped inside the soil. The electric field enhancements take place for two reasons; firstly, the air gaps inside the soil which are caused by irregular shape and size of the grains, and secondly by the different dielectric property of the soil and air voids. The ionisation zone extends as a result of increasing the charging voltage. The speed of the ionisation process and the final size of the ionisation region depend on the applied voltage and soil conductivity. The ionisation propagation model is illustrated in Figure 7.22.

Since the non-linear soil behaviour under high current was first obtained by Towne in 1928 [7.5], much more research work has been conducted investigating soil characterisation under high-impulse currents [7.7-7.8, 7.11, 7.25-7.28]. Computer models and equivalent circuit representations were also used to verify field and laboratory tests and to provide a detailed analysis of the soil parameter effects.

7.4.1. Proposed New Model

To find an equivalent circuit that represents the soil behaviour under a high impulse current, it is important to consider both the pre-ionisation and the post-ionisation regions. The pre-ionisation region is represented by a parallel resistance proportional to R_1 together with a capacitive component determined by the soil permittivity. The ionisation region is represented by a non-linear resistance. When the ionisation area expands, the resistance of the test soil will decrease and the overall resistance will be proportional to R2.

The soil ionisations occur after a period of time (time delay td), this time delay td is variable depending on the applied voltage. The EMTP simulations consider the variation of td as a function of the applied voltage. Therefore, two different ways were used to simulate the time delay:

- Using a time-controlled switch (SW2): this switch is connected in parallel to both branches a and b, and it is closed at a time specified from the case study, e.g. for sand mixed with 3% water subjected to 30kV charging voltage, the time delay values were inserted manually as recorded in the test results.
- Using non-linear inductance results very high impedance in branch b to start with, this causes the current to build up slowly up to a certain point. After that the current grows quickly introducing the second peak (soil ionisation). The non linear inductance, therefore, has the double function of switching and simulating the time delay required before soil ionisation occurs.

Therefore, the proposed equivalent-circuit contains two branches: the pre-ionisation region is represented by a non-linear resistance (R1) connected in parallel with a capacitance, while the ionisation region is represented by a non-linear resistance (R2) in series with an inductance L to account for the ionisation time delay. The test rod is represented by its resistance and inductance elements.

7.4.2. Simulation of Proposed Model

The laboratory test circuit together with the equivalent circuit were simulated using EMTP (ATP Draw). The values of R1 and R2 were taken from the test results shown in Figures

7.17 to 7.20. Figure 7.23 and 7.24 show the equivalent circuit model including soil ionisation and complete laboratory test-circuit as simulated in EMTP. Switches SW1 and SW2 were added to represent the impulse generator spark gap and to initiate the ionisation process respectively.

Figure 7.25 shows a simulated and measured current and voltage traces for water wetted with 3 % water and a charging voltage of 32 kV. It is clear that the proposed equivalent circuit model was able to produce the nonlinearities found in the test measurement of the current impulse. The simulated current and voltage were found to be in good agreement with values obtained from the laboratory test. Simulations of other charging voltages and different soil media were also found to be in a good agreement.

Figure 7.26 shows a complete laboratory test-circuit as simulated in EMTP, using the non-linear inductance to represent the ionisation time delay. A comparison of the (EMTP) simulation results using the time controlled switch and the nonlinear inductance are shown in Figure 7.27. The current and voltage simulated were for sand wetted with 3% water and subjected to a charging voltage of 30 kV. The similarity between the results obtained in both cases is clear.

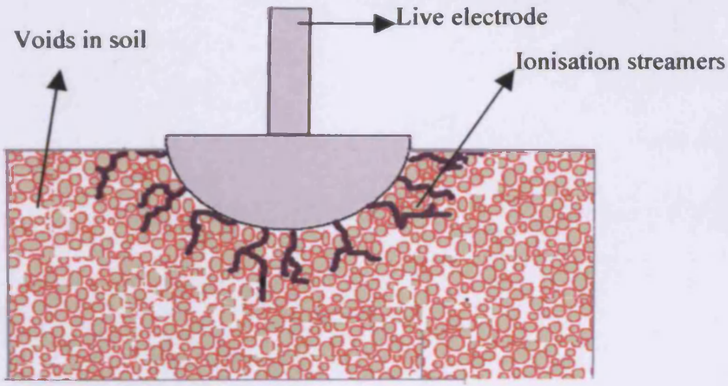

Fig.7.22 Ionisation propagation model.

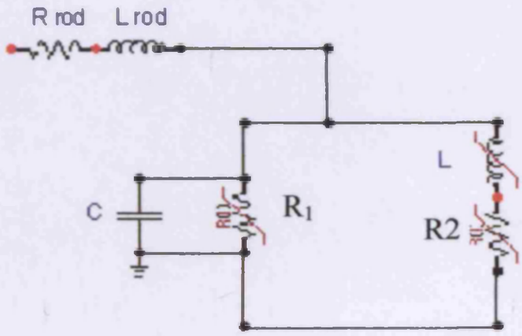

Figure 7.23 Proposed equivalent circuit of soil with ionisation.

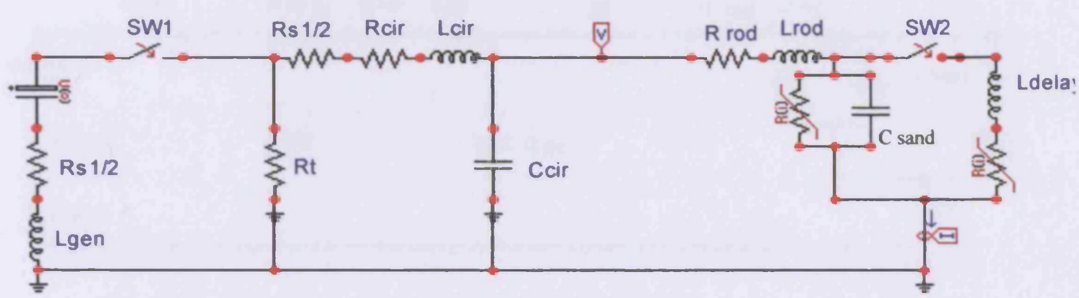

Rs1/2 = 3.3 Ω, Lgen = 0.02 mH, C = 0.5 μF, Rt = 9600 Ω,
Rcir = 0.01 Ω, Lcir = 0.03 mH, Ccir = 5E-6 μF
Rrod = 0.0001 Ω, Lrod = 0.0001 mH, Csand = 1.5E-5μF
SW1: closing time = 10 μs and opening time = 1 s
SW2: closing time was selected from t_d of wet 3 % sand tests and opening time = 1 s

Figure 6.24 EMTP Simulation circuit.

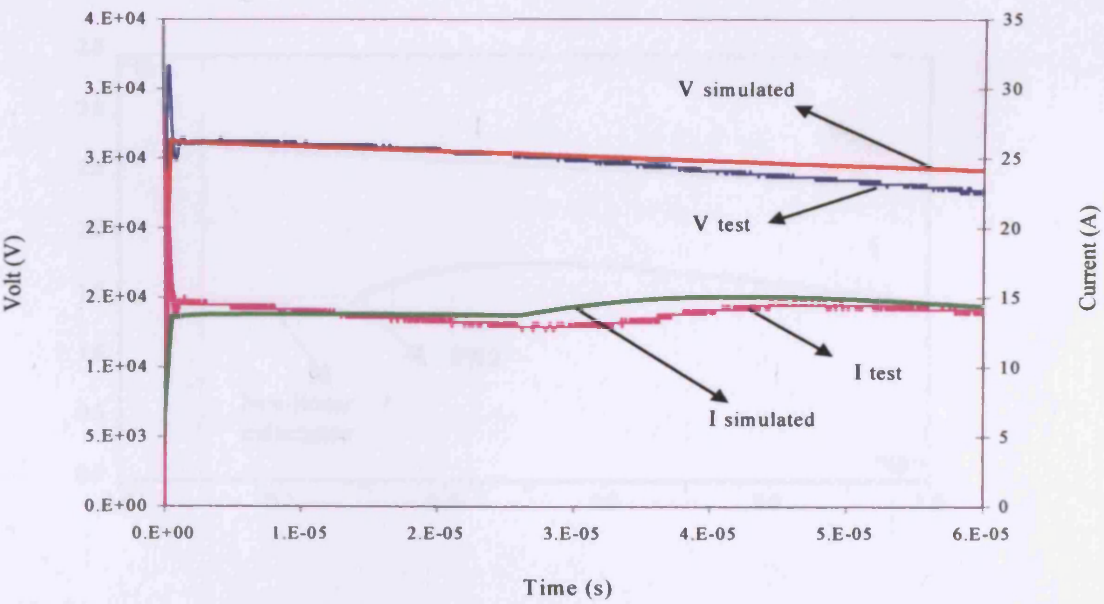

Figure 7.25 Simulated and measured current and voltage for a 32kV charging voltage (3% water content).

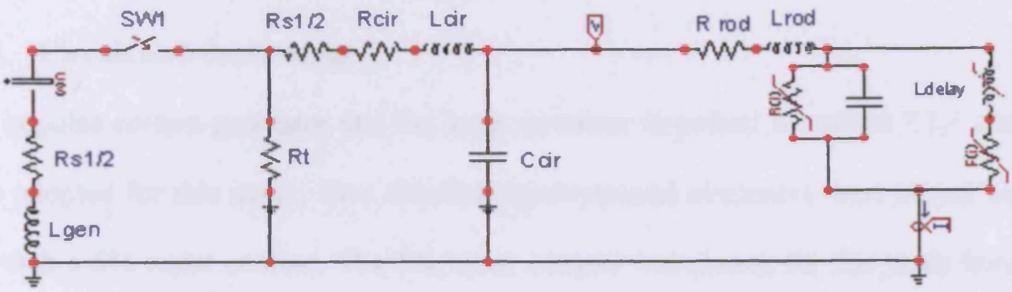

Rs1/2 = 3.3 Ω, Lgen = 0.02 mH, C = 0.5 μF, Rt = 9600 Ω,
Rcir = 0.01 Ω, Lcir = 0.03 mH, Ccir = 5E-6 μF
Rrod = 0.0001 Ω, Lrod = 0.0001 mH, Csand = 1.5E-5μF
SW1: closing time = 10 μs and opening time = 1 s

Figure 7.26 EMTP Simulation circuit (using non-linear inductance).

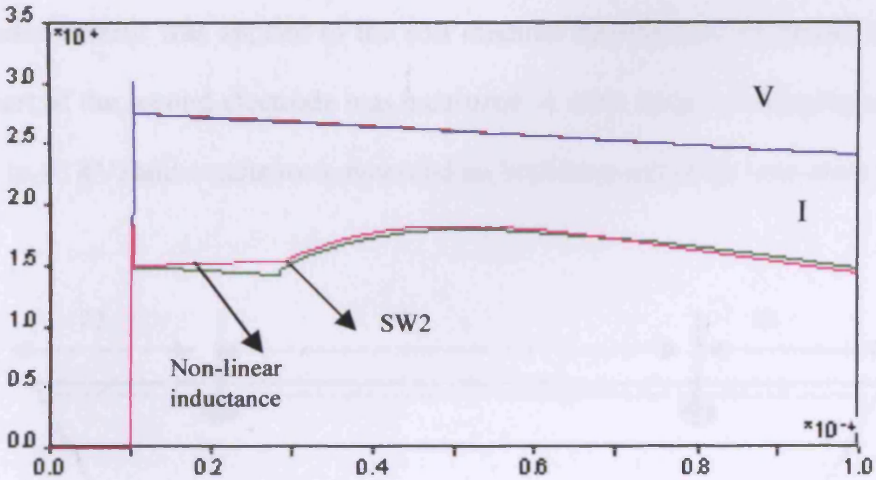

Figure 7.27 Compare simulated V and I resulting from using SW2 and non-linear inductance. (3% water content, 30kV).

7.5 Tests with Two Electrodes in Unbounded Medium

7.5.1 Circuit and Procedures

The impulse current-generator and the large container described in section 7.3.1 and 7.2.1 were adopted for this study. Two identical hemispherical electrodes were buried into wet soil with a 5% water content. The 5% water content was chosen for this study because it provides more uniform wetting of the sand during the test period, while it was very hard to handle the sand with 3% or 10 % water content due to vaporisation and water settling. Both electrodes were placed at an exact distance from the container boundaries. In an attempt to eliminate the capacitive effect between both electrodes, a wider distance was chosen to separate the electrodes. The location of both electrodes within the test cell is shown in Figure 7.28. All test-circuit elements are as described in section 7.3.1

The impulse current was applied to the soil medium through one electrode; the current at the top part of the second electrode was measured. A wide range of charging voltages were used (15 to 45 kV) and results were recorded on both long and short time-scales.

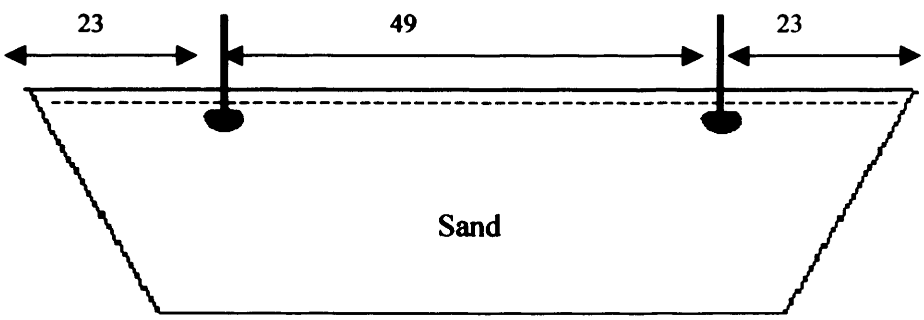

Figure 7.28 The location of electrodes within the test container.

7.5.2 Results and Analysis

Typical voltage and current impulse shapes for sand mixed with 5% water at a charging voltage of 25 kV are illustrated in Figure 7.30 for both long and short time-scales.

In the long time-scale records, it can be seen that both current and voltage increase rapidly to reach their peak values after about 0.6 and 0.03 μs respectively. Initial oscillations observed here could be the result of capacitive effects. On the impulse tail, both current and voltage decay slowly to reach zero. No second current peak was observed on the current impulse, indicating that soil ionisation did not take place in these arrangements.

The short time-scale traces provide more detailed current and voltage impulse for up to 3.5 μs. The detailed current-impulse exhibits an unexpected initial reduction of current wave to negative values, before the current starts increasing rapidly to reach its peak value. This initial current reduction has thus far not been explained. It is however thought that it could be due to inductive component in the current measurement circuit.

The impulse resistance R of the test electrode system is calculated as the instantaneous ratio of voltage to current. This impulse resistance is plotted as a function of its corresponding instantaneous current for different charging voltages. The results are presented in Figure 7.31(a and b) for both the long and short time-scale records. Both graphs show that the resistance R decreases as the current magnitude is increased. This indicates a non-linear conduction process in the test medium possibly resulting from either heating effects or low level ionisation effects.

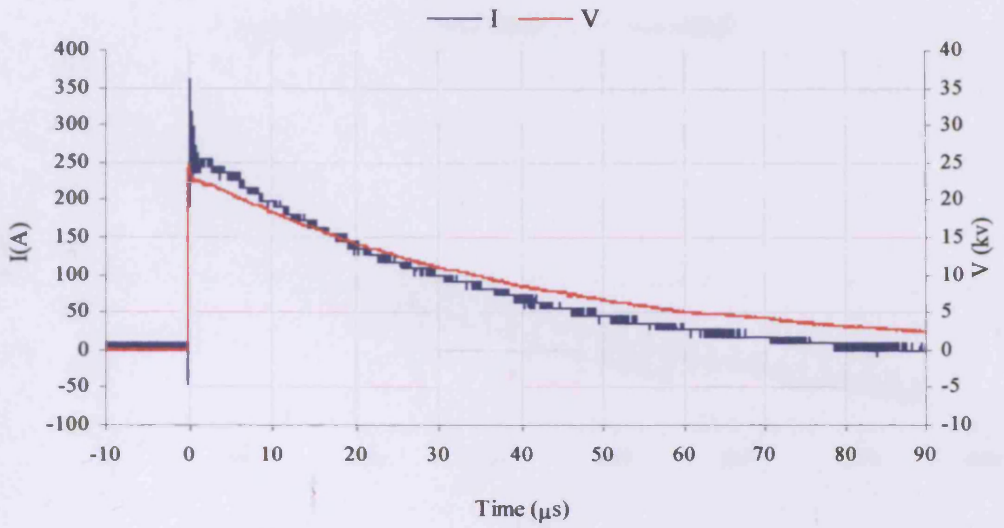

(a) Long time scale

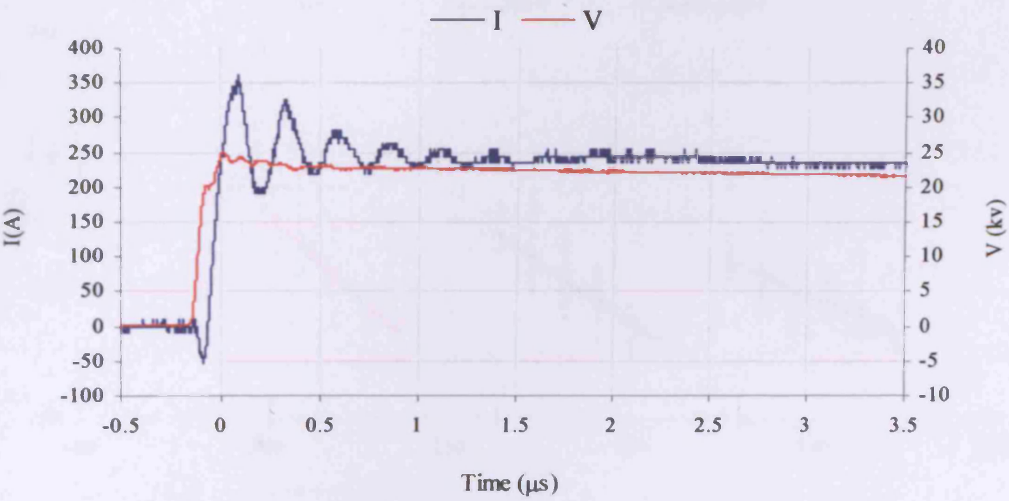

(b) Short time scale

Figure 7.30 Voltage and current impulse shape for sand mixed with 5% water (charging voltage of 25 kV).

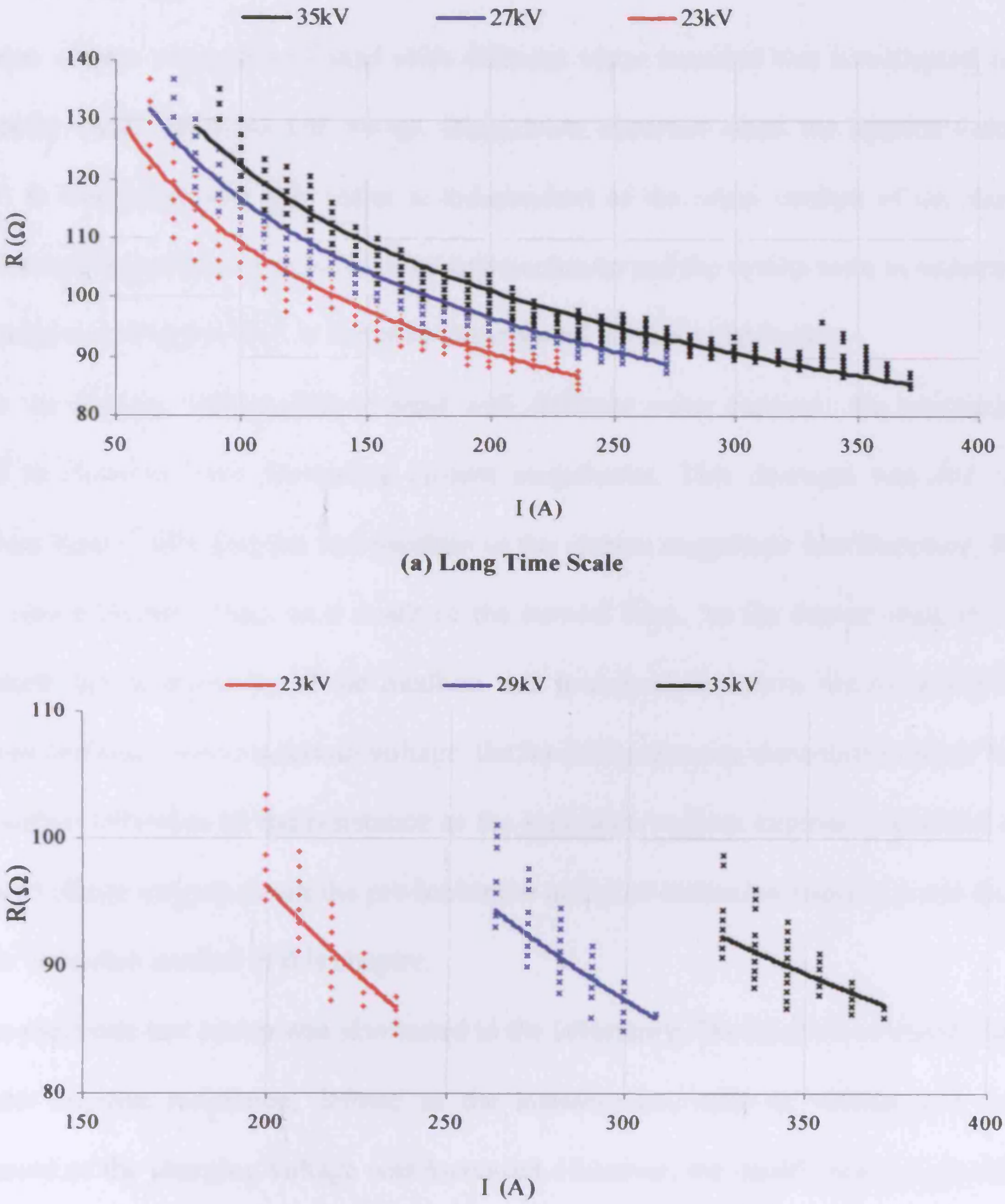

(a) Long Time Scale

(b) Short Time Scale

Figure 7.31 Impulse resistance (R) as a function of its corresponding current for different charging voltages.

7.5 Conclusions

The non –linear behaviour of sand with different water contents was investigated using a laboratory earth electrode test set-up. Breakdown occurred when the applied voltage is 34kV. It was found that this value is independent of the water content of the sand. An impulse test was also conducted on a resistive solution and the results were as expected; the resistance was found to have a constant value for all current magnitudes.

When the impulse was applied to sand with different water contents, the resistance was found to decrease with increasing current magnitudes. This decrease was due to two different factors affecting the test medium as the current magnitude was increased. Firstly, there was a thermal effect as a result of the current flow. As the current magnitude was increased, the conductivity of the medium was increased, therefore, the resistivity of the soil was reduced. Above a certain voltage, the ionisation process starts to take place leading to a further reduction of the resistance as the ionisation regions expand. The effect of the applied voltage magnitude on the pre-ionisation and post-ionisation resistance and the time delays were also studied in this chapter.

A two-electrode test set-up was also tested in the laboratory. The analysis of results showed that the impulse resistance, defined as the instantaneous ratio of voltage and current, decreased as the charging voltage was increased. However, the double peak observation in the case of the hemispherical test cell did not occur for the two-electrode system. Further investigations are required to determine whether ionisation takes place in the two electrode test set-up.

CHAPTER EIGHT

General Conclusions and Suggestions for Further Work

8.1 Conclusions

An examination of published research relating to electrical and lightning injuries has revealed the danger of these injuries. Investigators have attempted to determine the factors that affect the severity of an electrical injury. These factors include the amount of energy dissipated inside the body (this is dependent on the body weight), the current magnitude and the shock duration. The type of current is a very important factor as it was found that direct current is safer than alternating current. The severity of lightning injury depends on the frequency, voltage, current magnitude, the duration, pathway, and the behaviour of the tissue. Victims may survive the lightning strike but they could suffer from long-term injuries such as neurological and other physical or psychological injuries.

All the statistical information in the published work confirms that the number of deaths by lightning is reducing with years. One of the most important reasons for this reduction is the increasing use of earthing systems. The earthing system should provide a low earth impedance magnitude in order to dissipate the current to earth. To achieve a low earth impedance magnitude, two different parameters should be considered in designing the earthing system: the electrode geometry and the soil properties.

An extensive parametric study of earthing systems response to high frequencies has been conducted. The earthing systems analysed were vertical rods, horizontal electrodes and earth grids. The earthing system performance primarily depends on the soil resistivity, soil permittivity, the dimensions of the earthing system and the location of the injection points. The frequency is an important factor that affects the performance of the earthing systems. The impedance of earthing systems increases noticeably at high frequencies due to the inductive effect of the earthing system, especially in a medium with low soil resistivity. The capacitive effects become pronounced at high frequencies in a soil of resistivity higher than 1kΩm, especially with high relative permittivity. The earthing systems impedance increases with the increase of soil resistivity.

The impedance magnitude decreases with increasing the electrode length up to a certain point when the electrode reaches its effective length, beyond which increasing the length no longer affects the earth impedance. The concept of effective length has been confirmed and extended to the effective area of the grid. Increasing the grid size has a significant effect on reducing the earth grid impedance until it reaches its effective area beyond which increasing the size no longer reduce the earth grid impedance.

The effect of the injection point position has been investigated, it has been found that injection point position has no effect on the earth grid impedance at low frequency range. At higher frequencies, however, the impedance of a central injected grid is smaller than that of corner injected grid. This effect becomes very small at 10MHz, when the impedance magnitude is almost the same for central and corner injected point.

Increasing the number of meshes for a grid earthing system, results in a reduction on the earth grid impedance over a particular range of frequency depending on the soil resistivity. This behaviour could be attributed to the effective area of the earthing system. Increasing the mesh density locally, around the injection point, has been found to result in a reduction on the earth grid impedance. However, this arrangement is not as effective as increasing the overall mesh density.

In addition, adding vertical rods to the earth grid results in a reduction of the earth grid impedance for all soil resistivities, at low frequencies before the inductive effect becomes dominant. Increasing the number of rods introduces an extra reduction in the earth grid impedance.

An above ground enhancement has been suggested and has been proved to play a significant role in reducing the earth grid impedance over a particular range of frequencies where the inductive effect is dominant. This may be due to the fact that the inductance of the earth grid itself is smaller at this frequency range, therefore, the effect of the downleads is more pronounced, especially in a medium with low soil resistivity.

The effect of the above-ground enhancement on the transferred potential has also been investigated. It has been found that connecting downleads has an advantage of reducing the potential and therefore, the earth impedance at the injection point. However, it was shown to transfer a higher potential over a larger area.

The transient behaviour of the earthing system has also been investigated. With high soil resistivity, the transient ground potential rise peak magnitude and front-time increase with increasing soil resistivity and decrease with soil permittivity for all configurations. Increasing the length of the electrode or the grid size has an important effect on reducing the TGPR peak magnitude up to specific length/size beyond which increasing the length/size does not affect the TGPR magnitude.

The TGPR magnitude is affected by the current-impulse shape. For slow current impulses, the earth electrode is dominantly resistive and the front-time for both current impulse and resulting TGPR are very close in values. However, for fast-current impulses the front-time depends mainly on the soil resistivity, where the capacitive effect is dominant. The front-time for TGPR is greater than that for the current impulse, with very high soil resistivity. For low soil resistivity, the inductive effect is dominant and the TGPR font-time is shorter than the front-time of the current impulse.

The earthing system of an operational substation has been used as a case study. The frequency response and the transient behaviour of the earthing system have been studied. Results obtained from simulating this operational substation earthing system are similar to those obtained from the generic grid. Two important differences were observed: 1) a capacitive effect is present at high frequencies for all soil resistivities selected for this study. 2) for basic earth grid, the oscillations observed above 1MHz and for 10kΩm soil resistivities, have not been seen in this substation study.

The transient step and touch voltage magnitudes have been calculated within and around substation area under fast-impulse current conditions. It is very important to note that both transient step and touch voltages have been calculated for the worst case scenario when the current impulse hits the substation and at the instant of its peak value. There are no standard recommendations for the safety limits under these conditions. Therefore, it was not possible to conclude whether this earthing system is safe under these conditions or not.

The soil behaviour under impulse current has been investigated. Sand with different water content was tested using a laboratory earth electrode test set-up. Two main factors were found to control the sand behaviour under impulse conditions. Firstly, there is a thermal effect as a result of current flow. As the current magnitude was increased, the conductivity of the medium was increased, therefore, the resistivity of the soil was reduced. Secondly, an ionisation process which takes place above a certain voltage, leading to a further reduction in resistance as the ionisation regions expand.

A two electrode test set up has also been analysed. Soil ionisation was not observed at any point of the test indicating that the reduction of the resistance magnitude was due to a thermal effect as a result of the current flow.

8.2 Suggestions for Further Work

Further investigations are required to provide a better understanding of the earth grid response at a frequencies higher than 1MHz in a medium of soil resistivity higher than 1 kΩm.

New practical arrangements such as above ground enhancements and additional rods need to be investigated under transient conditions for different soil conditions.

The laboratory test for the two electrodes arrangement requires further examination under different water content conditions.

Chapter One

[1.1] M.A. Cooper et al.: 'Lightning Injuries', Wilderness Medicine by Paul S. Auerbach, 4th Edition, Inc. pp. 73-110, 2001.

[1.2] Electricity Association, Technical Specification 41-24 (EA TS 41-24), 'Guidelines for the Design, Testing and Maintenance of Main Earthing Systems in Substations', Electricity Association Services Limited, 1992.

[1.3] E.D. Sunde: 'Surge Characteristics of a Buried Bare Wire', AIEE Transactions, Vol. 59, pp. 987, 1940.

[1.4] ANSI/IEEE Std 80, 'IEEE Guide for Safety in AC Substation Grounding', The Institute of Electrical and Electronic Engineers, 2000.

[1.5] HD 637 S1, 'Power Installation Exceeding 1kV AC', European Committee for Electrotechnical Standardisations (CENELEC), 1999.

[1.6] BS 6651, 'Code of Practice for Protection of Structures against Lightning', British Standard 1999.

[1.7] IEC 479, 'Guide to Effects of Current on Human Beings and Livestock'. British Standards institution.

[1.8]. R.H Golde: 'Lightning' Vol. 1: Physics of Lightning, Academic Press, London, ISBN 0-12-287801-9, 1977.

[1.9] IEC-BS 923: "Guide on High Voltage Testing Techniques", British Standards institution, 1990

[1.10] R. H. Golde, W. R. Lee: 'Death by Lightning', Proc. IEE, , Vol. 123, No. 10R, pp. 1163-1180. October 1976.

[1.11] R.E Lopes and R.L. Holle: 'Changes in Number of Lightning Death in the United States During the Twentieth Centuries', Journal of Climate, Vol. 2, pp. 2070-2077. Oct 1997.

[1.12] T. Ishikawa: 'Prevention against Lightning Accidents in Japan', Nihon Univeristy, J. Med. 24, pp. 1-14, 1982.

[1.13] J.B. Wareing: 'Novel Protection from Lightning for 11kV Pole Mounted Transformers', Report No. 2967, EA Technology, August 1993.

[1.14] P. Hardaker: 'No More Bolts from the Blue', IEE Review, Vol. 43, No. 5, pp. 199, September 1997.

[1.15] H. Muir:'Striking Back at Lightning', New Scientist, Vol. 148, No. 1998, pp. 27, October 1995.

[1.16] CDEGS User Group Meeting Report: 1994, Safe Engineering Services Ltd., Montreal, 1994.

Chapter Two

[2.1] A.M. Davies: 'High Frequency and Transient Performance of Earthing Systems', PhD Thesis, University of Wales, Cardiff, 1999.

[2.2] ANSI/IEEE Std 80, 'IEEE Guide for Safety in AC Substation Grounding', The Institute of Electrical and Electronic Engineers, 2000.

[2.3] IEC-479, 'Guide to Effects of Currents Passing through the Human Body' BSI standards 1995.

[2.4] C. F. Dalziel, J. B. Lagen, J. L. Thurston: 'Electric Shock', Eelectr. Eng., 1941, 60, pp. 1073-1078.

[2.5] C. F. Dalziel: 'A Study of Hazards of Impulse Current', Trans. Am. Inst. Eelectr. Eng., 1953, 72, pp. 1032-1043.

[2.6] C. F. Dalziel, W. R. Lee: 'Reevaluation of Lethal Electric Currents', IEEE Trans, 1968, IGA-4, pp. 467-476.

[2.7] R.J. Scott: 'Ventricular Fibrillation in Dogs with Normal Acid Base State', Brit. J. Industr. Med., 1973, 30, pp. 155-161.

[2.8] N. Kitagawa, K. Kinoshita, T. Ishikawa: 'Discharge Experiments Using Dummies and Rabbits Simulating Lightning Strokes on Human Bodies', Int. J. Biometeor, 1973, Vol. 17, No 3, pp. 239-241.

[2.9] T. Ishikawa, et al.: 'Experimental Study on the Lethal Threshold Value of Multiple Successive Voltage Impulses to Rabbits Simulating Multi-stroke Lightning Flash', Int. J. Biometeor, 1985, Vol. 29, No. 2, pp. 157-168.

[2.10] R. H. Golde, W. R. Lee: 'Death by Lightning', Proc. IEE, October 1976, Vol. 123, No. 10R.

[2.11] P. Osyoka,: 'Messtechnische Untersuchungen Uber Stromstarke, Einwirkungsdauer und Stromweg bei elektrischen wechselstromunfallen an mensch und Tier', Elektromedizin, 1936, Vol. 8, pp 153-179 and 193-214.

[2.12] M. A. Cooper: 'Emergent Care of Lightning and Electrical Injuries', Seminar in Neurology, Vol. 15, No. 3 , September 1995.

[2.13] M.A. Cooper et al: 'Lightning Injuries', Wilderness Medicine by Paul S. Auerbach, 4th Edition Inc. pp. 73-110, 2001

[2.14] M. Daniel, et al.: 'Neuropsychological and Emotional Consequences of Accident, High-Voltage Electric Shock', Inter. J. Clinical Neuropsycology, 1985, Vol. 7, 102-106.

[2.15] H. Hooshmand, et al: 'The Neurophysiological Aspects of Electrical Injuries', Clinical Electroencephalography, 1989, Vol. 20, No. 2, pp. 111-120.

[2.16] A.R.Grossman et al: 'Auditory and Neuropsychiatric Behaviour Patterns after Electrical Injury', Journal of Burn Care and Rehabilitation, Vol. 14, No. 2, part 1, pp. 169-175.

[2.17] R.H.Golde: 'Lightning Protection'. Edward Arnold Publishers Ltd, ISBN 0 7131 3289 2, 1973.

[2.18] C. Andrews, M.A. Copper et al: 'Disease-a-Month', 1997. 43, 871-891.

[2.19] R. Zane: 'Lightning Injuries', Emergency Medicine Clinics of North America, Vol. 22, pp. 369-403, 2004.

[2.20] E. Gourbiere: 'Lightning Effect on Human Being', International Conference of Lightning Protection (ICLP), 2004, Vol. 1, INV2.

[2.21] C. Cooray et al.: 'Lightning Caused Injuries in Human', International Conference of Lightning Protection (ICLP), 2004, Vol. 2, pp. 857-862.

[2.22] T. Ishikawa: 'Prevention against Lightning Accidents in Japan', Nihon University. J. Med. 24, 1-14, 1982.

[2.23] T. Ishikawa et al: 'Lightning Injury Caused by Discharges Accompanying Flashovers- A Clinical and Experimental Study of Death and Survival', Seventh International Congress of Burn Injuries, Melbourne, Australia, Vol. 12, No. 7, pp. 496-501, 1986.

[2.24] C. J. Andrews, M. Darveniza, D. Mackerras: 'Lightning Injury- A Review of Clinical Aspects, Pathophyiology, and Treatment', Adv Trauma 4, 241-288, 1989.

[2.25] C. J Andrews, M. Darveniza: 'Telephone Mediated Lightning Injury: an Australian Survey', The Journal of Trauma, Vol. 29, No. 5, pp. 665-671. 1989.

[2.26] C. J Andrews et al: 'Lightning Injuries: Electrical, Medical and Legal Aspects', CRC Press, Boca Raton, 1992.

[2.27] C. J Andrews, 'Structural Changes after Lightning Strike, with Special Emphasis on Special Sense Orifices as Portals of Entry', Seminars in Neurology, Vol. 15, Number 3, September 1995.

[2.28] M. Primeau, G. Engelstatter, K Bares: 'Behavioral Consequences of Lightning and Electrical Injury', Seminar in Neurology, Vol. 15, No. 3, September 1995.

Chapter Three

[3.1] E.D. Sunde: 'Earth Conduction Effect in Transmission System'. New Dover Publications Inc., New York, 1968.

[3.2] A.M. Davies: 'High Frequency and Transient Performance of Earthing Systems', PhD Thesis, University of Wales, Cardiff, 1999.

[3.3] A.M. Davies, H. Griffiths, T.E. Charlton: 'High Frequency Performance of a Vertical Earth Electrode', Proceedings of the 24th International Conference on Lightning Protection (ICLP), Birmingham UK, pp. 536-540, 1998.

[3.4] F. Van der Linde, B. Zedan, H. Griffiths, A. Haddad: 'Impulse Response of Earth Electrode Systems', 37th International Universities Power Engineering Conference (UPEC), Stafford, UK, pp. 827 – 831, September 2002.

[3.5] M. I. Lorentzou, and N. D. Hatziargyriou,: 'EMTP Modeling of Grounding Electrodes' 34th International Universities Power Engineering Conference (UPEC), pp. 351 – 354, September 1997.

[3.6] M. I. Lorentzou, and N. D. Hatziargyriou: 'Effective Dimensioning off Extended Grounding Systems for Lightning Protection'. 25th International Conference on Lightning Protection, (ICLP), Greece. 2000.

[3.7] H. Griffiths, and A.M. Davies: 'Effective Length of Earth Electrodes Under High Frequency and Transient Conditions', 25th International Conference on Lightning Protection, Vol. 1, Rhodes (Greece), pp. 536-540, 2000.

[3.8] H. Griffiths, B. Zedan, A. Haddad: 'Frequency Response of Earthing Systems', 28th International Universities Power Engineering Conference, Vol. 2, pp. 717-720, Thessaloniki (Greece), 2003.

[3.9] F. Van der Linde, B. Zedan, , H. Griffiths, A. Haddad: 'Impulse Response of Earth Grid' 13th International Symposium on High Voltage Engineering. Greece. 2003.

[3.10] B. R. Gupta, and V. K. Singh: 'Impulse Impedance of Rectangular Grounding Grids', IEEE Transactions on Power Apparatus and Systems, Vol. 7, No. 1, pp. 214, Jan 1992.

[3.11] L. D. Grecv, and M. Heimbach: 'Frequency Dependent and Transient Characteristics of Substation Grounding Systems', IEEE Transactions on Power Delivery. Vol. 12, No. 1, 1997.

[3.12] B. Zedan, H. Griffiths, A. Haddad: 'The Effect of Grid Mesh Density on Substation Earth Impedance', Proceedings of the 36th Universities Power Engineering Conference, Swansea, UK, pp. 3C3.1-4, 2001.

[3.13] M. Heimbach, and, L. D. Grecv: 'Simulation of Grounding Structures within EMTP', 10th International Symposium on High Voltage Engineering", 1997.

[3.14] L. D Grecv, and M. Heimbach: 'Computer Simulation of Transient Ground Potential Rise in Large Earthing Systems', Proceedings of the 23rd International Conference on Lightning Protection, Florence, pp.585. , September 1996.

[3.15] M. Heimbach, and L. D. Grecv: 'Grounding System Analysis In Transient Programs Applying Electromagnetic Field Approach', IEEE Transactions on Power Delivery. Vol. 12, No. 1, pp. 186-193, January 1997.

/

[3.16] A. D Papalexopoulos, and A. P. Meliopoulos: 'Frequency Dependent Characteristics of Grounding Systems', IEEE Trans. Vol. PWRD-2, No. 4, pp. 1073-1081,1987.

[3.17] B. R. Gupta, and B. Thapar: 'Impulse Impedance of Grounding Grids', IEEE Trans. Vol. PAS-99, No. 6, pp. 2357-2362, 1980.

[3.18] Verma, R. and Mukhedkar, D.: 'Fundamental Consideration and Impulse of Ground Grids', IEEE Trans. PAS-100, Vol., No. 3, pp. 1023-1030, 1981.

[3.19] IEEE80, 'IEEE Guide for Safety in AC Substation Grounding', Revision IEEE Std 80-2000, IEEE Inc, New York, 2000.

[3.20] Electricity Association: Technical Specification 41-24, 'Guidelines for the Design, Installation, Testing and Maintenance of Main Earthing Systems in Substations', Issue 1, 1992.

[3.21] G. J. Burke, and E. K. Miller: 'Modelling Antennas Near to and Penetrating a loosy Interface', IEEE Transactions on Antennas and Propagation, Vol. AP-32, No. 10, pp. 1040-1049, October 1984.

[3.22] L.Grecv, F. Dawalibi: 'An Electromagnetic Model for Transients in Grounding Systems', IEEE Transactions on Power Delivery, Vol. 5 , No. 4, 1990, pp. 1773-1781.

[3.23] R. G. Olsen and C. W. Willis: 'A Comparison of Exact and Quasi-Static Methods for Evaluating Grounding Systems at High Frequencies', IEEE Transactions on Power Delivery, Vol. 11, No. 2, pp. 1071-1081, 1996.

[3.24] SES, 'CDEGS: Getting Started Manual', Safe Engineering Services and Technologies Ltd, Canada , 1968.

Chapter Four

[4.1] ANSI/IEEE Std 80, 'IEEE Guide for Safety in AC Substation Grounding', The Institute of Electrical and Electronic Engineers, 2000.

[4.2 Electricity Association, Technical Specification 41-24 (EA TS 41-24), 'Guidelines for the Design, Testing and Maintenance of Main Earthing Systems in Substations', Electricity Association Services Limited, 1992.

[4.3] CENELEC (HD) 637 S1, 'Power Installation Exceeding 1kV AC', European Committee for Electrotechnical Standardisations, 1999.

[4.4] H. Griffiths, and A.M. Davies: 'Effective Length of Earth Electrodes Under High Frequency and Transient Conditions', 25th International Conference on Lightning Protection, Vol. 1, Rhodes (Greece). pp. 536-540, 2000.

(

Chapter Five

[5.1] E. Kuffel, W. S. Zaengl and J. Kuffel: 'High-Voltage Engineering: Fundamentals'Butterworth-Heinemann, Oxford, 2000.

[5.2] IEC-BS 923: "Guide on High Voltage Testing Techniques", British Standards institution, 1990

[5.3] P.L. Bellaschi and R.E. Armington: 'Impulse and 60-cycle Characteristics of Driven Grounds- III: Effect of Lead in Ground Installation', AIEE Transactions on Electrical Engineering, Vol. 62, PP. 335-345, 1943.

[5.4] A.M. Davies, (1999): 'High Frequency and Transient Performance of an Earthing System', PhD Thesis, University of Wales, Cardiff, 1999.

[5.5] F.P. Dawalibi, W. Ruan, and S. O. Fortine: 'Lightning Transient of Communication Towers and Associated Grounding Networks' , Malaysia paper from CDEGS: Getting started manual, Safe Engineering Services and Technologies Ltd, Quebec, Canada, 1998.

[5.6] F. P. Dawalibi, W. Xiong, J. Ma: 'Transient Performance of Substation Structures and Associated Grounding System', IEEE Transactions on Industrial Applications, Vol. 31, No. 3, PP 520-527, 1995.

[5.7] A. Geri: 'Practical Design Criteria of Grounding Systems under Surge Conditions', 25th ICLP, Rhodes, Greece, pp. 458-463, September 2000.

[5.8] L. D. Grecv: 'Computer Analysis of Transient Voltages in Large Grounding Systems' IEEE Transactions on Power Delivery, Vol. 11, No. 2, pp. 815-823, April 1996.

[5.9] L.D. Grecv, M. Heimbach, (1997): 'Frequency Dependent and Transient Characteristics of Substation Grounding System', IEEE Transaction on Power Delivery, Vol. 12, No. 1, pp. 172-178 , January 1997.

[5.10] L. D. Grecv, F. E, Menter: 'Transient Electromagnetic Field near Large Earthing Systems', IEEE Transaction on Magnetics, Vol. 32, No. 3, pp. 1525- 1528, May 1996.

[5.11] H. Griffiths, A.M. Davies: 'Frequency Performance of Concentrated Earthing Systems', 12th International Symposium on High Voltage Engineering (ISH), Bangalore, India, Vol. 1, pp. 142- 45, August 2001.

[5.12] H.Griffiths, A.M. Davies: 'Effective Length of Earth Electrodes under High Frequency and Transient Conditions', 25th ICLP, Rhodes, Greece, pp. 469-473, September 2000.

[5.13] B.R. Gupta B. Thapar: 'Impulse Impedance of Grounding Grids', IEEE Transaction on Power Apparatus and Systems, Vol. PAS- 99, No. 6, pp. 469-473, Nov/Dec 1980.

[5.14] B. R. Gupta, V. K. Singh: 'Inductance of Rectangular Grids', IEEE Transaction on Power Delivery, Vol. 7, No. 3, pp. 1218-1222, July 1992.

[5.15] B. R. Gupta, V. K. Singh: 'Impulse Impedance of Rectangular Grounding Grids', IEEE Transaction on Power Delivery, Vol. 7, No. 1, pp. 214-218, January 1992.

[5.16] M. Heimbach, L. D. Grecv: 'Grounding System Analysis in Transient Programs Applying Electromagnetic Field Approach', IEEE Transactions on Power Delivery, Vol. 12, No. 1, pp. 186-193, January 1997.

[5.17] Y. Liu, M. Zitnik, R. Thottappillil: 'A Time Domain Transmission Line Model of Grounding System', 12th International Symposium on High Voltage Engineering (ISH), Bangalore, India, Vol. 1, pp. 154-157, 20-24 August 2001.

[5.18] M.I. Lorentzou, N. D. Hatziargyriou: 'Effective Dimensioning of Extended Grounding System for Lightning Protection', 25th International Conference of Lightning Protection (ICLP), Rhodes, Greece, pp. 435-439, 18-22 September 2000.

[5.19] A.P. Meliopoulos, M.G. Moharam: 'Transient Analysis of Grounding Systems', IEEE Transaction on Power Apparatus and Systems, Vol. PAS 102, No. 2, pp. 389-399, February 1983.

[5.20] F. E. Menter, L. Grecv: 'EMTP-Based Model for Grounding System Analysis', IEEE transaction on Power Delivery, Vol. 9, No. 4, pp. 1838-1849, October 1994.

[5.21] K.J. Nixon, I. R. Jandrell, H. J. Geldenhuys: 'Sensitivity Analysis of Parameters Influencing the Lightning Impulse Current Behaviour of Earth Electrode Components', 25th International Conference of Lightning Protection (ICLP) Rhodes, Greece, 18-22, pp. 484-489, September ,2000.

[5.22] A. D. Papalexopoulos, A. P. Meliopoulos: 'Frequency Dependent Characteristics of Grounding Systems', IEEE transaction on Power Delivery, Vol. PWRD-2, No. 4, pp. 1073-1081, October 1987.

[5.23] M. Ramamoorty et al.: 'Transient Performance of Grounding Grids', IEEE Transaction on Power Delivery, Vol. 4, No. 4, pp. 2053-2059, October 1989.

[5.24] T. Sonoda, Takesue, Hidemi S. Sekioka: 'Measurements on Surge Characteristics of Grounding Resistance of Counterpoise for Impulse Currents', 23rd International Conference of Lightning Protection (ICLP), Rhodes, Greece, pp. 411-416, September, 2000.

[5.25] R. Velazquez, D. Mukhedkar: 'Analytical Model of Grounding Electrodes Transient Behaviour', IEEE transaction on Power Apparatus and Systems, Vol. PAS 103, No. 3, pp. 1314-1322, June 1984.

[5,26] W. Xiong, F. P. Dawalibi: 'Transient Performance of Substation Grounding Systems Subjected to Lightning and Similar Surge Currents', IEEE Transaction on Power Delivery, Vol. 9, No. 3, pp. 1412-1420, July 1994.

[5,27] P. L. Bellaschi: 'Impulse and 60-Cycle Characteristics of Driven Grounds-I' AIEE Transaction on Electrical Engineering, Vol. 60, pp. 123-128, March 1941.

[5.28] P. L. Bellaschi, R. E. Armington, A. E. Snowden: 'Impulse and 60-Cycle Characterises of Driven Grounds-II', AIEE Transaction on Electrical Engineering, Vol. 61, pp. 349-363, 1942.

[5.29] L. V. Bewley: 'Theory and Tests of the Counterpoise', AIEE Transaction on Electrical Engineering, 12632, pp. 1163-1172.

[5.30] I. F. Gonos, F.V. Topalis, I. A. Stathopulos: 'Modeling of Grounding Grid Using an Electrolytic Tank', 12th International Symposium on High Voltage Engineering (ISH), Bangalore, India, 20-24, Vol. 1, pp. 146- 149 August 2001.

[5.31] R. Kosztaluk, M. Loboda, D. Mukhedkar: 'Experimental Study of Transient Ground Impedances', IEEE Transaction on Power Apparatus and Systems, Vol. PAS-100, No. 11, pp. 4653-4660, November 1981.

[5.32] R. Rudenberg: 'Electrical Shock Waves in Power Systems', Harvard University Press, Cambridge, Mass. 1968.

\

[5.33] SES, 'CDEGS: Getting Started Manual', Safe Engineering Services and Technologies Ltd, Canada , 1968.

[5.34] F. Van der Linde, B. Zedan, H. Griffiths, A. Haddad: 'Impulse Response of Earth Electrode Systems', 37th International Universities Power Engineering Conference (UPEC), Stafford, UK, pp. 827 – 831, September 2002.

[5.35] F. Van der Linde, B. Zedan, H. Griffiths, A. Haddad: 'Impulse Response of Earth Grid' 13th International Symposium on High Voltage Engineering". Greece. 2003.

Chapter Six

[6.1] ANSI/IEEE Std 80, 'IEEE Guide for Safety in AC Substation Grounding', The Institute of Electrical and Electronic Engineers, 2000.

[6.2] IEC 479, 'Guide to Effects of Current on Human Beings and Livestock'. British Standard.

[6.3] M. Heimbach, and L. D. Grcev: 'Grounding System Analysis in Transient Programs Applying Electromagnetic Field Approach'. IEEE Transactions on Power Delivery. Vol. 12, No.1, pp.186-193, January 1997.

Chapter Seven :

[7.1] BS 7430-1998, 'Earthing', British Standard Code of Practice.

[7.2] ANSI/IEEE Std 81-1983, 'IEEE Guide for Measuring Earth Resistivity, Ground Impedance, and Earth Surface Potentials of a Ground System'.

[7.3] ANSI/IEEE Std 142-1991, IEEE Recommended Practice for Grounding Industrial and Commercial Power System.

[7.4] ANSI/IEEE Std 80, 'IEEE Guide for Safety in AC Substation Grounding', The Institute of Electrical and Electronic Engineers, 2000.

[7.5] H. M. Towne: 'Impulse Characteristics of Driven Grounds', General Electric Review, Vol. 31, No. 11, pp.605-609, November, 1928.

[7.6] P.L. Bellaschi, R. E. Aemington, and A. E. Snowden: 'Impulse and 60-Cycle Characteristics of Driven Grounds-II', AIEE Transaction on Power Apparatus and Systems, Vol.61, pp. 349-363, 1942.

[7.7] A.C.Liew ans M. darveniza: 'Dynamic Model of Impulse Characteristics of Concentrated Earths', Proceeding IEE, Vol. 121, No. 2, pp. 123-135, February 1974.

[7.8] R. Kosztaluk, M. Loboda, and D. Mukhedkar: 'Experimental Study of Transient Ground Impedances', IEEE Transaction on Power Apparatus and Systems, Vol. PAS 100, No. 11, pp. 4653-4660, November 1981.

[7.9] K. Berger: 'The Behaviour of Earth Connections Under High Intensity Impulse Current', CIGRE, Vol. 95, 1946.

[7.10] G. M. Petropoulos: 'The High-Voltage Characteristics of Earth Resistances', Journal of IEE, Part 11, Vol. 95, pp. 172-174, February 1948.

[7.11] W. Kalat, M. Loboda and Z. Pochanke: 'Implementation of Dynamic Model of Surge Soil Condition for Transient Behaviour Of Grounding Electrode Simulation Using ATP of EMTP', 22nd International Conference on lightning Protection Proceedings, Budapest, pp. 1-6, September 1994.

[7.12] S. Visacro and A. Soares J: 'Sensitivity Analysis for the Effect of Lightning Current Intensity on the Behaviour of Earthing System', 22nd International Conference on Lightning Protection Proceedings, Budapest, pp. 1-5, September 1994.

[7.13] A. Haddad, I.A. Metwally, P. Nayllor, R. T. Waters: 'Fast Pulse Current Measurement: Design and Comparative Test Data', 8th International Symposium on High Voltage Engineering (ISH 1993) Yokohama, Japan, Vol. 2, pp. 459-462, 23-27, August 1993.

[7.14] R. Malewski: ' Wire wound Shunts for Measurement of Fast Current Impulses', IEEE Transactions on Power Apparatus and Systems, Vol -PAS 103, No. 6, pp. 2927-2933, 1984.

[7.15] D. G. Pellinen, M. S. Di Capua, S. E. Sampayan, H. Gerbracht, M. Wang: ' Rogowski Coil for Measuring Fast, High-Level Pulsed Currents', Review of Scientific Instruments, Vol. 51. No. 11, pp. 1535-1540, 1980.

[7.16] D. A. Doglass: 'Current Transformer Accuracy with Asymmetric and High Frequency Fault Current', IEEE Transaction on Power Apparatus and Systems, Vol. PAS-100, No. 3, pp. 1006-1011, March, 1981.

[7.17] E. D. Simmon, A. H. Rose, G. J. Fitz Patrick: 'An Optical Current Transducer for Calibration Studies', 8th International Symposium on High Voltage Engineering (ISH), Yokohama, Japan, Vol. 2, pp. 399-402, 23-27 August 1993.

[7.18] B. Richter: 'Application of Fibre Optics to the Measurement of Leakage Current in Metal Oxide Surge Arresters', 4th International Symposium on High Voltage Engineering (ISH), Athens, Greece, Series 64.05, pp. 1-4, 5-9, September 1983.

[7.19] Z. Abul-Malek: 'Fast Transient Response of High-Voltage Surge Arresters', Ph.D Thesis University of Wales Cardiff, United Kingdon, 1999.

[7.20] N. M. Nor: 'Investigations of Soil Characterisation under High Impulse Currents', PhD Thesis University of Wales Cardiff, United Kingdom, 2001.

[7.21] IEC-60: 'Guide on High-Voltage Testing Techniques' Standards, 1989.

[7.22] Haefely: 'Impulse Voltage Test System SGSA. 100-800kV, 5-40 kJ' User Manual.

[7.23] BS 1377: Part 3: 'Soil for Civil Engineering Purposes: Chemical and Elctro-Chemical Tests', British Standard Code of Practice. 1990.

[7.24] S. Srisakot: 'Characterisation of Soil Ionisation in Earthing Systems', PhD Thesis University of Wales Cardiff, United Kingdom, 2001.

[7.25] D. P. Snowden and J. W. Erler: 'Initiation of Electrical Breakdown of Soil by Water Vaporization', IEEE Transactions on Nuclear Science, Vol. 30, No. 6, pp. 4568-4571, December 1983.

[7.26] R. Velazquez and D. Mukhedkar: 'Analytical Modelling of Grounding Electrodes Transient Behaviour', IEEE Transactions on Power Apparatus and Systems, Vol. PAS 103, No. 6, pp. 1314-1322, July 1984.

[7.27] C. Mazzetti and G. M. Veca: 'Impulse Behaviour Of Ground Electrodes', IEEE Transaction on Power Apparatus and Systems, Vol. PAS-102, No. 9, pp. 3148-3156, July 1983.

[7.28] K. J. Nixon, I. R. Jandrell, J. M. Van Coller: 'Development of Earth Electrode System Models Suitable for South African Conditions', 24th International Conference of Lightning protection, (ICLP), Birmingham, United Kingdom, pp. 550.555, September 1998.

List of Publications

B. Zedan, H. Griffiths and A. Haddad: 'The Effect of Grid Mesh Density on Substation Earth Impedance', Proceedings of the 36^{th} Universities Power Engineering Conference (UPEC), Swansea, UK, pp. 3C3.1-4, 2001.

F. Van der Linde, B. Zedan, H. Griffiths and A. Haddad: 'Impulse Response of Earth Electrode Systems', 37^{th} International Universities Power Engineering Conference (UPEC), Stafford, UK, pp. 827 – 831, September 2002.

H. Griffiths, B. Zedan and A. Haddad: 'Frequency Response of Earthing Systems', 28^{th} International Universities Power Engineering Conference (UPEC), Vol. 2, pp. 717-720, Thessaloniki (Greece), 2003.

F. Van der Linde, B. Zedan, H. Griffiths and A. Haddad: 'Impulse Response of Earth Grid' 13^{th} International Symposium on High Voltage Engineering. Greece. 2003.

ADDENDUM

THE EFFECT OF GRID MESH DENSITY ON SUBSTATION EARTH IMPEDANCE

B Zedan, H Griffiths, A Haddad Cardiff University,UK **K Walker** NGC,UK **C Horne** PowerGen, **D Frame, N MacDonald** Scottish Power,UK

ABSTRACT

An investigation was carried out to examine the effect of grid mesh density on earth grid impedance. Simulations were carried out using a field-theory based software to evaluate the response of the earth grid for different soil conditions over a range of frequencies, from DC to 1 MHz. It is shown that increasing the mesh density of the grid lowers the earth grid impedance over a specific frequency range corresponding to a particular soil resistivity.

1 Introduction

In high voltage substations, the buried earth grid provides a low impedance connection to earth. As a result, high magnitude earth fault currents can flow and result in large potential differences across the surface of the ground in the vicinity of the substation. The mesh density of earth grid controls these potential differences within the substation, and this is important for human safety. Detailed guidelines are provided in national standards [1,2] for designing grids for this safety purpose. However, connections are also made to earth grids from high voltage devices such as surge arresters and capacitor voltage transformers (CVTs). An industry standard [2] specifies that there should be a 'high frequency' earth electrode placed directly beneath devices which are likely to conduct transient currents. However, these recommendations are only qualitative and provide little guidance for the practical design of earth grids or rod systems.

Earthing systems behaviour at power frequencies is well understood. The analysis of earthing systems subjected to lightning current impulses is more complex, and much of the previous work on this subject has concerned only simple ground arrangements such as horizontal or vertical electrodes. More recently, the transient and frequency response of earth grids has been studied [3,4]. Investigations have been carried out using simple lumped parameter equivalent circuit models [3,4] and transmission line models [5-8]. An electromagnetic field theory technique for earthing systems analysis has also been used [9].
Some of this recent work [7,8] has specifically considered the frequency response of earth electrodes and has indicated that inductive and capacitive effects are significant at high frequency.

The aim of the present work is to carry out a more comprehensive parametric study of the frequency response of simple earth grids. In particular, the effect of varying the mesh density is considered. A range of soil conditions is examined by varying both the soil resistivity and permittivity over a frequency range from DC to 1 MHz. An established earthing software package was used to carry out the simulation [9].

2 Earth grid models

Figure 1 shows the four arrangements of substation earth grid adopted for the simulations.

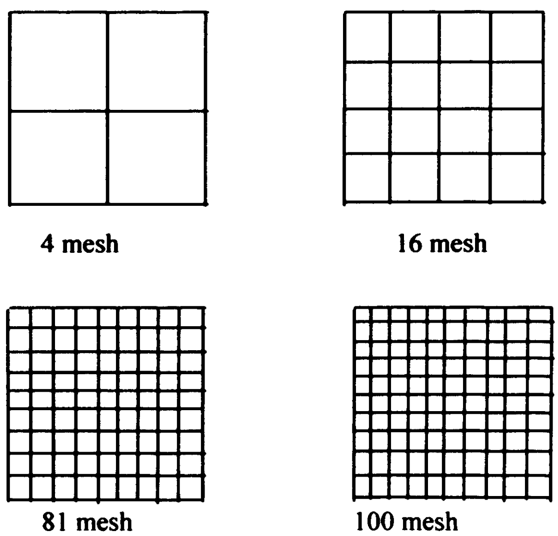

Figure 1: Earth grid models (100m x 100m)

Each grid has overall dimensions of 100m x 100m and the number of meshes is varied between 4 and 100. The grids' copper conductors are assumed to have a diameter of 1 cm and buried at a depth of 1 m. In the simulations, the grid is energised at the centre point.

3 Simulation results

3.1 Frequency response

Figure 2a shows the variation of the impedance magnitude of the 4-mesh earth grid with frequency (up to 1 MHz) for different soil resistivities (10 to 10000Ωm). Each curve has a lower frequency range over which the impedance is nearly constant. Above a particular frequency, which is related to the value of soil resistivity, the impedance increase markedly with frequency. This increase in impedance can be attributed to the inductance of the earth grid, which is illustrated in the plot of impedance angle shown in Figure 2b. As expected, the inductive effects, are more significant at low frequencies for low resistivity soil conditions. These impedance results exhibit similar trends to those obtained by Grcev and Heimbach [8].

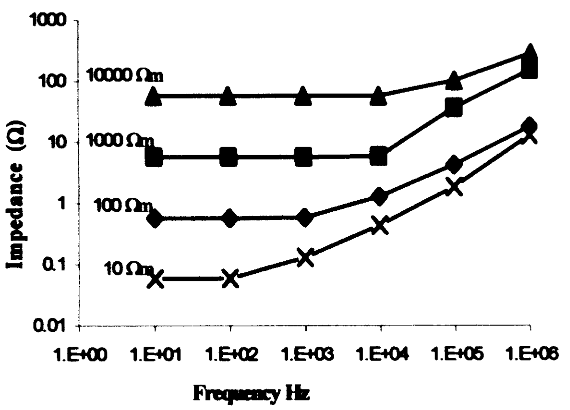

(a) Impedance magnitude

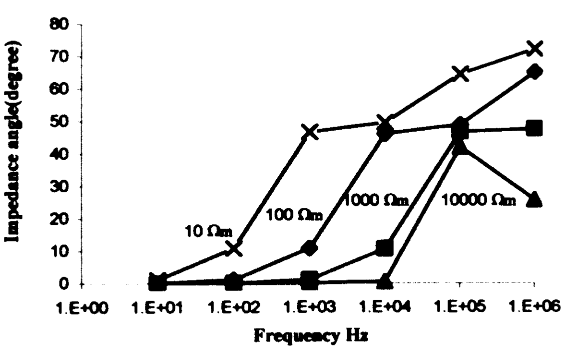

(b) Impedance angle

Figure 2: Frequency response of a 4 mesh earth grid for different soil resistivity and $\varepsilon_r = 1$

3.2 Effect of soil permittivity

Figures 3a and 3b illustrate the effect of soil permittivity on the earth impedance of the 81-mesh grid. The frequency response was investigated over the same range (DC to 1 MHz), and the results are shown for one low and one high soil resistivity conditions. For the low value of soil resistivity (ρ=10Ωm), there is no significant influence of soil permittivity on impedance. Also, for the high resistivity condition (ρ=10000Ωm), there is no noticeable permittivity effect up to 10kHz. However, at 100kHz, increasing the relative permittivity from 1 to 30 results in significant reduction in earth impedance. For ε_r=30 at 100kHz, the capacitive current is of the same order as the conductive current . The impedance angle at this frequency indicates a significant capacitive effect. At the higher frequency of 1MHz, the impedance magnitudes for all values of permittivity are higher. The impedance angle indicates that the grid behaves inductively at this frequency.

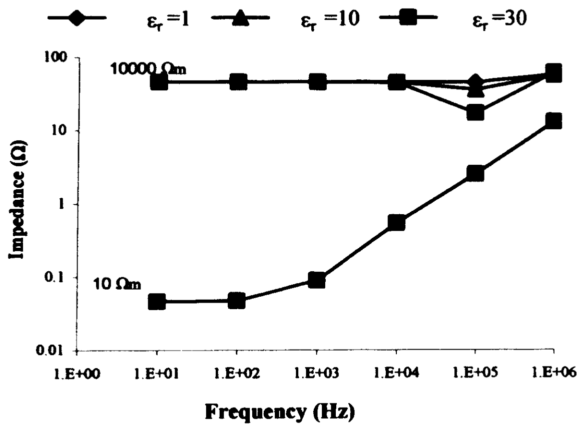

(a) Impedance magnitude

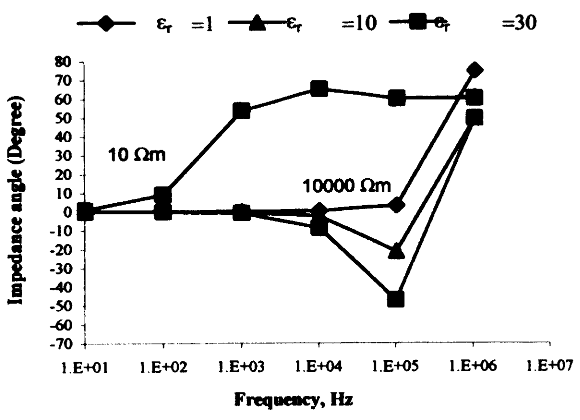

(b) Impedance angle

Figure 3: Effect of soil permittivity on earth grid impedance (81 mesh earth grid)

3.3 Effect of mesh density

Figure 4 shows the influence of grid mesh density on earth impedance for different frequencies. Again, results are presented for one low and one high soil resistivity conditions. As expected, at power frequencies, varying the mesh density has little effect on the earth grid impedance since the impedance is predominantly resistive. At higher frequencies, increasing the mesh density has a significant effect in lowering the earth grid impedance. As can be seen in Figure 4, there is a particular frequency range, where the mesh density has a pronounced effect, and this frequency range is different for low and high soil resistivity conditions. This behaviour could be attributed to the different effective areas of the earthing system for different soil resistivities as argued in reference [10].

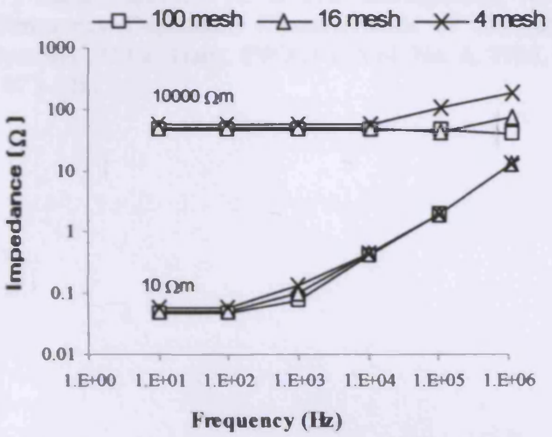

Figure 4: Frequency response for different mesh densities with different soil resisitivity (ε_r =1)

3.4 Effect of conductor segmentation

In the simulation software, the grid conductors are modelled as cylindrical segments. The degree of segmentation used can affect the accuracy of the results, particularly at higher frequencies. Accordingly, a sensitivity analysis was carried out to determine appropriate levels of segmentation for the main simulations.

Tables 1 and 2 summarise the influence of conductor segmentation on the impedance magnitude results for the 100m x 100m earth grid and for different mesh densities. The results are for a soil resistivity of 100Ωm and a unity relative permittivity.

It was found that increasing the segmentation affected the computed impedance, particlulary for the 100-mesh grid. At 1 MHz for the 4-mesh grid, 20 segments per conductor is sufficient while for 100-mesh grid, 35 segments per conductor are required.

Table 1: Influence of conductor segmentation on the calculated earth grid impedance at 1MHz.

No. Segments	4 mesh		16 mesh		100mesh	
	Z	ϕ	Z	ϕ	Z	ϕ
5	18.309	69.113	18.423	69.087	25.079	60.035
10	18.533	69.056	18.533	69.063	18.958	68.368
15	17.873	66.626	17.966	64.915	18.272	64.482
20	17.765	65.414	17.768	65.419	18.049	65.027
25	17.817	64.979	17.820	64.984	18.105	64.639
30	17.763	64.917	17.766	64.922	18.045	64.857
35	17.765	64.888	17.768	64.892	18.051	64.571

Table 2: Influence of conductor segmentation on the calculated earth grid impedance at 100kHz.

No. Segments	4 mesh		16 mesh		100mesh	
	Z	ϕ	Z	ϕ	Z	ϕ
5	4.373	49.596	4.550	50.974	5.395	65.173
10	4.298	49.182	4.507	50.852	3.988	61.755
15	4.312	48.965	4.523	50.689	4.012	60.721
20	4.312	48.860	4.522	50.564	3.986	61.332
25	4.309	48.861	4.518	50.593	3.977	61.350
30	4.312	48.834	4.521	50.573	3.981	61.313
35	4.308	48.835	4.517	50.583	3.973	61.322

4 Conclusions

This paper has demonstrated the influence of soil resistivity, soil permittivity and mesh density on the frequency response of a 100x100m earth grid. The parametric studies considered for frequencies ranging from DC to 1 MHz and for soil resistivity values between 10Ωm and 10000 Ωm. The relative permittivity was varied between 1 and 30.

The investigations have shown that the earth grid impedance increases with frequency with the inductive effects becoming significant above specific frequencies. These inductive effects are found to be more significant at lower frequencies for low soil resistivity media. In addition, it was shown that soil permittivity has an effect at high frequencies in high soil resistivity, and the increase in grid density lowers the earth grid impedance for a specific frequency range depending on the soil resistivity of the media.

REFERENCES

[1] Electricity Association: Technical specification 41-24, 'Guidelines for The Design, Installation, Testing and Maintenance of Main Earthing Systems in Substations', issue 1,1992.

[2] IEEE80: 2000: 'Guide for Safety in AC Substation Grounding', IEEE, New York, 2000.

[3] Gupta, B.R. and Thapar, B.: 'Impulse Impedance of Grounding Grids', IEEE Trans.PAS-99, Vol., No.6, 1980, pp. 2357-2362.

[4] Verma, R. and Mukhedkar, D.: 'Fundamental Consideration and Impulse of Ground Grids', IEEE Trans. PAS-100, Vol., No.3, 1981, pp. 1023-1030.

[5] Rammoorty, M. et al.: 'Transient performance of Ground Grid', IEEE Trans. PWRD. Vol. 4, No. 4, 1989, pp. 2053-2059.

[6] Meliopoulos, A. P. and Moharam, M. G.: 'Transient analysis of Grounding System', IEEE Trans. PAS-102, Vol. No. 2, 1983, pp. 389-399.

[7] Papalexopoulos, A. D and Meliopoulos, A. P.: 'Frequency Dependent Characteristics of Grounding Systems', IEEE Trans. PWRD-2, Vol. No. 4, 1987, pp. 1073-1081.

[8] Grcev, L. D. and Heimbach, M.: 'Frequency Dependent and Transient Characteristics of Substation Grounding Systems', IEEE Transactions on Power Delivery. Vol. 12, No.1, 1997.

[9] CDEGS, HIFREQ Module, Safe Engineering services, Montreal Canada, 1996

[10] Griffiths, H. and Davies, A.M.: 'Effective Length of Earth Electrodes Under High Frequency and Transient Conditions', 25th International Conference on Lightning Protection, Vol.1, Rhodes (Greece), 2000. pp. 536-540.

Address:
Electrical Division,
School of Engineering,
Cardiff University,
PO Box 687,
Cardiff CF24 3TD
Wales, UK
Tel: 44 029 20874608
E-mail ZedanB@Cardiff.ac.uk
http://www.cf.ac.uk/engin/research/highvolt

IMPULSE RESPONSE OF EARTH ELECTRODE SYSTEMS

F. van der Linde, B. Zedan, H. Griffiths, A. Haddad
Cardiff University

In collaboration with

K. Walker[1], D. Frame[2], N. MacDonald[3], C. Horne[4], J. Porter[4]
1. National Grid UK 2. Ingenco 3. Scottish Power 4. Powergen

ABSTRACT

The impulse behaviour of a number of earth electrode systems was determined using numerical calculations. Three different current impulse shapes were considered: 1/5μs, 8/20μs and 30/80μs. In order to simulate a realistic range of soil conditions, the soil resistivity was varied from 10Ωm to 10kΩm and the relative permittivity from 1 to 30. The performances of a 5m vertical rod, 5m horizontal electrode, 20m horizontal electrode and 100m x 100m 4-mesh grid were quantified by examining the transient ground potential rise; in particular, its peak magnitude and front-time. The potential distribution along the electrodes was also computed. A simple lumped-parameter circuit model is proposed for the simulation of the 5m vertical electrode. Comparison with the detailed analysis gave satisfactory agreement for specific soil parameters.

1. INTRODUCTION

Earth electrode systems are subjected to high-magnitude, fast-front surge currents caused by lightning strikes and switching operations on the power system. The earth electrode system should be able to disperse these surges into the ground without damage to equipment or interference between power system plant and ancillary equipment. The safety of humans in the vicinity of the earth electrode systems during the dissipation of these surges should also be ensured. Mitigation of these effects can, in some cases, be ensured by limiting the earth electrode system potential rise at the injection point. The rise of earth potential depends on many factors, such as electrode geometry, soil characteristics and parameters of the dissipated current, some of which are investigated here.

The reported theoretical studies [1–10] have analysed vertical rods, horizontal extended electrodes, substation grids and their combinations using a variety of analytical techniques. These studies have shown that there is a difference between the power-frequency and transient behaviour of earth electrode systems [1]. In particular, the peak magnitude of the transient impedance, defined as the ratio of the instantaneous voltage to the instantaneous current, increases as the transient front-time decreases [4, 6, 10] and the transient impedance magnitude also depends on the point of injection on the earth electrode system [3, 4, 9, 10]. The transient impedance generally decreases with increasing earth electrode system size [4, 7, 9] and its value depends on the electrode configuration [5]. It was also found that the impulse reduces in peak magnitude and the impulse steepness decreases as it propagates from the point of injection [7, 10].

The investigations into the impulse behaviour of earth electrode systems described in this paper were carried out using an electromagnetic-field analysis programme (CDEGS). Studies were also undertaken using a proposed simple lumped-parameter circuit model applied in both the time and frequency domains in order to investigate simpler methods of analysis of earth electrode arrangements. Non-linear phenomena in the medium such as soil ionisation and thermal effects have been neglected.

2. MODEL CONFIGURATIONS AND PARAMETERS

Four different earth electrode systems were selected for this study; 5m vertical and horizontal rods, a 20m horizontal electrode and a 100m x 100m 4-mesh grid. Each electrode system was injected with a current of 1A peak magnitude from 1m above ground level via a 20cm diameter lead. This lead is connected to the electrodes buried at a depth of 0.6m underground.

In this work, three impulse shapes were selected to represent particular practical events; 1/5μs for fast transients, 8/20μs for standard lightning impulses and 30/80μs for switching surges. The electrode systems were studied for soils with a wide range of resistivity (10Ωm - 10000Ωm) and relative permittivity (1 – 30).

3. RESULTS OF ELECTROMAGNETIC STUDIES

3.1 5m vertical electrode

The time-domain behaviour of the 5m vertical configuration was studied for a range of resistivity and relative permittivity values and current impulse shapes. The transient ground potential rise (TGPR) was always determined at a point 0.75m above ground level on the energisation lead.

3.1.1 Effect of soil properties on voltage magnitude and impulse shape

a) Magnitude observations

As expected, it was found that the TGPR peak magnitude increases with soil resistivity. The relationship between the TGPR peak magnitude and relative permittivity is, however, more complex. The TGPR peak magnitude decreases with increasing relative permittivity in soils with very high resistivity (10kΩm) (Figure 1). However, in soils with resistivity values between 10Ωm and 10kΩm, permittivity has little effect.

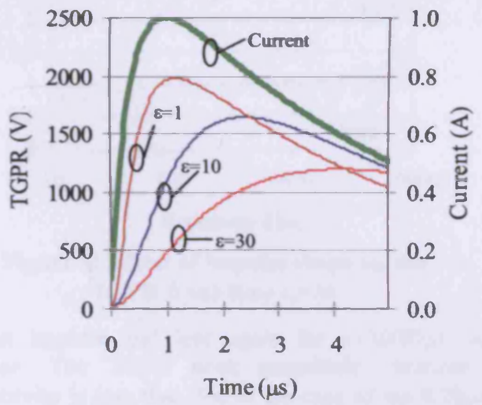

Figure 1: Effect of permittivity on TGPR (5m vertical rod, 1/5μs current impulse, ρ=10kΩm)

b) TGPR impulse shape

It was found that the TGPR steepness decreases with increasing resistivity and decreases with increasing relative permittivity (Figures 1 & 2). For soils with resistivity below 100Ωm, inductive effects dominate and the voltage front-time is shorter than that of the impulse current (Figure 2). In contrast, in soils with a resistivity above 1kΩm, the voltage front-time is longer than that of the current, and capacitive effects are seen such that changes in relative permittivity have a noticeable influence on the TGPR front-time.

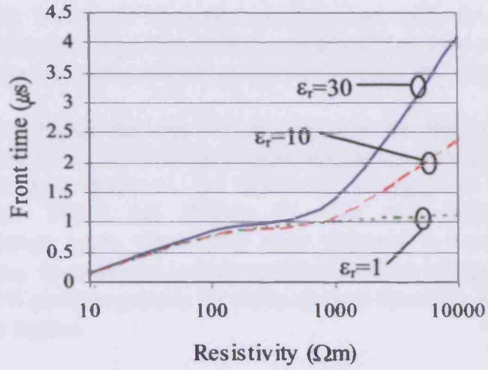

Figure 2: Effect of resistivity on front-time (5m vertical rod, 1/5μs current impulse)

3.1.2 Potential profile along the electrode

Typical TGPR magnitudes along the length of the electrode are shown in Figure 3. The TGPR peak magnitude decreases and its steepness decreases with distance from the injection point, which can be attributed to leakage from the electrode. Detailed studies have shown that in soils with moderate or high resistivity (>100Ωm), there is little change in TGPR peak magnitude between the point of injection and the end of the electrode. However, in soils with a resistivity of 10Ωm, the inductance of the energisation lead has a significant effect.

3.1.3 Effect of current impulse shape

The relatively "slow" 8/20μs and 30/80μs current impulse shapes produce similar trends in TGPR peak magnitudes and front-times to those calculated for 1/5μs shapes (Figure 4). It was found that the decrease in TGPR front-time with increasing soil resistivity is less for an 8/20μs than for a 1/5μs current impulse and less again for a 30/80μs current impulse. For 8/20μs and 30/80μs impulse shapes, both inductive and capacitive effects are less pronounced. Figure 4 summarises these trends by showing the normalised front-time of the TGPR. In this figure, each curve is normalised to the front-time of the current impulse shape for that curve.

Similarly, the increase in TGPR peak magnitude in soil with low resistivity is less for an 8/20μs than for a 1/5μs

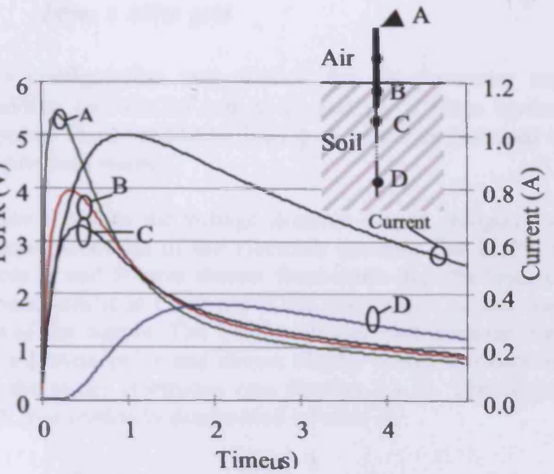

Figure 3: TGPR along a 5m vertical rod (1/5µs current, ρ=10Ωm ε_r=30, A: injection point, B:0.15m, C:0.725m, D: rod end)

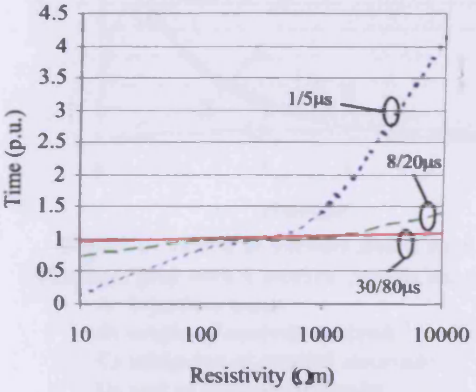

Figure 4: Effect of impulse shape on the TGPR front-time ε_r=30

current impulse and less again for a 30/80µs current impulse. The TGPR peak magnitude variation with permittivity is less than 3% in the case of the 8/20µs and 30/80µs impulses compared with 40% variation for 1/5µs impulse shapes. For the "faster" 1/5µs current impulses, the TGPR peak magnitude is higher in low resistivity soils due to inductive effects but lower in high resistivity soils.

When studying interference effects between electrode elements, the impulse sharpening that occurs in low resistivity soil (Figures 2 and 3) may enhance coupling between the earth electrode system and nearby metallic objects. The extent of this possible coupling enhancement needs to be further investigated.

3.2 Performance comparison of a 5m vertical electrode, 5m horizontal electrode and 20m horizontal electrode

A 5m horizontal electrode configuration with the same downlead arrangement as the vertical rod was also studied for the same range of soil properties and impulse shapes.

It was found that the voltage impulses for the two 5m arrangements have the same peak magnitude and the same front-time. However, the horizontal arrangement has a higher TGPR tail (Figure 5). The two waveforms converge again when they have decayed to very low values. In moderate to high resistivity soil (>100Ωm), the TGPR peak magnitude for the horizontal electrode is up to 23% higher.

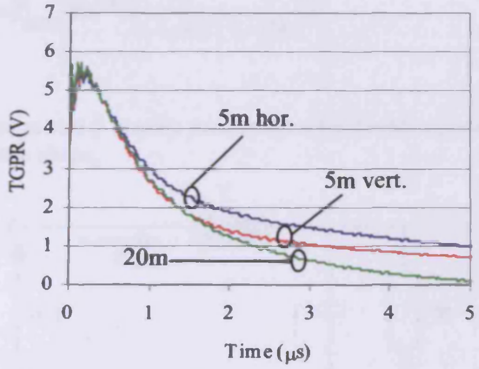

Figure 5: Performance comparison of a 5m vertical, 5m horizontal and 20m horizontal electrode (ρ=10Ωm, ε_r=1)

Comparison of the TGPR of the 5m electrodes with that of the 20m horizontal electrodes reveals that in low resistivity soil, the TGPR peak magnitude is the same (Figure 5). The TGPR for the 20m electrode becomes negative before converging with the curve for the 5m electrode after approximately 25µs. This "sharpening" of the TGPR impulse shape for the 20m compared with the 5m electrodes also occurs in higher resistivity soil.

In high resistivity soil, the 20m electrode exhibits significantly lower TGPR peak magnitude than both 5m electrodes. The TGPR peak magnitude was found to be 60% lower in soils with resistivity 1kΩm and 10kΩm compared with the 5m vertical arrangement. These results confirm earlier findings [11].

Moreover, the change in TGPR along the electrode length was found to be very small in soil with a resistivity greater than 100Ωm for the 5m electrodes. For the 20m electrode, the corresponding soil resistivity was found to be 1kΩm.

3.3 100m x 100m grid

This configuration was studied for the particular soil condition (ρ=100Ωm and ε_r=1) and for a 1/5μs current impulse. The energisation lead is the same as that used in the previous studies.

Figure 6 shows the voltage impulse shapes computed at selected locations of the electrode system. The TGPR at points A and B have shorter front-times than the injected current, whilst at C, D and E the rise-time is slower than that of the current. The TGPR reduces with distance from the injection point and shows similar trends as observed for the single electrodes (see Section 3.1.2). This agrees with independently determined results [7].

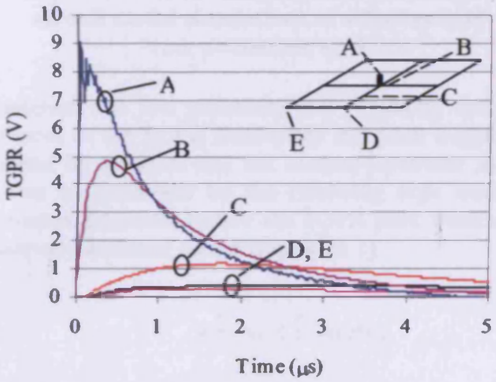

Figure 6: TGPR at various points on a 100x100m grid with 4 meshes, ρ=100Ωm, ε_r=1
A: injection point
B: origin of central electrode
C: midpoint of central electrode
D: end of central electrode
E: corner of grid

Although the grid is much larger than the 20m electrode, the TGPR peak magnitude is reduced by a factor of only 2. In addition, the grid produces a shorter front-time than the 20m electrode. By comparing the TGPR "origin" plot (B) of the grid with that of the injection point (A), the relatively large contribution made by the short (1.6m) injection lead to the overall behaviour of the grid can be seen (Figure 6).

4. COMPARISON WITH THE LUMPED PARAMETER MODEL

4.1 Proposed circuit model

The results shown in the previous sections were determined using field computation software requiring long run-times on powerful PCs. Here, a simple model is proposed to conduct these computations.

The lumped-parameter model consists of a series inductance (L) and a parallel combination of conductance (G) and capacitance (C) (Figure 7). R and L represent the impedance of the earth electrode conductor, and G and C represent the leakage from the conductor to the surrounding medium. Rudenberg's [11] definition of the model parameters was used. The circuit was solved in the time-domain and implemented in Mathcad using the following equation:

$$v(t)=I_{max}\left[L(-\alpha e^{-\alpha t}+\beta e^{-\beta t})+R\left(\frac{e^{-\alpha t}}{1-\alpha RC}-\frac{e^{-\beta t}}{1-\beta RC}\right)\right]$$
$$+I_{max}\left[\mathrm{R}e^{\frac{-t}{RC}}\left(\frac{-1}{1-\alpha RC}+\frac{1}{1-\beta RC}\right)\right] \qquad (1)$$

Where α and β are the parameters of a double-exponential impulse shape.

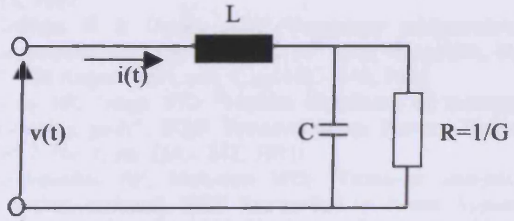

Figure 7: Simple equivalent circuit of an earth electrode system

4.2 Circuit simulation results

The TGPR calculated using CDEGS and the lumped-parameter model are compared for a 5m vertical electrode in high resistivity soil (Figure 8). In high resistivity soil (>1kΩm), there is agreement between the two calculations in terms of the front-time of the TGPR. However, the TGPR magnitude calculated with CDEGS is consistently lower than that calculated with the lumped-parameter model. In frequency domain studies, CDEGS was also found to produce lower conductor impedance than the lumped-parameter model. This is due to the value of the circuit parameters used and these can be refined to improve the results. For the case illustrated in Figure 8, the best fit was obtained when the conductance value (G) calculated according to Rudenberg's definition, was reduced by 14%.

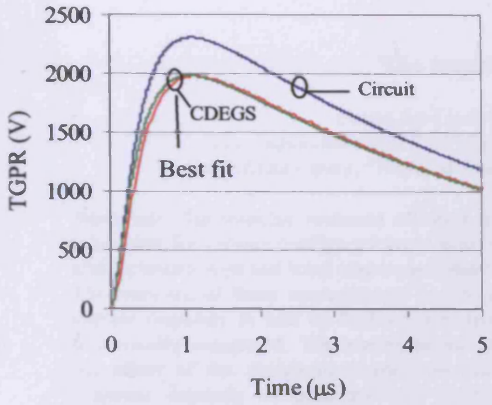

Figure 8: TGPR using CDEGS and lumped circuit model simulations of a 5m vertical rod, ρ=10kΩm, ε_r=1

In moderate and low resistivity soil (<1kΩm), there are differences in the TGPR front-times and peak magnitudes calculated by CDEGS and the lumped-parameter model. This can be explained by the relatively high inductive components generated before the TGPR peak when using the lumped-parameter model (Equation 1).

5. CONCLUSIONS

The impulse responses of 4 simple electrode configurations were studied (5m vertical rod, 5m horizontal electrode, 20m horizontal electrode and 100m x 100m grid). Three impulse shapes and a wide range of soil conditions were considered.

As expected, it was found that the TGPR peak of all the electrode configurations increases with resistivity. The TGPR peak decreases significantly with permittivity in very high resistivity soil.

The TGPR front-time is close to the impulse current front-time for the slow impulse shapes and the earth electrode system behaviour is predominantly resistive. However, for fast current impulses, the front-time varies significantly with resistivity. In very high resistivity soil, the TGPR front-time is longer than that of the impulse current front-time. In medium to high resistivity soil, the TGPR front-time is of the same order as the impulse current. In low resistivity soil, inductive behaviour dominates the transient response.

The voltage profile along the electrode systems was also investigated. In low resistivity soil, the TGPR peak magnitude decreases and the front-time increases with increasing distance from the point of injection.

In medium to high resistivity soil, the 20m electrode has a significantly lower TGPR peak magnitude compared with the 5m vertical and horizontal electrodes. For the longer electrode there is "sharpening" of the waveform, probably due to its increased inductance.

REFERENCES

1. Bellaschi PL, Armington RE: "Impulse and 60-cycle characteristics of driven gounds - III: Effect of lead in ground installation", AIEE Transactions on Electrical Engineering, 1943, Vol. 62, pp. 335 – 345, 1943
2. Dawalibi FP, Ruan W & Fortin S: "Lightning transient response of communication towers and associated grounding networks", The Malaysia Paper from CDEGS: Getting started manual, Safe Engineering Services and Technologies Ltd, Quebec, Canada, 1998
3. Geri A: "Practical design criteria of grounding systems under surge conditions", 25rd ICLP, Rhodes, Greece, 18-22 September, 2000, pp. 458 – 463, 2000
4. Grcev LD, Heimbach M: "Frequency dependent and transient characteristics of substation grounding systems", IEEE Transactions on Power Delivery, Vol. 12, No. 1, pp. 172 – 178, 1997
5. Griffiths H & Davies AM: "Frequency performance of concentrated earthing systems", 12th ISH, Bangalore, India, 20 – 24 August 2001, vol. 1, pp.142 – 145, 2001
6. Gupta BR, Singh VK: "Impulse impedance of rectangular grounding grids", IEEE Transactions on Power Delivery, Vol. 7, No. 1, pp. 214 – 218, 1992
7. Meliopoulos AP, Moharam MG: "Transient analysis of grounding systems", IEEE Transaction on Power Apparatus and Systems, Vol. PAS 102, No. 2, pp. 389 – 399, 1983
8. Ramamoorty M, Babu MM, Parameswaran S, Mukhedkar D: "Transient performance of grounding grids", IEEE Transactions on Power Delivery, Vol. 4 , No. 4, pp. 2053 – 2059, 1989
9. Sonoda T, Takesue H, Sekioka S: "Measurements on surge characteristics of grounding resistance of counterpoise for impulse currents", 23rd ICLP, Rhodes, Greece, 18-22 September, 2000, pp. 411 – 416, 2000
10. Velazquez R, Mukhedkar D: "Analytical modelling of grounding electrodes transient behaviour", IEEE Transaction on Power Apparatus and Systems, Vol. PAS 103, No. 3, pp. 1314 – 1322, 1984
11. Rudenberg R: "Electrical shock waves in power systems", Harvard University Press, Cambridge, Mass., 1968

Authors' Address: High Voltage Laboratory
Electrical Engineering Division
School of Engineering
Cardiff University
Newport Road
PO Box 687
Cardiff
CF24 3TD
Wales UK.
Tel: +44(0)29 2087 5953
E mail: vdlindefj@cf.ac.uk

XIIIth International Symposium on High Voltage Engineering, Netherlands 2003, Smit (ed.)
 ISBN 90-77017-79-8

The impulse response of earth grids

F. van der Linde[1], B. Zedan[1], H. Griffiths[1], A. Haddad[1]
In collaboration with K. Walker[2], D. Frame[3], N. MacDonald[4], C. Horne[5], J. Porter[5]
[1] Cardiff University, [2] National Grid UK, [3] PCS Ltd, [4] Scottish Power, [5] Powergen (All UK)

Abstract: The impulse response of earth grids was calculated for various configurations of grid size, local and perimeter rods and local and overall mesh density. The response of these arrangements to 1/5 and 30/80 current impulses in soil of different resistivities was numerically computed. The computations show that the effect of the design parameters on the impulse response depends on both the soil resistivity and impulse waveshape. In low resistivity soil, enhancement of the grid within an area of approximately 20x20m from the injection point improves the impulse performance. In high resistivity soil, a much larger part of the grid plays a role in the dispersal of the impulse current. The response to 1/5 current impulses is more strongly affected by changes in the grid close to the injection point compared with the response to 30/80 current impulses. However, rods at the perimeter of grids in high resistivity soil have a larger effect on the response of 1/5 current impulses than 30/80 current impulses.

1. Introduction

Currently, guidelines for the design of substation earth grids primarily satisfy power frequency performance requirements. Measures used to meet these requirements are based on increasing the area occupied by the grid, increasing the density of grid meshing and using rods to penetrate deeper low resistivity soil [1, 2]. Acknowledgement is also made of the requirement of grids to disperse impulse currents, such as lightning or switching surges, and high-frequency currents as caused by disconnect operations. However, the guidance given in the standards concerning high-frequency and transient performance focus on local enhancements to the grid at the point of injection and is qualitative in nature. The local enhancements suggested include: rods (connected to the main earth grid) [1, 2], horizontal electrodes [2] and increased mesh density [3].

In order to incorporate these measures in quantitative design guidelines, an extensive investigation has been carried out to study earth grid performance under high-frequency and transient conditions. These studies include variation of grid size, the number of local and total rods and local and overall mesh density.

The performance of an earth grid can be measured in terms of the potential rise of the grid and the exported potentials that give rise to electromagnetic fields in the vicinity of the grid. Here, the potential rise of the grid is used to quantify the earth grid performance.

This paper summarises the main findings of these investigations, taking into account such factors as impulse shape, soil resistivity and the point of injection. All the simulations were carried out using CDEGS' 'Hifreq' and 'FFTSES' modules. Non-linear phenomena in the medium such as soil ionisation and thermal effects have been neglected.

2. Previous work

In a previous study by the present authors [4] of simple earth electrodes, it was found that the electrodes behaved differently in soil with a low resistivity compared with soil of high resistivity. Transient simulations of these electrodes also revealed that the impulse shape had a considerable effect [4] and that the response to 8/20 and 30/80 current impulses is similar.

In reference [4] published previous work was reviewed and revealed that:

(i) the transient impedance, which depends on the injection point and grid configuration, increases with surge steepness and decreases with grid size.

(ii) for an injected current impulse, the peak transient ground potential rise (TGPR) and its steepness decrease with distance from the injection point.

3. Effect of grid size

The impulse performance of a square 4-mesh earth grid buried at a depth of 1m (Figure 1) was studied for different sizes (10x10m, 20x20m, 30x30m, 40x40m, 50x50m and 100x100m). The grid was energised through a 2m downlead at one corner and also at the centre.

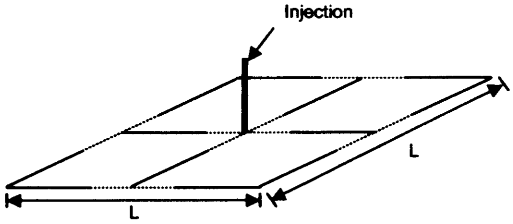

Figure 1: Configuration of the 4-mesh grids used to study the effect of grid size

The impulse response of these grids in low and high resistivity soil is summarised in Figure 2. As can be seen in Figure 2.a, in low resistivity soil, there is generally little change in TGPR peak magnitude for different sized grids. However, the TGPR for the 10x10m centrally injected grid with a 30/80 current impulse is 30% higher than that of the larger grids. In contrast, in high resistivity soil, grid size is more important (Figure 2.b). For example, a 10x10m grid injected with 1/5 current impulses at its corner has a TGPR peak magnitude 1.55 times that of a 50x50m grid. For grids injected with 1/5 current impulses, the performance improves significantly up to a grid size of up to 50x50m while for 30/80 current impulses, an improvement in performance is still seen up to at least 100x100m.

These studies indicate that there may be an effective area beyond which increasing the grid size has a limited or negligible effect. In low resistivity soil, this area may be of the order of $100m^2$ while in high resistivity soil it may be in excess of $2500m^2$.

Studies of simple earth electrode systems have shown that the impedance and peak TGPR decrease as the length of the electrodes increases but there is a minimum corresponding to the effective length, determined by the soil resistivity and frequency of the injected current [4 - 6].

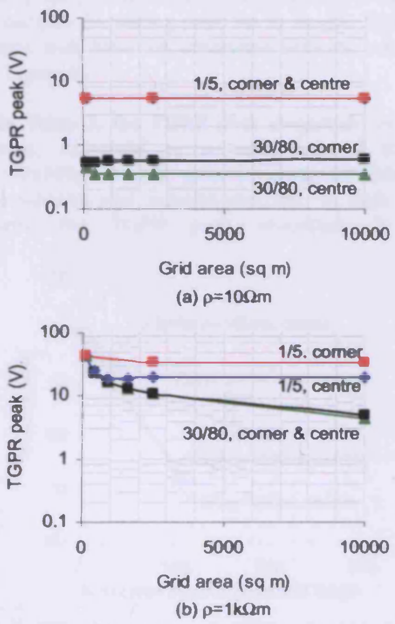

Figure 2 Effect of grid size on the TGPR peak magnitude for square centre and corner injected 4-mesh grids

4. Effect of rods

Both IEEE80 [1] and EA 41-24 [2] standards recommend that rods are applied at the perimeter of grids to improve power frequency performance. It is also recommended that rods are applied at points where high-frequency and transient currents will be discharged into the grid. These two cases will be examined separately.

4.1 The effect of rods at the perimeter of grids

The basic grid configuration for these studies is shown in Figure 3.a and consists of a 100x100m 4-mesh grid. Rods, 5m in length, are added according to the arrangements shown. The first rod is located at the point of injection and the remainder of the rods is evenly distributed around the perimeter of the grid. Configurations with 45, 129 and 237 rods were also studied. The case of 129 rods was studied for corner injection and all other cases for corner and centre injection.

Figure 4 shows the results of transient simulations for injection with 30/80 current impulses in high resistivity soil. The TGPR peak magnitude decreases with an increasing numbers of rods, although adding a single rod at the point of injection has little effect. The decrease in the TGPR as a result of adding 237 rods is 21% and 14% for centre and corner injected grids respectively. This reduction of TGPR could, therefore, be attributed to a reduction in the overall resistance of the grid.

Evidence supporting this argument is that the front-time of the TGPR becomes shorter as the number of rods increases, which suggest that the inductance of the system becomes more significant as a result of a reduction in resistance.

Studies of similar arrangements under 1/5 current impulses indicate that adding rods has a more significant effect in high resistivity soil (Figure 5).

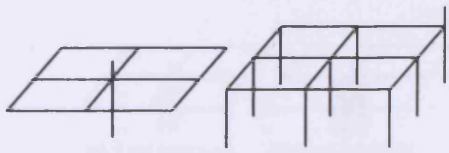

(a) 1 rod, centre inj. (b) 9 rods, corner inj.

Figure 3 Examples of 100x100m grid configurations with 5m rods (not to scale).

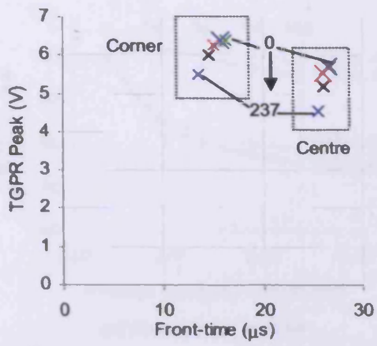

Figure 4 The effect of rods at the perimeter of a 100x100m 4-mesh grid on the TGPR peak magnitude when injected with 30/80 current impulses ρ=1kΩm

4.2 The effect of rods close to the point of injection

A separate study of the effect of rods local to the point of injection on the transient performance of earth grids is important for two reasons:

i) Their use is recommended in standards as so-called "high frequency" electrodes.

ii) Previous studies indicate that during the dispersal of impulse currents, the region local to the point of injection is important.

Figure 3.a shows the basic configuration studied. As with the previous studies, a 100x100m 4-mesh grid is modified by adding rods 5m in length. The three and nine rods have 5m separation between adjacent rods (Figure 6).

In Table 3, the TGRP peak magnitude of the 9-rod case, expressed as a percentage of that for a 100x100m 4-mesh grid, is given for different soil conditions and impulse currents. In high resistivity soil, the TGPR peak magnitude is virtually

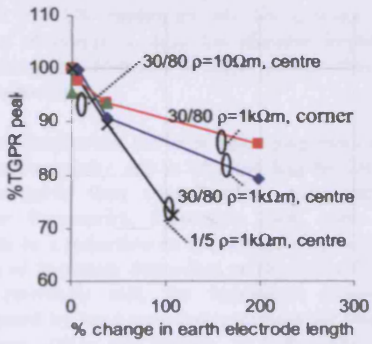

Figure 5 The effect of rods on the TGPR peak magnitude of a 100x100m 4-mesh grid

independent of the number of rods when the grids are injected with 30/80 current impulses. In low resistivity soil, there is a decrease in the TGPR peak magnitude as the number of rods increases. In low resistivity soil, the TGPR peak magnitude is reduced for slow but not fast current impulses, unlike in high resistivity soil where the reverse is true. These results can be expected based on the frequency response which show that at low frequencies, the addition of these small numbers of rods causes very little change in the impedance magnitude. Above 1MHz in high resistivity soil, the impedance magnitude reduces with the addition of rods.

Table 3: Effect of 9 local rods on TGPR peak magnitude of a 100x100m 4 mesh grid.

Impulse current	30/80		1/5	
Resistivity	1kΩm	10Ωm	1kΩm	10Ωm
%TGPR peak	100	84	86	97

5. Effect of mesh density

Grid mesh density was varied in two ways for the following studies; (a) the overall mesh density was varied by adding conductors evenly to a 100x100m grid, (b) the local mesh density was varied by increasing the mesh density in a 20x20m area around the injection point.

5.1 Overall mesh density

In Figure 7.a, the time-domain performance of grids with various mesh densities are shown for injection with slow current impulses. The number of conductors per metre describes the mesh density in this figure. In low resistivity soil, there is little improvement in the performance of the grid by increasing the overall mesh density. In high resistivity soil, there is an improvement in the transient performance of the grid with increasing mesh-density up to 36 meshes. In Figure 7.b, the effect of the overall mesh density for 1/5 and 30/80 current impulses in high resistivity soil is given. The transient performance gained by increasing the mesh-density is less for the 1/5 than for the 30/80 current impulse in the range of mesh densities studied here. However, the rate of change in the TGPR is better for 1/5 current impulses.

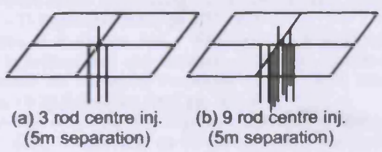

Figure 6 Examples of 100x100m grid configurations with local rods with 5m spacing.

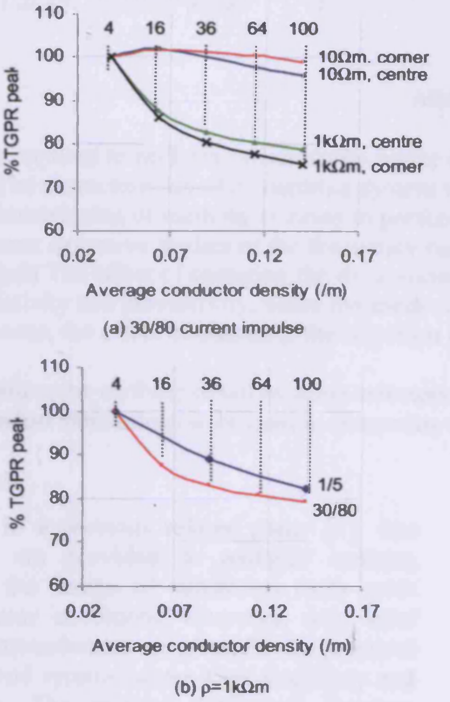

Figure 7 The effect of overall mesh density on the TGPR peak magnitude of a 100x100m grid. The top scale indicates the number of meshes.

5.2 Local mesh density

In high resistivity soil, local enhancement of the meshes (Figure 8) causes a decrease in the TGPR peak magnitude, but increasing the overall mesh density has greater effect (Figure 7.b). However, in low resistivity soil, local mesh enhancement has a greater impact (Figure 8). In this case, a 4-mesh grid locally enhanced to 100 meshes has a better performance than a grid with 100 meshes overall. These results confirm earlier observations about the effective impulse area. The frequency response of these systems also predicts this behaviour.

At low frequencies the impedance magnitude of a grid in low resistivity soil is affected less by local mesh enhancement than overall mesh enhancement. At higher frequencies, increasing local mesh density results in a reduction in impedance over a particular range of frequency dependent on the soil resistivity. In low resistivity soil, the impedance magnitude is decreased by local mesh enhancement for frequencies between 100Hz and 100kHz. In high resistivity soil, the impedance magnitude is noticeably reduced by

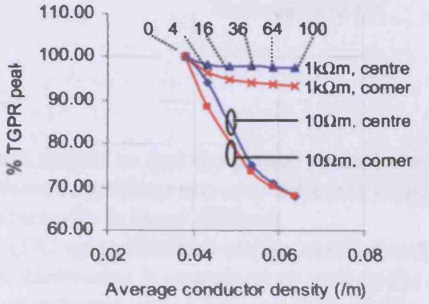

Figure 8 The effect of local mesh density on the TGPR peak magnitude of a 100x100m grid injected with 30/80 current impulses. The top scale indicates the number of local meshes.

local mesh enhancement for frequencies greater than 100kHz.

6. Conclusions

Many of the measures recommended in standards for improving earth grid performance for power frequency and impulses are effective at improving impulse performance. However, the degree to which they enhance performance depends on several parameters such as number and location of rods and mesh density enhancement. Indiscriminate application of these measures should be replaced by selective application determined by the local soil resistivity and the type of impulses that will be dispersed.

Further studies are required to determine the relationship between the effective lengths/areas and potential distributions of earth electrode systems at high frequencies and during the dispersal of impulse currents.

7. References

[1] IEEE80, 'IEEE guide for safety in AC substation grounding', Revision IEEE Std 80-2000, IEEE Inc, New York, 2000.

[2] EA 41-24, 'Guidelines for the design, installation, testing and maintenance of main earthing systems in substations', Issue 1:1992, Electricity Association, London, 1992

[3] CENELEC HD 637 S1, 'Power installation exceeding 1kV a.c.', CENELEC Harmonization document, 1999

[4] Van der Linde F, Zedan B, Griffiths H, Haddad A, Walker K, Frame D, MacDonald N, Horne C & Porter J, 'Impulse response of earth electrode systems', 37th International Universities Power Engineering Conference (UPEC), Stafford, UK, 9 – 11 September 2002, pp. 827 - 831

[5] Griffiths H & Davies AM, ' Effective length of electrodes under high-frequency and transient conditions', International Conference on Lightning Protection (ICLP) 2000, Rhodes, Greece, 18-22 September 2000, pp. 469-473.

[6] Gupta BR & Thapar B, 'Impulse impedance of grounding grids', IEEE Transactions on Power Apparatus and Systems, Vol. PAS-99, No. 6, Nov/Dec 1980, pp. 2357- 2362.

Author address: High Voltage Laboratory, School of Engineering, Cardiff University, Newport Road, PO Box 687, Cardiff, CF24 3TD, Wales UK. E mail: haddad@cf.ac.uk

FREQUENCY RESPONSE OF EARTHING SYSTEMS

B. Zedan, H. Griffiths andA. Haddad
High-Voltage Group, CardiffUniversiiy, Wales

Keith walker
National Grid, UK

ABSTRACT

Earthing systems are required to perform satisfactorily under fast-front surges so that the power system can be protected against excessive voltages. The characteristics of an earthing system under these conditions are very different from power frequency and, therefore, the dimensioning of earthing systems to perform satisfactorily is more difficult.

In this paper, we present extensive studies of the frequency response (DC up to 10MHz) of (i) a vertical rod, (ii) a horizontal electrode and (iii) a grid The effect of changing the dimensions of the electrodes is examined as well as the consideration of variations in soil resistivity and permittivity. Since the earth conductor inductance can have an appreciable effect on the overall earthing system response, the effect of changing the injection point is considered and the benefits of above ground meshing is quantified.

Finally, the application to the earthing detail of surge arresters is considered. The effect of bonding to surge arrester bases were investigated and transient simulations were used to determine the corresponding protective levels.

1. INTRODUCTION

It has been noted. in a previous related paper [1], that detailed guidelines are provided in national earthing standards [2,3] for the design of substation earth grids under power frequency conditions. However, only brief and qualitative recommendations are given for the practical design of grids and rod systems under high frequency and transient conditions. The marked difference between power-frequency and transient behaviour of such systems has been the subject of a number of investigations that have been reviewed previously [4].

In [1], the influence of soil resistivity, soil permittivity and mesh density on the frequency response, up to 1MHz, of a large grid was demonstrated. It was shown that earth grid impedance increases with frequency and that inductive effects become significant above specific frequencies. The inductive effects are significant at lower frequencies in low soil resistivity media, while soil permittivity has an effect at high frequencies in high soil resistivity. An increase in grid mesh density was shown to lower earth grid impedance for a specific frequency range depending on soil resistivity.

In this paper , the frequency response of rod, horizontal and grid earth electrodes is investigated with the frequency range extended to 10MHz. For the rod and horizontal electrode configurations the effect of length is considered. For a 100x100m grid, the difference between central and corner grid injection is examined. Finally, the effect of increasing the number of downleads is considered.

This effect is important to examine in the context of practical earthing arrangements for surge arresters.

2. MODEL CONFIGURATIONS, PARAMETERS AND SIMULATION METHOD

Figure 1 shows the general arrangements for the *rod*, horizontal and grid electrode considered in the study.

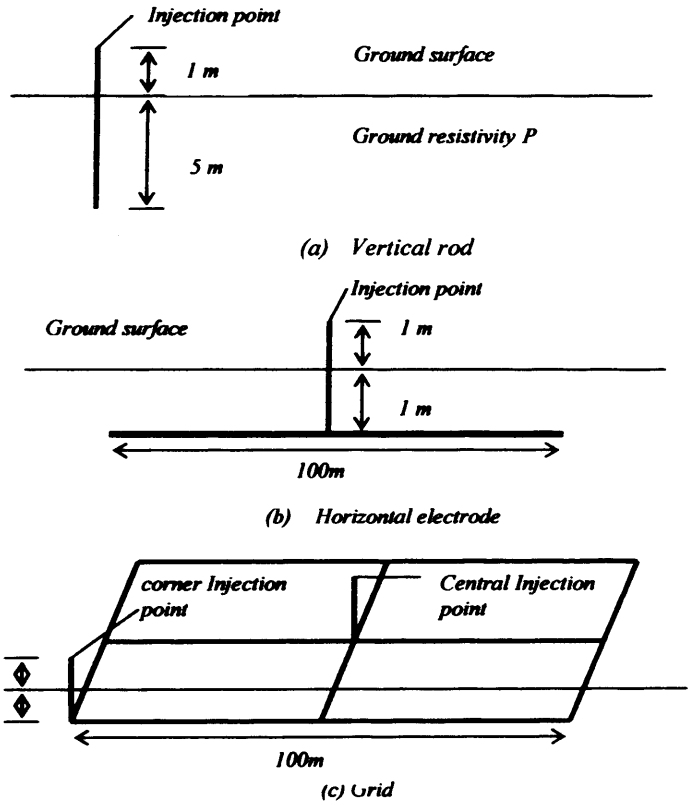

Fig. 1 Earth models(a)rod,(b) horizontal electrode, (c)4-mesh earth grid

Each electrode system is assumed to be made of cylindrical copper conductors with radii of 0.5cm. The systems were studied for earth conditions with a wide range of resistivity (10.Ω.m-10,000.Ω.m) and relative permittivity (1-30). In the simulations to compute earth impedance values, a 1A current energisation was selected. The simulations were carried out using an electromagnetic-field analysis program (CDEGS) [5].

3. SIMULA N RESULTS

3.1 *Frequency response of a vertical rod*

The frequency response for the 5m vertical rod detailed in Fig.1a is shown in Fig. 2 for a relative permittivity of 1.

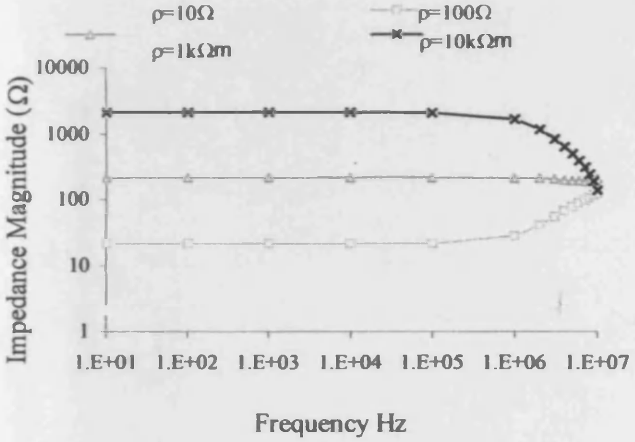

(a)

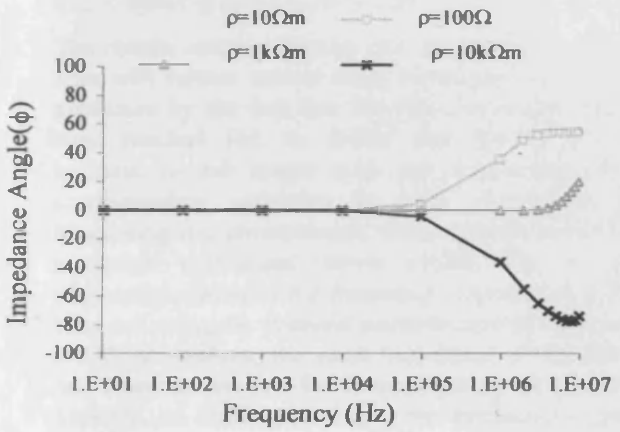

(b)

Fig.2 Frequency response of 5m vertical rod(a) Impedance magnitude,(b) Impedance angle

Each curve has a lower frequency range over which the impedance is nearly constant. For low earth resistivity values (10-100Ωm), the impedance increase rapidly above a particular frequency. This trend is similar to the response for the 4-mesh grid analysed in [1] and can be attributed to the inductance of the conductor. In contmst, however, in high resistivity earth (1000-10,000.Ω.m) the earth impedance of the rod decreases above a particular frequency also related to resistivity. The impedance angle at 100kHz and above, in the 10k.Ωm medium, is negative and tends towards -900 just below 10MHz. This indicates that capacitive effects may be highly significant under these conditions and may explain the reduction in impedance magnitude.

3.2 *Frequency response of a horizontal electrode*

The corresponding frequency response for the 100m horizontal earth electrode shown in Fig. 1b.

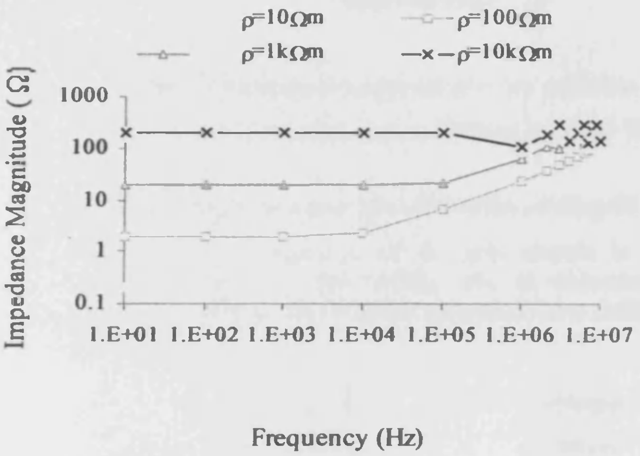

(a)

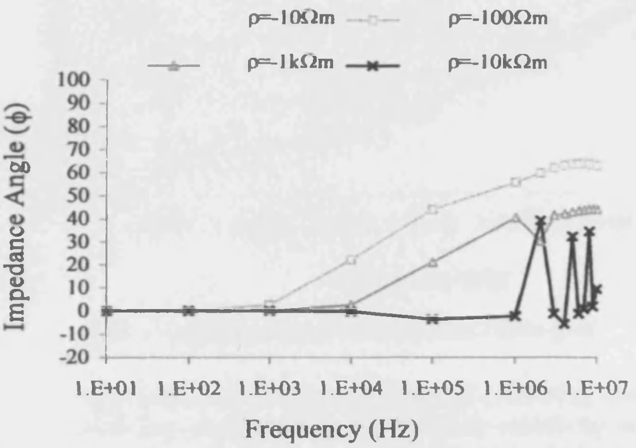

(b)

Fig.3 Frequency response of a 100 Horizontal electrode

(a) Impedance magnitude, (b) Impedance angle

The results of Fig. 3 shows that the behaviour of the 100m horizontal electrode is similar to the 100x100m earth grid investigated in [1], viz., inductive effects become significant above a particular frequency related to resistivity. Above 1MHz in a high resistivity medium, there is evidence of resonant effects in the impedance response.

3.3 *Effect of rod length*

Variations in rod length were considered in the range from 5m to 15m. Over this range, for the same values of resistivities previously considered. and for frequencies up to 100kHz, increases in length produced corresponding decreases in earth impedance. The results for a frequency of 100kHz are shown in Fig. 4.

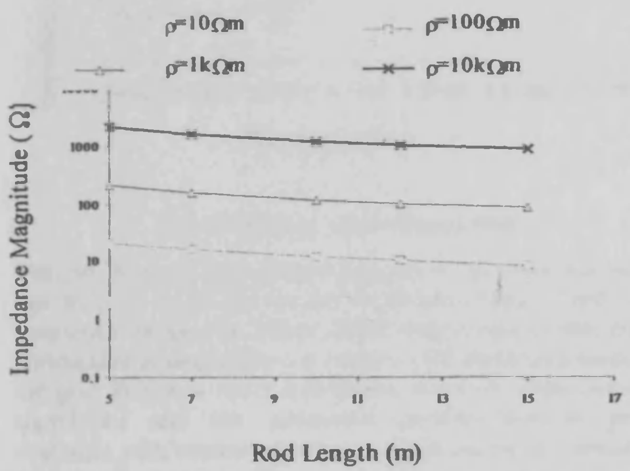

Fig. 4 Effect of rod length on earth impedance at 100kHz

The results indicate that an increase in rod length beyond 15m will further reduce earth impedance and this can be explained by the fact that the effective length has not yet been reached [6]. At 1MHz and above, however, an increase in rod length does not necessarily produce a corresponding reduction in earth impedance. Results, illustrating this phenomenon. were reported in [6] based on a simple equivalent circuit model. Fig 5. shows a comparison between the frequency response of a 5m and a 10m rod using the detailed electromagnetic-field model. In a 100Ωm medium, the earth impedance of the 10m rod is less than the 5m rod for frequencies up to approximately 100kHz. At 1MHz and above, the frequency responses of the two rods of different length converge indicating that an effective length of approximately 5m has been reaches at 1MHz. In the higher resistivity 10Ωm medium, the impedance of the 10m rod is less than the 5 m rod for frequencies up to 5MHz. At this frequency, the impedance of the 10m rod reaches a minimum value. As the frequency is increases from 5MHz to 10 MHz, the impedance of 10m rod increases markedly and at 10MHz exceeds that of the 5m rod.

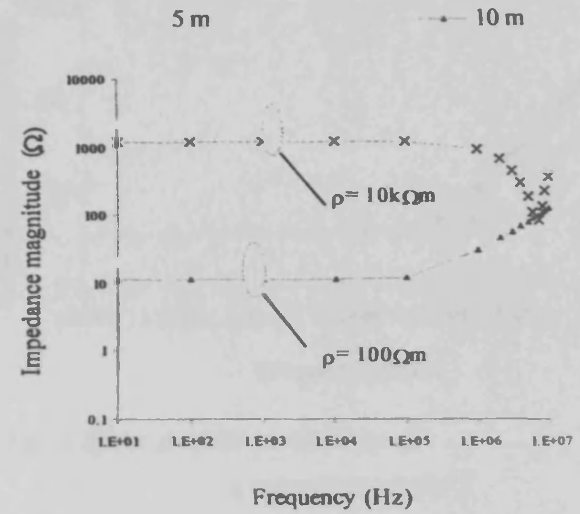

Fig. 5 *Frequency response of a 5m and 10m* rod

3.4 *Frequency response of a 100x100m earth grid*

The frequency response of the grid shown in Fig.1c is shown in Fig. 6. The results are in accordance with previous findings, but here are extended from 1MHz *to* 10MHz.

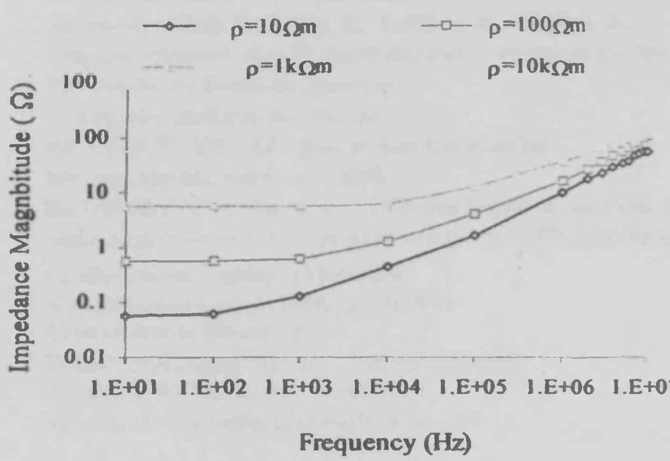

Fig.6 Frequency response of a 100x100m grid

Fig.6 shows that at high frequency (10MHz), the range of earth impedance values for different resistivity media is at least three orders of magnitude less than at dc. This illustrates that inductive effects become very significant as frequency increases, and how they influence the effective length of an electrode, or effective area in the case of a grid.

3.5 *Effect of injection position*

Considering how important inductive effects, Fig. 7 compares the impedance response, in 1000m earth, of a 100x100m earth grid for the cases of central and corner injection (See Fig.1c).

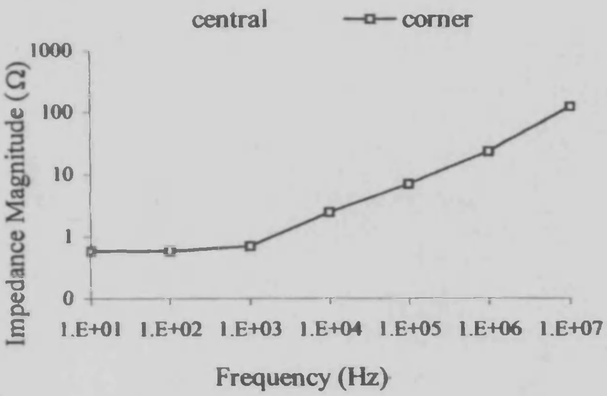

Fig. 7 Effect of injection position

The results show how, at low frequency, the injection point has little or no effect on the earth impedance. Over this frequency range, the longitudinal impedance of the earth conductors is negligible compared to the earth resistance of the grid. Between 1kHz and 1MHz, however, inductance is significant and the additional parallel current paths available with central injections conditions (four instead of two) results in a significant reduction in earth impedance for this case. However, at high frequency (10MHz), the reduction in effective area combined with the high inductance of the downlead means that the impedance values converge once more.

3.6 *Effect of enhancing above-ground connections*

It is recognised that at high frequencies, the impedance of the downleads connecting plant to the earthing system may become dominant. As a result, it may be beneficial to consider enhancements to the above-ground system in the form of meshed interconnections. A 12x12m, 16 mesh grid, buried at 1m was selected to for this study. In its basic arrangement the grid is energized with a single, centrally-connected 4 m downlead. This arrangement is then enhanced with a mesh identical to the buried grid, 3m above the ground. The two meshes are connected firstly by 17 downleads arranged at equally-spaced intervals around the grid periphery and then by a further 7 downleads connected to the grid crossing points(25 downleads in total). Fig.8 shows that the earth impedance, as seen from the point of injection, can be considerable reduced, using above –ground interconnections.

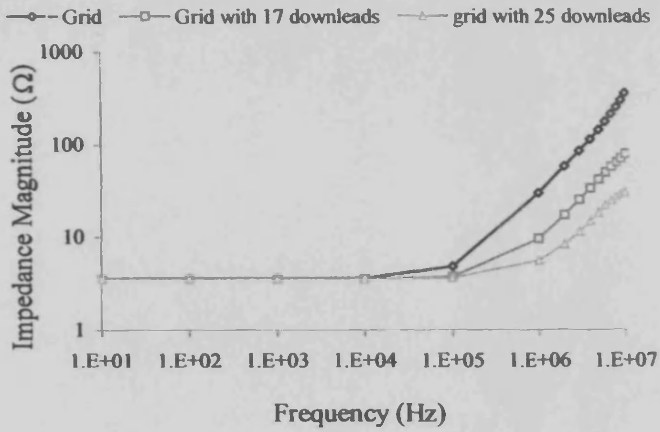

Fig. 8 Effect of additional downleads

4. CONCLUSIONS

5. REFERENCES **[1]** Zedan, B., Griffiths, H., Haddad, A. : 'The effect of grid mesh density on substation earth impedance', Proceedings of the 36th Universities Power Engineering Conference, Swansea, UK, 2001, pp.4

[2] Electricity Association: Technical specification 41-24, 'Guidelines for The Design, fustallation, Testing and Maintenance of Main Earthing Systems in Substations', issue 1,1992.

[3] IEEE80: 2000: 'Guide for Safety in AC Substation Grounding', IEEE, New York, 2000.

[4] van der Linde, F., Zedan, B., Griffiths, H., Haddad, A.,: 'Impulse response of earth electrode systm', Proceeding of the 27th University Power Engineering Conference.Stafford,UK,2002,pp.4

[5] 'CDEGS', HIFREQ Module,Safe Engineering Services,Canada,Versionx.x,2002

[6] Griffiths, H., davies,A.M.,:' Effective length of earth electrode under high frequency and transient conditions' 25th International Conference on Lightning Protection, Vol.1,Rhodos(Greece),2000,pp.536-540

Contact details for authors:
E-mail: griffithsh@cf.ac.uk , haddad@cf.ac.uk
Tel:44 29 20874608, 44 29 20875904
http://www.cf.ac.uk/engin/research/highvolt